VOLUME 79 JANUARY 2, 1975 NUMBER 1

JPCHAx

THE JOURNAL OF PHYSICAL CHEMISTRY

PUBLISHED BIWEEKLY BY THE AMERICAN CHEMICAL SOCIETY

THE JOURNAL OF

PHYSICAL CHEMISTRY

AMERICAN CHEMICAL SOCIETY, *1155 Sixteenth St., N.W., Washington, D.C. 20036*

Books and Journals Division

JOHN K CRUM *Director*
RUTH REYNARD and VIRGINIA E. STEWART *Assistants to the Director*

CHARLES R. BERTSCH *Head, Editorial Processing Department*
D. H. MICHAEL BOWEN *Head, Journals Department*
BACIL GUILEY *Head, Graphics and Production Department*
SELDON W. TERRANT *Head, Research and Development Department*

 Published biweekly by the American Chemical Society at 20th and Northampton Sts., Easton, Pa. 18042. Second-class postage paid at Washington, D.C., and at additional mailing offices.

All manuscripts should be sent to *The Journal of Physical Chemistry,* Department of Chemistry, University of Minnesota, Minneapolis, Minn. 55455.

Additions and Corrections are published once yearly in the final issue. See Volume 78, Number 26 for the proper form.

Extensive or unusual alterations in an article after it has been set in type are made at the author's expense, and it is understood that by requesting such alterations the author agrees to defray the cost thereof.

The American Chemical Society and the Editor of *The Journal of Physical Chemistry* assume no responsibility for the statements and opinions advanced by contributors.

Correspondence regarding accepted copy, proofs, and reprints should be directed to Editorial Processing Department, American Chemical Society, 20th and Northampton Sts., Easton, Pa. 18042. Department Head: CHARLES R. BERTSCH. Assistant Department Head: MARIANNE C. BROGAN. Assistant Editor: CELIA B. MCFARLAND. Editorial Assistant: JOSEPH E. YURVATI.

Advertising Office: Centcom, Ltd., 50 W. State St., Westport, Conn. 06880.

Business and Subscription Information

Send all new and renewal subscriptions *with payment* to: Office of the Controller, 1155 16th Street, N.W., Washington, D.C. 20036. Subscriptions should be renewed promptly to avoid a break in your series. All correspondence and telephone calls regarding changes of address, claims for missing issues, subscription service, the status of records, and accounts should be directed to Manager, Membership and Subscription Services, American Chemical Society, P.O. Box 3337, Columbus, Ohio 43210. Telephone (614) 421-7230. For microfiche service, contact ACS Journals Department, 1155 16th St. N.W., Washington, D.C. 20036. Telephone (202) 872-4444.

On changes of address, include both old and new addresses with ZIP code numbers, accompanied by mailing label from a recent issue. Allow four weeks for change to become effective.

Claims for missing numbers will not be allowed (1) if loss was due to failure of notice of change in address to be received before the date specified, (2) if received more than sixty days from date of issue plus time normally required for postal delivery of journal and claim, or (3) if the reason for the claim is "issue missing from files."

Subscription rates (hard copy or microfiche) in 1975: $20.00 for 1 year to ACS members; $80.00 to nonmembers. Extra postage $4.50 in Canada and PUAS, $5.00 other foreign. Supplementary material (on microfiche only) available on subscription basis, 1975 rates: $15.00 in U.S., $19.00 in Canada and PUAS, $20.00 elsewhere. All microfiche airmailed to non-U.S. addresses; air freight rates for hard-copy subscriptions available on request.

Single copies for current year: $4.00. Rates for back issues from Volume 56 to date are available from the Special Issues Sales Department, 1155 Sixteenth St., N.W., Washington, D.C. 20036.

Subscriptions to this and the other ACS periodical publications are available on microfilm. For information on microfilm write Special Issues Sales Department at the address above.

Notice to Authors last printed in the issue of June 6, 1974

THE JOURNAL OF

PHYSICAL CHEMISTRY

Volume 79, Number 1 January 2, 1975

JPCHAx 79(1) 1-94 1975

ISSN 0022-3654

COMMUNICATIONS TO THE EDITOR

There is no supplementary material for this issue.

* In papers with more than one author, the asterisk indicates the name of the author to whom inquiries about the paper should be addressed.

AUTHOR INDEX

THE JOURNAL OF
PHYSICAL CHEMISTRY

VOLUME 79, NUMBER 1 JANUARY 2, 1975

Rate Constants for the Reaction of O^- Radicals with Organic Substrates in Aqueous Solution[1]

P. Neta and Robert H. Schuler*

Radiation Research Laboratories, Center for Special Studies and Department of Chemistry, Mellon Institute of Science, Carnegie-Mellon University, Pittsburgh, Pennsylvania 15213 *(Received June 21, 1974)*

Publication costs assisted by Carnegie-Mellon University and the U. S. Atomic Energy Commission

In strong base OH radical is rapidly converted into O^- so that reactions of the latter radical can be conveniently studied by radiolyzing solutions at high pH. The absolute rate constants for reaction of O^- with unsaturated compounds have been measured in 1 *M* NaOH by following the increase in absorption of the allylic radicals resulting from H atom abstraction. The radical produced from 3-hexenedioic acid has a very strong absorption at a relatively long wavelength (λ(max) 266 nm, ϵ(266) 16,350 M^{-1} cm^{-1}) so that this compound was chosen as an appropriate reference for competitive experiments. Detailed examination of the competition against ethanol indicates that relative rate constants for the reaction of O^- can be determined accurately (±10%) and placed on an absolute scale by reference to the measurements on 3-hexenedioic acid. The rate constant measured for reaction of O^- with ethanol has been determined to be 1.2×10^9 M^{-1} sec^{-1} and this reaction can, in turn, be used as a secondary reference in cases where the radical produced from a second solute absorbs significantly. Measurement of the rate constants for H abstraction from a number of saturated alcohols and monocarboxylic acids by O^- gives values ~50% of those for abstraction by OH. More highly charged anions exhibit markedly lower rate constants. Partial rate constants for various H atom configurations are suggested. Rate constants for reaction with most unsaturated compounds having allylic hydrogens are higher than expected from the partial rates for the saturated system showing that a main path of reaction involves abstraction of these hydrogen atoms. The data indicate that the rate for abstraction from allylic positions is increased by a factor of 2–3 over the rates in similar saturated systems. Addition of O^- to double bonds and aromatic systems has again been shown to be relatively slow ($<5 \times 10^7$ M^{-1} sec^{-1}) so that in most cases abstraction dominates addition.

Introduction

At high pH the hydroxyl radical produced in irradiated aqueous solutions is rapidly converted into its basic form, the oxide anion radical, to a degree controlled by the equilibrium[2]

$$OH + OH^- \underset{}{\overset{pK = 11.85}{\rightleftharpoons}} O^- + H_2O \qquad (1)$$

Although many rate constants for reaction of OH have been determined only a few values are known for O^- reactions. The compilation by Dorfman and Adams[3] lists, for example, only five rate constants for reaction with organic compounds. Several additional values have been reported more recently.[4-6] From the known rates for reaction with methanol, ethanol, and formate ion[3] it appears that hydrogen abstraction by O^- is about half as rapid as abstraction by OH. On the other hand, the limited information available on the addition of O^- to double bonds or to aromatic systems indicates that these reactions are relatively slow, usually more than 2 orders of magnitude slower than addition of OH.[3,4] Because of these differences in reactivities, compounds which contain sites for both addition and abstraction react mainly with OH by addition but with O^- by abstraction. The O^- radicals are, therefore, useful for the production of certain radicals which cannot easily be obtained by other means.[4] For example, in a recent esr study a series of substituted benzyl radicals was produced by abstraction from the corresponding toluenes.[7] Similarly, abstraction from olefinic compounds can produce allylic radicals.[4,6]

Because of the limited amount of data currently available on O^- reaction rate constants and particularly because

of the importance of O^- reactions for selectively producing certain radicals in unsaturated and aromatic systems, it appeared worthwhile to develop a simple technique for measuring such rate constants and to apply it to a series of organic compounds. Establishment of the systematics of the dependence of rate constant on structure is useful in assigning partial rate constants to different reaction sites. In recent spectrophotometric studies of allylic radicals produced by O^- reactions[8,9] it became apparent that determination of extinction coefficients for these radicals required detailed knowledge of these partial rates so that one could predict, with reasonable accuracy, the relative frequency for attack at the different sites. In the present study a number of absolute rate constants were determined by direct observation of the buildup of the product radical in pulse radiolysis experiments. A competitive method, which examined the reduction in yield of a reference radical when a second solute was introduced into the system, was then developed and cross checked between several different solutes. This method was then used to survey the rate constants for reaction of O^- with some 30 organic substrates. The results and systematics of the observed rate constants are summarized here.

Experimental Section

The computer-controlled pulse radiolysis system described by Patterson and Lilie[10] was used in these studies. The absolute rates for reaction of O^- with selected reference compounds at known concentrations were determined by following the growth in absorption of the product radicals. Most studies were carried out in 1 *M* NaOH solutions where OH is over 99% dissociated into O^- with the period for dissociation being $\sim 10^{-10}$ sec. Absolute measurements were made at a number of solute concentrations such that the growth periods were in the range 0.5–15 μsec. The pulse length used was 0.5 μsec and the time constant of the detecting electronics was ~0.1 μsec. Observations were carried out at absorbed doses limited to $1–2 \times 10^{16}$ eV/g per pulse at which doses the initial radical concentrations (1–2 μM) were sufficiently lower than the solute concentration that pseudo-first-order kinetics applied. The median radical lifetime for second-order reactions at these concentrations is greater than 100 μsec. Despite this, in order to obtain reasonably complete scavenging of O^-, it was found necessary to use concentrations of organic solutes such that the reaction periods were in the range of a few microseconds. At lower concentrations the scavenging was incomplete and a limiting reaction period ~35 μsec was observed, apparently as the result of reaction with impurities in the solutions. Since even the purest sodium hydroxide commonly available contains significant carbonate (~0.4%) reaction with the carbonate was suspected (because of the high concentration of base used the solutions contained a minimum of 1.5 m*M* carbonate). The reaction of O^- with carbonate was examined by use of the competition method developed here and found to have an apparent rate constant of $2.7 \times 10^6\ M^{-1}\ \text{sec}^{-1}$. In 1 *M* base this reaction is, in fact, controlled by reaction of the equilibrium concentration of OH with the carbonate ($k_{(OH + CO_3^{2-})} = 4 \times 10^8\ M^{-1}\ \text{sec}^{-1}$)[3] so that the rate constant for reaction of O^- with the carbonate must be $<10^6\ M^{-1}\ \text{sec}^{-1}$. At a concentration of 1.5 m*M* CO_3^{2-} the reaction period should be ~170 μsec. The shorter observed reaction period must, therefore, either result from a higher concentration of carbonate or reaction of O^- with other impurities initially present in the solution. In fact it was found that at low concentrations both the extent of scavenging and the reaction period were very sensitively dependent on the sample of base used and the way in which the solutions was handled. As a standard procedure water was purged with N_2O for at least 20 min before the base was added (40 g/l. of Baker Analyzed NaOH containing 0.4% Na_2CO_3; sample freshly opened on the day of the experiment) and this procedure gave very consistent results throughout this series of experiments.

Most studies were carried out *via* competitive experiments in which the decrease in the concentration of the radical produced from 3-hexenedioic acid was observed at 266 nm. In these studies the results from a large number of pulses (25–50) were averaged to give relative absorbances known to 1–2% so that reliable measurements could be made over a wide range of concentrations of added solute. The reproducibility and rapid reduction of data provided by the computerized pulse radiolysis system is important here. Appropriate corrections were made for light absorption by radicals produced from the second solutes but, except for very high concentrations, these corrections were usually small. A 2-cm single pass absorption cell was used for most experiments. In a few cases (fumarate, maleate, the aromatic compounds) the added solutes themselves absorbed strongly and it was necessary to use a 0.5-cm cell and to make an appropriate correction for transmission of scattered light of long wavelength.

In the absence of side reactions of e_{aq}^- and H atoms with the solutes present in solution, the O^- radical yield in N_2O saturated solution is $G = 6.6$; 2.8 directly from the water, 3.2 from reaction of e_{aq}^- with N_2O and 0.6 from conversion of H through e_{aq}^- to O^-. In treating the experimental results we have assumed that reaction with the solutes added is entirely that of O^-. From the known rate constants, interference by side reactions of e_{aq}^- and H are, in most cases, unimportant. This is particularly true for saturated systems and for unsaturated systems which react rapidly with O^- ($>3 \times 10^8\ M^{-1}\ \text{sec}^{-1}$). For unsaturated systems which react only slowly with O^-, interference with the reaction between e_{aq}^- and N_2O can contribute somewhat to the reduction in the observed signal. These cases are appropriately corrected and footnoted in the results.

Most chemicals used were of the purest grade available from J. T. Baker Chemical Co., Aldrich Chemical Co. or the Eastman Chemical Co. *t*-BuOH was Mallinckrodt Analytical Reagent and glycine was Cyclochemical Co. NRC Grade. Crotononitrile was from the Bader collection (Aldrich) and aconitic acid from Nutritional Biochemicals Corp.

Results and Discussion

In general, carboxyallyl radicals exhibit a very strong absorption band in the region 250–300 nm so that their production by abstraction from unsaturated acids provides a convenient reference reaction for the study of O^- rate constants. After a survey of a number of typical examples, 3-hexenedioic acid was chosen as the most suitable reference since the rate of reaction 2 is reasonably high and the resultant radical has appropriate optical properties. The spectrum of radical I (Figure 1) shows a very intense, moderate-

$$O^- + {}^-O_2CCH_2CH{=}{=}CHCH_2CO_2^- \xrightarrow{k_2} OH^- + {}^-O_2CCH_2\overline{CHCHCH}CO_2^- \quad (2)$$

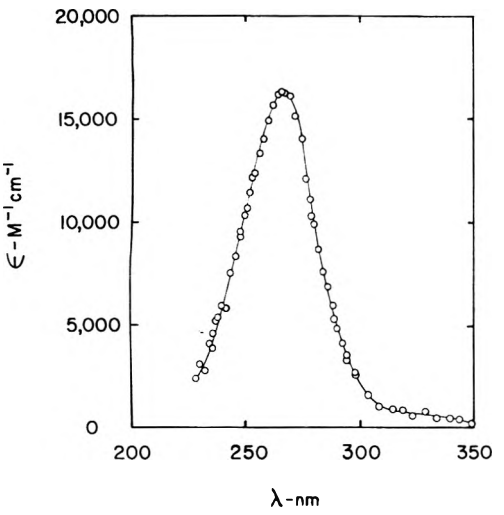

Figure 1. Optical absorption spectrum of radical I (^-O_2C-$CH_2CHCHCHCO_2^-$) produced in the radiolysis of 3-hexenedioic acid in 1 *M* NaOH solution saturated with N_2O. Extinction coefficients are calculated from the limiting absorbances at high solute concentrations assuming a yield for radical I of 6.0 and using $(SCN)_2^-$ dosimetry taking ϵ_{480} $(SCN)_2^-$ 7600 M^{-1} cm^{-1}.

ly narrow band (37 nm at half-maximum) at 266 nm. This wavelength is sufficiently high to provide a good signal-to-noise ratio in our apparatus at radical concentrations in the region of 10^{-6} *M*. Absorption by the base (which at 1 *M* cuts off below 230 nm) is unimportant.

Absolute Rate Determinations. The period for reaction was measured from 5×10^{-5} to 1.5×10^{-3} *M* 3-hexenedioic acid and typical data are illustrated in Figure 2. The quality of the data obtainable with this system is obvious. The limiting absorbance levels determined from observations on longer time scales (as is illustrated in Figure 2 for the measurements at 8×10^{-4} *M*) are reported in Table I. The growth during the initial period was fitted to an exponential by a weighted least-squares approach. A plot of $1/t_{1/2}$ *vs.* solute concentration was linear with the slope corresponding to a rate constant (k_2) of 6.3×10^8 M^{-1} sec^{-1}. The intercept corresponded to a background rate (k') of 2.0×10^4 sec^{-1} (half period of 35 μsec). Multiplication of the observed limiting absorbances by $(1 + k'/k_2[S])$ to take into account the portion of O^- radicals reacting by other paths gave the corrected absorbances in the third column. The constancy of these corrected absorbances indicated that other complications are unimportant and that the background rate is being properly taken into account. A limiting value of 16,350 M^{-1} cm^{-1} is obtained for the extinction coefficient of radical I at 266 nm. Correcting the observed period by 16,350 over the observed absorbance gives the period for reaction with the 3-hexenedioic acid in the absence of other reactions. The data of Figure 2 were then fitted by a weighted least-squares approach to an exponential growth assuming that the limiting absorbance was $16{,}350/(1 + k'/k_2[S])$ (with k' and k_2 as obtained from the first approximations) and the resultant curves are those plotted in Figure 2. The measured periods and rate constants for the individual experiments are given in Table I. A plot of $A/(16{,}350\ t_{1/2})$ *vs.* [S] goes through the origin and has a slope corresponding to $k_2 = 6.3 \times 10^8$ M^{-1} sec^{-1}. Least-squares treatment of this data gives the 90% confidence level as $\pm 0.3 \times 10^8$ M^{-1} sec^{-1}. For 3-hexenedioic acid solutions at 1 m*M*, where most of the competitive measurements reported below were measured, the effective

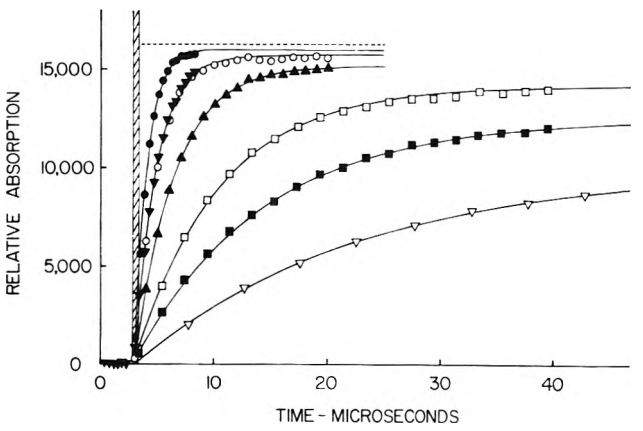

Figure 2. Time dependence for the production of radical I in 1 *M* NaOH solutions containing 5×10^{-5} *M* (▽), 1×10^{-4} *M* (■), 2×10^{-4} *M* (□), 4×10^{-4} *M* (▲), 8×10^{-4} *M* (▼ and ↄ), and 1.5×10^{-3} *M* (●) 3-hexenedioic acid. Observations were at 266 nm. The pulse duration is indicated by the shaded area. For a solution 2×10^{-2} *M* in 3-hexenedioic acid the transient signal was found to rise to better than 95% of the plateau level within 1 μsec after the pulse so that instrumental time constants do not perturb these results significantly. The solid curves represent the results of weighted least-squares treatment of the data with the limiting value being $16{,}350/(1 + k'/k_2[S])$ as described in the text. The periods and rate constants determined from these calculations are reported in Table I.

reference rate is 6.5×10^5 sec^{-1} if one takes into account the slight effect of background reactions.

The other compounds for which absolute rate measurements were made were 2-hexenedioic, glutaconic, and crotonic acids. The allylic radicals from all these compounds have intense absorption bands in the region 250–270 nm and were easily studied as described above. The absolute rate constants for all these compounds are summarized in Table II.

Competitive Experiments Against Ethanol. Ethanol reduces the yield of allylic radicals from 3-hexenedioic acid according to simple competition as is illustrated in Figure 3. The limiting absorbance observed upon completion of the reaction was measured in pulse experiments and a plot of $(A_0/A - 1)$ was found to be linear in ethanol concentration. (A and A_0 are the absorbances of the reference radical per unit dose in the presence and absence of a second solute.) Measurements were carried out at 0.5, 1.0, 1.5, and 2.5 m*M* 3-hexenedioic and the relative reductions found to be dependent only on the relative concentrations of the two solutes as is shown in Figure 3. The relative rates for reactions 2 and 3 were found to be equal (*i.e.*, $A_0/A - 1 = 1$) at

$$O^- + S \xrightarrow{k_3} \text{products} \qquad (3)$$

[EtOH]/[3-hexenedioic] = 0.53. From this the absolute rate for reaction of O^- with ethanol is 12.2×10^8 M^{-1} sec^{-1}.

Similar competitive experiments were carried out with the other reference compounds and the rates were determined by reference to the above rate constant for reaction with ethanol. In all cases good linearity of the competition plots over the range of A/A_0 from 0.2 to 5 indicates that complications due to side reactions (particularly of e_{aq}^- with the solute) are unimportant. These rate constants agree very well with the absolute measurements as is illustrated in Table II. In general, if the product radical absorbs significantly, studies of the effect of ethanol in reducing this absorption provide a simple means of measuring the rate constant. This approach is applied in a number of other measurements reported below.

TABLE I: Rate of Reaction of O^- with 3-Hexenedioic Acid

10^{-4} [3-hexenedioic acid], M	Relative absorbance, A[a]	Corrected absorbance[b]	$t_{1/2}$, μsec[c]	$t_{1/2}(16,350/A)$	$10^{-8}k$, M^{-1} sec^{-1}
0.5	9,800	16,000	14.3	23.8	5.8
1.0	12,200	16,200	7.9	10.6	6.6
2.0	13,850	16,000	5.15	6.07	5.7
4.0	15,100	16,350	2.38	2.58	6.7
8.0	16,000	16,600	1.31	1.34	6.5
15.0	16,000	16,350	0.76	0.78	6.0
					(6.3 ± 0.3)[d]

[a] Observed at 266 nm at times >5 $t_{1/2}$; decay of the radicals occurred only at much longer times (milliseconds) and is unimportant here. [b] Relative absorbance corrected by a factor of $1 + k'/k_2[S]$ where k' is the limiting rate of 2×10^4 sec^{-1} and k is taken as 6.3×10^8 M^{-1} sec^{-1}. [c] From least-squares treatment of the data of Figure 2. [d] From least-squares analysis of a plot of $A/(16,350t_{1/2})$ *vs.* [S].

TABLE II: Absolute Rate Constants for Reaction of O^-

Compound	Rate constant $\times 10^{-8}$, M^{-1} sec^{-1}: Absolute determn[a]	Competition with EtOH[b]
3-Hexenedioic acid	6.3	(6.3)[c]
2-Hexenedioic acid	6.9	6.5
Glutaconic acid	3.0	3.5
Crotonic acid	9.0	8.5 (8.7)[d]

[a] Carried out with 1 M NaOH, 0.5–15 $\times 10^{-4}$ M of the organic compound in N_2O saturated solutions, by observing the rise time of the absorption at 250–270 nm. [b] Carried out using a constant concentration of the organic acid and varying the ethanol concentration. Rate constants are corrected for the background rate of 2×10^4 sec^{-1} which contribute 2–4% under the conditions of these competition experiments. [c] Taken as the reference rate constant. [d] Determined by competition of crotonic against 3-hexenedioic acid.

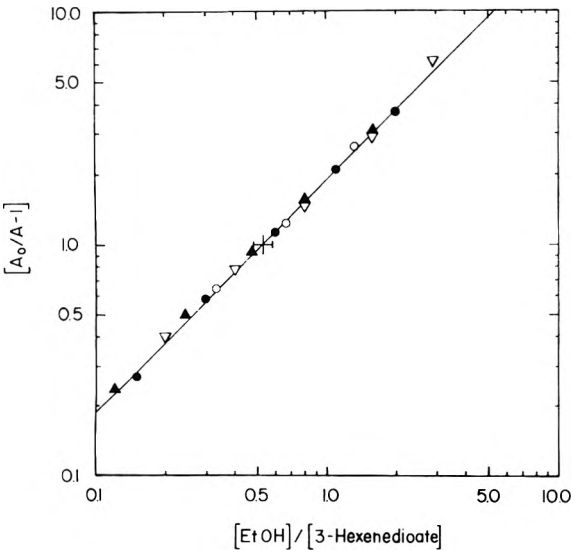

Figure 3. A plot of the results of competition between the reaction of O^- with 3-hexenedioic acid and ethanol in N_2O saturated 1 M NaOH solution. Solutions containing 0.5 (▽), 1.0 (●), 1.5 (○), and 2.5 (▲) mM 3-hexenedioic acid and increasing concentrations of ethanol. The reduction in the absorption of radical I is linear in the ratio of ethanol to 3-hexenedioic acid concentration (the solid line has a slope of unity) and independent of the 3-hexenedioic acid concentration. The rates of reaction 2 and 3 are equal at a solute concentration ratio of 0.53 indicated by the cross in the figure.

The allylic radical from crotonic acid absorbs at 250 nm and has only a modest extinction coefficient at 270 nm (~2000 M^{-1} cm^{-1}) so that it was possible to study the effect of crotonic acid in reducing the absorption from the 3-hexenedioic acid radical. The measured rate constant (8.7×10^8 M^{-1} sec^{-1}) is in excellent agreement with the absolute rate constant (9.0×10^8 M^{-1} sec^{-1}) directly measured at 250 nm and also with the rate constant (8.4×10^8 M^{-1} sec^{-1}) determined by competition with ethanol.

Rate Constants for Reactions of O^- with Saturated Organic Solutes. Rate constants for reaction of O^- with a number of saturated compounds, determined by competition with 3-hexenedioic acid as described above for ethanol, are summarized in Table III. For all five alcohols studied the rate of abstraction by O^- is found to be ~0.6 of that for abstraction by OH. The same situation holds for monocarboxylic acids, except that the ratio in this case is somewhat lower, ~0.4. The constancy of these ratios indicates that the reactivities of both OH and O^- are affected by structure and substituents in a similar fashion. The lower ratio observed for the acids is most probably a result of the effect of charge on the rate, which becomes more pronounced in the case of di and tricarboxylic acids. In order to estimate the effect of charge and of substitution, partial rates have to be derived. From the rate constants in Table III partial rates can be derived as shown in Table IV. The values in this table give good agreement with the overall rate constants for alcohols and monocarboxylic acids. In the case of substitution by CO_2^- the reactivity decreases by a factor of ~2 which is about as expected for reaction between singly charged anions. The CO_2^-, therefore, has no large deactivating effect on the reaction although it may decrease the reactivity of adjacent H atoms slightly. As in the case of abstraction by OH radicals OH groups activate the adjacent H atoms appreciably (by a factor ~4). As expected the reactivity of secondary hydrogen atoms is considerably greater than that of primary hydrogens (by a factor ~5).

It will be noted in Table III that the dicarboxylates are about a factor of 3 less reactive than their singly charged counterparts. The effect of charge is emphasized in the case of triply charged citrate where the measured rate of 0.42×10^8 is a factor of 3 less than for succinate, with which it can be directly compared, and an order of magnitude lower than expected from the partial rate data of Table IV. If we take the interaction distance as 4 Å then, at low ionic strength, the coulombic term introduces factors of 0.36, 0.10, and 0.03 into the rate expression for reaction between a singly charged anion and singly, doubly, and triply charged anions. The measured rate constants essentially reflect decreases in the rate constants of these magnitudes but one must remember that the measurements are carried

TABLE III: Rate Constants for Reaction of O^- with Saturated Compounds

	Compd	$10^{-8}k_{O^-}$, M^{-1} sec^{-1}	k_{O^-}/k_{OH}
Methanol	CH_3OH	5.5[a]	0.61
Ethanol	CH_3CH_2OH	12.2 (11.3)[a]	0.68
1-Propanol	$CH_3CH_2CH_2OH$	15.1	0.56
2-Propanol	$(CH_3)_2CHOH$	12.2	0.61
2-Methyl-2-propanol	$(CH_3)_3COH$	3.3	0.66
Formate	HCO_2^-	14[a]	0.47
Acetate	$CH_3CO_2^-$	0.5	0.71
Propionate	$CH_3CH_2CO_2^-$	3.3	0.42
n-Butyrate	$CH_3CH_2CH_2CO_2^-$	6.5	0.36
n-Hexanoate	$CH_3CH_2CH_2CH_2CH_2CO_2^-$	14.4	0.37
Malonate	$^-O_2CCH_2CO_2^-$	0.21	0.38
Succinate	$^-O_2CCH_2CH_2CO_2^-$	1.35	
Adipate	$^-O_2CCH_2CH_2CH_2CH_2CO_2^-$	4.5	
Citrate	$^-O_2CCH_2C(OH)(CO_2^-)CH_2CO_2^-$	0.42	
Glycine	$H_2NCH_2CO_2^-$	5.6	0.19
Acetonitrile	CH_3CN	2.2	10[b]
Propionitrile	CH_3CH_2CN	10	14
Cyanoacetate	$^-O_2CCH_2CN$	4.1	27

[a] Previous determinations. [b] k_{OH} redetermined in the present work by competition with *p*-nitrobenzoate (see P. Neta and L. M. Dorfman, *Advan. Chem. Ser.*, **No. 81**, 222 (1968)).

TABLE IV: Partial Rates for Abstraction by O^- from Saturated Systems[a]

	$10^{-8}k$, M^{-1} sec^{-1}		
Group	R = alkyl	R = CO_2^-	R = OH
CH_3–R	1.1	0.5	5.5
$-CH_2$–R	3.5	2.2	11
>CH–R			10

[a] Partial rates increased by a factor ~3 for hydrogen atoms in allylic positions.

out at an ionic strength of ~1 so that effects of charge should be reduced considerably.

The nitriles examined show anomalously high rate constants, an order of magnitude higher than their rate of reaction with OH. It was suspected that O^-, contrary to OH, might react directly with the cyano group. However, steady-state esr experiments with acetonitrile did not indicate any such reaction. Only the radical $\cdot CH_2CN$ was observed in 1 *M* NaOH and the intensity was comparable to that found at pH 10 so that all radicals appear to abstract efficiently on the time scale of the esr experiments (*i.e.*, 100 μsec). Pulse radiolysis of cyanoacetate at pH 14 and doses an order of magnitude greater than used here showed the formation of a strongly absorbing secondary species which was not produced in neutral solutions. This species was suspected to affect the O^- rate determination, but thorough examination of the system showed no such complications. It has to be concluded, therefore, that the nitriles undergo H abstraction by O^- with rate constants appreciably higher than those by OH, but the reason is, at the moment, unclear.

Rate Constants for Reaction of O^- with Unsaturated Systems. The measured rate constants for reaction of O^- with unsaturated compounds are summarized in Table V. Since the rate constants for the reaction of OH with most unsaturated systems are in the range 3–6 × 10^9 M^{-1} sec^{-1} the ~1% equilibrium concentration of OH present in 1 *M* base is expected to result in a contribution of ~0.5 × 10^8 M^{-1} sec^{-1} to the rate constant. Measurements with acetylenedicarboxylate and fumarate both gave rate constants of 0.4 × 10^8 which can be ascribed almost entirely to the OH contribution. The latter, which absorbs significantly in the region of 270 nm, had to be studied in the 0.5-cm path length cell, but gave a reliable value. The rate constant for reaction on OH with fumarate anion was measured at pH 9 by competition with *p*-nitrobenzoate and found to be 5.0 × 10^9 M^{-1} sec^{-1}. Correcting for this contribution, the rate constant for reaction of O^- with the fumarate cannot be greater than 10^7 M^{-1} sec^{-1}. A similar rate should apply to acetylenedicarboxylate. Addition of O^- to unsaturated systems appears to be, for the most part, unimportant. Maleate does not absorb nearly as strongly in the region of 270 nm as does fumarate and can be studied somewhat more easily. A careful comparison between the reactions with fumarate and maleate indicated that the latter was somewhat more reactive and in fact, after correction for the OH contribution, exhibits a rate constant ~3 × 10^7 M^{-1} sec^{-1} for the reaction of O^-. Very probably this higher rate can be ascribed to the abstraction of vinylic protons.

The observed rate constants for the reaction of O^- with the other unsaturated compounds are considerably greater than can be ascribed to the contribution for reaction of OH. Where allylic protons exist, rate constants are mostly above 5 × 10^8 M^{-1} sec^{-1}. Comparison of the measured rate constants with the expectation from the partial rates for abstraction given in Table IV indicates that activation of the allylic protons increases the rate of those positions by a factor ~3. As a result, the main radical produced in many of these systems is the allylic radical and radiolysis of strongly basic solutions of these compounds becomes a convenient way of producing allylic radicals for spectroscopic purposes. One would like to know the yields of these radicals and, as mentioned in the Introduction, one of the purposes of the present work was to provide appropriate rate information for estimation of yields. In most cases side reactions should not contribute more than 20–30%. One exception is aconitic acid which, because of its triple charge, reacts only slowly with O^- so that reactions of OH become quite important and one is not able to produce high concentrations of the tricarboxylated allyl radical. Comparison of the rate constants for reaction with singly charged 3-butenoate and

TABLE V: Rate Constants for Reaction of O^- with Unsaturated Compounds in 1 *M* NaOH

Compd		$10^{-8}k$,[a] M^{-1} sec^{-1}
Acetylenedicarboxylate	$^-O_2CC{\equiv}CCO_2^-$	0.4[b]
Fumarate	$^-O_2CCH{=}CHCO_2^-$	0.4[b]
Maleate	$^-O_2CCH{=}CHCO_2^-$	0.8[b]
Acrylate	$CH_2{=}CHCO_2^-$	2.0[b]
Crotonate	$CH_3CH{=}CHCO_2^-$	8.7[c]
3-Butenoate	$CH_2{=}CHCH_2CO_2^-$	7.2
Methacrylate	$CH_2{=}C(CH_3)CO_2^-$	4.8
Glutaconate	$^-O_2CCH_2CH{=}CHCO_2^-$	3.2[c]
Aconitate	$^-O_2CCH_2C(CO_2^-){=}CHCO_2^-$	~1.5[d]
2-Hexenedioate	$^-O_2CCH{=}CHCH_2CH_2CO_2^-$	6.7[c]
3-Hexenedioate	$^-O_2CCH_2CH{=}CHCH_2CO_2^-$	(6.5)[d]
Crotononitrile	$CH_3CH{=}CHCN$	9.9
Allyl cyanide	$CH_2{=}CHCH_2CN$	10.5
Methacrylonitrile	$CH_2{=}C(CH_3)CN$	17.6
Allyl alcohol	$CH_2{=}CHCH_2OH$	22[e] (29)[f]
2-Butene-1,4-diol	$HOCH_2CH{=}CHCH_2OH$	23[e]
Muconate	$^-O_2CCH{=}CHCH{=}CHCO_2^-$	~20
Allylbenzene	$C_6H_5CH_2CH{=}CH_2$	5[d]
Benzonitrile	C_6H_5CN	1.0

[a] Determined by competition with 3-hexenedioic acid unless otherwise stated. These rate constants include a contribution ~0.5 × 10^8 M^{-1} sec^{-1} for addition of OH to the unsaturated systems. [b] Correction has been applied for interference of the solute with the reaction between e_{aq}^- and N_2O. [c] Average value from several determinations (see Table II). [d] Absolute determination. [e] Determined by competition with ethanol. [f] Previously determined in ref 6.

doubly charged glutaconate again indicates a factor ~2 reduction in the rate constant resulting from the additional charge in the latter case. The reactivities of neutral olefinic substrates are all high, and where hydrogen atoms in allylic positions are additionally activated by an OH group the rate constants approach the diffusion-controlled limit. Rate constants for reaction with allyl cyanide and crotononitrile are about as expected but that with methacrylonitrile appears to be anomalously high. This latter value was checked with two samples which gave comparable results.

The rate constant for reaction of O^- with benzoate is known to be low (0.4 × 10^8 M^{-1} sec^{-1}).[5] Measurements on benzonitrile gave an observed rate constant of 1.0 × 10^8 M^{-1} sec^{-1} which, correcting for the OH contribution of 0.5 × 10^8 M^{-1} sec^{-1}, gives a net rate for O^- reactions of 0.5 × 10^8 M^{-1} sec^{-1}. In this case the rate constant does not exhibit any appreciable contribution for reaction of O^- with the cyano group, in support of the above comment on the reaction with saturated nitriles.

References and Notes

(1) Supported in part by the U. S. Atomic Energy Commission.
(2) J. Rabani and M. S. Matheson, *J. Phys. Chem.*, **70**, 761 (1966); J. L Weeks and J. Rabani, *ibid.*, **70**, 2100 (1966).
(3) L. M. Dorfman and G. E. Adams, *Nat. Stand. Ref. Data Ser., Nat. Bur. Stand.* **No. 46**, (1973).
(4) P. Neta, M. Z. Hoffman, and M. Simic, *J. Phys. Chem.*, **76**, 847 (1972).
(5) M. Simic, M. Z. Hoffman, and M. Ebert, *J. Phys. Chem.*, **77**, 1117 (1973).
(6) M. Simic, P. Neta, and E. Hayon, *J. Phys. Chem.*, **77**, 2662 (1973).
(7) P. Neta and R. H. Schuler, *J. Phys. Chem.*, **77**, 1368 (1973).
(8) T. Soylemez and R. H. Schuler, *J. Phys. Chem.*, **78**, 1052 (1974).
(9) R. H. Schuler and L. K. Patterson, *Chem. Phys. Lett.*, **27**, 369 (1974).
(10) L. K. Patterson and J. Lilie, *Int. J. Radiat. Phys. Chem.*, **6**, 129 (1974).

Chlorine-Atom Sensitized Oxidation of Dichloromethane and Chloromethane[1a]

Eugenio Sanhueza[1b] and Julian Heicklen*

Department of Chemistry and Center for Air Environment Studies, The Pennsylvania State University, University Park, Pennsylvania 16802
(Received July 1, 1974)

Publication costs assisted by the Center for Air Environment Studies

Mixtures of Cl_2, O_2, and either CH_2Cl_2 or CH_3Cl were irradiated at 3655 Å and 32°. The Cl_2 photodissociates and $CHCl_2$ or CH_2Cl radicals are produced *via* hydrogen abstraction from the corresponding chlorinated methane. In the CH_2Cl_2 system, there is a long chain process, the initial products are HCl, CHClO, CCl_2O, and possibly CO. $\Phi\{CHClO\} = 49$ and $\Phi\{CCl_2O\} = 4.1$ independent of CH_2Cl_2 or O_2 pressure or I_a. A complete mechanism is proposed. In the CH_3Cl system, the initial products are exclusively HCl and CHClO, the quantum yield of the latter being 2.0 independent of reaction conditions. Thus in this system there is no chain at all, and the mechanism is similar to that for CH_3 oxidation, except that no alcohol is produced. In both systems the CHClO produced is removed by chlorine atom attack $Cl + CHClO \rightarrow HCl + ClCO \rightarrow Cl + CO$ (10) with $k_{10} = 7 \times 10^8\ M^{-1}\ sec^{-1}$.

Introduction

As far as we know the oxidation of $CHCl_2$ and CH_2Cl radicals has not been studied, previously. Therefore in our continuing program on halocarbon oxidation, we have studied these oxidations and report the results here. The radicals were prepared from the reaction of Cl atoms with CH_2Cl_2 and CH_3Cl, respectively.

Experimental Section

Much of the experimental procedure has been described previously.[2,3] The experiments were performed in a conventional Hg-free high-vacuum glass line equipped with Teflon stopcocks and Viton O rings.

The light source was a Hanovia medium-pressure mercury lamp. The radiation passed through a Corning 7-54 filter and Pyrex glass to isolate the 3655-Å line before entering the stem of the T-shaped reaction cell. The reaction cell was situated in the sample beam of a Beckman IR-10 infrared spectrometer for continual analysis. Absolute light intensities were obtained from the chlorine-atom sensitized oxidation of C_2Cl_4 at high O_2 pressures, where the oxidation quantum yield was taken to be 300.[4]

The CH_2Cl_2 was Eastman Kodak Spectro ACS grade, and the fraction volatile at −80° but condensable at −130° was used. The CH_3Cl was from the Matheson Co., and the fraction volatile at −80° but condensable at −196° was used.

The chlorocarbon reactants and products were monitored by *in situ* infrared spectroscopy by monitoring the following bands with the listed peak extinction coefficients (to base 10).

Molecule	Band, cm^{-1}	Peak extinction coeff, $Torr^{-1}\ cm^{-1}$
CH_2Cl_2	1320	3.05×10^{-2}
CH_3Cl	3020	1.03×10^{-3}
CH_3Cl	1380	4.4×10^{-4}
CHClO	1783	1.5×10^{-2}
CCl_2O	950	1.85×10^{-2}

Unfortunately with CH_3Cl, both bands were overlapped by product bands, so that analysis was difficult and not very accurate. For short conversions the stronger band at 3020 cm^{-1} was used, with corrections made for the overlapping HCl band at 3020 cm^{-1}, using the HCl band at 2810 cm^{-1} to estimate the correction. For longer exposures, the weaker band of CH_3Cl at 1380 cm^{-1} was used.

CHClO is thermally unstable, so that a direct measure of its extinction coefficient is not possible. The value above was obtained from the initial rates in the rapid chlorine-atom sensitized photooxidation of CH_2Cl_2. Under these conditions thermal decay of CHClO is unimportant, and calibrations were made from mass balance considerations (*i.e.*, CH_2Cl_2 consumed equals $CHClO + CCl_2O + CO$ produced). The extinction coefficient obtained in this manner is reasonable, being only slightly larger than that of the carbonyl stretch in CCl_2O.

CO and CO_2 were analyzed by gas chromatography after irradiation was terminated. For a few runs mass spectral analysis was also made after the termination of irradiation.

Results

CH_2Cl_2. When mixtures of Cl_2, O_2, and CH_2Cl_2 are irradiated at 3655 Å, the initial major products are CHClO and HCl, with smaller amounts of CCl_2O and CO being produced. As the photolysis times increase the CHClO yields decrease, ultimately to zero, and the CO yields increase. Thus CO is a secondary product resulting from the decomposition of CHClO.

Table I lists the initial quantum yields for CH_2Cl_2 consumption and CHClO and CCl_2O production. The yields show some scatter but essentially are independent of the CH_2Cl_2 pressure, the O_2 pressure, or the absorbed intensity, I_a, which were varied by factors of 4.3, 14, and 5.3, respectively. The average quantum yields are $-\Phi\{CH_2Cl_2\} = 56 \pm 4$, $\Phi\{CHClO\} = 49 \pm 3$, and $\Phi\{CCl_2O\} = 4.1 \pm 0.4$.

Three runs were taken to completion so that all the CH_2Cl_2 and CHClO were consumed. Then if the sole carbon-containing products are CO and CCl_2O, their sum should equal the initial CH_2Cl_2 pressure. This relationship is well obeyed for the second run in Table I, which was done at a relatively low O_2 pressure. For two other runs at very high O_2 pressures, there is a mass deficiency in the products. Presumably under these conditions some CO_2 is

TABLE I: Chlorine-Atom Sensitized Oxidation of CH_2Cl_2 at 32 ± 2°

Symbol for Figures 1–3	$[CH_2Cl_2]$, Torr	$[O_2]$, Torr	$[Cl_2]$, Torr	I_a,[a] mTorr/sec	$-\Phi\{CH_2Cl_2\}$	$\Phi\{CHClO\}$[b]	$\Phi\{CCl_2O\}$	Footnote
□	4.43	79.5	9.41	1.41	50	43	3.3	*d*
●	7.05	19.4	1.80	0.27	57	50	4.1	*e*
◐	8.46	5.65	5.33	0.80	60	52	4.2	
■	8.66	23.0	5.37	0.805	53	54	3.9	
◑	8.73	70.7	5.29	0.80	52	47	3.3	*c*
○	10.7	53.7	9.45	1.42	62	50	4.5	
▲	16.5	59.6	2.04	0.31	54	47	4.9	
△	18.9	68.3	9.37	1.41	61	50	4.5	*f*
					Av = 56 ± 4	Av = 49 ± 3	Av = 4.1 ± 0.4	

[a] Assuming quantum yield of C_2Cl_4 oxidation to be 300 at high O_2 pressure. [b] From initial rates. [c] $\Phi\{CO\} < 4$ after photolysis time of 20 sec. [d] $(\Delta[CO] + \Delta[CCl_2O])/-\Delta[CH_2Cl_2] = 0.65$ at the end of the run when $[CH_2Cl_2] \sim 0$ and $[CHClO] \sim 0$. [e] $(\Delta[CO] + \Delta[CCl_2O])/-\Delta[CH_2Cl_2] = 1.0$ at the end of the run when $[CH_2Cl_2] \sim 0$ and $[CHClO] \sim 0$. Photolysis time = 500 sec. [f] $(\Delta[CO] + \Delta[CCl_2O])/\Delta[CH_2Cl_2] = 0.85$ at the end of the run when $[CH_2Cl_2] \sim 0$ and $[CHClO] \sim 0$. Photolysis time = 220 sec.

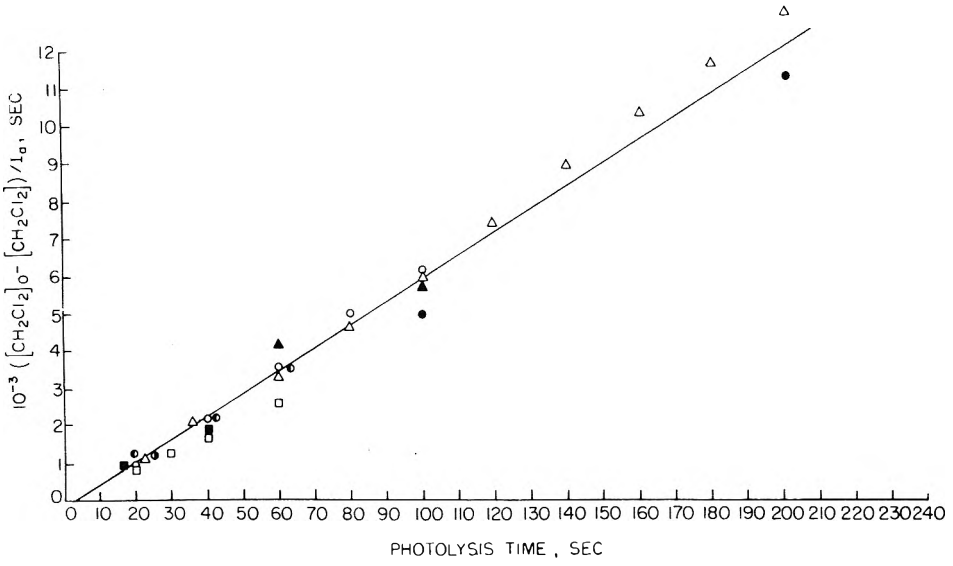

Figure 1. Plot of the loss of CH_2Cl_2 divided by I_a *vs.* the photolysis time in the chlorine-atom sensitized oxidation of CH_2Cl_2 at 32°. The symbol key is listed in Table I.

also produced, which could account for the deficiency. We did not analyze for CO_2, since on our chromatographic column, CCl_2O interfered with the analysis.

More complete time histories of the data in Table I are displayed in Figures 1–3. The loss of CH_2Cl_2 is shown in Figure 1. When normalized for I_a, all the data can be fitted by the same straight line. The best fit of the data shows a slight induction period of about 4 sec, but this is probably an experimental artifact. The slope of the line, which is now heavily weighted by the longer conversion experiments, gives $-\Phi\{CH_2Cl_2\} = 62$, slightly higher than the value of 56 obtained from Table I.

Figure 2 displays the CCl_2O data. All the data can be fitted by a straight line passing through the origin. The slope of the line gives $\Phi\{CCl_2O\} = 4.4$, again slightly higher than the value of 4.1 obtained from Table I.

Figure 3 shows three typical time histories for CHClO. This molecule is an initial product, but the CHClO pressure passes through a maximum, and then falls to zero as the irradiation proceeds. The peak CHClO pressures, $[CHClO]_{max}$, and the corresponding CH_2Cl_2 pressures, $[CH_2Cl_2]_{max}$, at the [CHClO] maximum are

$[CHClO]_{max}$, Torr	$[CH_2Cl_2]_{max}$, Torr	$[CH_2Cl_2]_{max}/[CHClO]_{max}$
1.25	2.0	1.6
3.15	5.20	1.65
5.45	9.45	1.74

CH_3Cl. When mixtures of CH_3Cl, O_2, and Cl_2 are irradiated at 3655 Å, the main products are CHClO and HCl. CO is also produced with a quantum yield ≤0.2 for short conversions, and, as with CH_2Cl_2, it is a secondary product resulting from the decay of CHClO. The CO_2 produced was negligible, its quantum yield being about 0.01.

Mass spectral analysis also showed the presence of H_2O as a product as well as mass spectral cracking peak at *m/e* 79–81 ($ClCO_2^+$) and 80–82 ($ClCHO_2^+$). These high mass peaks suggest $CClH_2O_2H$ and/or $(CClH_2O)_2$ as products. Absent were peaks at *m/e* 31, 65, and 66, indicating that $CClH_2OH$ was not a product.

Formic acid, HCOOH, was also produced as a secondary product, and can be attributed to CHClO decay in the presence of H_2O.[5] There was no evidence for either CCl_2O or CH_2O production.

TABLE II: Chlorine-Atom Sensitized Oxidation of CH_3Cl at 32 ± 2°

$[CH_3Cl]$, Torr	$[O_2]$, Torr	$[Cl_2]$, Torr	I_a,[a] mTorr/sec	$-\Phi\{CH_3Cl\}$	$\Phi\{CHClO\}$[b]	Footnotes
5.72	358	9.41	1.41	~2.2	2.0	*c*
6.90	64.3	9.76	1.46	~2.0	2.05	*d*
7.13	20.4	9.49	1.42	~1.8	2.0	*c*
13.1	37.2	5.68	0.85		2.05	
15.8	65.3	1.88	0.28		2.1	*f*
16.3	62.2	9.49	1.42		2.0	*e*
20.7	59.7	19.6	2.94	~1.7	1.9	*d,g*
33.8	43.8	9.45	1.42		2.0	
60.0	104	30.2	4.5	~2.0	1.81	*d*

[a] Assuming quantum yield of C_2Cl_4 oxidation to be 300 at high O_2 pressure. [b] From initial rates. [c] $-\Phi\{CH_3Cl\}$ estimated at high conversion. [d] $-\Phi\{CH_3Cl\}$ estimated from initial rates. [e] $\Phi\{CO\} \leq 0.2$ after photolysis time of 200 sec. [f] $\Phi\{CO_2\} \sim 10^{-2}$ after photolysis time of 1252 sec. [g] $\Phi\{HCOOH\} \sim 0.8$ after photolysis time of 1500 sec followed by dark thermal decay of CHClO to completion. $\Phi\{CO\} \leq 0.2$, $\Phi\{CO_2\} \sim 10^{-2}$.

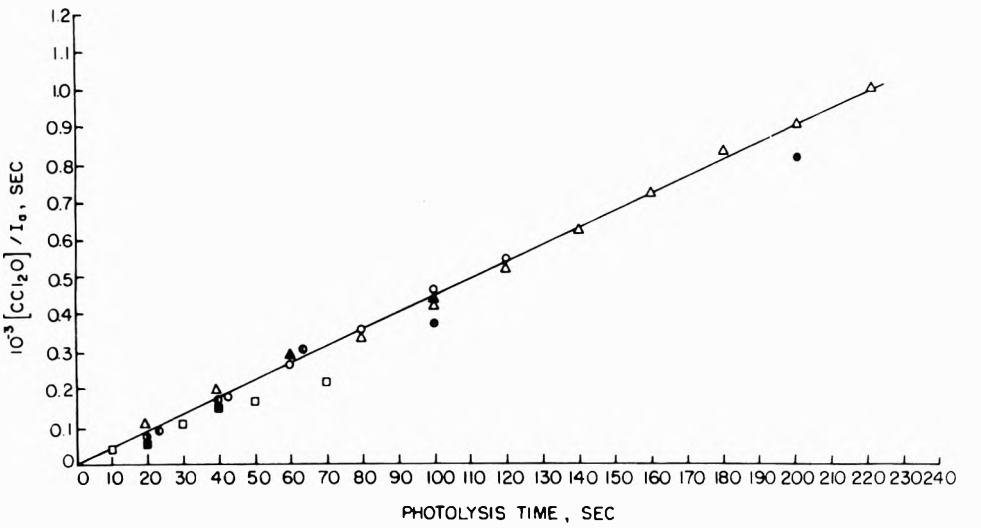

Figure 2. Plot of $[CCl_2O]/I_a$ *vs.* the photolysis time in the chlorine-atom sensitized oxidation of CH_2Cl_2 at 32°. The symbol key is listed in Table I.

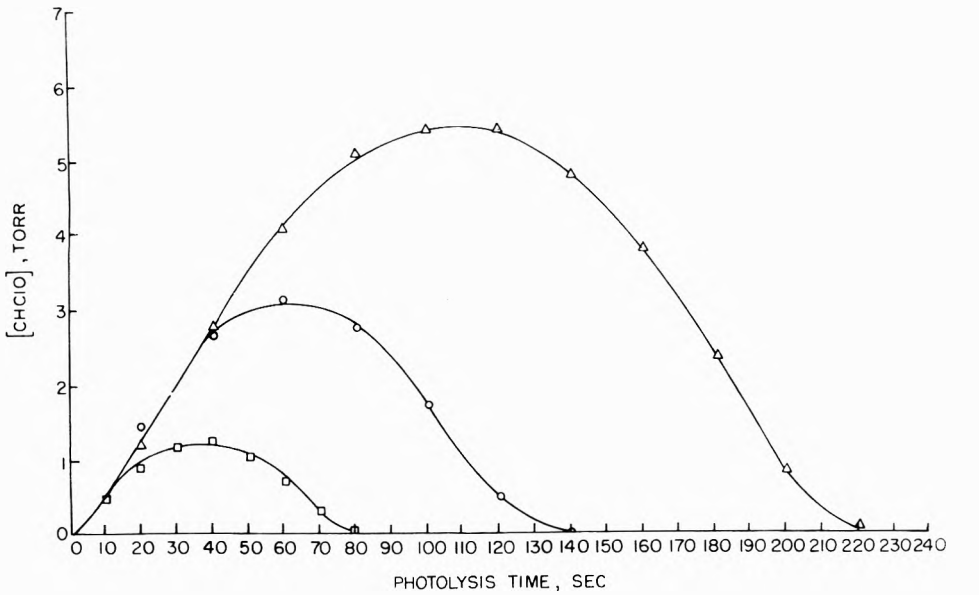

Figure 3. Plot of [CHClO] *vs.* photolysis time in the chlorine-atom sensitized oxidation of CH_2Cl_2 at 32°. The symbol key is listed in Table I.

In Table II are listed the initial quantum yields for CH_3Cl removal and CHClO production. Both quantum yields are 2.0 invariant to a change in $[CH_3Cl]$ by a factor of 10.5, a change in $[O_2]$ by a factor of 17.6, or a change in I_a by a factor of 16.1.

The quantum yield for CH_3Cl removal is invariant to the

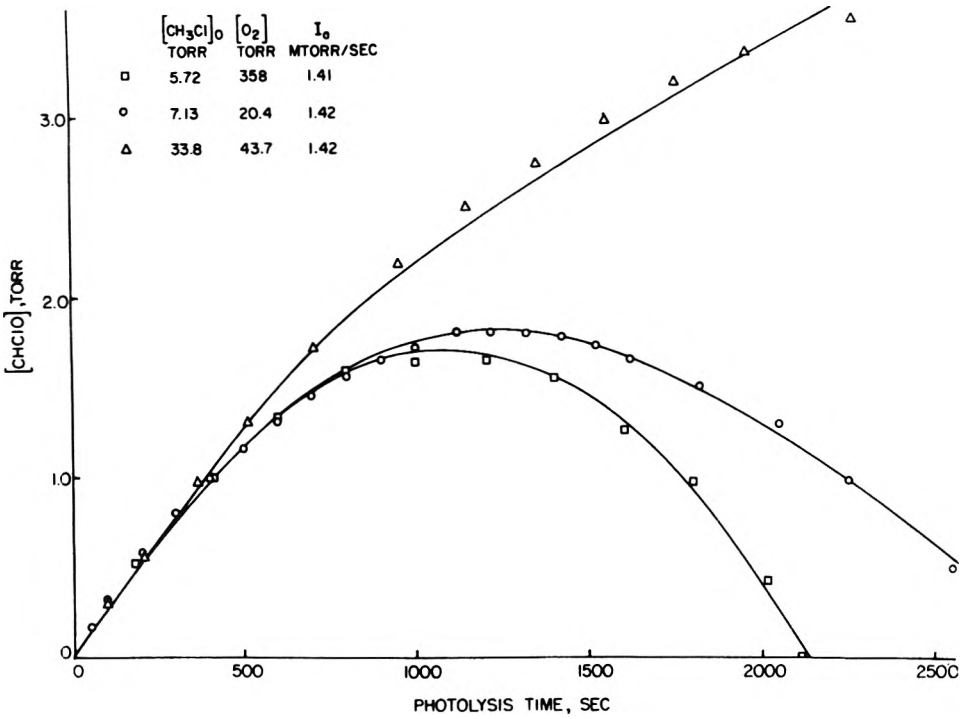

Figure 4. Plot of [CHClO] *vs.* photolysis time in the chlorine-atom sensitized oxidation of CH_3Cl at 32°.

duration of the photolysis, but CHClO behaves as in the CH_2Cl_2 system. First CHClO is produced, its pressure passes through a maximum, and then it decays to zero as the irradiation progresses. This effect is shown graphically for three runs in Figure 4. For the two runs in which the maximum has been reached, the values of $[CHClO]_{max}$ and the corresponding value of $[CH_3Cl]$ at the maximum, $[CHCl_3]_{max}$, are

$[CHClO]_{max}$, Torr	$[CH_3Cl]_{max}$, Torr	$[CH_3Cl]_{max}/[CHClO]_{max}$
1.70	2.9	1.7
1.81	3.6	2.0

Discussion

CH_2Cl_2. The main chain sequence appears to be analogous to that for CCl_3 oxidation[4]

$$Cl_2 + h\nu \longrightarrow 2Cl \quad (1)$$

$$Cl + CH_2Cl_2 \longrightarrow CHCl_2 + HCl \quad (2)$$

$$CHCl_2 + O_2 \longrightarrow CHCl_2O_2 \quad (3)$$

$$2CHCl_2O_2 \longrightarrow 2CHCl_2O + O_2 \quad (4a)$$

$$CHCl_2O \longrightarrow CHClO + Cl \quad (5)$$

The two features that are not obvious are (1) how is CCl_2O produced? and (2) how are the chains terminated?

The reactions of termination must involve two radicals. One of these cannot be $CHCl_2O$, for then there would be an intensity dependence on the quantum yields. Thus we propose

$$2CHCl_2O_2 \longrightarrow (CHCl_2O)_2 + O_2 \quad (4b)$$

$$(CHCl_2O)_2 \longrightarrow CHClO + CCl_2O + HCl \quad (6a)$$

$$\longrightarrow CCl_2O + H_2O + CCl_2 \quad (6b)$$

where reaction 6a produces CCl_2O by termination, but reaction 6b gives CCl_2O by chain propogation since it is known[6] that CCl_2 reacts with O_2 *via*

$$CCl_2 + O_2 \longrightarrow ClO + ClCO \longrightarrow Cl + CO \quad (7)$$

and the predominant fate of ClO is[7]

$$2ClO \longrightarrow 2Cl + O_2 \quad (8)$$

Then part of the CO would come from reaction 7 and part from CHClO decomposition.

The above mechanism predicts the initial rate laws

$$\Phi\{CHClO\} = 1 + 2k_{4a}k_6/k_{4b}k_{6a}$$

$$\Phi\{CCl_2O\} = k_6/k_{6a}$$

$$\Phi\{CO\} = k_{6b}/k_{6a}$$

Since $\Phi\{CHClO\} = 49$ and $\Phi\{CCl_2O\} = 4.1$, then $k_6/k_{6a} = 4.1$, $k_{4a}/k_{4b} = 5.9$, and the initial value for $\Phi\{CO\}$ should be 3.1.

As the reaction progresses, the CHClO decays. This decay could come from the thermal decay[5]

$$CHClO \longrightarrow CO + HCl \quad (9)$$

or from the reaction

$$Cl + CHClO \longrightarrow HCl + ClCO \longrightarrow Cl + CO \quad (10)$$

The thermal decay has been reported[5] to have a half-life of about 10 min, much too slow to be of importance here. Thus at the maximum in [CHClO], its rate of formation *via* reaction 2 must equal its rate of removal *via* reaction 10, or

$$[CH_2Cl_2]_{max}/[CHClO]_{max} = k_{10}/k_2$$

The ratio $[CH_2Cl_2]_{max}/[CHClO]_{max}$ was found to be constant at 1.7 for three runs. Since $k_2 = 4.4 \times 10^8\ M^{-1}\ sec^{-1}$ at 32°,[8] then $k_{10} = 7.4 \times 10^8\ M^{-1}\ sec^{-1}$.

CH_3Cl. In this system, there is no chain, and presumably CH_2Cl oxidizes in a similar manner to CH_3 radicals, except that no alcohol is formed. The sequence of reactions is

$$Cl_2 + h\nu \longrightarrow 2Cl \quad (1)$$

$$Cl + CH_3Cl \longrightarrow HCl + CH_2Cl \quad (11)$$

$$CH_2Cl + O_2 \longrightarrow CH_2ClO_2 \quad (12)$$

$$2CH_2ClO_2 \longrightarrow 2CH_2ClO + O_2 \quad (13)$$

The CH_2ClO radicals must disappear by one of two routes

$$CH_2ClO_2 + CH_2ClO \longrightarrow CHClO + CH_2ClO_2H \quad (14)$$

or

$$CH_2ClO + O_2 \longrightarrow CHClO + HO_2 \quad (15)$$

followed by

$$HO_2 + CH_2ClO_2 \longrightarrow O_2 + CH_2ClO_2H \quad (16)$$

Presumably the CH_2ClO_2H has some stability since its expected mass spectral peaks were detected. However most of it decomposes, possibly on the walls, *via*

$$CH_2ClO_2H \longrightarrow CHClO + H_2O \quad (17)$$

Thus $\Phi\{CHClO\} = 2.0$ and there is no chain process.

As the reaction proceeds the CHClO can decay *via* reactions 9 and 10. Since the times to reach the maximum in [CHClO] are greater in the CH_3Cl than in the CH_2Cl_2 system, reaction 11 may play a more important role. However if we ignore reaction 11, then

$$[CH_3Cl]_{max}/[CHClO]_{max} = k_{10}/k_{11}$$

The ratio $[CH_3Cl]_{max}/[CHClO]_{max}$ was found to be ~1.8. Since $k_{11} = 3.6 \times 10^8\ M^{-1}\ sec^{-1}$ at 32°,[8] then $k_{10} \sim 6.5 \times 10^8\ M^{-1}\ sec^{-1}$, a value in reasonable agreement with the value of $7.4 \times 10^8\ M^{-1}\ sec^{-1}$ found in the CH_2Cl_2 system.

Acknowledgment. This work was supported by the Environmental Protection Agency through Grant No. 800949 for which we are grateful.

References and Notes

(1) (a) CAES Report No. 349–74. (b) Fulbright Fellow.
(2) E. Mathias, E. Sanhueza, I. C. Hisatsune, and J. Heicklen, Center for Air Environment Studies, Report No. 304-73, The Pennsylvania State University, University Park, Pa., 1973.
(3) E. Sanhueza and J. Heicklen, Center for Air Environment Studies, Report No. 306-73. The Pennsylvania State University, University Park, Pa., 1973.
(4) J. Heicklen, *Advan. Photochem.*, **7**, 57 (1969).
(5) I. C. Hisatsune and J. Heicklen, *Can. J. Spectrosc.*, **18**, 77 (1973).
(6) E. Sanhueza and J. Heicklen, Center for Air Environment Studies, Report No. 305-73. The Pennsylvania State University, University Park, Pa., 1973.
(7) M. A. A. Clyne and J. A. Coxon, *Proc. Roy. Soc., Sec. A*, **303**, 207 (1968).
(8) M. A. A. Clyne and R. F. Walker, *J. Chem. Soc., Faraday Trans. 1*, **69**, 1547 (1973).

Effect of Wavelength in the Gas-Phase Photolysis of Carbon Tetrachloride at 253.7, 184.9, 147.0, and 106.7 nm

Douglas D. Davis, John F. Schmidt, Charles M. Neeley, and Robert J. Hanrahan*[1]

Department of Chemistry, University of Florida, Gainesville, Florida 32611 *(Received June 17, 1974)*

Publication costs assisted by the U. S. Atomic Energy Commission

The photolysis of gaseous carbon tetrachloride at pressures from 30 to 100 Torr and 25° has been studied using light of 253.7, 184.9, 147.0, and 106.7 nm produced by electrodeless discharge lamps. Qualitatively, there is a clear trend toward increasing molecular fragmentation with increasing photon energy. At 253.7 nm, only Cl_2 and C_2Cl_6 are formed; $\phi(Cl_2) = \phi(C_2Cl_6) = 0.11$. Added Br_2 is consumed with a quantum yield of unity, and CCl_3Br is the only organic product. At 184.9 nm, $\phi(Cl_2) = \phi(C_2Cl_6) = 0.048$, but a small amount of C_2Cl_4 is also formed. With added Br_2, $\phi(-Br_2) = 1.6$, and both CCl_3Br and CCl_2Br_2 are produced. Formation of 1,1-dichlorocyclopropane in the presence of added ethylene gives strong evidence for the presence of dichlorocarbene at 184.9 nm (and presumably also at lower wavelengths). At 147.0 nm, $\phi(Cl_2) \simeq \phi(C_2Cl_6) = 0.085$, but a yield of C_2Cl_4 equal to 40–90% of the C_2Cl_6 yield was also noted. Preliminary results at 106.7 nm indicate that C_2Cl_4 is the predominant organic product at that wavelength. It is suggested that $CCl_3\cdot$ radicals are formed at all wavelengths, that CCl_2 becomes important at 184.9 nm and below, and that $CCl\cdot$ fragments contribute at 147.0 and 106.7 nm.

Introduction

A search of the literature on photolysis of carbon tetrachloride reveals several papers on the liquid-phase system[2–4] as well as papers on the radiolysis of the liquid compound.[5,6] Several research groups have been concerned with the photolysis of carbon tetrachloride mixed with various hydrocarbons.[7] Apparently, no work on the photolysis of the pure compound in the gas phase has been reported. The present study was initiated because of our interest in other aspects of the reaction dynamics of carbon tetrachloride, including radiolysis of CCl_4–NH_3 mixtures in the liquid phase,[8] radiolysis of CF_4–CCl_4 mixtures in the gas phase,[9] and fast-flow microwave discharge studies of gaseous CF_4–CCl_4 mixtures.[10]

The present work includes measurements of the production of Cl_2 and organic products (C_2Cl_6, C_2Cl_4) from the pure compound at 253.7, 184.9, 147.0 and 106.7 nm; quantum yields are reported for all wavelengths. Scavenging by Br_2 was also studied at the same wavelengths (except 106.7), including consumption of bromine and production

of organic bromides. A brief investigation of the role of added O_2 was made at 253.7 nm. Furthermore, several experiments were performed at 184.9 nm to assess the role of dichlorocarbene in the photolysis mechanism, including trapping of CCl_2 with ethylene and an investigation of the effect of the concentration of added Br_2 on the ratio of product yields CCl_2Br_2/CCl_3Br. The observation of a marked pressure effect on the Cl_2 yield at 184.9 nm is also interpreted on the basis of the role of CCl_2 in the mechanism.

Experimental Section

The carbon tetrachloride used in this work was Fischer reagent grade purified by preirradiation according to the method of Firestone.[5] It was immediately placed under vacuum at liquid nitrogen temperature on a mercury-free high-vacuum line, which was used for all of the present experiments. The light sources were electrodeless glow discharge lamps fabricated from 34/45 male standard taper joints, which plugged directly into matching joints of 5-l. (for 253.7-nm work) or 1-l. (184.9 nm and lower) reaction vessels. For 253.7-nm work a 3-mm Vycor window was used and for 184.9 nm an extremely thin Vitrosil quartz window was used; LiF was used at the lower wavelengths. Since CCl_4 absorbs 184.9-nm light much more strongly than 253.7-nm light, presence of light of the higher wavelength was not significant. Photolysis lamps were activated by a Raytheon PGM 10 × 1 microwave generator operating at 2450 mHz; a Type C antenna was used. Analyses for Cl_2 and Br_2 were done using a Beckman DU spectrometer; the entire sample was frozen into a removable cuvet for analysis, and was redegassed before continuing the experiment. For higher boiling products, the sample was condensed into the liquid state and an appropriate sample taken with a microsyringe. Analyses were done on a Microtek GC2000R gas chromatograph with a hydrogen flame detector. The entire glass system used for photolysis was grease free. All stopcocks were Fischer-Porter O ring sealed Teflon-glass valves. Connections were made using glass O-ring joints with Teflon O rings. The lamp was sealed in place using Kel-F wax. The lamp window was sealed to the glass body by epoxy cement. During the course of the photolysis at 184.9 nm and lower wavelengths, the cell contents were stirred with a solenoid-driven gas circulating pump. This was not necessary for 253.7-nm work since the light beam traversed the entire diameter of the photolysis cell with only 20% attenuation.

At 253.7 nm actinometry was done by measuring H_2 production from HBr ($\phi_{H_2} = 1.00$).[11] At 184.9 nm the N_2O actinometer was used; N_2 production was measured ($\phi_{N_2} = 1.44$).[12] The light sources were found to vary by ±10% during the experiments. Actinometry at 147.0 and 106.7 nm was based on production of CO from CO_2 ($\phi_{CO} = 1.00$).[13] Properties of the light sources and actinometry data are summarized in Table I. This table also gives the extinction coefficient of gaseous CCl_4 at the several wavelengths employed. The absorption spectrum of CCl_4 was determined using a McPherson Model 218 vacuum ultraviolet monochrometer with double-beam attachment and ratio-recording electronics. A typical spectral scan of CCl_4 at a pressure of 0.075 Torr (as measured by an MKS Baratron capacitive micromanometer) in an 8.0-cm cell is shown in Figure 1. (A partial description of the vacuum ultraviolet spectrum of CCl_4, and some related discussion, can be found in the literature.[14,15])

TABLE I: Summary of Light Sources

Wavelength, nm	253.7	184.9	147.0	106.7[a]
Gas	Hg	Hg	Xe	Ar
Window	Vicor	Quartz	LiF	LiF
Actinometry gas	HBr	N_2O	CO_2	CO_2
Measured product	H_2	N_2	CO	CO
Assumed ϕ	1.00	1.44	1.00	1.00
Measured I_0, quanta/sec	1×10^{16}	4×10^{16}	7×10^{14}	1×10^{15}
$\epsilon(CCl_4)$, atm^{-1}/cm^{-1}	0.08	46	240	*b*

[a] The Ar resonance lamp emits light at both 104.8 and 106.7 nm; we refer to the more intense, higher wavelength line for convenience. [b] May be small.

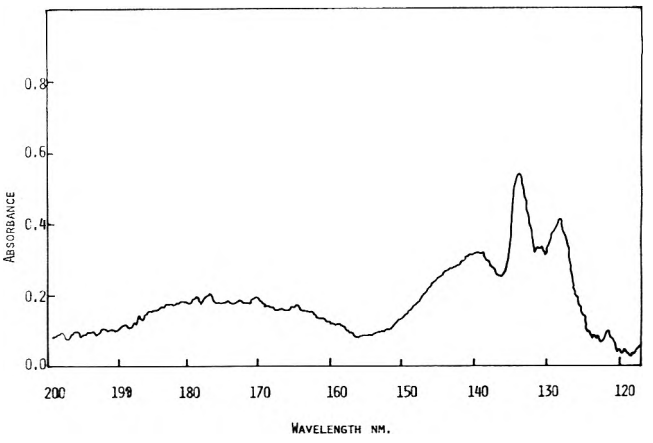

Figure 1. Absorption spectrum of CCl_4 in the gas phase at 0.075 Torr pressure and 25°, as determined using a McPherson Model 218 scanning vacuum ultraviolet spectrophotometer with a 8-cm cell.

Experimental Results

Photolysis at 253.7 nm. Chlorine Production. A series of experiments was performed to measure the production of Cl_2 from pure degassed CCl_4 at 253.7 nm. In these runs the CCl_4 pressure was chosen as 100 Torr (close to its saturation value) because of the very low extinction coefficient of the compound at this wavelength. In four duplicate runs, initial Cl_2 quantum yields were 0.108, 0.084, 0.112, and 0.129, giving an average value of 0.108 ± 0.016. A typical plot of chlorine concentration *vs.* photolysis time (Figure 2) shows that the rate of chlorine production decreases with increasing photolysis time. (A summary of quantum yields for chlorine production at 253.7, 184.9, 147.0, and 106.7 nm is given in Table II.)

Bromine Scavenging. Several experiments with *ca.* 0.2 Torr added Br_2 gave initial quantum yields for Br_2 consumption of 0.78, 0.92, and 0.97. It appears reasonable to assume that the primary quantum yield for C–Cl bond rupture is unity, particularly since a correction for light absorption by product BrCl was not made. (Absorption measurements were made at 500 nm, somewhat on the long wavelength side of the Br_2 maximum and even farther above the BrCl maximum, in order to minimize interference by BrCl.) A typical graph of Br_2 concentration *vs.* photolysis time is shown in Figure 3; Br_2 is consumed linearly at short times, but the rate falls off somewhat as the

TABLE II: Product Yields in CCl_4 Photolysis

Wavelength, nm	253.7	184.9	147.0	106.7
$\phi(Cl_2)$[a]	0.11 ± 0.02	0.048	0.083	0.013
$\phi(C_2Cl_6)$	($\simeq Cl_2$)	0.05	0.087	(0.034)[b]
$\phi(C_2Cl_4)$	0	~0.0005	0.05	0.027

[a] Chlorine quantum yields refer to 100 Torr for 253.7- and 184.9-nm photolyses, and to 30 Torr for 147.0- and 106.7-nm experiments. At 184.9 nm the chlorine quantum yield was found to be pressure dependent; see Figure 6. Pressure effects were not investigated at other wavelengths. The apparent low quantum yield at 106.7 nm may be due to inefficient light absorption by CCl_4, or to development of color centers in the LiF window. [b] Maximum C_2Cl_6 yield at 120-min photolysis time; see text.

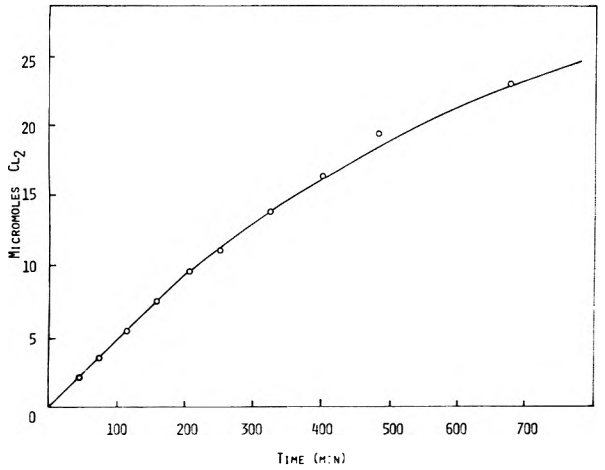

Figure 2. Production of Cl_2 in the gas-phase photolysis of CCl_4 at 253.7 nm. The experimental conditions were 100 Torr of CCl_4, 25°, 5-l. reaction vessel.

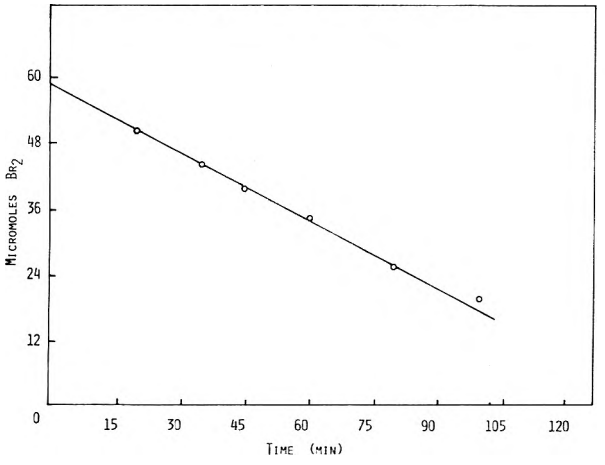

Figure 3. Consumption of added Br_2 scavenger in the gas-phase photolysis of CCl_4 at 253.7 nm. The experimental conditions were 100 Torr of CCl_4, 25°, 5-l. reaction vessel.

Br_2 concentration is depleted, possibly due to competition between Br_2 and BrCl for free radicals. (Table III summarizes bromine scavenging results at 253.7, 184.9, and 147.0 nm.)

Oxygen Scavenging. Primarily to assess the consequences of (possibly) imperfect degassing of CCl_4, a brief investigation was made of the effect of added O_2 on CCl_4 photolysis. It will be seen in Figure 4 that addition of several milliTorr of O_2 has only a slight effect, but addition of several Torr O_2 pressure causes $\phi(Cl_2)$ to increase to about 1.0. We conclude that the system displays no abnormal sensitivity to added O_2; the results are broadly consistent with our conclusion that ϕ of the primary process is unity. (A more definite conclusion would require further investigation, particularly identification of products. Formation of phosgene and Cl_2 is reasonable, and compatible with $\phi(Cl_2) \simeq 1.0$, however.)

TABLE III: Bromine Scavenging in CCl_4 Photolysis

Wavelength, nm	253.7	184.9	147.0
$\phi(-Br_2)$	0.9 ± 0.1	1.6 ± 0.1	
Organic products	CCl_3Br[a] ($\phi \simeq 1$)	CCl_3Br[b] CCl_2Br_2	CCl_3Br CCl_2Br_2 $CClBr_3$

[a] 2% residual C_2Cl_6. [b] Ratio CCl_2Br_2/CCl_3Br varies from less than 0.1 to 0.6, depending on the Br_2 concentration (1–20%).

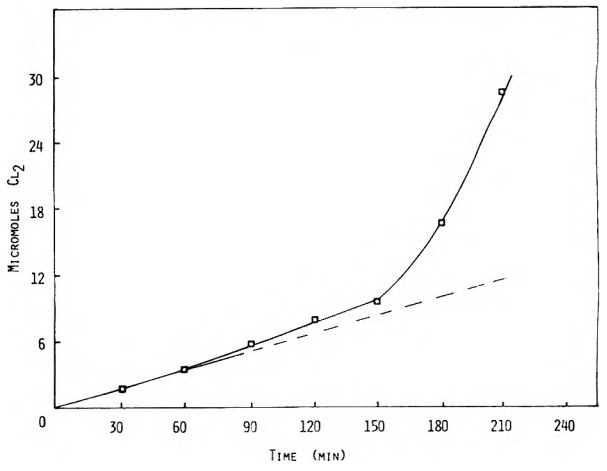

Figure 4. Effect of added O_2 on the production of Cl_2 in the gas-phase photolysis of CCl_4 at 253.7 nm. From 0 to 60 min photolysis time, no added O_2; from 60 to 150 min, several milliTorr added O_2; from 150 to 210 min, several Torr added O_2. The experimental conditions were 100 Torr of CCl_4, 25°, 5-l. reaction vessel.

Organic Products. In the photolysis of pure CCl_4 at 253.7 nm, the only organic product detected was C_2Cl_6. Measurement of its yield at two different photolysis times showed that $\phi(C_2Cl_6) = \phi(Cl_2)$ within experimental error (±10%). (Quantum yields for the formation of organic products in the photolysis of CCl_4 at the four wavelengths studied are included in Table II.)

In the presence of added Br_2, $\phi(CCl_3Br) = 0.9$, and this was the only significant organic product. A small amount of C_2Cl_6, about 2% of the CCl_3Br yield, was also found.

Photolysis at 184.9 nm. Pure CCl_4. The photolysis of CCl_4 at 184.9 nm is superficially similar to the photolysis at 253.7 nm; in experiments with CCl_4 pressure of 100 Torr, $\phi(Cl_2) = 0.048$. A typical graph showing chlorine production as a function of photolysis time is shown in Figure 5. Again, C_2Cl_6 is the main organic product, with $\phi(C_2Cl_6) = \phi(Cl_2)$ at several different photolysis times; typically, a ratio of C_2Cl_6/Cl_2 of 51/49 was found. However, a small yield of C_2Cl_4, equal to about 1% of the C_2Cl_6 yield, was also found There appeared to be a small yield of polymer on the photolysis vessel walls, but no attempt was made to measure it. This deposit was removed by intermittent photolysis of oxygen after approximately 90 min of CCl_4 photolysis.

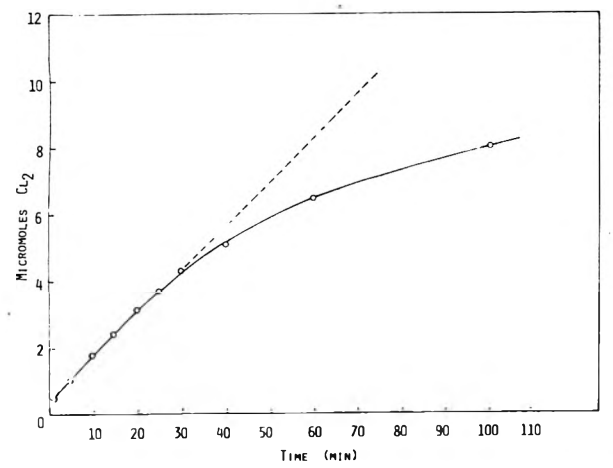

Figure 5. Production of Cl_2 in the gas-phase photolysis of CCl_4 at 184.9 nm. The experimental conditions were 100 Torr of CCl_4, 25°, 1-l. reaction vessel.

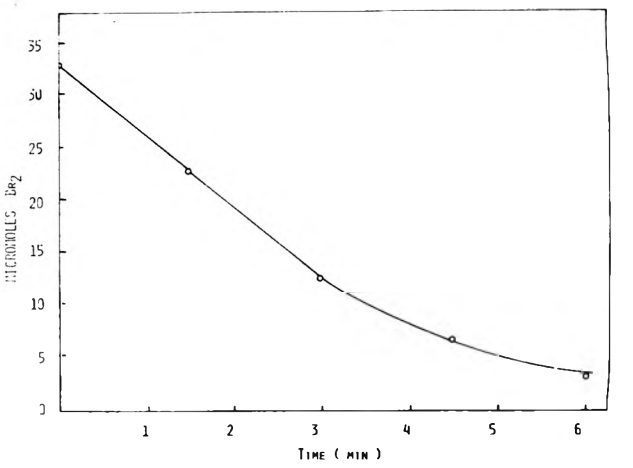

Figure 7. Consumption of added Br_2 scavenger in the gas-phase photolysis of CCl_4 at 184.9 nm. The experimental conditions were 100 Torr of CCl_4, 25°, 1-l. reaction vessel.

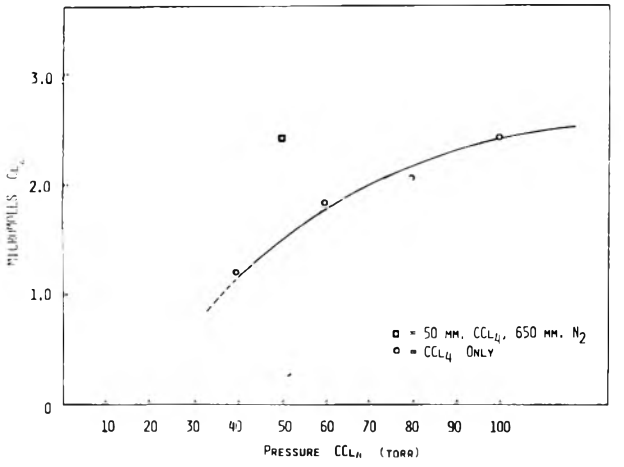

Figure 6. Production of Cl_2 at a fixed photolysis time vs. pressure in the photolysis of CCl_4 at 184.0 nm: (O) pure CCl_4; (□) 50 Torr of CCl_4, 650 Torr of N_2. Experiments done at 25° using a 1-l. reaction vessel.

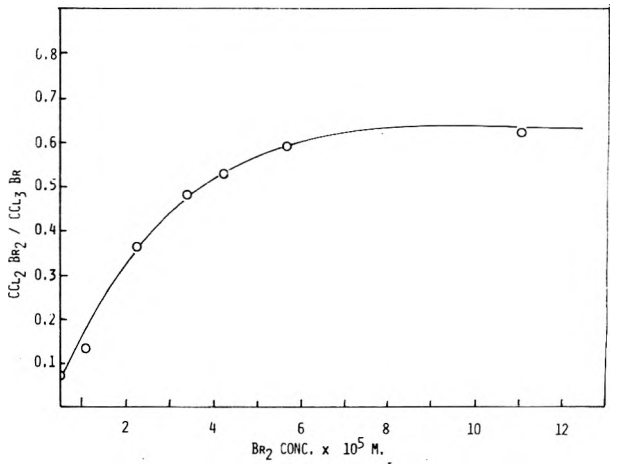

Figure 8. Effect of the Br_2 concentration on the ratio of CCl_2Br_2 to CCl_3Br produced in the gas-phase photolysis of CCl_4 at 184.9 nm. Pressure of CCl_4 100 Torr at 25° in a 1-l. reaction vessel. Concentration range corresponds to 0.05–1 mol % Br_2.

Several lines of speculation suggested to us that the photolysis of CCl_4 at 184.9 nm might be pressure dependent. To provide evidence on this point, the effect of CCl_4 pressure on the Cl_2 production rate was measured in a series of experiments. The results are shown in Figure 6. It can be seen that the chlorine yield increases by a factor of about 2.5 between a CCl_4 pressure of 30 and 100 Torr. Addition of 650 Torr of N_2 to a sample of 50 Torr of CCl_4 increased the chlorine yield to the limiting value expected at large carbon tetrachloride pressures.

Scavenger Experiments. As in the photolysis at 253.7 nm, initially added bromine is removed by photolysis at 184.9 nm; a typical experiment is shown in Figure 7. In two experiments, we found $\phi(-Br_2) = 1.6 \pm 0.1$.

A separate set of bromine scavenger experiments was done to measure organic products. To make sure that Br_2 was the exclusive scavenging agent, photolysis time was limited to 1 min or less. In a typical experiment, the product mixture had the following composition: CCl_3Br, 73%; CCl_2Br_2, 26%; C_2Cl_6, 0.15%; $C_2Cl_4Br_2$, 0.07%; and C_2Cl_5Br, trace.

In a further experiment, an investigation was made of the effect of bromine concentration on the relative yields of organic bromide products. In Figure 8 the ratio of the yield of CCl_2Br_2 to CCl_3Br is plotted. It can be seen that the relative yield of CCl_2Br_2 increases toward a limiting value of about 0.7, with added Br_2.

As will be discussed further below, we interpret the production of CCl_2Br_2 in the photolysis at 184.9 nm as evidence for the participation of dichlorocarbene in the photolysis mechanism. In an effort to obtain further evidence on this point, experiments were conducted with ethylene added as a carbene scavenger. Figure 9 shows a graph of the quantum yield of the adduct, 1,1-dichlorocyclopropane, as a function of the composition of the photolysis mixture. This is not a simple experiment to interpret, since C_2H_4 absorps light at 184.9 nm. The upper curve in Figure 9 is calculated assuming that only the fraction of the light absorped by CCl_4 gives the adduct; the lower curve utilizes the entire absorped light intensity in the calculation. Assuming that the activation must reach CCl_4 (either directly or by energy transfer) in order to form the adduct, $\phi(CCl_2)$ equals approximately 0.5–1.0 according to this experiment. (It should be noted that excited $C_3H_4Cl_2$ might be formed, isomerizing to give $CH_2{=}CH{-}CCl_2H$ or $CCl_2{=}CH{-}CH_3$. Due to experimental difficulties, neither of these would have been detected in our gas chromotography experiments. The latter superimposes on the tail of the CCl_4

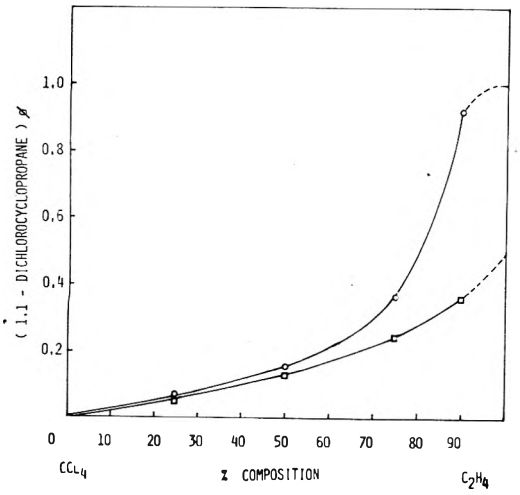

Figure 9. Quantum yield for production of 1,1-dichlorocyclopropane as a function of per cent added ethylene in the gas-phase photolysis of CCl_4–C_2H_4 mixtures at 184.9 nm: (O) calculation of ϕ based on energy absorbed in CCl_4 only; (□) calculation of ϕ based on all energy absorbed in systems. Total pressure 100 Torr at 25°, 1-l. reaction vessel.

peak, and the former should appear at the same point on the chromatogram as $C_2H_4Cl_2$, which is also produced. Hence, a portion of the CCl_2 yield may be masked in the ethylene scavenging experiments.)

Photolysis 147.0 and 106.7 nm. Pure CCl_4. Photolysis of pure degassed CCl_4 with a xenon resonance lamp at 147.0 nm produced Cl_2, C_2Cl_6, and C_2Cl_4; quantum yields were 0.083, 0.087, and 0.05, respectively. We suggest that the increase of the quantum yield of C_2Cl_4, compared with the higher wavelengths, is particularly significant. Preliminary experiments were done at 106.7 nm, using an argon resonance lamp. Although the intensity of the photolysis lamp was measured as 1.3 (±0.1) × 10^{-5} quanta per sec, we cannot confirm its spectral purity, since our McPherson monochromator has little if any light transmission below 110 nm. We could see nothing in the spectrum below the Lyman α line at 121.7 nm. Fairly rapid development of color centers in the LiF windows does suggest substantial light intensity below 110 nm, however.

The chemical behavior of the system under photolysis at 106.7 nm appears to be rather complex. The Cl_2 and C_2Cl_4 yields increase regularly with dose, but the total moles of C_2Cl_6 formed maximize at short photolysis times and actually decrease regularly between 120 and 360 min of photolysis. Average quantum yields for Cl_2 and C_2Cl_4 were 0.013 and 0.027, respectively; the apparent quantum yield of C_2Cl_6 was 0.034 at 120 min of photolysis, 0.012 at 240 min, and 0.002 at 360 min. (Due to the rapid production of color centers in the windows at this wavelength, our reported quantum yield measurements should be interpreted with caution.) The ratio of C_2Cl_4 to C_2Cl_6 varies from 0.8 at 120 min to 13 at 360 min, and in general is much larger than at higher wavelengths. It appears that C_2Cl_6 is labile under photolysis at 106.7 nm; it may absorb light of this wavelength much more efficiently than the parent CCl_4.

Scavenger Experiments. Although bromine scavenging was not attempted at 106.7 nm, some preliminary work was done at 147.0 nm. Organic products included not only CCl_3Br and CCl_2Br_2, formed at 184.9 nm, but also $CClBr_3$. We suggest that formation of this compound, as well as the increasing proportion of C_2Cl_4 among the products at the lower wavelength, is evidence of increasing fragmentation of CCl_4 with decreasing wavelengths of the photolysis light.

TABLE IV: Lamp Aging in CCl_4 Photolysis at 147.0 nm

Lamp age, hr	Lamp intensity, quanta sec^{-1}	$\phi(Cl_2)$	$\phi(C_2Cl_6)$
35–42	7.6×10^{14}	0.083	0.087
52–54	7.1×10^{14}	0.031	0.039
65–67	6.5×10^{14}	0.020	0.020

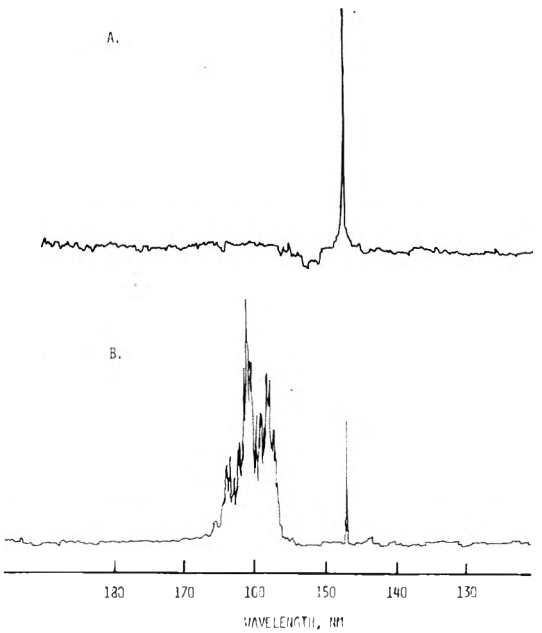

Figure 10. Output spectra of newly prepared (A) and aged (B) xenon resonance lamps. See text for details.

Actinometry Problems

We report here a problem with actinometry at 147.0 nm, since it could be of significance to other workers in vacuum ultraviolet photochemistry. During a series of measurements using the xenon resonance lamp, intermittent measurements of the intensity of the lamp were made, and the results appeared to indicate only moderate lamp aging; the results are summarized in Table IV. Measurements at approximately 35, 55, and 65 hr of lamp life indicated a slow decrease in lamp intensity from 7.6 × 10^{14} to 6.5 × 10^{14} quanta/sec. Nevertheless, there appeared to be a continuing decrease in product yield per unit photolysis time as the lamp aged. The apparent quantum yields for Cl_2 and C_2Cl_6 production fell from about 0.08 when the lamp was 35 hr old, to 0.02 when the lamp was 65 hr old. This apparently contradictory situation can be resolved by examining the output spectrum from the newly prepared and an aged lamp, as shown in Figure 10, and comparing this with the spectrum of CCl_4 shown in Figure 1. It will be seen that the newly prepared lamp has a strong output of nearly pure 147.0-nm light; this wavelength is well absorbed by CCl_4, as can be seen in Figure 1. In the case of an aged lamp, however, the intensity at 147.0 nm has decreased markedly, and a complex and unidentified spectrum at 160 nm had developed. Figure 1 shows that, coincidentally, the absorption spectrum of CCl_4 has a minimum at about 155 nm, amounting at that wavelength to less than 10% of its maximum value. In contrast, the CO_2 actinometer gas absorbs

well through out this wavelength region. It appears that the "impurities spectrum" may efficiently decompose CO_2, but may be nearly nonactinic for CCl_4.

Discussion

The results at 253.7 nm appear to be readily explained by a mechanism involving only chlorine atoms and trichloromethyl radicals at intermediates

$$h\nu + CCl_4 \longrightarrow CCl_3\cdot + Cl\cdot \qquad \phi_1 \qquad (1)$$

$$Cl\cdot + Cl\cdot - M \longrightarrow Cl_2 + M \qquad k_2 \qquad (2)$$

$$Cl\cdot + CCl_3\cdot \longrightarrow CCl_4 \qquad k_3 \qquad (3)$$

$$CCl_3\cdot + CCl_3\cdot \longrightarrow C_2Cl_6 \qquad k_4 \qquad (4)$$

$$CCl_3\cdot + Cl_2 \longrightarrow CCl_4 + Cl\cdot \qquad k_5 \qquad (5)$$

The fact that any appreciable product yield can be found in this system is due to the circumstances that reaction 5, perhaps surprisingly, has an activation energy of 8 kcal/mol[16] and therefore a collisional probability very much less than unity. (From simple collision theory, the collision efficiency would be $e^{-8000/RT}$ or about 10^{-6}.) This reaction must become important in the photolysis of pure carbon tetrachloride at long photolysis times, which undoubtedly explains the tendency toward a plateau in Figure 2. It is reasonable, on the basis of the present results, to conclude that $\phi_1 = 1$. Although $\phi(-Br_2)$ was found to be 0.9, the difference between this value and 1.00 is probably within experimental error. During the early stages of photolysis with added Br_2, the stoichiometry of the scavenging reaction is expected to be

$$CCl_4 + Br_2 \longrightarrow CCl_3Br + BrCl \qquad (6)$$

so that the quantum yield of CCl bond rupture corresponds to $\phi(-Br_2) = 1.0$. Since the primary absorption act in CCl_4, in the broad band extending from about 170 to 250 nm, is probably an n-σ^* transition to a repulsive state,[15] it is reasonable that this step should have unit efficiency. We propose here a simple kinetic scheme which allows a reasonable interpretation of the magnitude of the quantum yields for Cl_2 and C_2Cl_6 production, during the short time photolysis regime in which reaction 5 can be neglected. The key step in the mechanism is the competition represented by reactions 3 and 4, which controls whether a net production of C_2Cl_6 occurs, or whether back reaction to give the original CCl_4 takes place. This competition can be formulated as

$$\text{rate (4)}/\text{rate (3)} = k_4[CCl_3\cdot]^2/k_3[CCl_3\cdot][Cl\cdot] \qquad (7)$$

From the steady-state calculation for Cl and CCl_3 concentrations

$$[CCl_3]/[Cl] = (k_2M/k_4)^{1/2} \qquad (8)$$

and

$$\frac{\text{rate (4)}}{\text{rate (3)}} = \left(\frac{k_4}{k_3}\right)\left(\frac{k_2M}{k_4}\right)^{1/2} \qquad (9)$$

It can be seen that

$$\phi_{C_2Cl_6} = \left(\frac{\text{rate (4)}}{\text{rate (3)} + 2\ \text{rate (4)}}\right)\phi_1 \qquad (10)$$

where $\phi_1 = 1$

$$\simeq \text{rate (4)}/\text{rate (3)} \qquad (11)$$

and if $k_3 \simeq k_4$

$$\phi_{C_2Cl_6} = \left(\frac{k_2M}{k_4}\right)^{1/2} = \left(\frac{\text{rate 3 - body}}{\text{rate 2 - body}}\right)^{1/2} \qquad (12)$$

Since the C_2Cl_6 quantum yield is predicted to be approximately equal to the square root of the ratio of the three-body to a two-body rate process, it would be reasonable to expect a C_2Cl_6 yield of a magnitude of 0.1 or even smaller. Unfortunately, it was not practical to investigate the pressure dependence suggested by eq 12, since CCl_4 absorbs light of 253.7 nm very poorly even at 100 Torr pressure.

It is clear that there must be an additional primary process at 184.9 nm. A mechanism involving only $CCl_3\cdot$ radicals could not account for the substantial yield of CCl_2Br_2 formed in the presence of added Br_2. Production of 1,1-dichlorocyclopropane in the presence of added ethylene is additional evidence for the formation of CCl_2 as an intermediate. Participation of reactions 1–5 as in the photolysis at higher wavelengths probably persists, but the fragments involved may possess excess translational or internal energy.

In order to interpret the photolysis at 184.9 nm and lower wavelengths, we propose the following additional reactions

$$CCl_4 + h\nu \longrightarrow CCl_2 + Cl_2\ (\text{or } 2Cl\cdot) \qquad (13)$$

$$CCl_2 + CCl_4 \longrightarrow C_2Cl_6^* \qquad (14)$$

$$C_2Cl_6^* + M \longrightarrow C_2Cl_6 \qquad (15)$$

$$C_2Cl_6^* \longrightarrow 2CCl_3\cdot \qquad (16)$$

$$CCl_4 + h\nu \longrightarrow CCl\cdot + Cl_2 + Cl\cdot \qquad (17)$$

$$CCl\cdot + CCl_4 \longrightarrow C_2Cl_5^* \qquad (18)$$

$$C_2Cl_5^* \longrightarrow C_2Cl_4 + Cl\cdot \qquad (19)$$

Production of dichlorocarbene (reaction 13) accounts for the formation of CCl_2Br_2 at 184.9 nm and all lower wavelengths, as well as formation of 1,1-dichlorocyclopropane in the presence of added ethylene. The marked pressure dependence of the Cl_2 yield (and presumably also the C_2Cl_6 yield) at 184.9 nm is probably due, at least in part, to the necessity of a subsequent collision (reaction 15) to dispose of the internal energy resulting from formation of a new C–C bond in reaction 14. A simple analysis of the pressure dependence data does not appear feasible, however, because the dynamic scheme represented by eq 7–12 must also participate at 184.9 nm. The necessity of adding a rather substantial amount of Br_2 to reach the limiting yield of CCl_2Br_2 relative to CCl_3Br, as shown in Figure 8, suggests that reaction 14 is rather efficient and difficult to compete with.

Production of $CClBr_3$ at 147.0 nm strongly suggests a new process producing CCl· fragments at this wavelength. It also appears reasonable to relate the emergence of a significant yield of C_2Cl_4 at the lower wavelengths to CCl· fragments, and the reaction sequence 17–18–19 seems to be a reasonable interpretation. If CCl_2 were the precursor, it would be hard to explain the lack of C_2Cl_4 at 184.9 nm.

It is possible to make an estimate of the primary quantum yields of CCl_3 and CCl_2 at 184.9 nm from the yield for bromine consumption, using the relation

$$2\phi(CCl_2) + \phi(CCl_3) = 1.6 \qquad (20)$$

We assume that the sum of the two quantum yields is unity, giving $\phi(CCl_2) = 0.6$ and $\phi(CCl_3\cdot) = 0.4$. The stoichi-

ometry implied by eq 20 is valid either if CCl_2 reacts directly with Br_2, or if it inserts into CCl_4 giving two CCl_3· radicals *via* reaction 16. In the latter case, one CCl_2 fragment gives two molecules of CCl_3Br in place of one CCl_2Br_2. Since the maximum ratio of CCl_2Br_2 to CCl_3Br achieved at high scavenger concentration is 0.7, it again appears that the insertion reaction is quite efficient. (Another possible assumption is that these are two types of CCl_2 fragments, presumably singled and triplet states, and that one of them (the singlet) is almost immune to bromine scavenging.)

The data shown in Figure 9 for production of 1,1-dichlorocyclopropane at 184.9 nm are not incompatible with a yield of CCl_2 as high as 0.6, but the data are hard to interpret because C_2H_4 also absorbs light at this wavelength. Other complications include the possible production of an open-chain dichloropropene (which may have been masked in the analysis) and the low efficiency of C_2H_4 as a carbene scavenger. Qualitatively, however, formation of 1,1-dichlorocyclopropane is strong evidence for participation of CCl_2 in the reaction.

Interpretation of the O_2 scavenging experiment at 253.7 nm appears straightforward. It is evident from Figure 4 that the primary quantum yield for C–Cl bond rupture must be considerably greater than the net yield of Cl_2 and C_2Cl_6 in the unscavenged system. This conclusion is in qualitative agreement with the bromine scavenger data. Additionally, if the stoichiometry of the reaction in the presence of O_2 is assumed to be

$$CCl_4 + \tfrac{1}{2}O_2 \longrightarrow Cl-\overset{\overset{O}{\|}}{C}-Cl + Cl_2 \qquad (21)$$

then the oxygen scavenging results are in quantitative agreement with bromine scavenging. It has been known for many years that phosgene is formed when CCl_3· radicals are generated in the presence of oxygen; Steacie[16] gives a discussion of the possible mechanisms involved.

An interesting and fundamental question concerns the nature of the primary photophysical act at the several wavelengths studied; in particular, is there more than one electronic state involved? Based on detailed studies of several halomethanes,[14,15,17] it is likely that the entire broad band extending from about 160 nm to over 200 nm (with a slight tail out as far as 254 nm) is attributable to a single process, the $n\sigma^*$ transition. One or more other processes come in below 160 nm, generally interpreted as transitions of nonbonding halogen electrons to Rydberg states.[14,17]

It is particularly significant that the same $n\sigma^*$ transition gives only reaction 1 at 254 nm, but gives both reactions 1 and 13 at 185 nm. It is strongly suggested that additional vibrational energy makes possible the split giving CCl_2 at 185 nm. This observation suggests that photolysis of CCl_4 at 254 nm, but at an elevated temperature, might also give dichlorocarbene. This process has, in fact, recently been observed by Tedder and coworkers.[7] For this reason we suggest that the conjugate product in reaction 7 is probably Cl_2 rather than 2Cl·, since the latter would not be energetically feasible at 254 nm, even at elevated temperature.

Extending to lower wavelengths the concept that higher vibrational levels in the $n-\sigma^*$ excited state lead to further fragmentation, we suggest that the same model applies to formation of Cl· fragments. We suggest that the initially formed Rydberg state undergoes internal conversion to a high vibrational level of the lower-lying $n-\sigma^*$ state,[18] which can fragment to give Cl·, CCl_2, or CCl_3·, depending on how much energy may be lost in deactivating collisions before dissociation occurs. The implicit assumption that predissociating states are involved is not unreasonable, since fine structure has been observed in Rydberg bands of CF_2Cl_2 and $CFCl_3$·.[15]

Acknowledgment. These results were presented in part in Paper No. 89, Division of Physical Chemistry, 153rd National Meeting of the American Chemical Society, Miami Beach, Fla, April 1967, and in Paper No. 117, Division of Physical Chemistry, 166th National Meeting of the American Chemical Society, Chicago, Ill., August 1973. We thank Professor John Tedder for sending us a preprint of his recent paper dealing with CCl_4 photolysis.[7] This work was supported in part by the University of Florida Nuclear Science Program and by The U.S. Atomic Energy Commission under Contract No. AT-(40-1)-3106. This is document No. ORO-3106-50.

References and Notes

(1) Author to whom correspondence should be addressed.
(2) E. H. Lyons, Jr., and R. G. Dickinson, *J. Amer. Chem. Soc.*, **57**, 443 (1935).
(3) V. K. Pfondte, *J. Prakt. Chem.*, **5**, 196 (1957).
(4) H. B. Silber, M.S. Thesis, Lehigh University, Bethlehem, Pa., 1964.
(5) F. P. Abramson, B. M. Buckhold, and R. F. Firestone, *J. Amer. Chem. Soc.*, **84**, 2285 (1962).
(6) N. E. Bibler, *J. Phys. Chem.*, **75**, 24 (1971); **77**, 167 (1973).
(7) J. Currie, H. Sidebottom, and J. Tedder, *Int. J. Chem. Kinet.*, **6**, 481 (1974). (See earlier references cited therein.)
(8) D. D. Davis and R. J. Hanrahan, *J. Amer. Chem. Soc.*, **87**, 3088 (1965).
(9) R. E. Marcotte and R. J. Hanrahan, *J. Phys. Chem.*, **76**, 3734 (1972).
(10) R. E. Marcotte and R. J. Hanrahan, *J. Fluorine Chem.*, **2**, 87 (1972).
(11) G. S. Forbes, J. E. Cline, and B. C. Bradshaw, *J. Amer. Chem. Soc.*, **60**, 1431 (1938).
(12) G. A. Castellion and W. A. Noyes, Jr., *J. Amer. Chem. Soc.*, **79**, 290 (1957).
(13) (a) B. H. Mahan, *J. Chem. Phys.*, **33**, 959 (1960); (b) H. Jacker and E. K. Rideal, *J. Chem. Soc.*, 1058 (1957); (c) W. Groth, *Z. Phys. Chem. (Leipzig)*, **B37**, 307 (1937).
(14) C. R. Zobel and A. B. F. Duncan, *J. Amer. Chem. Soc.*, **77**, 2611 (1955).
(15) H. Tsubomura, K. Kimura, K. Kaya, J. Tanaka, and S. Nagakura, *Bull. Chem. Soc. Jap.*, **37**, 417 (1964).
(16) E. W. R. Steacie, "Atomic and Free Radical Reactions," Reinhold, New York, N.Y., 1954, p 682.
(17) J. Doucet, P. Sauvageau, and C. Sandorfy, *J. Chem. Phys.*, **58**, 3708 (1973).
(18) As pointed out by one of the referees of this paper, the low wavelength spectrum of CCl_4 is not fully understood, and it is possible that more than one $n-\sigma^*$ transition may be involved. This possibility does not affect the gist of our conclusions, however.

Excited Charge-Transfer Complex as an Intermediate in Photochemical Iodination Reactions

Robert F. Cozzens

Department of Chemistry, George Mason University, Fairfax, Virginia 22030 *(Received October 26, 1973; Revised Manuscript Received October 10, 1974)*

Publication costs assisted by George Mason University

The photochemical reaction between molecular iodine and benzene or methyl-substituted benzenes is studied in fluid solution at room temperature. By control of the wavelength of the exciting radiation and by varying the concentration of iodine it is shown that the reaction may be caused to proceed by way of the electronically excited charge-transfer complex formed between molecular iodine and the aromatic hydrocarbon. The reaction is first order in iodine when the hydrocarbon is directly irradiated but zero order when the charge-transfer band alone absorbs all of the incident radiation. The reaction rate increases with stability of the complex.

Introduction

It has been known for many years that molecular complexes form as the result of weak interaction between an electron "rich" group (electron donor) and an electron-accepting group.[1,2] The enthalpy of formation of these complexes is generally less than 10 kcal/mol and thus they are not normally isolatable. Various mechanisms involving these charge-transfer complexes (electron donor–acceptor complex) as a chemical intermediate have been proposed for numerous chemical and biochemical processes. Actual experimental evidence for charge-transfer intermediates in chemical reactions is, however, quite limited. Akamatsu, Inokuchi, and Matsunaga[3] and other workers[4] have observed a bromination reaction taking place in the solid bromine–hydrocarbon complex, one of the few complexes which may be isolated. The dissociation energy for molecular bromine, however, is large enough that free-radical reactions may compete with other mechanisms. It has also been observed[5] that the photooxidation of several hydrocarbons takes place when ultraviolet light is absorbed by the O_2–hydrocarbon contact charge-transfer absorption band which generally lies at slightly lower energies than the lowest energy absorption band of the deoxygenated hydrocarbon.

The charge-transfer complex was first described by Mulliken[6] as a resonance hybrid between a nonbound form and an ionic form. The ground state is predominantly nonbonding while the excited state is predominantly ionic in nature. In the case of the aromatic hydrocarbon–molecular iodine complex (Ar–I_2) absorption of light by the ground state charge-transfer complex results in transfer of an electron from the aromatic species (electron donor) to the iodine (electron acceptor) resulting in an ionic excited state. Such a process is described by

$$\text{Ar-I}_2 \xrightarrow{h\nu_{ct}} \cdot\text{Ar}^+\text{I}_2^{-}\cdot$$

where the diradical ion pair represents the excited state charge-transfer complex. This excited species may undergo chemical reaction during its lifetime, just as any other species, and thus may serve as a reactive chemical intermediate, or it may return to the ground state complex by either a radiative or nonradiative process. The radiative process is only observed in certain special systems. The nature of the excited state of the charge-transfer complex has been studied[7-11] and reviewed by numerous workers.

Experimental Section

The benzene used was Baker reagent grade solvent which was washed twice with reagent grade concentrated sulfuric acid. It was then washed with distilled water until no acid residue was detected in the water layer and dried over reagent grade anhydrous sodium carbonate. The solvent was then cooled until 90% was crystallized and the remaining liquid was discarded. This fractional crystallization process was repeated twice. The toluene and *o*-, *m*-, and *p*-xylene were chromatographic grade solvents distributed by the Matheson Coleman and Bell and mesitylene was Baker reagent grade. The toluene, xylenes, and mesitylene were each washed with H_2SO_4 and then water, and dried over sodium carbonate. The iodine was freshly resublimed reagent grade crystals manufactured by the Allied Chemical Co.

Irradiation was performed at room temperature directly in 1-cm Beckman quartz cells which were subsequently used in the uv spectrophotometer. These were suspended in a quartz container which was filled with a solution which served as a filter jacket permitting only desired wavelengths to be incident upon the reaction cell and as a constant temperature bath. All light reaching the sample passed through a minimum of 1.5 cm of filter solution. The irradiation source was a 250-W medium-pressure mercury arc with quartz housing. Actinometry using solutions of potassium ferrioxlate was according to the method described by Melville and Gowenlock[12] and showed $3.7 \pm 0.1 \times 10^{16}$ quanta/sec to be incident upon the reaction cell.

All spectra were measured on a Beckman Model DK-2 or Model DB-6 recording spectrophotometer. The gas chromatograph used for analysis purposes was manufactured by MicroTec Instruments, Inc. using a glass column packed with Apiezon-J on Chromasorb Q and a thermal conductivity detector. Glass columns were necessary due to the catalytic effect of stainless steel and copper on the decomposition of organo–iodine compounds at elevated temperatures. Monochromatic light for kinetic studies was supplied by a Baush and Lomb monochromater furnished with a 100-W

mercury arc. Thin layer chromotograms were run using commercially available plates manufactured by E. Merck AG of Germany, employing fluorescent silica gel on aluminum. Chromatograms were developed by ultraviolet irradiation followed by treatment with a starch solution or by exposure of the plate to iodine vapor as well as by observing the quenching of the fluorescence of the adsorbent.

Results

When solutions of 10^{-3} to 10^{-4} M iodine in either benzene, xylene, or mesitylene were irradiated through a filter consisting of the pure hydrocarbon, the reddish color characteristic of iodine in these complexing solvents slowly and permanently bleached out. The filter solution allowed excitation of only the molecular iodine and the charge-transfer absorption bands. Similar samples were stored in dark containers and maintained at ambient temperature and others at 70° for 24 hr. No change in the spectroscopically determined iodine concentration was observed in either sample.

A 7.0×10^{-4} M sample of iodine in toluene was irradiated through an aqueous $CuCl_2$ filter solution. The concentration of the $CuCl_2$ was adjusted such that the absorbance at 4000 Å was greater than two, thus allowing light absorption by only the molecular iodine band of the toluene–iodine solution. No detectable change in the concentration of iodine was observed after 6 hr of irradiation at ambient temperature.

The effect of the initial iodine concentration on the rate of disappearance of iodine from the various samples was studied. The samples were irradiated through a filter jacket consisting of the respective hydrocarbon, allowing absorption by the charge-transfer band and not by the hydrocarbon itself. The absorbance of the charge-transfer band was greater than two. Results of these studies showed the rate to be independent of iodine concentration within the range of 10^{-3} to 10^{-4} M iodine, indicating zero-order dependance on I_2 concentrations. By adding iodine to compensate for that which reacted it was found that the formation of products did not affect the observed net reaction rate. Studies of the effect of iodine concentration on the rate of iodine consumption when no filter was used indicated an increase in reaction rate with an increase in iodine concentration. Without a filter solution, the aromatic hydrocarbon bands, as well as the charge-transfer band, are excited by the intense 2537- and 2880-Å lines emitted by the mercury arc source. Direct excitation of the hydrocarbon resulted in first-order disappearance of molecular iodine for all hydrocarbons used. Results for the I_2–*m*-xylene systems are shown in Figure 1.

Samples of 7.0×10^{-4} M iodine in the solvents benzene, toluene, *o*-xylene, *m*-xylene, *p*-xylene, and mesitylene were irradiated for 1 hr through a filter solution of the respective aromatic hydrocarbon. Absorption spectra were taken before and after irradiation and the change in absorbance of the molecular iodine was noted and taken as a measure of the loss of I_2 from the system and thus a measure of the relative rate of the overall iodination reaction. The results are shown in Figure 2.

A 50-ml sample of 10^{-3} M iodine in benzene was irradiated through a benzene filter solution for 19.5 hr at ambient temperature and vacuum evaporated to a volumn of 1.0 ml. A portion of this residue was separated by gas chromatography at 197°. A small peak was observed which was not common to a sample of the solution analyzed before irradiation. The retention time for this new peak was identical

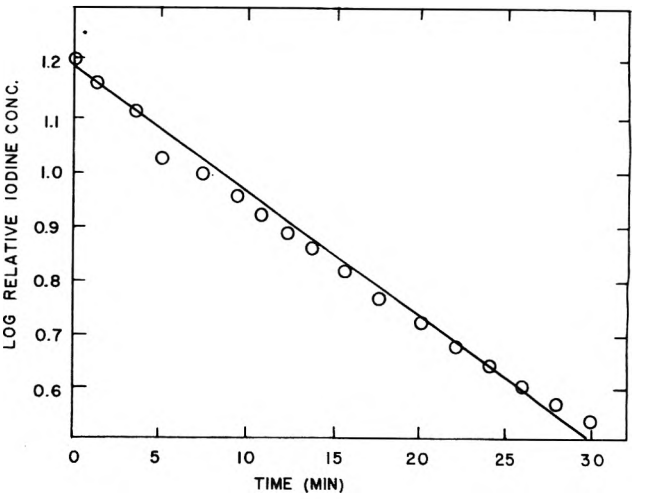

Figure 1. A typical plot of the log of the spectroscopically determined iodine concentration as a function of time of irradiation for *m*-xylene at 340 nm.

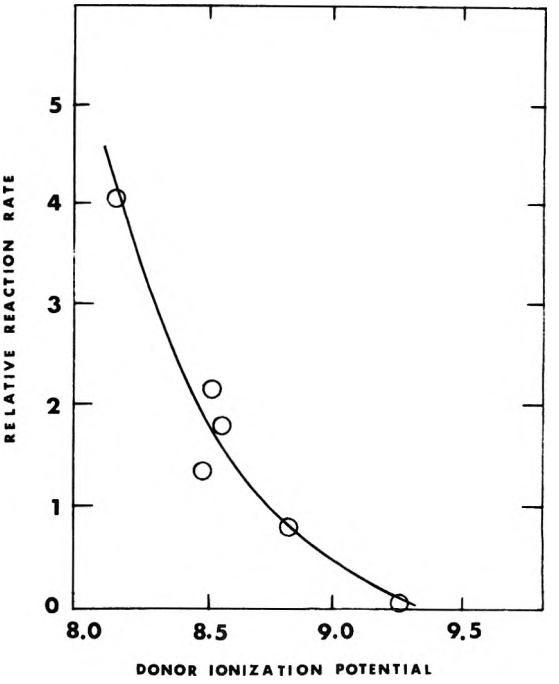

Figure 2. Relative rate of photochemical iodination for various substituted benzenes upon irradiation of the charge-transfer absorption band as a function of the ionization potential of the electron donor. In order of decreasing reaction rate the hydrocarbons are 1,3,5-trimethylbenzene, o-xylene, *p*-xylene, *m*-xylene, toluene, and benzene.

with that observed for iodobenzene in a benzene solution. Gas chromatographic separation of the reaction products of the substituted benzenes was found to be impossible with our apparatus due to decomposition of the iodinated compounds, even in glass columns, at the temperature required for separation.

The reaction of iodine with toluene was also studied using a thoroughly vacuum degassed solution. No difference in the reaction rate was observed between the degassed sample and one irradiated while in equilibrium with the atmosphere. Thin layer chromatographic separation of the concentrated mixture of toluene–iodine following irra-

diation through a toluene filter and subsequent removal of excess molecular iodine with clean copper wire or with triple distilled mercury indicated a single product whose R_f value in several solvents was identical with that of a known sample of benzyl iodide. Similar treatment of a *p*-xylene–iodine reaction mixture resulted in the thin layer separation of only the α-iodo-substituted xylene as identified by comparison with thin layer chromatograms of known samples. No other products were discovered to be present.

Excess molecular iodine remaining in a mesitylene–iodine solution which had been irradiated through a mesitylene filter solution was removed by reaction with elemental mercury. The sample was concentrated by vacuum evaporation at room temperature followed by reaction with pyridine to form a solid derivative which was recrystallized from an alcohol–ether solution. Comparison of physical properties of the pyridine derivative with known compounds resulted in the identification of 3,5-dimethylbenzyl iodide as the principle reaction product.

Discussion

The experimental evidence presented above can be explained only by a photochemical iodination reaction taking place by way of an excited charge-transfer complex intermediate. The absorbance of the charge-transfer band of the reaction sample was greater than 2.0 for all experiments and appropriate filters were used to avoid direct absorption by the hydrocarbon, thus it can be assumed that nearly all of the light in the region of the charge-transfer absorption band incident upon the sample was absorbed by the complex. Changes in the iodine concentration when only the complex was irradiated did not affect the net rate of reaction over the range where essentially all exciting light was absorbed by the complex. Direct excitation of the π–π^* band of the aromatic hydrocarbon, when no filter was used, resulted in a reaction whose rate showed a first-order dependance upon the iodine concentration as shown in Figure 1. Such a reaction would be expected for reaction between electronically excited aromatic hydrocarbon molecules or resulting free radicals and molecular iodine. Thus, it can be concluded that the reaction occuring when *only* the charge-transfer band was irradiated took place by way of the excited complex and not as a result of the direct formation of excited or free-radical donor species or by direct excitation of molecular iodine.

The effect of various electron-donor molecules on the rate of reaction with molecular iodine by way of the excited complex is shown in Figure 2. This effect appears to be related to the ease of formation or the thermodynamic stability of the ground state complex. Similarly, the effect can be related to the increase in the number of protons or reactive sites as well as changes in geometry as the benzene becomes more highly substituted. The relative effect of molecular structure on the quantum yield for this iodination reaction compared to the thermodynamic stability of the ground state complex as measured by its absorbtivity can not be determined by any simple experiment due to the interdependence of these properties. The energy required for the dissociation of a side chain hydrogen is 77.5 kcal/mol as compared to 102 kcal/mol for that of a ring hydrogen. Thus, substitution of iodine for a benzyl hydrogen would be the energetically more favored reaction.

The mechanism for the iodination reaction when only the charge-transfer band is irradiated must be one which directly involves the excited state of the charge-transfer complex as an intermediate and thus can be represented by the following process

$$Ar + I_2 \rightleftharpoons (Ar\text{-}I_2) \overset{h\nu_{ct}}{\rightleftharpoons} (Ar^{\cdot+}\cdots I_2^{\cdot-}) \longrightarrow ArI + HI$$

where $(Ar\text{–}I_2)$ represents the ground state complex and ArI is the iodinated product. The diradical ion pair excited state of the complex may reassociated and lose its excess energy or rearrange, forming the iodination product. The excited state of the complex may be represented by an ion pair held together by coulombic forces. The ionic species probably does not escape the solvent cage during its lifetime. If the radical ions were to escape the cage, numerous free-radical reactions including the solvent as well as radical reactions would be possible.

References and Notes

(1) G. M. Bennett and G. H. Willis, *J. Chem. Soc.*, 256 (1929).
(2) P. Pfeiffer, "Organische Molelculverbindunger," 2nd ed, Ferdinand Enke, Stuttgart, Germany, 1927.
(3) H. Akamatsu, H. Inokuchi, and Y. Matsunaga, *Bull. Chem. Soc. Jap.*, **29**, 213 (1956).
(4) M. Labes, H. W. Blaeslee, and J. E. Bloor, *J. Amer. Chem. Soc.*, **87**, 4251 (1965).
(5) J. C. W. Chien, *J. Phys. Chem.*, **69**, 4317 (1965).
(6) (a) R. S. Mulliken, *J. Amer. Chem. Soc.*, **72**, 600 (1950); (b) R. S. Mulliken, *J. Phys. Chem.*, **56** 801 (1952).
(7) R. F. Cozzens and T. A. Gover, *J. Phys. Chem.*, **74**, 3003 (1970).
(8) (a) E. M. Kosower, *J. Amer. Chem. Soc.*, **27**, 3883 (1955); (b) E. M. Kosower and P. E. Klinedinst, *ibid.*, **78**, 3493 (1956).
(9) G. Porter, *Discuss. Faraday Soc.*, **33**, 198 (1962).
(10) S. P. McGlynn, *Chem. Rev.*, 58, 1113 (1958).
(11) R. S. Mulliken and W. B. Person, *Annu. Rev. Phys. Chem.*, **13**, 113 (1962).
(12) H. Melville and B. G. Gowenock, "Experimental Methods in Gas Reactions," MacMillan, New York, N.Y., 1964.

Excited State Reactivity of Aza Aromatics. III. Quenching of Fluorescence and Photoisomerization of Azastilbenes by Inorganic Anions

P. Bortolus,

Laboratorio di Fotochimica e Radiazioni d'Alta Energia of the Consiglio Nazionale delle Ricerche, I-40126 Bologna, Italy

G. Bartocci, and U. Mazzucato*

Istituto di Chimica Fisica, Università di Perugia, I-06100 Perugia, Italy *(Received April 23, 1974; Revised Manuscript Received October 3, 1974)*

Publication costs assisted by the Consiglio Nazionale delle Ricerche (Roma)

The quenching of fluorescence of azastilbenes (styrylpyridines and styrylpyridinium cations) by inorganic anions has been investigated to obtain information on the quenching mechanism and on the relevance of this deactivation for the trans → cis photoisomerization of azastilbenes. The quenching rate constants are much higher in acidic medium when both the species are charged. The observed correlation between the quenching rate constants and the redox potentials of the anions implies an electron transfer mechanism. The parallel study of the photoisomerization quenching of 3-styrylpyridinium cations shows important differences between the quenching efficiency on emission and photoreaction when Br^- and I^- are the quenchers. The results, which indicate that the CT complex decays through the triplet manifold, at least in the presence of heavy atom quenchers, imply a concurrency of both heavy atom effect and charge transfer interaction in the quenching mechanism. They are promising as they can give an indication of the excited state responsible for the photoisomerization.

Introduction

Several examples of fluorescence quenching by inorganic anions have been reported.[1-3] The quenching mechanism might be interpreted as an external heavy atom induced intersystem crossing (ISC) or as an electron transfer from the anion to the substrate depending on whether the quenching rate constant is correlated with the square of the atomic spin–orbit coupling parameter of the anions or with their redox potential, respectively. Since the correlation with the redox potential has been demonstrated often, the charge transfer (CT) mechanism is considered that which best explains most of the experimental results.[1,4]

Any such intermediate, either an exciplex or merely a collisional complex may be nonfluorescent because of preferential radiationless deactivation.

Quenching by inorganic anions may be a useful probe to monitor decay processes of excited azastilbenes[6] and thus give an indication of the excited state responsible for the isomerization following direct excitation. In fact, while there is general agreement that the sensitized isomerization occurs at the triplet level, the assumption that in the absence of heavy substituents the direct isomerization takes place in the singlet manifold is not yet conclusively proved.[7]

In a previous paper we have found that the photochemical behavior of azastilbenes depends markedly upon the nature of the solvent and salts present in the solutions.[7] In particular, the yield of trans → cis photoisomerization (ϕ_t) for the protonated 3-styrylpyridine (3-$StPH^+$) has been found to be strongly lowered by NaCl added to buffer the ionic strength. The effect, which was absent when Na_2SO_4 or $NaClO_4$ were used, has been assigned to a specific interaction between the chloride ion and the excited 3-$StPH^+$. The yield of fluorescence (ϕ_f) has shown a similar behavior, the Stern–Volmer plots of ϕ_t and ϕ_f against NaCl concentration having practically the same slopes. The effect of NaCl on neutral StP's was negligible, in comparison.

These observations led us to investigate in greater detail the effect of inorganic anions on fluorescence and trans → cis photoisomerization of styrylpyridines. The results obtained are important in the interpretation of both the quenching mechanism and the photochemical behavior of azastilbenes.

Experimental Section

The azastilbenes, synthesized for previous work, were purified by crystallization from *n*-hexane and/or water–ethanol.

Potassium and sodium halides and thiocyanate were of analytical grade from Merck (sodium salts were used as quenchers in acidic medium, where $NaClO_4$ was the buffer of the ionic strength, in order to avoid precipitation of $KClO_4$); potassium selenocyanate was a British Drug House product.

The luminescence quenching experiments were carried out by measuring the relative fluorescence intensities at different quencher concentrations at room temperature (25 ± 1°). The solutions were deaerated by bubbling pure nitrogen. Both a CGA DC-3000/1 and a Turner 210 spectrofluorimeter were used. The azastilbene concentration was about 10^{-5} *M*; quencher concentrations were in the range from 10^{-3} to 10^{-1} *M* in the acidic medium and from 10^{-2} to 1 *M* in the alkaline medium. A solution of anthracene was used to correct for the fluctuations in the intensity of the exciting light (300 nm, with the exception of the measurements with $SeCN^-$, when 350-nm excitation was used). The ionic strength was kept at a constant value of 1 by addition of $NaClO_4$ or Na_2SO_4. Quenching constants K_Q were obtained from the Stern–Volmer (S–V) equation

$$(I^0 - I)/I = K_Q[X^-] = k_q\tau[X^-] \quad (1)$$

where I^0 and I are the uncorrected intensities of fluorescence in the absence and in the presence of quencher, respectively. The measurements were made at the wavelength corresponding to the maximum of the emission spectrum of StP's. The quenching rate constant k_q (M^{-1} sec^{-1}) can be obtained if the lifetime of the first excited singlet state at infinite dilution, τ, is known.

In our experimental conditions there was not any direct evidence, from the absorption spectrum, of complex formation in the ground state neither could any new emission characteristic of complex formed under irradiation be detected. As a matter of fact, with the heaviest quencher, k_q in an acidic medium is higher than the diffusional rate constant ($k_d \sim 5 \times 10^9$ M^{-1} sec^{-1}). This behavior, which is not surprising as the radius of interaction increases for charged species, might also imply that a static quenching process is partially operative; its contribution, however, should be very small in polar solvent, as indicated also by some experiments on the effect of quencher concentration on the azastilbene lifetimes.

Britton buffers and NaOH solutions were used for the measurements at pH 2 and 13.5, respectively. At these pH values the azastibenes are in the cationic and neutral forms, respectively, in both the ground (pK ~5) and first excited singlet (pK^* ~12) states.[8] For the 4'-OCH_3 derivative, which is a stronger base in the excited state,[8] NaOH 1 N was used.

The photoisomerization quenching was studied spectrophotometrically by S–V plots of ϕ_t^0/ϕ_t against [X^-] in the same medium as fluorescence. The trans → cis quantum yields were determined at different salt concentrations by the method already described.[7] An Unicam SP500 single-beam spectrophotometer was used. Singlet lifetimes were measured by a sampling technique previously described.[9]

Results and Discussion

Fluorescence Quenching. Table I shows the quenching constants obtained with alkali halides, thiocyanate, and selenocyanate as quenchers of 3-styrylpyridine fluorescence in water–ethanol 90/10 (v/v), in basic and acidic solutions. Table II shows the quenching constants and the quenching rate constants of the three isomeric StP's and some 4' derivatives of the 3 isomer by iodide ion in basic medium and by chloride, bromide, and iodide ions in acidic medium.

Data at pH 2 in Table I show that the quenching efficiency depends considerably on the ionic strength of the solution. A more detailed investigation of this effect has shown (as expected from the Brønsted–Bjerrum theory for a complexation between unlike ions) that log ($k_q\tau$) decreases linearly with increase of the square root of the ionic strength, the effect being practically suppressed at high ionic strength. The slope of the plot is about 0.4, a value rather smaller than that predicted by the Brønsted–Bjerrum equation. Both this observation and the less pronounced effect of the ionic strength with quenchers of high efficiency are similar to the results reported for the quenching of the N-methylacridinium ion by counterions.[1] Owing to these effects, which will receive further attention in our laboratory, the measurements were carried out at a constant ionic strength of $\mu = 1$.

The 3 isomer has the longest fluorescence lifetime[8] of the three isomeric StP's and thus it is the most convenient isomer for the study of the effect of the anion nature on the deactivation. The quenching efficiency on the free base fluorescence by the anions reported in Table I is in the order of $Cl^- < Br^- < SCN^- < I^- < SeCN^-$. The same order was found for the halides with the cation 3-$StPH^+$. The quenching was much more effective on the protonated form which has, however, τ about a factor of 6 longer. The quenching rate constants of Table II were obtained on the basis of the measured lifetimes of the first excited singlet state of protonated 3-StP's and of those approximately calculated from fluorimetric measurements of the excited state pK^* of the neutral 3-StP's.[8] The k_q values are still higher for the protonated forms, the differences becoming less pronounced with the increasing size of the quencher. The similar quenching effect found in two experiments with sodium and cesium chlorides showed that the interaction does not effectively depend on the nature of the cation under our experimental conditions. A semilog plot of the K_Q values reported in Table I *vs.* the oxidation potential of the anions showed a linear correlation for both the basic and acidic species. This behavior reflects an associative CT mechanism which contributes to the quenching process, *e.g.*, for the free base

$$^1StP^* + X^- \rightleftharpoons {}^1(StP^* \cdots X)^- \longrightarrow {}^3StP^* \text{ (or StP)} + X^- \quad (2)$$

although, in the absence of complex emission, a contribution of collisional deactivation cannot be ruled out.[1] The intermediate complex may facilitate ISC to the triplet state of the acceptor as has been shown by flash experiments in the system biphenyl + inorganic anions[3] as well as in other systems where both partners were neutral molecules.[10] This behavior is generally assumed with heavy atom quenchers, when excited complex formation is often followed by enhanced ISC to the triplet complex which then normally dissociates to yield the triplet substrate. The rate constant for the complex ISC is generally higher than for the free substrate ISC.[11] In our case, some evidence for the formation of triplet 3-$StPH^+$ through the CT complex comes from the photoisomerization quenching experiments with Br^- and I^- (see below). The free energy associated with the transfer process (assuming that the entropy does not change with excitation and neglecting solvent effects) will be given, *e.g.*, for the free base, by

$$\Delta G_{CT} = [E_{1/2}(X^{\cdot}/X) - E_{1/2}(StP^{\cdot}/StP)] - \Delta E_{00}(^1StP^*) \quad (3)$$

where the first term on the right is the difference between the half-wave potentials for the one-electron oxidation of the inorganic anion X^- and the one-electron reduction of the azastilbene; ΔE_{00} is the energy of the first excited singlet state of the azastilbene.[3,5,10] Equation 3 gives, for a given acceptor, the observed relation of the quenching ability with the oxidation potential of the donor anions, and, for a given anion, a relation with the reduction potential of azastilbenes. An interesting correlation has in fact been found in a similar case[3] between log k_q and the excited

TABLE I: Quenching Constants K_Q (M^{-1}) of the Fluorescence of 3-Styrylpyridine by Inorganic Anions in 90/10 (v/v) Water–Ethanol (Sodium Sulfate or Perchlorate as Ionic Buffers)

Quencher	pH 2		pH 13.5
	Unbuffered	$\mu = 1$	$\mu = 1$
Cl^-	17	6	<0.1
Br^-	52.5	19	0.46
I^-	88	39	4.6
SCN^-			3.65
$SeCN^-$			6.1

TABLE II: Quenching Constants K_Q (M^{-1}) and Quenching Rate Constants k_q (10^9 M^{-1} sec^{-1})[a] for the Fluorescence of *trans*-Styrylpyridines by Inorganic Anions in 90/10 (v/v) Water–Ethanol at μ = 1

	pH 13.5		pH 2					
Compd	$(K_Q)_{I^-}$	$(k_q)_{I^-}$	$(K_Q)_{I^-}$	$(k_q)_{I^-}$	$(K_Q)_{Br^-}$	$(k_q)_{Br^-}$	$(K_Q)_{Cl^-}$	$(k_q)_{Cl^-}$
2-StP	0.5		1.6					
3-StP	4.6	5.1	39.0	7.0	18.8	3.4	6.0	1.1
4-StP	0.5		1.3					
4′-CH_3-3-StP	2.5	1.5	25.3	4.2	7.5	1.3	0.5	0.1
4′-OCH_3-3-StP	0.4	1.3	2.0	1.2	0.14	0.1		
4′-Cl-3-StP	4.0	0.8	37.8	7.1	18.7	3.5	4.4	0.83
4′-Br-3-StP	3.4	1.7	26.8	8.4	12.2	3.8	2.7	0.84
4′-I-3-StP	1.3		11.0		4.6		1.1	

[a] Calculated using the lifetimes from ref 8.

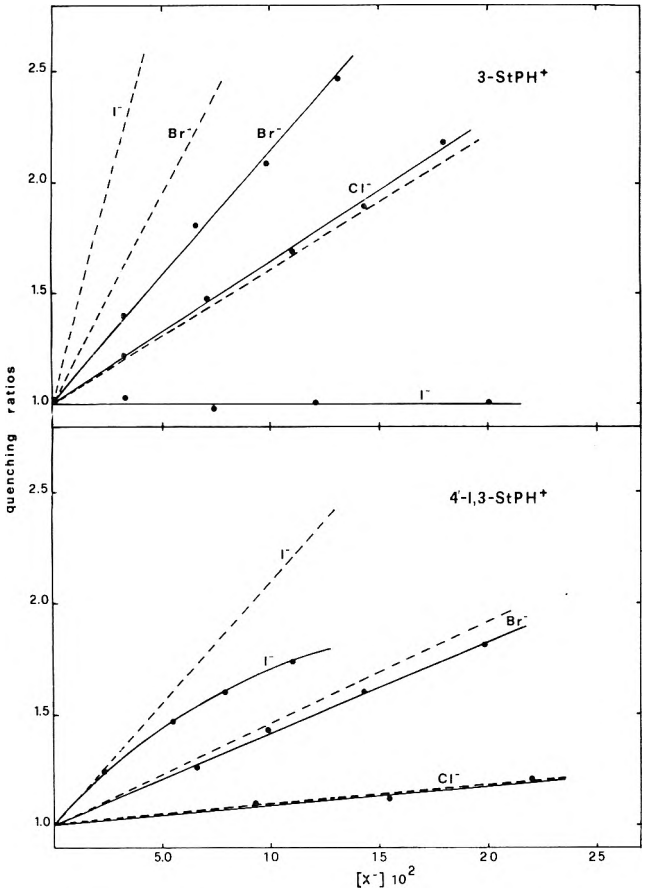

Figure 1. Stern–Volmer plots for the trans → cis photoisomerization quenching of 3-styrylpyridine and its 4′-I derivative by halide anions in 90/10 (v/v) water–ethanol at pH 2 and μ = 1. Dashed lines show the corresponding fluorescence quenching.

state reduction potential of the acceptors, calculated by the sum $E_{1/2}(A^-/A) + \Delta E_{00}$ of the polarographic half-wave reduction potential of the acceptor and the energy of its excited singlet state obtained from the absorption and fluorescence spectra. The latter relationship cannot be verified in our case both because k_q values are not obtainable for the short-lived 2- and 4-StP's and because reliable reduction potentials in water–ethanol are not available for all the isomers. For the unsubstituted StP's, the reduction potentials in 25% water–75% dioxane are reported in the literature.[12] The value for the reduction potential of 3-StP is more negative than for the other isomers in both neutral and protonated forms. If the $\bar{\nu}_{00}$ of the $S_1 \leftarrow S_0$ transitions are taken into account (29,220, 29,450 and 29,570 cm^{-1} for the neutral isomers 2, 3, and 4, respectively),[8] it results that the 3 isomer has a smaller electron affinity in the excited state also. This isomer having the highest K_Q, the lifetime turns out to be the determining factor in the slope of its S–V plot. The order of the excited state reduction potentials is in fact 3 > 2 > 4. As the quenching constants are in the order 3 ≫ 2 ≃ 4 in both acidic and basic media, a singlet lifetime at least one order of magnitude smaller for the isomers 2 and 4 can be inferred.

By using the singlet lifetimes of the 4′ derivatives of 3-StP,[8] the substituent effect on k_q can be evaluated. Some k_q values of Table II are close to the diffusion limit, indicating that the quenching is diffusion controlled for these relatively long-lived acceptors. Looking at the k_q values for neutral StP's and to those at pH 2 with Cl^- and Br^-, which are certainly below the diffusion limit, it is interesting to note that the electron-donating methyl and methoxy groups lower the quenching rate noticeably with respect to the unsubstituted compound. The relative effect of different substituents cannot, however, be discussed owing to the large uncertainty of the τ values. Another interesting point concerning the 4′-methyl derivative is that the dependence of its log K_Q on $E_{1/2}$ of the anions is characterized by a greater slope than for the unsubstituted 3-$StPH^+$. This indicates that an electron density increase in azastilbene plays a role in the quenching mechanism, so that a CT process contributes to the deactivation of the excited state.

Photoisomerization Quenching. In the case of photoisomerization quenching, different kinetic situations may arise depending on whether one or more excited states are reactive and one or more are quenched by the added salt.[13] The kinetics may also depend on whether the path for nonradiative decay of the complex is one leading to the ground state azastilbene directly or *via* the triplet manifold. Figure 1 shows the S–V plots for the quenching of trans → cis photoisomerization of 3-$StPH^+$ and its 4′-I derivative by halide anions up to about a 0.1 M quencher concentration, together with the corresponding plot for the emission quenching for comparison purposes. Table III reports the corresponding quenching constants together with the quenching ratios measured at a fixed 1 M quencher concentration for 3-$StPH^+$ and its 4′-Br and 4′-I derivatives.

Examining first the results obtained with the unsubstituted compound, it is interesting to note that the trend of the anion effect is quite different from that reported for fluorescence. The same effect of Cl^- on ϕ_f and ϕ_t even at high ionic quencher concentration, is compatible with the reaction occurring either at the S_1 or T_1 levels. The quenching of the S_1 state does not result significantly in triplet formation, since this would result in a less quenched

TABLE III: Quenching Constants $k_q\tau$ (M^{-1}) of Fluorescence and Trans → Cis Photoisomerization of 3-Styrylpyridinium Cations (pH 2) by Sodium Halides in 90/10 (v/v) Water–Ethanol at μ = 1 by $NaClO_4$[a]

	3-StPH$^+$		4′-Br-3-StPH$^+$		4′-I-3-StPH$^+$	
Quencher	Fluor	Isomerm	Fluor	Isomerm	Fluor	Isomerm
Cl^-	6.0 (8.4)[b]	6.5 (7.9)	2.7 (4.0)	2.7 (4.0)	1.1 (1.8)	1.0 (1.9)
Br^-	18.8 (46)	11.3 (4.1)	12.2 (24)	9.0 (5.1)	4.6 (7.4)	4.2 (5.1)
I^-	39 (~500)	0 (1.0)	26.8 (240)	10[c] (1.3)	11.0 (69)	11[c] (3.4)

[a] The quenching ratios at 1 M quencher concentrations are shown in parentheses. [b] The quenching ratios at $[X^-] = 1$ expected from a linear S–V plot should be obtained by $(k_q\tau + 1)$. [c] Initial slope of the nonlinear S–V plot.

isomerization. In fact, previous energy transfer experiments with triplet donors[14] had shown that all StPH$^+$'s are able to isomerize at the T_1 level with good efficiency. It is to be noted in this respect that the triplet state was not quenched by Cl^- up to $[Cl^-] = 0.1$ M, as demonstrated by the unquenched biacetyl-sensitized photoisomerization of 3-StPH$^+$. However, biacetyl phosphorescence was quenched by Cl^- at higher concentrations. The quenching efficiency of Br^- in dilute solutions is slightly greater for fluorescence than for isomerization. When $[Br^-] = 1$ M, the fluorescence intensity ratio is higher than the value extrapolated from the S–V plot, while the ratio of photoreaction yields is lower, indicating that the T_1 level population is increased in the presence of high quencher concentration. The heavy anion I^-, which quenches fluorescence strongly in the concentration range of the S–V plot and much more at 1 M concentration, has no effect on the photoreaction.

The behavior with the heavy atom quenchers is probably due to the concurrency of heavy atom effects by both the free (external) and complexed (internal) X^-. This results in a more effective quenching of S_1 and an increased T_1 concentration by enhanced ISC of both ^{1}3-StPH$^+$ and the complex, which then dissociates to X^- and ^{3}3-StPH$^+$, following eq 2. In the case of I^-, a balance of different processes is probably operative.[15] The possible implication of a quenching of ^{3}StP's by Br^- and I^- in this balance is difficult to prove; some experiments in the presence of triplet donor sensitizers did not give useful results due to specific interactions of the anions with the excited sensitizer.

A quenching experiment on the free base ([NaOH] = 0.4 M, $[I^-] = 0.6$ M; experiments with the other anions are of less significance because the K_Q values are too small) showed that also in this case the isomerization is practically unquenched.

As some of the results described seemed to indicate an important pathway to the triplet manifold in the decay of the CT complexes, it was interesting to investigate the 4′-Br and 4′-I derivatives of 3-StP which have higher yields of the singlet to triplet ISC compared to the unsubstituted compound. This was shown by the fluorescence yield at 77 K, which becomes quite high (>0.6) for the unsubstituted StP's and some derivatives but remains low for the 4′-Br (<0.2) and particularly for the 4′-I derivative (<0.01).[7] The results obtained with these two compounds in acidic medium are also reported in Table III. Looking at the heaviest substrate, a somewhat different behavior with respect to the 3-StPH$^+$ can be observed. In fact, only Cl^- has a similar effect, the S–V plot being linear even at high concentration and with equal slope for emission and photoreaction. The Br^- ion quenching shows a linear trend up to high concentrations and practically with the same slope for the two phenomena. The fluorescence is weak for this derivative (ϕ_f = 0.03), and probably ϕ_{ISC} is high, so a small number of quanta are here recovered for the photoreactive T_1 state. The quenching by I^-, like that by Br^- of 3-StPH$^+$, is less on the reaction than on the emission and the plot bends downward from origin. Here more quanta are recovered as the heavy atom effect is greater.

The 4′-Br derivative has an intermediate behavior, in the sense that the differences found in the quenching of emission and photoreaction by heavy quenchers are intermediate between those found for 3-StPH$^+$ and 4′-I-3-StPH$^+$.

Conclusions

Inorganic anions are efficient quenchers of the excited states of azastilbenes mainly in acidic medium. The interaction seems to imply both some sort of CT complex formation and a heavy atom enhanced ISC to the triplet manifold, the latter becoming more important at high quencher concentrations. Photoisomerization is quenched to a different extent than fluorescence as the enhanced ISC enables the photoconversion to proceed at the triplet level. The results seem to confirm that both S_1 and T_1 states are reactive in the absence of quenchers, the first being mainly responsible for the direct photoisomerization of 3-StP, the latter for the reaction of the 4′-Br and 4′-I derivatives, as assumed for the corresponding stibenes.[6] More conclusive information cannot be drawn on the reaction mechanism without further studies on the quenching of the T_1 state.

Acknowledgments. The financial supports of the Italian Consiglio Nazionale delle Ricerche (Contract No. 72.00155.03) and of NATO (Research Grant No. 630) are gratefully acknowledged.

References and Notes

(1) See, *e.g.*, T. G. Beaumont and K. M. C. Davis, *J. Chem. Soc. B*, 456 (1970); C. A. G. Brooks and K. M. C. Davis, *J. Chem. Soc., Perkin Trans. 2*, 1649 (1972).
(2) R. S. Davidson and A. Lewis, *J. Chem. Soc., Chem. Commun.*, 262 (1973).
(3) A. R. Watkins, *J. Phys. Chem.*, **77**, 1207 (1973).
(4) Direct evidence for exciplex formation has been recently reported by the appearance of a new emission band characteric of the complex for the salts of *N,N*-(diethyl)-2-(1-naphthyl)ethylamine with hydrogen halides and alkyl halides.[2] The CT interpretation of the fluorescence quenching mechanism has been verified in many other systems with donor partners different from inorganic anions;[5] other mechanisms, implying, *e.g.*, hydrogen transfer, have been sometimes hypothesized, being CT energetically improbable.
(5) D. Rehm and A. Weller, *Ber. Bunsenges. Phys. Chem.*, **73**, 834 (1969); *Isr. J. Chem.* **8**, 259 (1970); K. H. Grellmann, A. R. Watkins, and A. Weller, *J. Phys. Chem.*, **76**, 3132 (1972).
(6) See also I. G. Lopp, R. W. Hendren, P. D. Wildes, and D. G. Whitten, *J. Amer. Chem. Soc.*, **92**, 6440 (1970).
(7) G. Bartocci, P. Bortolus, and U. Mazzucato, *J. Phys. Chem.*, **77**, 605 (1973) (part II of this series).
(8) G. Favaro, U. Mazzucato, and F. Masetti, *J. Phys. Chem.*, **77**, 601 (1973).

(9) F. Masetti and U. Mazzucato, *Ann. Chim. (Rome)*, **62**, 519 (1972).
(10) K. H. Grellmann, A. R. Watkins, and A. Weller, *J. Phys. Chem.*, **76**, 469 (1972).
(11) See, e.g., J. B. Birks, "Photophysics of Aromatic Molecules," Wiley-Interscience, London, 1970, p 436.
(12) J. Chodkowski and T. Giovanoli-Jakubczak, *Rocz. Chem.*, **41**, 373 (1967).
(13) See, e.g., P. J. Wagner, "Energy Transfer Kinetics in Solution" in "Creation and Detection of the Excited State," Vol. 1, Part A, A. A. Lamola, Ed., Marcel Dekker, New York, N.Y., 1971, p 173.
(14) G. Favaro, G. Bartocci, and P. Bortolus, in press.
(15) The possibility that a nonrelaxed CT collision complex undergoes a very fast ISC cannot be excluded.
(16) J. Saltiel and E. D. Megarity, *J. Amer. Chem. Soc.*, **94**, 2742 (1972).

Chemical Reaction Rates of Quasifree Electrons in Nonpolar Liquids. II[1]

Augustine O. Allen,* Thomas E. Gangwer, and Richard A. Holroyd

Chemistry Department, Brookhaven National Laboratory, Upton, New York 11973 *(Received July 15, 1974)*

Publication costs assisted by Brookhaven National Laboratory

Reaction rates of the electron, generated by X-ray ionization in various solvents, with a number of compounds which are known as good electron scavengers (*e.g.*, SF_6, N_2O, CCl_4, C_2H_5Br, and trichloroethylene) have been determined as a function of temperature. The results are correlated with the quantity V_0, the energy of the electron in its mobile state, previously determined by photoelectric threshold measurements in the various solvents. The measured rate constants exhibit maxima for characteristic values of V_0, reminiscent of the resonant energy maxima in the dissociative attachment cross sections for electron reaction shown by the same molecules in the gas phase. Since V_0 shifts toward more positive values with decreasing temperature, it is found that, for a particular solute, in a solvent having V_0 lower than the value for the maximum electron–solute reaction rate, the reaction has a negative temperature coefficient. In solvents with higher V_0 than corresponding to the maximum rate, the temperature coefficient of the reaction rate is positive. Thus the kinetics of these reactions appear quite different from those of ordinary chemical reactions. New data are presented on electron mobilities in various solvents, obtained incidentally in the course of the measurement of the rate constants. The relative reaction rates for quasifree electrons with various solutes in cyclohexane are in good general agreement with Schuler and Klein's values for relative reaction rates with transient "geminate" electrons.

Introduction

The reactions of electrons formed by ionization in liquid or amorphous materials are little understood, and yet are of considerable importance in a number of applications ranging from radiobiology to dielectric breakdown in insulators. The present paper extends our earlier work[2] on the interaction rates of electrons with scavenger molecules in liquid hydrocarbons and tetramethylsilane (TMS). The present work has resulted in some clarification of the nature of the reactions occurring and their relation to the dissociative attachment reactions of molecules with electrons in the gas phase.

Experimental Section

Our method for determining rate constants has been described in detail.[2] The mobility of electrons in the purified solvent is first determined by measuring the rate of approach of the electron current to a steady-state value (Hudson method); the total steady-state current is then determined and the deviation of the ratio of the electron current to the total current from the value one-half provides a measure of the amount of electron-trapping impurities in the solvent preparation. The measurements are made over a range of temperatures. Small amounts of solute are then added to the liquid in the cell and new measurements are then made of the electron current. The amount by which the electron current is reduced by the presence of scavenger provides a measure of the ratio (k/μ_e) of the rate of reaction of the electron with the solute to the mobility of the electron in the solvent. All hydrocarbon solvents (Phillips Research Grade) and tetramethylsilane (nmr grade) were passed through activated silica gel, deaerated by bubbling with N_2, degassed and stirred over NaK, and finally the solvent vapor was bubbled through NaK at 200°. All solutes (CP grade) were degassed prior to use.

The Biomation Model 802 recorder used in the previous work was employed for all k/μ measurements. For some of the mobility measurements the faster Biomation Model 8100, which can record 2048 data points over a time range which can be as small as 20 μsec, was used. This recorder was on the output of a Keithley Model 105 pulse amplifier; the terminating resistance on the amplifier input provided a time constant of less than 0.2 μsec. Temperature control was improved by the use of a Thermo Electric Co. Model 32422 indicating proportional temperature controller.

Results

Electron Mobilities. New mobility data obtained in the course of this work are shown in Table I. The values for *n*-hexane agree fairly well with previous studies (Figure 1).

TABLE I: Electron Mobilities

Solvent	Temp, °C	Preparation[a]	μ_e, cm V^{-1} sec^{-1}
n-Hexane	21	H1	0.069
	21	H2	0.060
	20	H3	0.060
	0	H3	0.032
Cyclohexane	21	C1	0.23
		C2	0.21
		C3	0.20
		C4	0.21
		C5	0.23
2,2,4-Trimethylpentane	68	I1	8.1
	50	I1	6.5
	50	I2	6.9
	35	I1	5.6
	20	I1	5.1
	20	I2	5.3
	20	I3	5.6
	−25	I2	3.6
	−25	I3	4.2
	−60	I2	2.6
	−83	I3	1.85
Tetramethylsilane	19	T1	97
	0	T1	96
	−25	T1	99
	−50	T1	103

[a] The use of different samples of each liquid is indicated by different numbers; where the number is the same it indicates the same sample of liquid was used in these experiments.

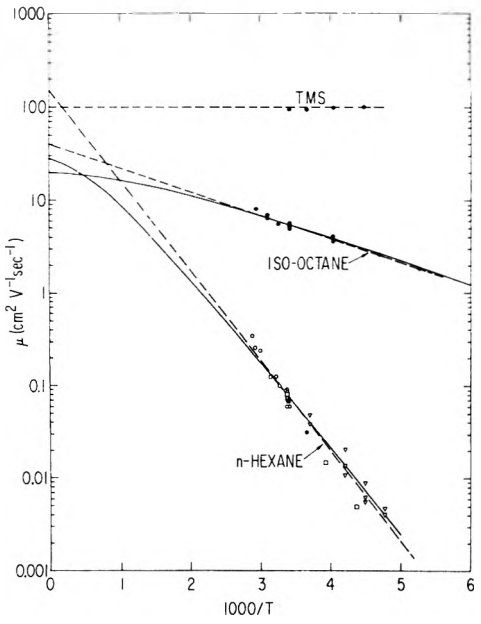

Figure 1. Mobilities as a function of $1/T$ for tetramethylsilane, 2,2,4-trimethylpentane, and *n*-hexane: data for TMS and isooctane from this work; for hexane (●) this work, (O) ref 4, (□) ref 2, (▽) ref 5. Dotted lines are fit to eq 1. Solid curves are fit to eq 2.

The values for cyclohexane confirm our previous value, which was in disagreement with earlier determinations. The values obtained for TMS and for 2,2,4-trimethylpentane (isooctane) are graphed in Figure 1. The values for TMS at low temperatures must be regarded as superseding the values that we published earlier. At the lowest temperature used in the earlier work, the ions were so slow that it was difficult to judge the correct value of the total steady-state current. The present results were also improved by

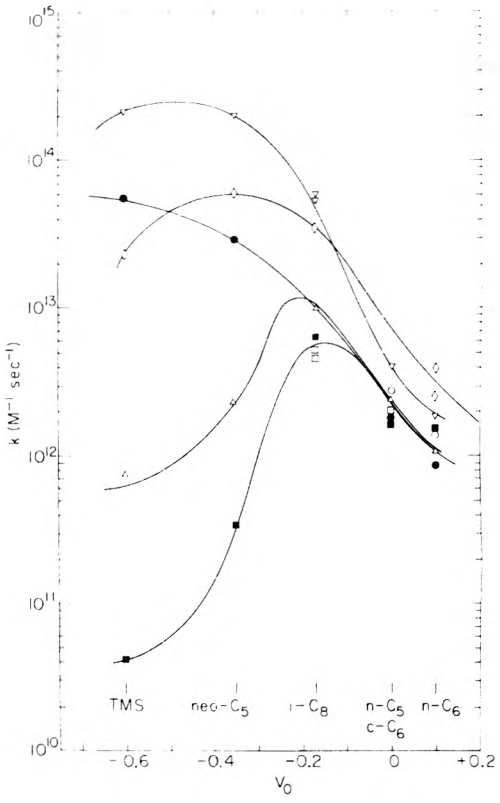

Figure 2. Electron rate constants at room temperature as a function of V_0 (in eV) for reaction with (▽) SF_6, (◇) C_2HCl_3, (O) CCl_4, (△) N_2O, and (□) C_2H_5Br: open symbols, this work; filled symbols, ref 2.

use of the faster Biomation recording equipment. It now appears that the electron mobility in TMS is independent of temperature over the range studied within the experimental accuracy.

Since the electrical current measurements give a value of k/μ, values of μ, the electron mobility in each solvent at each temperature used, had to be assumed in the light of available data to obtain the rate constants. For neopentane, the field-dependent values of μ were taken from the recent work of Bakale and Schmidt.[3] For TMS, where the field was always kept below 2000 V/cm, a value of 100 for μ was assumed at all temperatures. For isooctane and *n*-hexane values were read from the lines shown in Figure 1 (see Table II). The hexane points in Figure 1 include, besides values found in the present work, data previously published from our laboratory[2,4] and that of Davis.[5]

Rate Constants. The new data on the second-order rate constants of reactions of electrons with trichloroethylene, sulfur hexafluoride, nitrous oxide, carbon tetrachloride, ethyl bromide, and methyl and ethyl chloride are assembled in Table II. Rate constants obtained from successive additions of the same compound to a given preparation were in agreement to within 5–10%. Agreement is frequently but not always as good between results obtained at different times on different preparations of the solvent. In Figure 2 the available data for the reaction of electrons with five solutes at room temperature are presented as a function of the electron energy V_0 for the various solvents. (Values of V_0 are discussed by Holroyd.[6]) A clear pattern emerges. The rate constant for reactions of electrons with each solute (with the exception of carbon tetrachloride) shows a pronounced maximum corresponding to some particular value of the energy V_0. For carbon tetrachloride no

TABLE II: Rate Constants for Reactions of Electrons with Various Compounds in Different Solvents

Solvent and assumed μ_e	Solute	Temp, °C	$k/\mu_e(\times 10^{-12})$,[a] V cm^{-2} M^{-1}	$k(\times 10^{-12})$,[a] M^{-1} sec^{-1}
n-Hexane	C_2HCl_3	50	36.5[b]	5.6
$\mu_e = 160 \exp(-2245/T)$		41	47.3[c]	6.0
		22	32.1[b]	2.6
		19	52.8[c]	3.9
		0	48.9[c]	2.1
		−20	28.6[b]	0.64
		−25	53.1[c]	1.00
		−52	23.3[c]	0.15
		−55	22.1[b]	0.12
	CCl_4	21	17.4	1.32
	SF_6	24	23.8	2.0
		22	23.8	1.9
		0	22.9	0.99
		−25	24.1	0.45
		−27	21.8	0.38
	N_2O	22	13.7	1.09
		1	11.3	0.50
		−25	10.7	0.20
Cyclohexane	SF_6	21	16.7	4.0
$\mu_e = 0.24$	N_2O	21	10.0	2.4
	CH_3Cl	21	6.02	1.40
	CCl_4	21	11.4	2.7
	C_2H_5Br	21	8.23	2.0
2,2,4-Trimethylpentane	C_2HCl_3	19	6.3	35
$\mu_e = 40.8 \exp(-585/T)$		0	6.2	30
		−25	5.9	23
		−52	5.5	16
	SF_6	50	9.4	63
		20	10.4	58
		19	9.5	52
		0	8.0	38
		−25	7.5	29
		−50	9.9	29
		−59	8.3	22
	N_2O	19	1.8	9.6
		0	2.0	9.5
		−25	2.2	8.3
		−50	3.2	9.6
	C_2H_5Br	50	0.41	2.7
		20	0.93	5.1
		19	0.80	4.4
		0	1.17	5.6
		−25	1.57	6.1
		−51	2.1	6.2
		−59	2.2	6.0
		−85	2.1	3.8
	C_2H_5Cl	19	<0.0016	<0.009
Neopentane	C_2HCl_3	21	*d*	58
μ_e from ref 3	SF_6	21		198
	N_2O	21		2.3
Tetramethylsilane	C_2HCl_3	21	0.23[c]	23
$\mu_e = 100$ at all temp[e]		0	0.26	26
		−25	0.33	33
		−50	0.40	40
	SF_6	21	2.09	209
		0	2.28	228
		−25	2.29	229
		−50	2.32	232
	N_2O	21	0.0075	0.75
		0	0.0087	0.87
		−25	0.0108	1.08
		−50	0.0133	1.33
	CH_3Cl	20	0.0066	0.66
		0	0.0055	0.55
		−25	0.0040	0.40
		−51	0.0028	0.28
	C_2H_5Cl	20	$<1.2 \times 10^{-5}$	<0.0012

[a] Average of determinations on solutions of up to five different concentrations, at two to four different field strengths for each concentration. [b] Runs of 5/13/74. [c] Runs of 1/10/74, a different preparation of hexane. [d] Field varied from 2.5 to 20.0 kV/cm; μ_e and hence k/μ_e varied with field. [e] Field kept below 2.2 kV/cm to avoid field variation of μ_e.

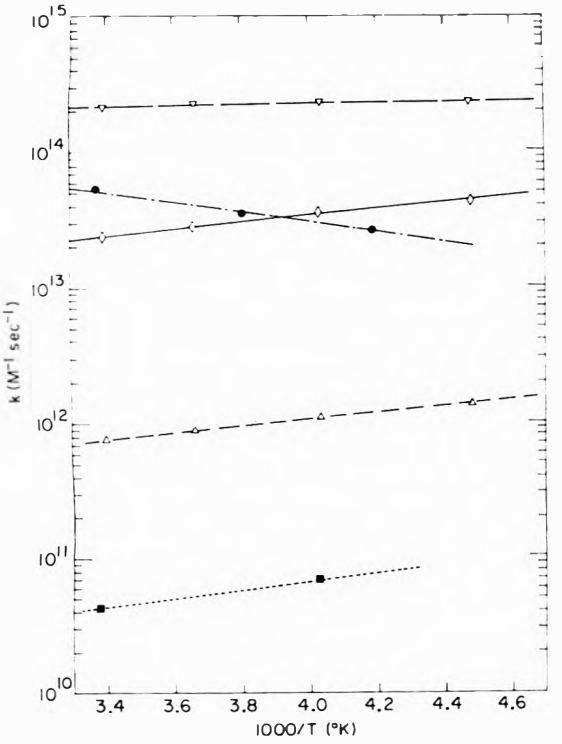

Figure 3. Electron rate constants in tetramethylsilane as a function of reciprocal absolute temperature. Symbols as in Figure 2.

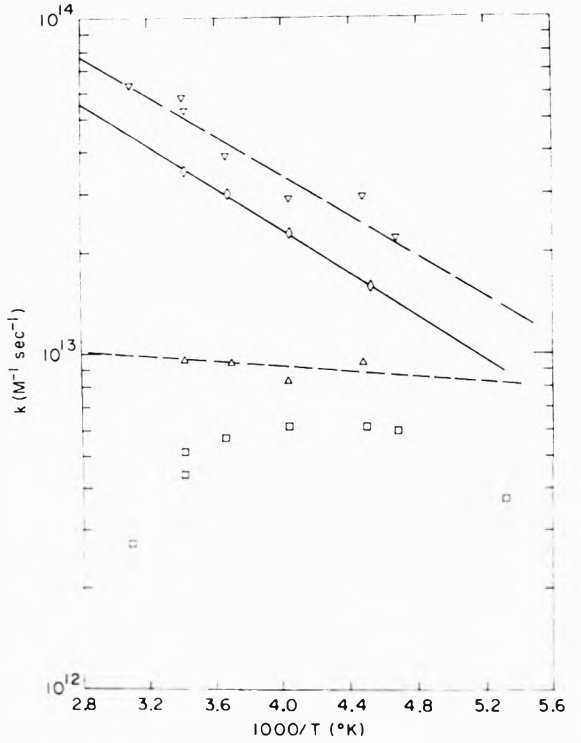

Figure 4. Electron rate constants in 2,2,4-trimethylpentane as a function of $1/T$. Symbols as in Figure 2.

maximum is seen but the data appear to suggest that one would occur if a solvent of lower V_0 could be found. In Figures 3–5 the rate constants for the different solutes in TMS, isooctane, and hexane, respectively, are plotted against reciprocal temperature. When the V_0 value corresponding to the maximum rate constant for the given solute–electron reaction is greater than the V_0 for the solvent, the temperature coefficient of the reaction is negative; that is, the reaction goes faster the lower the temperature. When the V_0 for the solvent is higher than the V_0 value corresponding to the maximum solute–electron rate constant the temperature coefficient is positive. For example, N_2O reaches a maximum at $V_0 = -0.2$ eV and the temperature coefficient of e^- with N_2O is positive in *n*-hexane and negative in TMS. For the case of ethyl bromide in isooctane, we seem to be right on the maximum V_0 value for the reaction of this solute with the electron, and as the temperature is lowered the reaction rate constant first increases and then decreases.

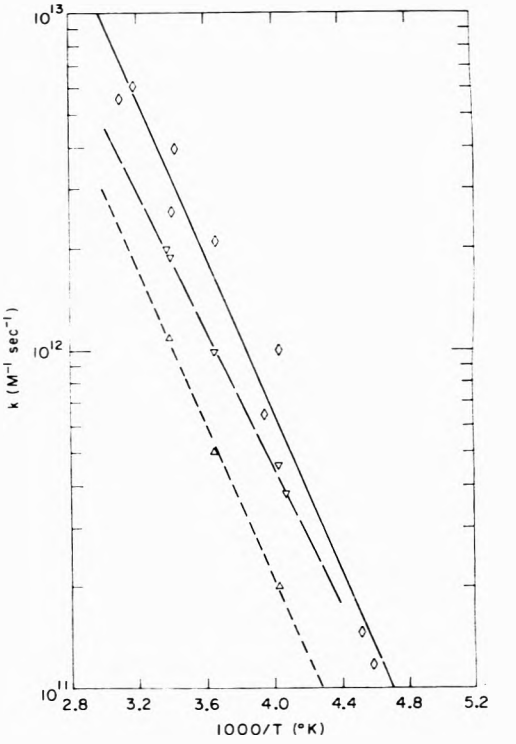

Figure 5. Electron rate constants in *n*-hexane as a function of $1/T$. Symbols as in Figure 2.

Discussion

Electron Mobilities. Electron mobilities in liquid hydrocarbons are generally explained by assuming that the electron alternates between extended mobile states and localized trapped states of lower energy in which the mobility is negligibly small. Then the observed mobility is given by $\mu_0 P(T)$, where μ_0 is the mean mobility in the mobile states and $P(T)$ is the probability of finding the electron in a mobile state. Previously[2] we discussed two possible forms for $P(T)$ which lead to the following equations for μ.

$$\mu = \mu_0 \exp(-E/RT) \quad (1)$$

$$\mu = \mu_0(1 + E/RT) \exp(-E/RT) \quad (2)$$

Figure 1 shows the data available from our laboratory and from Davis' laboratory at the University of Minnesota on electron mobilities in normal hexane, with the present data on mobilities in isooctane and TMS. The data given by Davis[5] suggest a somewhat smaller temperature coefficient for mobility in hexane than is suggested by the data from

our laboratory. However, we have fit the data giving all points from both laboratories equal weight; the straight lines in the figure give the best least-squares fit of the data to eq 1, while the curved lines give the best fit to eq 2. The intercepts on the axis of infinite temperature are of course the values calculated for μ_0. The values for μ_0 from eq 1 come out higher for normal hexane than for either TMS or isooctane. Equation 2 gives μ_0 for hexane lying between μ_0 for isooctane and for TMS. This result is somewhat unexpected and suggests that the molecular shapes affect the mobility in a more complicated way than has hitherto been supposed. These results indicate that neither eq 1 nor 2 is adequate for calculation of μ_0.

Rate Constants. A number of electron reaction rate constants have been determined[7,8] in hexane and cyclohexane solutions using nanosecond pulse radiolysis equipment, by noting either optical absorption changes or the decay of conductivity following a very short pulse of fast electrons. The results, in general agreement with those from our laboratory, show that for a large number of molecules, rate constants in hexane at room temperature lie between 1 and 2 × 10^{12} M^{-1} sec^{-1}, while in cyclohexane the rates lie between 2 and 4 × 10^{12}. A few molecules show lower rate constants, presumably because their reactions require activation. These results suggest that in liquids of relatively low electron mobility, the electron reactions are essentially diffusion controlled. Consistent with this idea is the present result (Table II) that for all solutes in *n*-hexane and for SF_6 in all solvents k/μ_e changes very little over a wide temperature range.

Electron-reactive solutes at sufficiently high concentrations will react, under ionizing radiation, not only with free electrons but with the more numerous "geminate" electrons which fail to escape the field of their parent ion and recombine with it after a very short lifetime. The solute concentration required to achieve a given amount of electron reaction, additional to the free ion yield, should be a measure of the relative reaction rate of electron with solute. Schuler[9] expresses this reactivity by a constant α, and Table III compares values of α for various solutes in cyclohexane with rate constants for reaction with quasifree electrons reported in the present work and elsewhere. The ratio α/k should be constant and equal to the mean lifetime of the geminate ion–electron pairs. With one exception, the ratios are constant, within the uncertainties in the determinations of both α and k. The mean lifetime in cyclohexane is 4 × 10^{-12} sec. The apparent exception, methyl iodide, warrants further study. The results support the assumption that molecules should react at the same specific rate with quasifree and with geminate electrons.

Comparison with Gas-Phase Data. Although the maxima in the rates shown in Figure 2 resemble the resonant gas-phase cross-section maxima in dissociative capture reactions, the situations are not the same, because (at least on the accepted model) the electrons in most of the hydrocarbon liquids spend the majority of the time resting in traps, and the reactions occur only while the electrons are moving through the liquid outside the traps. Further, while the gas-phase resonance peaks represent an energy requirement for maximum rate in both liquid and gas, the absolute magnitudes and shapes of the cross-section curves may be quite different. According to theory, at least for diatomic molecules, the peaks, taken as a function of electron energy, should be nearly symmetrical; but the observed gas-phase peaks, especially for polyatomic molecules, show a marked trailing or extension on the high-energy side. The effect may be due to the participation in the reaction of several excited vibronic levels of the molecule. In the liquid, where the molecules are touching and vibrational energy is readily shared, we expect vibrational modes of the solvent molecules surrounding the reacting molecule to participate in broadening the resonance. Since rather highly excited states of the ion complex, which in isolation quickly reemit the electron, could be stabilized by energy transfer to the solvent, we may expect to see no real peak in the liquid, the rate in the liquid remaining roughly constant for energies well above those corresponding to the gas-phase resonance region. Energy transfer to solvent would be expected also, for the same reason, to result in higher cross sections than can be obtained in the gas phase at any energy.

TABLE III: Comparison of Electron Rate Constants k with Relative Scavenging Constants α in Cyclohexane

Compd	α,[a] M^{-1}	$10^{-12}k$, M^{-1} sec^{-1}	$10^{12}(\alpha/k)$, sec
CH_3Cl	5.0	1.4	3.6
CH_3I	22	2.0[b]	11.0
C_2H_5Br	10	2.0	5.0
N_2O	8	2.4	3.3
SF_6	16	4.0	4.0
CCl_4	12	2.7, 1.8,[b] 4.3[c]	4.5, 6.7, 2.8
$(C_6H_5)_2$	15	3.3,[c] 2.3[d]	4.6, 6.5
CO_2	13	4.3[c]	3.0

[a] Reference 9. [b] Reference 2. [c] Reference 8b. [d] Reference 7.

In the mobile quasifree state, the electrons are in thermal equilibrium with the liquid, and have a mean kinetic energy of $\frac{3}{2}kT$, while their mean level of potential energy is V_0, relative to the free electron in the vacuum.[10] The source of this potential is the polarization energy U_p of the medium. However the wave function of the electron is so distorted by frequent scattering due to the irregularities in potential in the liquid that the wave number k_0 is much larger than for a free electron, and the energy of the electron is increased by a term $\hbar^2 k_0^2/2m$

$$V_0 = U_p + \hbar^2 k_0^2/2m \qquad (3)$$

Thus a high V_0 is due to multiple scattering effects,[11] which are stronger the more unsymmetrical the molecules of the liquid. The trapping of electrons is also favored by the molecular dissymmetry, so that there is a close inverse relation between the logarithm of the observed mobility and the value of V_0.[6] For a given liquid, V_0 increases with decreasing temperature.[12]

In comparing gas-phase and liquid-phase reactions, one more energy term must however be considered. A dissociative attachment reaction must generally proceed through an intermediate excited molecular-ion complex: $AB + e^- = AB^{-*} = A + B^-$. The energy of the ion complex is lower than *in vacuo*, owing to polarization of the solvent, by an amount P_-, which in general depends on the radius of the ion. We take the energy requirement for peak reaction rate in the gas phase to be determined by a characteristic difference (which can be zero) between the energy of the electron and a certain energy level of the complex. For reaction to occur at its maximum rate in the liquid, the same relation should hold between the mean electron energy V_0 and the energy level in the complex but the latter term will be changed by $-P_-$. Then if E_{max} is the electron energy at which the reaction cross-section peaks in the gas phase,

and $V_0(\max)$ is the energy requirement in the liquid, we have

$$V_0(\max) = E_{\max} - P_- \quad (4)$$

Though P_- depends on the molecular radius, the molecules treated here are all of comparable size, and the various solvents have closely similar dielectric constants. Hence in this discussion we take the term P_- to be roughly constant.

We suppose that in neopentane and especially TMS, as in liquid Ar, Kr, and Xe, trapping plays an unimportant role, so that $P(T) \sim 1$ and $\mu_0 \simeq \mu$. Here we expect a close relationship of the liquid-phase electron reaction rates, taken as functions of V_0, with the gas-phase cross sections σ, taken as functions of electron energy. For other hydrocarbons, the observed rate constant k has been decreased by the fraction of the time $P(T) = \mu/\mu_0$ in which the electrons are in a mobile reaction state, so that the true rate constant k_m, valid for the electron in the mobile reactive state, is

$$k_m = k\mu_0/\mu \quad (5)$$

For dissociative attachment of electrons to polyatomic molecules in the gas phase, the full-width at half-height of the resonance peaks lies in the range 0.5–1.0 eV. The molecule SF_6 is unusual in that, beside a normal dissociative attachment reaction leading to SF_5^-, which peaks at an electron energy of 0.15 eV, there is a very narrow (width <0.1 eV) nondissociative attachment reaction, leading to the ion SF_6^-, which peaks at <0.02 eV, with a maximum cross section at room temperature at least 20 times higher than for the SF_5^- reaction.[11] However, at higher temperatures (230°) the SF_5^- yield becomes greater than that of SF_6^-, even at thermal energies. In the liquid state, participation of surrounding molecules in the reaction should tend to perturb the symmetry and favor the dissociative electron capture reaction to form SF_5^-. Looking at our data on SF_6 in TMS and neopentane, we see that the temperature coefficient of the rate in TMS is slightly negative, possibly indicating that as V_0 becomes less negative with decreasing temperature the peak of the resonance is being approached. In neopentane, $V_0 = -0.35$, the rate is about the same, and the resonance peak probably lies between the two values, or about −0.5 eV. If this corresponds to a gas-phase resonance for SF_5^- at 0.15 eV, it would indicate that the term P_- is about −0.65 eV.

The rate of reaction of CCl_4 is still rising as we go from neopentane to TMS, indicating that its resonance peak lies at lower energies than SF_6, a finding not in disagreement with gas-phase data.[13]

In light of eq 5, one might suppose that k/μ for SF_6 and CCl_4 should decrease as we go to solvents of higher V_0. Instead, k/μ for SF_6 (Table II) increases by a factor of 10, and for CCl_4 apparently by a factor of 30, as we pass from TMS to *n*-hexane. The explanation must be that, in going from one hydrocarbon to another of higher V_0, μ_0 decreases faster than k_m. This is not unreasonable, since μ_0 should be affected qualitatively by molecular symmetry in much the same way as the electron wave vector k_0, and hence as V_0. We have seen that attempts to derive μ_0 by extrapolation of μ to infinite temperature may be misleading, and μ_0 itself could be a function of temperature as is certainly the case in liquid argon.[14] The CCl_4 data, on this interpretation, indicate that μ_0 in hexane should be less than 3.5 cm^2/V sec, or about 300 times smaller than is found by simple extrapolation of the Arrhenius equation for the mobility, which seems unreasonable. If we assume μ_0 is about 22 cm^2/V sec for isooctane, 13 for cyclohexane, and 8.4 for *n*-hexane, values of $k\mu_0/\mu$ remain about constant for SF_6 but appear to go through a minimum for CCl_4 at neopentane and reach their highest value in cyclohexane and *n*-hexane. These proposed values for μ_0 are empirical and have no theoretical basis. A theory of the density of states in these liquids, from which μ_0 might be calculated, is greatly needed.

Trichloroethylene in the gas phase shows[15] $E_{\max} = 0.4$ eV, suggesting that in solution $V_0(\max)$ should be about −0.25 eV, between neopentane and isooctane. We see that in isooctane, as the temperature is lowered and V_0 correspondingly increases, k/μ for C_2HCl_3 decreases slightly, showing that we are already, at $V_0 = -0.17$ eV, to the right of the peak for this substance. The high value for *n*-hexane seems anomalous.

For ethyl bromide, σ(gas) peaks[13] at a much higher value, 0.8 eV, while for nitrous oxide the main peak occurs at 2.3 eV, though there is a shoulder at about 1.0 eV which could become more important in solution. We see, however, that the rate constants for these two substances reach peaks at about $V_0 = -0.2$, and at higher V_0 they join CCl_4 in dropping to lower values. We suppose that in these cases as the electron mobility drops the rates become limited by the rate of electron diffusion, so that all the observed rates with these reactive molecules become about the same. There are obviously many molecules in which further activation is required so that their peaks are far to the right and the rates will be much lower; ethyl chloride in isooctane or TMS is an example (Table II).

All the above ideas are of course tentative, being based on a limited set of rate constant data. Rate constant measurements in a much larger number of solvents, to determine the k–V_0 relations more precisely, could be done by using mixtures of hydrocarbons. It would be particularly interesting to see if mixtures of different pairs of hydrocarbons, adjusted to a certain V_0, would show essentially the same electron rate constants with the various solutes, as the above discussion would lead one to expect.

Conclusions

For the five good electron scavengers we have studied (SF_6, CCl_4, C_2HCl_3, N_2O, and C_2H_5Br), the reaction rates with electrons in nonpolar solvents can be correlated with V_0, the energy level of the mobile conduction electrons in the various solvents. Those solutes that react rapidly in the gas phase with electrons of thermal energy react rapidly in all the solvents; those that require more energetic electrons for reaction in the gas phase react only slowly with electrons in high-mobility, very negative V_0 solvents, but more rapidly in solvents of more positive V_0, even though the electron mobility in these solvents is lower. In any given solvent, V_0 becomes more positive with decreasing temperature; so that solutes that require higher V_0 for rapid reaction show negative temperature coefficients for the electron reaction rate; those that have attained rapid rates show positive temperature coefficients. The data suggest that the mobility μ_0 of electrons while in the mobile conducting state may be lower than hitherto supposed.

References and Notes

(1) Research performed under the auspices of the U.S. Atomic Energy Commission.

(2) A. O. Allen and R. A. Holroyd, *J. Phys. Chem.* **78,** 796 (1974).
(3) G. Bakale and W. F. Schmidt, *Chem. Phys. Lett.*, **22,** 164 (1973).
(4) W. F. Schmidt and A. O. Allen, *J. Chem. Phys.*, **52,** 4788 (1970).
(5) R. M. Minday, L. D. Schmidt, and H. T. Davis, *J. Phys. Chem.*, **76,** 442 (1972).
(6) R. A. Holroyd, *Proc. 5th Int. Congr., Radiat. Res.*, in press.
(7) (a) G. Beck and J. K. Thomas, *J. Chem. Phys.*, **57,** 3649 (1972); (b) *ibid.*, **60,** 1705 (1974).
(8) (a) J. H. Baxendale and E. J. Rasburn, *J. Chem. Soc., Faraday Trans. 1*, **70,** 705 (1974); (b) J. H. Baxendale, J. P. Keene, and E. J. Rasburn, *ibid.*, **70,** 718 (1974).
(9) G. W. Klein and R. H. Schuler, *J. Phys. Chem.*, **77,** 978 (1973), and references therein.
(10) R. A. Holroyd and M. Allen, *J. Chem. Phys.*, **54,** 5014 (1971).
(11) B. E. Springett, J. Jortner, and M. H. Cohen, *J. Chem. Phys.*, **48,** 2720 (1968).
(12) R. A. Holroyd and R. L. Russell, *J. Phys. Chem.*, **78,** 2128 (1974).
(13) L. G. Christophorou, "Atomic and Molecular Radiation Physics," Wiley-Interscience, New York, N.Y., 1971.
(14) J. A. Jahnke, L. Meyer, and S. A. Rice, *Phys. Rev. A*, **3,** 734 (1971).
(15) R. P. Blaunstein and L. G. Christophorou, *J. Chem. Phys.*, **49,** 1526 (1968).

A Spectrophotometric Study of the Rate of the Aqueous Iodate–Iodide Reaction

Steven M. Schildcrout*[1] and Fred A. Fortunato

Department of Chemistry, Youngstown State University, Youngstown, Ohio 44555 *(Received April 18, 1974)*

Publication costs assisted by Youngstown State University

The initial rate of the reaction of IO_3^- with I^- in acetate buffer has been measured at fixed ionic strength and acetate concentration with varying concentrations of IO_3^-, I^-, and H^+ at temperatures between 293 and 308°K. The method involves spectrophotometic determination of the product I_3^- at a wavelength of 353 nm. In contrast to some previous results, the reaction is now found to be first order in IO_3^- and second order in H^+; the apparent order with respect to I^- increases with temperature in the concentration ranges considered. Agreement with some earlier amperometric results is found. The applicability of previously proposed rate laws and mechanisms is considered, and upper limits are estimated for the enthalpies of possible reactive intermediates.

Introduction

The reduction of iodate by iodide in acidic aqueous solution according to

$$IO_3^- + 5I^- + 6H^+ \longrightarrow 3I_2 + 3H_2O \quad (1)$$

or

$$IO_3^- + 8I^- + 6H^+ \longrightarrow 3I_3^- + 3H_2O \quad (2)$$

is important in the preparation of standard iodine solutions and in the analytical determination of acid content, iodide, and iodate.[2] Since the rate of (1) is conveniently measured by noting the sudden appearance of the blue starch–iodine complex when reaction proceeds in the presence of a reducing agent such as arsenite or thiosulfate ("iodine clock"), the reaction has been used also in teaching to illustrate principles of kinetics.[3]

The first successful kinetic study of this reaction was reported by Dushman[4] 70 years ago, and has been followed by many others with a variety of rate laws claimed and mechanisms proposed. Various previous workers have reported that the reaction is first or second order in IO_3^-; first, second, or third order in H^+; and first, second, or fractional order in I^-. Various multiterm rate laws have been given also. These previous studies have recently been critically reviewed.[5]

The present study was undertaken to establish a rate law, with possible mechanistic consequences, for reactions 1 and 2 based on precise spectrophotometric measurements and to compare the results with those of the previous studies, which used other techniques. In this study the reaction rate is determined by measuring the visible absorption by I_3^- as a function of time. This method has the following advantages. (a) The chemical system is simplified since there is no need for chemical indicators or other secondary reagents. (b) The subjective visual determination of a color at an end point is eliminated. (c) A linear increase in absorbance *vs.* time gives direct confirmation of the assumptions needed for the initial-rate method of interpretation used here. (d) Since the slope of an absorbance–time plot is used, it is not necessary to know the exact time of mixing of the reagents.

Experimental Section

Dried and weighed samples of KI and KIO_3 were each dissolved in acetic acid–potassium acetate buffer solutions made with freshly boiled distilled water. The acetate concentration and thus the ionic strength for all runs was held near 0.20 *M*. These iodate and iodide solutions were measured in clinical syringes after temperature equilibration and injected into 1.0-cm silica cells. The sample size was 3 ml.

Sample and reference cells were placed in the thermostatted sample compartment of a Cary 14 spectrophotometer, and the production of I_3^- was monitored from absorbance at 353 nm. This peak is preferred to another at 288 nm although the latter has a greater molar absorptivity, since the 288-nm peak is more subject to interference from I^- absorption and end absorption from the solvent.[6] Typically, absorption was measured for at least 1 min for each run.

Experiments were carried out at sample temperatures of 293, 298, 303, and 308°K. The bath water temperature was monitored with a calorimetric thermometer and was found to fluctuate less than ±0.2° for all runs at a given nominal temperature. A total of 231 runs were used, of which about half were at 298°K. For these the iodide concentrations ranged from 3×10^{-5} to 2×10^{-2} M and iodate from 2×10^{-4} to 1×10^{-3} M. The pH ranged from 4.0 to 5.2. Control runs carried out in the dark showed that the irradiating light of the spectrophotometer has no measurable effect on the rate of reaction.

Treatment of Data

Data were obtained in the form of strip chart recordings of absorbance at 353 nm *vs.* time. Some typical raw data are shown in Figure 1. All plots are linear, at least initially, as required for the initial-rate method.[3,7] The precision of the measured slopes is within 1%. The rate of formation of I_3^- is obtained from the slope by

$$\frac{d[I_3^-]}{dt} = \frac{1}{\epsilon l}\frac{\Delta E}{\Delta t} \tag{3}$$

where E is absorbance, t is time, l is cell path length, and ϵ is the molar absorptivity, which is given[8] with a small correction for I^- contribution as

$$\epsilon = 2.64 \times 10^4(1 + 0.164[I^-]) \tag{4}$$

Since we wish to consider the total rate of reactions 1 and 2 we calculate

$$-\frac{d[IO_3^-]}{dt} = \frac{1}{3}\frac{d[I_3^-]}{dt}\left(1 + \frac{1}{K[I^-]}\right) \tag{5}$$

where the second term on the right allows for the presence of uncomplexed I_2 and where K is the equilibrium constant for

$$I_2 + I^- \rightleftharpoons I_3^- \tag{6}$$

calculated for the appropriate temperature from thermodynamic data.[9] The value of K at 298°K is about 7×10^2. The assumption that reaction 6 is at equilibrium should be valid since equilibrium is rapidly achieved.[10]

Hydrogen ion concentration is calculated for each run from

$$[H^+] = K_a([CH_3COOH]/\gamma_\pm^2[CH_3COO^-]) \tag{7}$$

where K_a is the dissociation constant for acetic acid at the corresponding temperature[11a] and $\gamma_\pm$, the mean ionic activity coefficient, is calculated from

$$\log \gamma_\pm = -\frac{A\sqrt{I}}{1 + \sqrt{I}} + (0.10)I \tag{8}$$

where I is ionic strength and A is a temperature-dependent parameter from Debye–Hückel theory.[11b] The use of formal acetic acid and acetate concentrations in eq 7 is considered satisfactory since the pH is near the pK_a. Determination of hydrogen ion activity with a pH meter would be experimentally cumbersome here and would not improve the precision or accuracy of the results since use of eq 8 would still be necessary to obtain concentration. The values of $[H^+]$ thus calculated are expected to have a systematic error within 5%.

The test of the precision of the concentration and rate data is in the precision of the resulting rate law. This is considered in the next section.

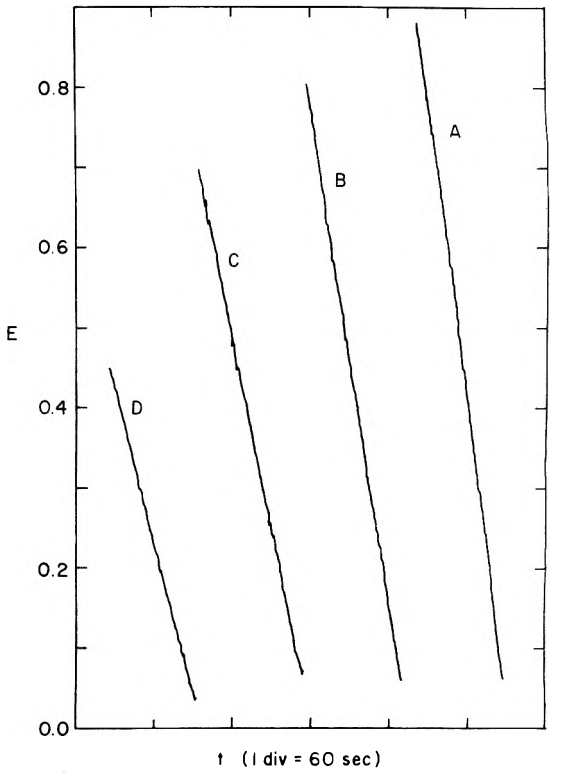

Figure 1. Recordings of absorbance at 353 nm *vs.* time (right to left) for some reaction mixtures at 298°K: $[IO_3^-] = 2.03 \times 10^{-4}$ M and $[H^+] = 4.50 \times 10^{-5}$ M. $[I^-]$ is varied for each curve: A, 3.00×10^{-2}; B, 2.66×10^{-2}; C, 2.33×10^{-2}; D, 2.00×10^{-2} M.

Calculations were performed on an IBM 360/50 computer.

Results and Discussion

The rates as calculated from eq 5 were fitted to a single term rate law

$$-\frac{d[IO_3^-]}{dt} = k[IO_3^-]^a[I^-]^b[H^+]^c \tag{9}$$

Reaction orders were obtained at each temperature from the slope of a linear least-squares plot of log (rate) *vs.* log (concentration) where other variables are constant. Points were rejected if they were more than two average deviations from the mean, and the average deviation and mean were recalculated. These results are given in Table I along with values of k. It is seen that a and c are essentially independent of temperature with average values $a = 0.97 \pm 0.01$ and $c = 1.99 \pm 0.01$ where the error limits are average deviations of the mean.

There is a significant variation with temperature in the order with respect to I^-, as Table I shows. If the rate law is to be given in a form where all exponents of concentrations are independent of temperature, a form more complex than eq 9 must be used.

Barton and Wright have studied the kinetics of (1) at 298°K and $I = 1.00$ by amperometric determination of I_2. They report catalysis by acetate and other nucleophiles commonly used in buffers and give the rate law

$$-\frac{d[IO_3^-]}{dt} = [IO_3^-][I^-]^2[H^+]^2\left(k_0 + \frac{k_b[CH_3COO^-]}{1 + k'[I^-]}\right) \tag{10}$$

This was rationalized by assuming an initial rapid equilibrium

TABLE I: Values of Parameters from Eq 9 for Reaction 2 at Various Temperatures[a]

Temp,[b] °K	a	No.	b	No.	c	No.	$10^{-10}k^c$	No.
293.2	1.02 ± 0.02	11(12)	1.51 ± 0.06	10(12)	1.99 ± 0.02	14(16)	1.44 ± 0.01	40
298.3	0.94 ± 0.01	22(25)	1.55 ± 0.03	23(25)	2.00 ± 0.01	22(25)	1.95 ± 0.01	108
303.3	0.96 ± 0.02	10(12)	1.69 ± 0.03	11(12)	1.98 ± 0.01	13(16)	2.62 ± 0.01	43
308.2	0.98 ± 0.02	7(8)	1.85 ± 0.01	5(6)	1.98 ± 0.01	10(12)	3.62 ± 0.01	21

[a] Error limits for a, b, c, and k are average deviations of the mean for the indicated number of measurements. Numbers in parentheses are the number of values available before the rejection process. The acetate concentration is 0.192 M and the ionic strength is 0.20. [b] Uncertainty ±0.2°. [c] k is evaluated for time in seconds and concentrations in molarity, assuming $a = 1$ and $c = 2$ exactly.

$$IO_3^- + 2H^+ + B^- \overset{K_{11}}{\rightleftharpoons} BIO_2 + H_2O \qquad (11)$$

where B^- is a nucleophile in the catalyzed pathway and where it is I^- for the uncatalyzed reaction. In the former case, iodide attacks the complex to form a steady-state concentration of $BI_2O_2^-$, which undergoes further I^- attack to yield I_2 and the reactive IO_2^-, releasing the B^-. In the uncatalyzed pathway, I_2O_2 yields IO_2^- and I_2 in a rate-determining attack by I^-.[12]

For the present runs at 298°K, the average ratio of the observed rate to that calculated from eq 10 is 0.667 ± 0.127 where the error is the average deviation of a single measurement for 115 values. Experiments where $[I^-] = 3 \times 10^{-3}$ M, the smallest concentration used here, showed anomalously high ratios. If we consider only those runs where $[I^-] > 6 \times 10^{-3}$ M, then the average ratio of observed rates to predicted rates (eq 10) becomes 0.595 ± 0.045 for 92 values. This relative average deviation of less than 8% indicates good agreement with eq 10. Rejecting the values for low $[I^-]$ may be justified by the greater uncertainty in the correction for uncomplexed I_2 when $[I^-]$ is small (eq 5). That the ratio is not unity is accounted for since the present results are at an ionic strength of 0.20 while those of Barton and Wright[12] are for $I = 1.00$. Accordingly these authors cite evidence that there is a positive salt effect in this range of ionic strength. Although the present results do not permit reliable determinations of the three rate constants in eq 10 at the various temperatures, they are consistent with this rate law and thus the proposed mechanism.

A rate law of the form

$$-d[IO_3^-]/dt = [IO_3^-][I^-][H^+]^2(k_1 + k_2[I^-]) \qquad (12)$$

has been used often, and the present data for each temperature were fitted to this equation. The results are shown in Table II. Morgan, *et al.*,[13] have assumed an initial equilibrium yielding IO_2^+

$$IO_3^- + 2H^+ \overset{K_{13}}{\rightleftharpoons} IO_2^+ + H_2O \qquad (13)$$

followed by the rate-determining attack of iodide in bimolecular and termolecular steps

$$IO_2^+ + I^- \overset{k_{14}}{\longrightarrow} IO^+ + IO^- \qquad (14)$$

$$IO_2^+ + 2I^- \overset{k_{15}}{\longrightarrow} I^+ + 2IO^- \qquad (15)$$

This mechanism yields the rate law 12 where $k_1 = K_{13}k_{14}$ and $k_2 = K_{13}k_{15}$. Then the slope of a plot of ln (k_1/k_2) *vs.* $1/T$ should give $E_{15} - E_{14}$, the difference between Arrhenius activation energies of reactions 14 and 15. Although, as shown in Figure 2, the linearity is not good, a least-squares treatment gives $E_{15} - E_{14} = 21$ kcal mol^{-1}. If (15) competes with (14) then this high relative activation energy of the former implies a frequency factor unreasonably large for a termolecular reaction or unusually small for the bimolecular one.

TABLE II: Values of Rate Constants from Eq 12 for Reaction 2 at Various Temperatures[a]

Temp,[b] °K	$10^{-6}k_1{}^c$	No.	$10^{-8}k_2{}^d$	No.
293.2	3.58 ± 0.45	10(11)	3.45 ± 0.34	10(11)
298.3	2.62 ± 0.19	23(25)	4.23 ± 0.16	22(25)
303.3	2.71 ± 0.27	11(12)	4.45 ± 0.19	11(12)
308.2	1.29 ± 0.16	5(6)	6.11 ± 0.12	6(6)

[a] Error limits for k_1 and k_2 are average deviations of the mean for the indicated number of measurements. Numbers in parentheses are the number of values available before the rejection process. The acetate concentration is 0.192 M and the ionic strength is 0.20. [b] Uncertainty ±0.2°. [c] M^{-3} sec^{-1}. [d] M^{-4} sec^{-1}.

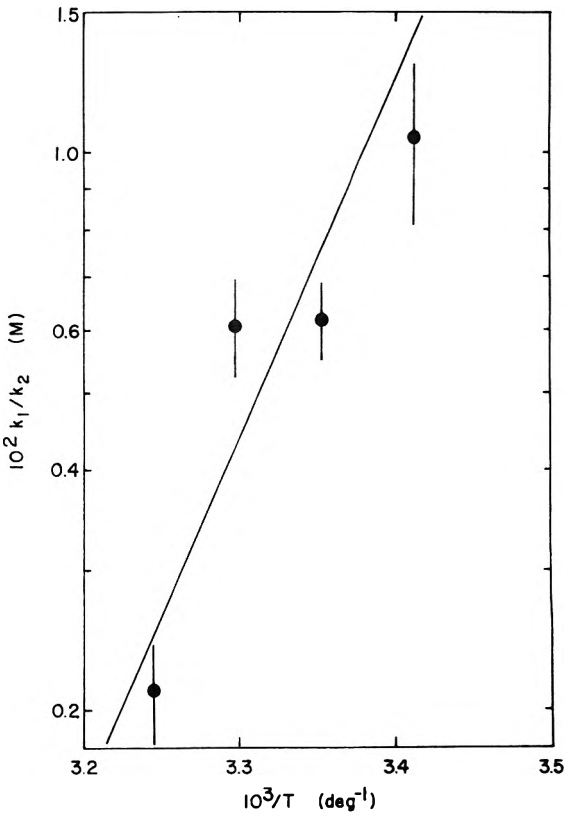

Figure 2. Temperature dependence of k_1/k_2 based on results in Table II.

The rate law 12 may be obtained also by modifying the mechanism of Morgan, *et al.*,[13] to involve, rather than (13), an initial equilibrium as in reaction 11 where B^- is I^-.

The I_2O_2 thus formed is assumed to react by the following pathways

$$I_2O_2 \overset{k_{16}}{\rightleftharpoons} IO^+ + IO^- \quad (16)$$

$$I_2O_2 + I^- \xrightarrow{k_{17}} I^+ + 2IO^- \quad (17)$$

which now replace reactions 14 and 15, respectively. Reactions 11 and 17 are similar to the mechanism proposed by Barton and Wright[12] for their uncatalyzed pathway. Now $k_1 = K_{11}k_{16}$ and $k_2 = K_{11}k_{17}$ so $E_{17} - E_{16} = 21$ kcal mol^{-1} from the data shown in Figure 2, and one must infer an extremely small frequency factor for 16 if 17 is to compete with it.

The temperature dependence of k_1 and k_2 yields apparent activation energies of -13 ± 2 and $+8 \pm 2$ kcal mol^{-1}, respectively. The former energy corresponds to $\Delta H°_{13} + E_{14}$ or $\Delta H°_{11} + E_{16}$. Since E_{14} or E_{16} should be nonnegative, an upper limit for $\Delta H°_{13}$ or $\Delta H°_{11}$ of -11 kcal is obtained. From thermodynamic data[9] the upper limit of +5 kcal mol^{-1} is obtained for the standard enthalpy of formation of aqueous IO_2^+ if eq 13 pertains and -8 kcal mol^{-1} for aqueous I_2O_2 if eq 11 pertains. Attempts to show the existence of a discrete monomeric IO_2^+ cation have not been successful.[14]

The present "activation energy" for k_1 of -13 kcal mol^{-1} conflicts with the positive value obtained from the recently reported results of Furuichi, *et al.*,[15] who studied reaction 1 at [I$^-$] below 10^{-7} M in the presence of solid AgI and $AgIO_3$, a method similar to that used in an early study.[16] These workers[15] assumed a rate law corresponding to the first term of (12).

The value of k_1 at 298° (Table II) is significantly greater than those previously reported.[15-18] Wilson[5] considered earlier k_1 values to be doubtful. Comparing eq 10 and 12 it is seen that k_1 should depend on nucleophile concentration. At low [I$^-$] eq 10 predicts a rate second order in I$^-$ while (12) requires it to be first order in I$^-$.

Although they conflict at low [I$^-$], eq 10 and 12 become equivalent when [I$^-$] is large with $k_0 = k_2$, the fifth-order rate constant. The "activation energy" for k_2 is now 9 ± 2 kcal mol^{-1}, whereas the value of 5.0 ± 0.1 kcal mol^{-1} was reported[12] for k_0. The present value of k_2 at 298° agrees very well with that of $(4.0 \pm 0.1) \times 10^8$ M^{-4} sec^{-1} reported by Barton and Wright[12] for k_0. Other values reported[5,19] for k_2 cover a range of an order of magnitude which includes the present result.

Conclusions

The rate of reactions 1 and 2 at a fixed ionic strength and acetate concentration, as determined by spectrophotometry, fits with high precision a one-term rate law (9) which is first order in IO_3^- and second order in H^+, where the apparent order in I$^-$ increases as temperature increases. Although eq 9 is satisfactory as an empirical result, the temperature dependence of the exponent b (Table I) makes it awkward for possible mechanistic interpretation.

There is consistency between the present results at 298°K and rates reported by Barton and Wright[12] (eq 10), who used amperometry and considered various concentrations of buffering nucleophiles at fixed ionic strength. It is significant that their results have now been corroborated using a different experimental method since the amperometric results have been criticized[5] for low precision and had not been reproduced. The present results do not, however, permit complete confirmation of the form of their rate law (10). Values for k_b and k' were not reported[12] for temperatures other than 298°K. This rate law nevertheless does predict that the apparent order with respect to I$^-$ should increase toward 2 as temperature increases, as is observed here. By absolute rate theory the uncatalyzed pathway must have a greater activation energy than the acetate-catalyzed pathway, so k_0/k_b should increase with temperature, and the reaction becomes fifth-order overall.

The simpler eq 12 with appropriate rate constants can be used with the present data for all temperatures studied. Although the precision of the fit here is not as good as with eq 10 at 298°K, eq 12 is considered satisfactory for correlating the present results. From the temperature dependence of k_1 and k_2, rough Arrhenius activation energies are obtained which imply an upper limit of 5 kcal mol^{-1} for the standard enthalpy of formation of aqueous IO_2^+ and a very low frequency factor for its reaction with iodide if the mechanism of Morgan, *et al.*,[13] is correct. Alternatively, if reaction proceeds *via* I_2O_2, its enthalpy of formation in aqueous solution is less than -8 kcal mol^{-1}, and its unimolecular decomposition is limited by an unfavorable entropy of activation.

Disagreements among the present results and those from previous studies in regard to values for rate constants and, in many cases, even the general form of the rate law may be understood where workers have failed to properly allow for or control side reactions, ionic strength, or catalytic effects, or where a statistical interpretation of the results was incomplete.

References and Notes

(1) Author to whom correspondence should be addressed.
(2) I. M. Kolthoff, E. B. Sandell, E. J. Meehan, and S. Bruckenstein, "Quantitative Chemical Analysis," 4th ed, Macmillan, New York, N.Y., 1969, pp 819, 842–860, 1131.
(3) D. P. Shoemaker, C. W. Garland, and J. I. Steinfeld, "Experiments in Physical Chemistry," 3rd ed, McGraw-Hill, New York, N.Y., 1974, pp 273–279.
(4) S. Dushman, *J. Phys. Chem.*, **8**, 453 (1904).
(5) I. R. Wilson in "Comprehensive Chemical Kinetics," Vol. 6, C. H. Bamford and C. F. H. Tipper, Ed., Elsevier, New York, N.Y., 1972, pp 381–385.
(6) H. H. Jaffé and M. Orchin, "Theory and Applications of Ultraviolet Spectroscopy," Wiley, New York, N.Y., 1962, p 173.
(7) A. A. Frost and R. G. Pearson, "Kinetics and Mechanism," 2nd ed, Wiley, New York, N.Y., 1961, p 45.
(8) E. E. Genser and R. E. Connick, *J. Chem. Phys.*, **58**, 990 (1973).
(9) M. Kh. Karapet'yants and M. L. Karapet'yants, "Thermodynamic Constants of Inorganic and Organic Compounds," J. Schmorak translation, Ann Arbor-Humphrey Science Publishers, Ann Arbor, Mich., 1970.
(10) O. E. Myers, *J. Chem. Phys.*, **28** 1027 (1958).
(11) (a) R. A. Robinson and R. H. Stokes, "Electrolyte Solutions," 2nd ed (revised), Butterworths, London, 1965, p 517. (b) *ibid.*, pp 231–232, 468.
(12) A. F. M. Barton and G. A. Wright, *J. Chem. Soc. A*, 2096 (1968).
(13) K. J. Morgan, M. G. Peard, and C. F. Cullis, *J. Chem. Soc.*, 1865 (1951).
(14) H. A. Carter and F. Aubke, *Inorg. Chem.*, **10**, 2296 (1971).
(15) R. Furuichi, I. Matsuzaki, R. Simic, and H. A. Liebhafsky, *Inorg. Chem.*, **11**, 952 (1972).
(16) E. Abel and K. Hilferding, *Z. Phys. Chem.*, **136A**, 186 (1928).
(17) P. Beran and S. Bruckenstein, *J. Phys. Chem.*, **72**, 3630 (1968).
(18) F. Magno and M. Fiorani, *Ric. Sci.*, **36**, 594 (1966).
(19) R. A. Hasty, *Mikrochim. Acta*, 925 (1973).

Mechanism of the Radiation-Induced Decomposition of Sodium Nitrate. I[1]

Arnold Frances and Everett R. Johnson*[2]

Department of Chemical Engineering, University of Maryland, College Park, Maryland 20742 *(Received April 5, 1974; Revised Manuscript Received September 9, 1974)*

Publication costs assisted by the University of Maryland

Experimental evidence is presented to show that the "apparent" increase in nitrite yield when nitrite is determined by the ceric sulfate method as compared to the method of Shinn is due to the presence of a color center and is not due to the presence of radicals such as NO_2, NO, N_2O_3, etc. as has been proposed. The color center is believed due to an O^- or O_2^- bound to the nitrite ion/or ions formed simultaneously.

The radiation-induced decomposition of the alkali nitrates has been extensively studied[3] and it is generally agreed that the overall reaction is

$$MNO_3 \longrightarrow MNO_2 + \tfrac{1}{2}O_2$$

This paper is concerned primarily with the observation by Cunningham[4] that when irradiated $NaNO_3$ or KNO_3 are analyzed for nitrite ion by ceric sulfate reduction, the apparent nitrite yield so determined is appreciably higher than when nitrite is determined by the conventional Shinn[5] method. The increase in apparent nitrite yield found using the ceric method of analysis was attributed by Cunningham to the presence of small amounts of reducing substances other than NO_2^- such as NO_2, NO, O_2^-, O^-, or O_2^{2-}. Cunningham[6-8] developed a very complex mechanism, supported by optical and esr studies, for the decomposition of nitrates based on the initial formation of species such as O_2^{2-}, NO_2^{2-}, NO_3, NO_3^{2-}, $N_2O_3^{2-}$ and reactions of these species to give final stable products, such as NO, NO_2, N_2O_4, and NO_2^-. Kaucic and Maddock[9] in their studies on the decomposition of $NaNO_3$ doped with $Ca(NO_3)_2$ confirmed the apparent increase in nitrite yield observed by Cunningham when the irradiated samples were analyzed by the ceric method as compared to the Shinn method. However, they observed that this apparent increase in the nitrite yield (ΔNO_2^-) was only evident in the early stages of the decomposition, *i.e.*, the ratio of the nitrite yield as determined by the ceric method to that determined by the Shinn method at very low absorbed dose was about 2.5, with increasing dose the ratio dropped to about 1.

There is, however, serious discrepancy in the literature concerning the optical and esr studies reported by Cunningham and that by others.[10-17] A review of all the papers pertaining to esr studies on irradiated $NaNO_3$ indicates that NO, O_2^{2-}, or O^- are not present. Weak resonance spectra have been reported in $NaNO_3$ irradiated at room temperature which have been tentatively assigned to either NO_2[10,13] or NO_3, however, these results are not supported by the studies of others.[16a,17]

Mass spectrographic analysis of the gas evolved when irradiated $NaNO_3$ or KNO_3 is heated,[4,18-20] or of the gas collected over water after dissolution of the irradiated salt,[20] and by chemical means[21] does not show the presence of NO or NO_2. Esr studies do reveal the presence of NO_2 at liquid nitrogen temperature,[11,14,16a,17] however, only if NO_2^- is present in the lattice,[16a,17] *i.e.*, if $NaNO_3$ is irradiated at 77°K and the esr spectrum examined at this temperature, NO_2 is not present, however, if the irradiated sample is first warmed to room temperature then cooled to 77°K and reirradiated, the spectrum of NO_2 is observed. This strongly suggests that the nitrite ion as such is not a primary product. The spectrum of NO_2 is observed if KNO_3 is doped with nitrite ion prior to irradiation at 77°K. There is, however, evidence for the presence of NO_3^{2-} at low temperatures.[16a,17]

As to the optical spectra, Pringsheim[22,23] has observed a single color band in irradiated $NaNO_3$ in contrast to five bands reported by Cunningham.[24]

The fact remains, however, that analysis for nitrite in irradiated $NaNO_3$ using the ceric sulfate method gives consistently higher values than the Shinn method, hence there must exist some reducing species which has not as yet been identified. The work reported here is an attempt to elucidate the nature of this reducing substance.

Experimental Section

The bulk of the experiments were performed using a cylindrical cobalt-60 source of about 1500 Ci. However, some experiments were performed using a cobalt-60 source whose activity was approximately 25,000 Ci.

Nitrite ion was determined by the method of Shinn[5] and the ceric sulfate method.[4] In the Shinn method sulfanilamide is diazotized and coupled with *N*-(1-naphthyl)ethylenediamine hydrochloride to form a colored azo compound with an absorption maximum at 545 mμ. The molar extinction at this wavelength was 54,100. In the ceric method an irradiated sample is dissolved directly in 0.4 *N* H_2SO_4 which is approximately 10^{-3} *M* in ceric ion. The ceric ion concentration was determined at 330 mμ; the molar extinction coefficient at this wavelength was 5,500.

Dosimetry was determined by ferrous oxidation using a *G* value of 15.45 molecules of ferrous ion oxidized per 100 eV absorbed. Ferric ion was determined at 305 mμ, and the molar extinction used was 2201.

All $NaNO_3$ was reagent grade.

Results and Discussion

More than 100 analyses of nitrite concentration comparing the ceric method and the Shinn method have been performed on irradiated $NaNO_3$. The ceric method gave very erratic results but in all cases the nitrite yield as determined by the ceric method was always greater than when determined by the method of Shinn. The difference in nitrite yield, ΔNO_2^- (ceric–Shinn), for room temperature irradiations, however, occurred during the initial absorbed

dose only; beyond the initial absorbed dose the difference in NO_2^- yield as determined by the two methods remained constant (see Figure 1). These results are consistent with those reported by Kaucic and Maddock.[9] As indicated in the introductory paragraph, there is no experimental support for the presence of oxides of nitrogen during the decomposition of $NaNO_3$. Since the ceric ion is very easily reduced, and ΔNO_2^- is relatively small ~0.15 μmol/g (for room temperature decompositions), it appeared that the erratic results could possibly be attributed to surface impurities which formed reducing radicals during irradiation. Accordingly, a series of experiments was done with $NaNO_3$ which had received a number of different treatments prior to irradiation. These pretreatments consisted of (1) recrystallization from boiling concentrated HNO_3 with subsequent recrystallization from deionized water, (2) repeated recrystallization from deionized water, (3) baking at 100° at high vacuum ($P < 10^{-7}$ Torr), and (4) combinations of these pretreatments. In addition, irradiation was also performed with $NaNO_3$ in the presence of about 3 atm pressure of N_2O. These results are summarized in Table I. As can be seen there is no apparent difference in the results between the $NaNO_3$ used as purchased, the $NaNO_3$ irradiated in the presence of N_2O, or the $NaNO_3$ that had received various pretreatments. Furthermore, the difference in nitrite yields by the two methods cannot be attributed to decomposition of any nitrite formed during irradiation. Pure $NaNO_2$ was irradiated to an absorbed dose of 7.5×10^{20} eV/g. Analysis for total nitrite by the two methods gave identical results. In addition, particle size did not cause any change in the difference in yields as determined by ceric and Shinn analyses.

Samples of irradiated $CsNO_3$ and KNO_3 when analyzed by these two methods gave results roughly comparable to the $NaNO_3$ *i.e.*, ΔNO_2^- ~0.1. However, this difference in NO_2^- was about the maximum observed. In many irradiated samples little or no difference was observed in NO_2^- content using the two methods.

It appeared, therefore, that the difference in "apparent" nitrite yield (ΔNO_2^-), as determined by the two methods could not be attributed to surface effects, particle size, or prior treatment of the salt. Nor could the difference in yields be attributed to any decomposition products of nitrite ion.

An important aspect, however, of the difference in apparent nitrite yields (ΔNO_2^-) using these two methods is the fact that the difference increases with decreasing temperature (Figure 2). Samples irradiated at liquid helium temperatures and subsequently warmed to room temperature and analyzed by the two methods gave results (ΔNO_2^-) roughly 5–10 times greater than those found in samples irradiated at room temperature to the same absorbed dose. These results indicated that the additional reducing substance may be a trapped electron (or color center). It is well known that defects (trapped electrons and holes) are formed in NaCl, MgO, and SiO_2 when these substances are irradiated and these color centers can be detected by chemical means[16b] consequently samples of NaCl, MgO and SiO_2 were irradiated to an absorbed dose of about 10^{21} eV/g and analyzed for the presence of reducing species using ceric sulfate. In addition, samples of Na_2SO_4, which are not known to contain defect centers, were also irradiated and analyzed. The insoluble irradiated MgO and SiO_2 were simply added to the ceric solution, stirred, and subsequently filtered off. These results reported as ΔNO_2^- are summarized in Table II. As can be seen all the samples with the exception of Na_2SO_4 contained reducing species. MgO and SiO_2 showed reducing properties if they were simply heated at 120° *in vacuo* for about 20 hr without irradiation (the reduction of ceric ion in these latter samples on a per gram basis was greater by a factor of 2–4 than that of the irradiated sample).

Most color centers in irradiated ionic crystals are easily bleached by thermal annealing at relatively low temperatures, however, when samples of $NaNO_3$ irradiated at room temperature to an absorbed dose of 1.05×10^{20} ev/g were annealed at 100° for 48 hr and subsequently analyzed, ΔNO_2^- remained essentially unchanged, *i.e.*, the equivalent nitrite yield as determined by the two methods remained the same (~0.15 μmol/g) despite annealing. However, when samples of $NaNO_3$ similarly irradiated were an-

TABLE I: Difference in Apparent Nitrite Yield (ΔNO_2^-) in $NaNO_3$ Irradiated in Different Atmospheres or after Different Pretreatments (Absorbed Dose = 1.4×10^{20} eV/g)

Treatment	ΔNO_2^- (av), μmol/g
Normal $NaNO_3$ (irradiated *in vacuo* or air)	~0.15
Irradiated in 3 atm pressure of N_2O	~0.15
Recrystallized from boiling HNO_3	~0.12
Recrystallized from deionized water	~0.14

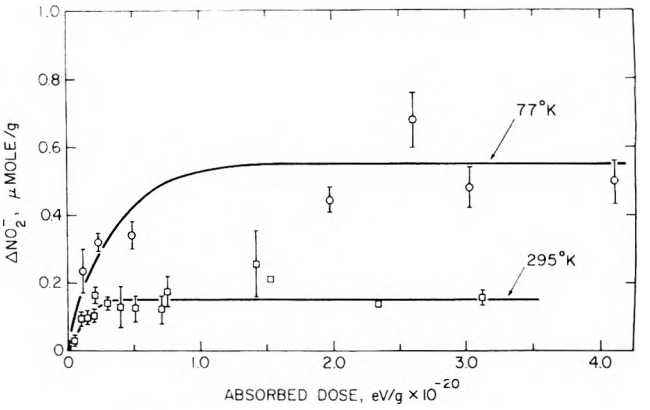

Figure 1. ΔNO_2^- (ceric–Shinn) as a function of absorbed dose.

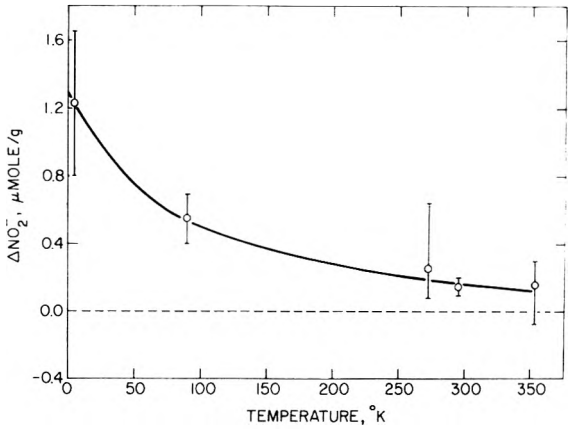

Figure 2. The increase in ΔNO_2^- (ceric–Shinn) as a function of temperature (absorbed dose = 1.4×10^{20} eV/g).

TABLE II: Reducing Properties of Various Irradiated Salts (Absorbed Dose = 10 × 10^{20} eV/g)

Salt	ΔNO_2^- (equivalent), mol of NO_2^-/g
NaCl	0.049
MgO	0.52
SiO_2	1.05
Na_2SO_4	0.00

nealed at 200°, although appreciable thermal decomposition occurred, analysis of these samples by the two methods gives identical results indicating that the substance or substances that gave rise to the difference in equivalent nitrite yields had disappeared during the heating. Subsequently, samples irradiated at −196° to an absorbed dose of 1.4 × 10^{20} eV/g were annealed at different temperatures for 18 hr and the annealed samples analyzed by the two methods (see Figure 3). These results are plotted as ΔNO_2^- (ceric–Shinn) *vs.* temperature. As can be seen there is a rather abrupt decrease in ΔNO_2^- at a temperature of about 160°. The abrupt character of this plot resembles a threshold event, such as a fairly deep electron trap rather than a chemical reaction or some diffusional process. Another group of samples irradiated at −196° to an absorbed dose of 1.2 × 10^{20} eV/g was heated at 200° for varying times (see Figure 4). As can be seen appreciable annealing occurs within the first hour.

Irradiated $NaNO_3$ (as well as KNO_3 and $CsNO_3$) has a slight yellow color which is intensified if the irradiation is done at low temperatures. The properties of this color band as observed by Pringsheim appears to have much in common with the reducing species identified chemically as ΔNO_2. For example, Pringsheim observed that the color band was bleached when the crystal was heated for 30 min at 200°, however, the color center was stable at 100°. This is consistent with the observations reported here. Pringsheim observed that at room temperature the color center intensity increases very rapidly with absorbed dose and then levels off, whereas at −196° the color center intensity rises more slowly with absorbed dose but reaches a value more than twice that found at room temperature. This is consistent with the chemical observations, *i.e.*, at room temperature ΔNO_2^-, after the first few minutes of irradiation, reaches its peak value and then remains relatively constant, whereas at liquid nitrogen temperatures ΔNO_2^- appears to reach its peak value more slowly than at room temperature; however, this value at −196° is about 3–4 times greater than at room temperature (see Figure 1). Pringsheim also observed that the color band formed when $NaNO_3$ was irradiated at −196°, could be reduced in intensity if the sample were subsequently irradiated at room temperature. Table III shows the decrease in ΔNO_2^- when samples of $NaNO_3$, irradiated at −196° are subsequently irradiated at room temperature. Another property observed by Pringsheim was that the color band was readily bleached by light from a high-intensity mercury arc lamp. Samples of $NaNO_3$ irradiated at −196° and ground to a fine mesh were placed in an open beaker and bleached at liquid nitrogen temperature and at room temperature. These results are summarized in Table IV. As can be seen a substantial reduction in ΔNO_2^- was achieved. Complete reduction in ΔNO_2^- did not occur because of the conditions of the experiment, *i.e.*, lack of penetration of the light plus poor stirring of the powders. In these experiments, however, it was virtually impossible to prevent photochemical decomposition. This is to be expected since the color band at 330 μm is very close to one of the nitrate bands at 300 μm.

TABLE III: Decrease in ΔNO_2^- of $NaNO_3$ Irradiated at 196° (Absorbed Dose = 1.7² × 10^{20} eV/g) as a Result of Post-Irradiation at Room Temperature

Absorbed dose, eV/g	ΔNO_2^-, mol of NO_2^-/g
0.00	0.72
2.6 × 10^{20}	0.37

TABLE IV: Decrease in ΔNO_2^- in $NaNO_3$ Irradiated at −196° (Absorbed Dose = 1.4 × 10^{20} eV/g) Bleached with Mercury Arc Lamp

Bleaching time, hr	Temp, °C	ΔNO_2^-, mol of NO_2^-/g
0.00	−196	0.68
0.5	−196	0.45
1.5	−196	0.14
4.0	25	0.49
8.0	25	0.34
20.0	25	0.22

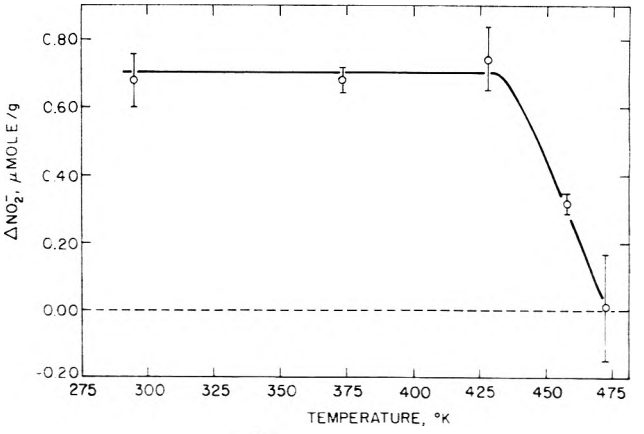

Figure 3. Change in ΔNO_2^- as a result of annealing for 18 hr at different temperatures.

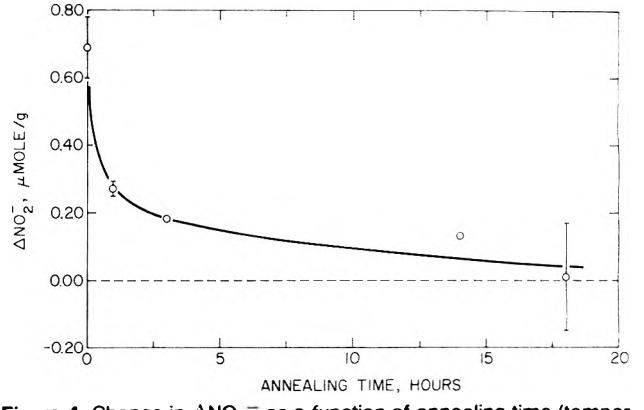

Figure 4. Change in ΔNO_2^- as a function of annealing time (temperature = 200°).

The lack of good reproducibility (at low absorbed doses) using the ceric method is readily explained for the determination of NO_2^- in these experiments if we assume that we are indeed determining color center concentration in addition to nitrite ion concentration. The production of color centers in $NaNO_3$, unlike nitrite ion production, is not quantitatively predictable, *i.e.*, the color center concentra-

tion will vary somewhat with different crystals and hence so will ΔNO_2^-.

It appears therefore that ΔNO_2^- is a measure of the color center concentration and that the reduction of ceric ion is another chemical method of determining these centers. The question remains, however, as to the nature of the color center. The center described by Pringsheim has its maximum at 335 mμ and cannot reasonably be attributed to either NO_2 or NO in the lattice, since the absorption spectra of these molecules when observed in an inert matrix[25,26] are very far removed from 335 mμ. Pringsheim attributes the color center to an electron trapped in the vicinity of the nitrite ion.

We do not think that the color center can be an electron trapped in an anion vacancy as are, for example, the color centers observed in the alkali halides. In these latter salts the color centers are easily annealed at room temperature and below whereas in $NaNO_3$ a minimum temperature of about 160° is required. We are inclined to accept the view that the color center is an electron trapped in the vicinity of a nitrite ion; however, it must be very tightly bound and is more likely associated with a relatively stable molecular species. The results of Zeldes and Livingston[16a] clearly indicate that the nitrite ion is the precursor of the NO_2 molecule observed in the esr spectra at low temperatures and that the actual formation of nitrite ion requires some thermal activation, *i.e.*, at liquid nitrogen temperature the nitrite ion is not formed but rather some intermediate which, when the irradiated sample is warmed to room temperature, produces nitrite ion.

The color center, we believe, is associated with this intermediate. Since the concentration of this species at room temperature is relatively high, ~0.15 μmol/g, it cannot be NO_3, NO_2^{2-}, or NO_3^{2-} since in this concentration range these species are easily detected by paramagnetic resonance techniques. We suggest that the center is an O^- or an O_2^- associated with the nitrite ion/or ions formed simultaneously in some sort of a complex.

References and Notes

(1) Research performed under the auspices of the U.S. Atomic Energy Commission Contract No. AT(40-1)-3660
(2) To whom correspondence should be addressed.
(3) For a general review of nitrate radiolysis see, E. R. Johnson "Radiation Induced Decomposition of Inorganic Molecular Ions," Gordon and Breach, New York, 1970.
(4) J. Cunningham, *J. Phys. Chem.*, **67**, 1772 (1963).
(5) M. B. Shinn, *Ind. Eng. Chem., Anal. Ed.*, **13**, 33 (1941).
(6) J. Cunningham, *J. Phys. Chem.*, **70**, 30 (1966).
(7) J. Cunningham, *Int. J. Phys. Chem. Solids*, **23**, 843 (1962).
(8) J. Cunningham, *J. Phys. Chem.*, **66**, 770 (1962).
(9) S. Kaucic and A. G. Maddock, *Trans. Faraday Soc.*, **65**, 1083 (1969).
(10) W. B. Ard, *J. Chem. Phys.*, **23**, 1967 (1955).
(11) B. Bleany, W. Hayes, and P. M. Llewellyn, *Nature (London)*, **179**, 140 (1957).
(12) H. Zeldes, "Paramagnetic Resonance," Vol. II, Academic Press, New York, N.Y., 1963, p 764.
(13) D. Shoemaker and E. Boesman, *C. R. Acad. Sci.*, **252**, 2099, 2865 (1961).
(14) R. Adde and P. Petit, *C. R. Acad. Sci.*, **256**, 4682 (1963).
(15) See also ref 1, p 80.
(16) (a) H. Zeldes and R. Livingston, *J. Chem. Phys.*, **35**, 563 (1961); **37**, 3017 (1962); (b) See W. G. Burns and T. F. Williams, *Nature (London)*, **175**, 1043 (1955); J. G. Rabe, B. Rabe, and A. O. Allen, *J. Phys. Chem.*, **70**, 1098 (1966); E. A. Roja and R. R. Hentz, *ibid.*, **70**, 2919 (1966).
(17) R. W. Holmberg, personal communication.
(18) H. Pogge, Thesis, Stevens Institute of Technology, Hoboken, N.J.; University Microfilm, Ann Arbor, Mich., No. 68-16, 222.
(19) E. Ladov and E. R. Johnson, *J. Amer. Chem. Soc.*, **91**, 7601 (1969).
(20) G. Hennig, R. Lees, and M. Matheson, *J. Chem. Phys.*, **21**, 664 (1953).
(21) T. H. Chen and E. R. Johnson, *J. Phys. Chem.*, **66**, 2249 (1962).
(22) P. Pringsheim, *J. Chem. Phys.*, **23**, 369 (1955).
(23) E. Hutchinson and P. Pringsheim, *J. Chem. Phys.*, **23**, 1113 (1955).
(24) J. Cunningham, *J. Chem. Phys.*, **41**, 3522 (1964).
(25) G. W. Robinson, M. McCarthy, and M. C. Keelty, *J. Chem. Phys.*, **27**, 972 (1957).
(26) H. Brion, C. Moser, and M. Yamazaki, *J. Chem. Phys.*, **30**, 673 (1959).

Kinetics of Malonic Acid Pyrolysis in Alkali Halide Matrices[1,2]

L. A. Cosby and G. L. Humphrey*

Department of Chemistry, West Virginia University, Morgantown, West Virginia 26506

(*Received June 12, 1974*)

The thermal decomposition of malonic acid dispersed in alkali halide pressed pellets has been studied. The study was made by heating the pellets and observing the changes in absorption of several infrared bands of the reactant and products. The reaction was found to be first order with respect to disappearance of malonic acid with an apparent rate constant of $k(\text{sec}^{-1}) = 6.0 \times 10^9 \exp[(-23{,}400 \pm 300)/RT]$. The effects of changing the matrix material are discussed.

Introduction

Although several studies[3-7] have been carried out on the kinetics of the thermal decomposition of pure malonic acid in the molten state, none appear to have been reported for the reaction in solid solution. By employing a technique similar to that of Bent and Crawford,[8] we have made an infrared spectroscopic study of the thermal decomposition of malonic acid in the solid state at, or above, its melting point. The reactant was incorporated in an alkali halide solid matrix and quantitative kinetic results were obtained by observing the change in infrared absorption of reactant and products as a function of time. Many investigations of the decarboxylation of malonic acid in numerous different solvents have been reported.[9] From the proposed mechanisms for the reactions in solution it appeared that a study of the reaction in a highly ionic solid medium would be beneficial.

Experimental Section

Chemicals. Malonic acid was obtained from K and K Laboratories, Plainview, N.Y., and recrystallized from acetone at low temperatures. The crystals were ground to a fine powder and placed under reduced pressure at room temperature for several hours. Analysis showed the material to be 99.9 ± 0.1% malonic acid with a melting point of 136°.

The alkali halides were obtained from Brinkman Instruments, Inc., Westbury, N.Y., and were manufactured by E. G. Merck, Darmstadt, Germany as Suprapur or Ultrapur.

Instruments. The constant temperature bath was a Fisher unitized bath, specially insulated, and filled with UCON fluid 50-HB-280-X obtained from Union Carbide Corp., Charleston, W. Va. Bath temperatures could be maintained by a mercury expansion controlled electronic relay system to ±0.05°. A wooden rack containing holes for the reaction tubes was constructed for the bath to facilitate placing the samples in the bath.

The alkali halide pellets were formed under 20,000 psi gauge pressure in a Carver hydraulic press using a 25 × 6 mm rectangular die manufactured by Beckman Instruments Co.

A Mettler semimicrobalance accurate to 5×10^{-5} g was used to weigh samples.

Spectra were obtained on a Beckman IR-12 spectrometer calibrated periodically by means of the polystyrene spectrum, or by scanning the atmospheric absorption in single beam mode. Absorption frequencies reported in this work are considered to be accurate to ±1.0 cm^{-1}. Absorbance values could, in general, be reproduced to better than ±0.002 absorbance unit.

Pellet Preparation. Pellets were prepared both from the commercial alkali halides as received and from the commercial salts ground to a very fine powder in agate and evacuated for several days at 250°. In the case of pellets pressed from predried salts, the salts were mixed with finely ground malonic acid in a rotating vacuum type evaporator which was simultaneously magnetically stirred. The die was filled in a dry box, closed, and sealed by applying pressure and then evacuated before pressing the pellet. Dry air was used to bring the pressure inside the die back to atmospheric after pressing the pellet. For the preparation of pellets from salts that were used as received, the die and salts were treated as above in a constant humidity room maintained at about 40% relative humidity.

Kinetics. In preparation for a kinetic run, 10 to 15 pellets were prepared as described above and weighed to the nearest 5×10^{-5} g, and the infrared spectrum of each was obtained. Absorbance values for the bands were determined by the baseline technique and the values from the initial spectra were used to establish the zero time absorbance values for each pellet. The pellets were then placed in individual sample tubes in the constant temperature bath. Each pellet was removed from the bath after elapse of the chosen specific time for the kinetic run, cooled to room temperature either in a desiccator, or in a constant humidity room, and the spectrum again obtained.

Timing for a kinetic run was made by means of a stop watch which was allowed to run continuously throughout the time period.

In order to obtain good spectra after heating a pellet, it was necessary to repress the pellet. Heating of the pellets caused them to become opaque and expand slightly (possibly due to CO_2 evolution) so that the edges of the pellet had to be sanded in order to replace it in the pellet die. The resulting weight loss from the repressing procedure necessitated correction of the absorbance values obtained after repressing a disk. By preparing a large number (50) of different weight pellets from a single mixture of malonic acid and alkali halide and obtaining absorbance values for each of the bands used in our study, it was determined that absorbance was a linear function of pellet weight. Furthermore, it was found that the intercept of a plot of absorbance *vs.* pellet weight was at the origin. These facts allowed the use of a simple weight ratio for correcting absorbance values to a value for a standard pellet weight, chosen as 0.20000 g. The average variance of the absorbance of the bands studied in this work as obtained from five different kinetic runs on the same bulk pellet mixture was 0.87×10^{-3} absorbance unit.

Results

By preparing pellets from mixtures of malonic acid and alkali halides in varying concentration ratios and comparing their spectra it was found that all major absorption bands in the malonic acid spectrum (3000, 1700, 1440, 1310, 1220, 1175, 900, 760, 650 cm^{-1}) obeyed Beer's law over the concentration range (0.05–1.0 wt %) employed for the pellets.

In the initial stages of a kinetic run, the absorbance values for the pellets showed an increase. Since the working temperatures were generally above the melting point (136°) of malonic acid, we attributed the initial increase in absorbance to malonic acid becoming more uniformly dispersed throughout the alkali halide matrix. Some workers[10] have resolved the problems associated with abnormal initial changes in absorbance by subjecting pellets to an annealing process, but such a procedure was impractical in our work since temperatures as low as 80° were found to bring about thermal decomposition of malonic acid. Annealing at lower temperatures had no effect on the initial absorbances of the pellets. The inability to anneal the pellets did not create major problems since the time required for the absorbance to reach maximum values was approximately 2 min at 140°, after which time the absorbance values decreased in a regular fashion reflecting decomposition of the malonic acid. It may be noted that the time required for the absorptions to reach a maximum was approximately equal to the time required for the pellet to reach bath temperature as measured by a thermocouple imbedded in some pellets.

Since absorbances of the bands under study were found to be proportional to concentrations of malonic acid present, the order of reaction was determined from plots of the logarithm of the change in absorbance per unit of time for a particular band *vs.* the logarithm of the absorbance for that band. The slope of the line obtained from such plots is equal to the order of the reaction. Applying this method to the 3000-cm^{-1} band gave reaction orders of 1.18 at 145°, 1.15 at 161°, and 1.08 at 167°. The other bands gave values for the order of the reaction ranging from 0.59 to 1.4 with the average value for all bands being 0.97 ± 0.10.

Rate constants were determined by plotting the logarithm of the ratio of the initial absorbance values to the absorbance values at time, t, each corrected to a standard weight pellet of 0.20000 g, *vs* time, t. Five of the nine absorption bands studied for malonic acid gave good straight line plots from which rate constants could be determined, and the results are presented in Table I. The placement of

TABLE I: Malonic Acid Decomposition Rate Constants (units = 10^{-3} sec^{-1})

Temp, °C ± 0.1°	3000 cm^{-1}	1700 cm^{-1}	1440 cm^{-1}	1220 cm^{-1}	900 cm^{-1}
	Potassium Bromide Matrix				
138.9	1.02	1.05	1.21	1.10	0.81
142.0	1.54	1.39	1.16	1.75	1.15
144.9	2.23	2.11	1.60	2.08	
149.0	2.38	2.39	2.56	2.61	
153.2	2.83	2.59	2.96	3.37	3.92
158.1	4.67	5.04	5.12	4.24	5.18
161.0	5.20	4.98	4.98	5.48	6.24
167.0	7.01	8.53	6.45	9.41	
	Rubidium Bromide Matrix				
158.5	4.65	4.20	4.21	4.28	

the lines from which the slopes (rate constants) were determined was made by a least-squares computer program which was a modification of the LSKIN1[11] program. The average variance of absorbances for the absorption bands of malonic acid used in determining the rate constants, which is based on five kinetic runs made from the same bulk pellet mixture, was 1.0×10^{-3} absorbance unit. This results in an uncertainty of 10% in the rate constant values.

The first-order rate constants for the decomposition of malonic acid in a rubidium bromide matrix gave results comparable to those obtained in the potassium bromide matrix. The spectra for malonic acid obtained in other matrix materials (NaCl, NaBr, NaI, KCl, KI, CsCl, CsBr, CsI, RbCl, RbI) were indicative of reaction of malonic acid with the matrix material.[12]

The 900-cm^{-1} absorption band in some instances (144.9, 149.0, and 167.0° in KBr and 158.5° in RbBr) gave such random points that no sensible least-squares fit for the data could be found.

From the experimentally determined rate constants and their corresponding temperatures, the thermodynamic parameters shown in Table II were calculated on the basis of the absolute reaction rate theory equation, k = (constant)(T) $\exp(\Delta S^{\ddagger}/R)$ $\exp(-\Delta H^{\ddagger}/RT)$ and $\Delta G_T^{\ddagger} = \Delta H^{\ddagger} - T\Delta S^{\ddagger}$. A comparison of values obtained by other investigators in other media is also presented in Table II. A plot of the negative logarithm of T/k *vs.* $1/T$ based on the absolute reaction rate theory equation, from which $\Delta S^{\ddagger}$ (intercept) and $-\Delta H^{\ddagger}$ (slope) were determined for the five absorption bands of malonic acid used in this work, is presented in Figure 1.

The activation energies and frequency factors for the bands studied are summarized in Table III.

Discussion

The thermal decomposition of malonic acid in potassium bromide and in rubidium bromide, as in some other media,[14,15] appears to be a straightforward decarboxylation to yield carbon dioxide and acetic acid. The infrared spectrum of carbon dioxide trapped in the pellets was evident in the early stages of heating and the infrared spectra of the pellets in the final stages of heating showed only acetic acid to be present.

Fraenkel, *et al.*,[16] have proposed a mechanism for the thermal decarboxylation of acids which appears to have been generally accepted. The mechanism involves the formation of an activated complex between an electrophilic carbonyl carbon atom and a nucleophilic center in the solvent medium, illustrated as follows

TABLE II: Activation Parameters for the Thermal Decomposition of Malonic Acid in Several Media

Medium	$-\Delta H^{\ddagger}$, kcal/mol	$\Delta S^{\ddagger}$, eu/mol	$-\Delta G^{\ddagger}$ at 135°, kcal/mol
1-Butanol[a]	27.2	−4.4	29.0
1-Hexanol[a]	26.0	−7.6	29.1
2-Ethylhexanol-1[a]	24.8	−10.4	29.05
Diisobutylcarbitol[a]	24.8	−10.7	29.16
Cyclohexanol[a]	23.0	−15.0	29.13
Acetanilide[a]	19.85	−22.66	29.1
Molten malonic acid[b]	35.8	+11.9	31.0
Malonic acid in KBr[c]	22.8 ± 1	−17.4 ± 1	29.8 ± 1

[a] Reference 13. [b] Reference 15. [c] This work.

TABLE III: Frequency Factor and Activation Energy for Malonic Acid Decomposition in Potassium Bromide

Ir band frequency, cm^{-1}	Activation energy, kcal/mol	Frequency factor, sec^{-1}
3000	23.0	2.0×10^{9}
1700	23.2	1.2×10^{10}
1440	23.6	3.9×10^{9}
1220	23.9	6.2×10^{9}

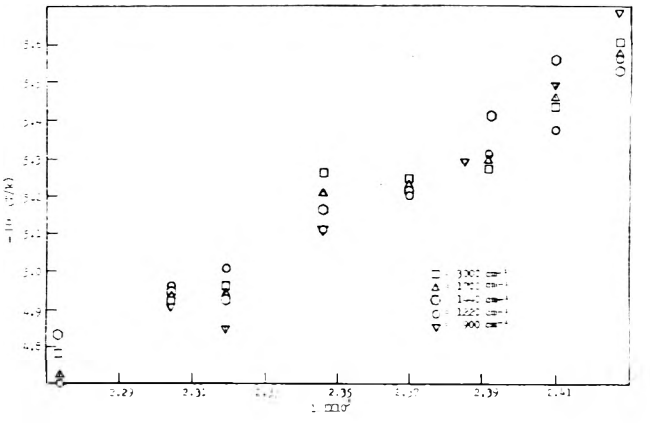

Figure 1. Combined enthalpy of activation plot for the thermal decarboxylation of malonic acid in KBr at temperatures from 138.9 to 167.0°.

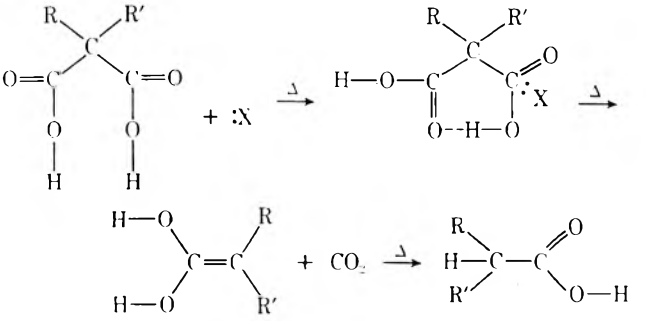

Support for the above mechanism is found in the fact that $\Delta H^{\ddagger}$ decreases with solvent basicity, and there is a linear dependence of the rate of decarboxylation upon concentration of a strong amine base, such as pyridine,[16] the reaction rate dependence disappearing at a 1:1 mole ratio of base to malonic acid, indicating a bimolecular reaction.

Kenyon and Ross[17] observed that unsymmetrically disubstituted malonic acid did not produce optically active di-

substituted acetic acid, which is further support for the above mechanism. The production of a racemic mixture of disubstituted acetic acid would require formation of a carbon–carbon double bond at some point in the reaction mechanism.

Blades and Wallbridge[18] observed that deuteriomalonic acid exhibits no kinetic isotope effect. The absence of a kinetic isotope effect suggests that the rate-determining step in the decarboxylation is the breaking of a carbon–carbon bond rather than the formation, or dissociation, of a hydrogen bond. Loudon, *et al.*,[7] also conclude from $^{13}C/^{12}C$ isotopic effects that both carbonyl groups must be involved in the transition state, and that bond breaking is almost complete between the leaving carbon and the central carbon atom. These workers also investigated an oxygen isotope effect by measuring the variation with per cent reaction in the ^{18}O content of the CO_2 released. Since no variation in ^{18}O content was found, bond breaking and bond making in the transition state is again suggested.

Clark[19] has shown that when $\Delta H^{\dagger}$ is plotted against $\Delta S^{\ddagger}$ for a given series of reactions in various solvents, the result is a straight line of slope T, the isokinetic temperature. Other workers[20] have pointed out limitation in the use of isokinetic temperatures for drawing valid conclusions, and have established requirements which must be met before valid conclusions can be drawn. The data obtained by Clark[21] appear to satisfy the requirements, and for the solvents studied thus far for the decarboxylation of malonic acid, $\Delta H^{\ddagger}$ and $\Delta S^{\ddagger}$ values, when plotted, form a straight line with a slope of 422 K (149°) for the isokinetic temperature. The $\Delta H^{\ddagger}$ and $\Delta S^{\ddagger}$ values for the decarboxylation of molten malonic acid also fall on the same straight line as those for various solvents including the solid alkali halides used in this work. Apparently the same mechanism of reaction prevails in each case, and the fact that the $\Delta H^{\ddagger}$ value for the decarboxylation of malonic acid is significantly lower in potassium bromide than for molten malonic acid could be the result of the activation effect of the bromide ion in the alkali halide medium.

A comparison of the reaction rates for the decarboxylation of malonic acid in KBr to those in RbBr reveals no significant differences. This might be expected if the mechanism does involve the nucleophilic halide ion. Investigation of the effect of the anion upon the reaction rate would be most meaningful in this case, but is impractical due to the interfering side reactions taking place between malonic acid and other alkali halides.[12]

An interesting observation made in this research was that solid malonic acid undergoes decarboxylation at measurable rates well below its melting point. We found that malonic acid decomposes slowly in a KBr matrix at 80° and the reaction half-life is approximately 6 weeks. This temperature is well below the reported solid state phase transition temperaure (130°),[22,23] and therefore it appears that malonic acid can decompose from the β phase as well as the α phase.

The multipellet technique developed for the kinetic studies in this work has enabled us to collect data for the decarboxylation of malonic acid at temperatures considerably higher than were previously possible, and allows the study of reactions with half-lives as low as 4 min or less without significant problems.

Acknowledgment. We are indebted to the National Science Foundation for funds to purchase the Beckman IR-12 spectrophotometer, and to Dr. G. A. Hall for many helpful discussions.

References and Notes

(1) Abstracted in part from the Ph.D. Dissertation of L. A. Cosby, West Virginia University, 1969.
(2) This work was supported by the National Aeronautics and Space Agency, Grant No. NLG-4900-001, formerly NsG-533.
(3) C. N. Hinshelwood, *J. Chem. Soc.*, **117**, 156 (1920).
(4) J. Laskin, *Trans. Sib. Acad. Agr. For.*, **6**, 7 (1926).
(5) J. Gyore and M. Ecet, *J. Therm. Anal.*, **2**, 397 (1970).
(6) A. S. Wipf, *Diss. Abstr., Int. T*, **31**, 4623 (1971).
(7) A. G. Loudon, A. Maccoll, and D. Smith, *J. Chem. Soc., Faraday Trans. 1*, **69**, 894 (1973).
(8) H. A. Bent and B. Crawford, *J. Amer. Chem. Soc.*, **79**, 1973 (1957).
(9) L. W. Clark, "Decarboxylation Reactions," in "The Chemistry of Carboxylic Acids Esters," S. Patai, Ed., Interscience, New York, N.Y., 1969, pp 589–622, Chapter XII.
(10) K. O. Hartman and I. C. Hisatsune, *J. Phys. Chem.*, **69**, 583 (1965).
(11) C. E. Detar and D. F. Detar, Program 80, Quantum Chemistry Program Exchange, Indiana University, 1967.
(12) L. A. Cosby and G. L. Humphrey, to be submitted for publication.
(13) L. W. Clark, *J. Phys. Chem.*, **66**, 125 (1962).
(14) L. W. Clark, *J. Phys. Chem.*, **71**, 302 (1967).
(15) L. W. Clark, *J. Phys. Chem.*, **67**, 138 (1963).
(16) G. Fraenkel, R. L. Belford, and P. E. Yankwich, *J. Amer. Chem. Soc.*, **76**, 15 (1954).
(17) J. Kenyon and W. A Ross, *J. Chem. Soc.*, 3407 (1951).
(18) A. T. Blades and M. G. H. Wallbridge, *J. Chem. Soc.*, 792 (1965).
(19) L. W. Clark, *J. Phys. Chem.*, **68**, 3048 (1964).
(20) R. C. Petersen, J. H. Markgraf, and S. D. Ross, *J. Amer. Chem. Soc.*, **83**, 3819 (1961).
(21) L. W. Clark, *J. Phys. Chem.*, **71**, 2597 (1967).
(22) W. W. Wendlandt and J. A. Hoiberg, *Anal. Chem. Acta*, **28**, 506 (1963).
(23) The temperature of the phase change was determined by differential thermal analysis[22] and is probably about 25–30° too high judging from our infrared spectral studies where we detected the phase change by means of reversible changes in the absorbtion spectrum in going through the transition temperature. From a comparison of the temperature of fusion for malonic acid as determined by the standard melting point technique (136°) and that determined by differential thermal analysis (160°),[22] we also conclude that the reported temperature of the phase change is too high. Our spectral studies of malonic acid in alkali halides show the β to α phase change occurring at about 90°.

Alternative Model for Nonstoichiometry in Uranium Hydride

J. B. Condon

Union Carbide Corporation, Nuclear Division, Oak Ridge, Tennessee 37830 *(Received January 21, 1974; Revised Manuscript Received September 27, 1974)*

Publication costs assisted by Union Carbide Corporation, Nuclear Division

A model is presented to account for the nonstoichiometry and observed hydrogen overpressures for uranium hydride. The model assumes that vacancies in the hydrogen lattice are disfavored when the hydride is contaminated by oxygen and favored when certain metallic contaminants are present. This model explains the literature data as well as, if not better than, the model involving vacancy–vacancy attractions. It is also better than the pure vacancy model. The presented model accounts for the observed hysteresis in the hydrogen pressure over uranium hydride and explains the first-order kinetics in uranium observed for hydriding.

I. Introduction

This article reconsiders the basic model used to explain the nonstoichiometry of uranium hydride and the observed hydrogen pressures at elevated temperatures. This reconsideration is prompted by the need to resolve a conflict that exists in the literature and to present a more consistent view of the kinetics and thermodynamics of this material. This consistency must be particularly applicable to recent findings with respect to contaminant effects.

The literature presents considerable contradictory data on the equilibrium hydrogen pressure of the U–UH_3–H_2 system. Plateau pressure measurements by several authors are inconsistent. The most striking inconsistency, however, is in the full-phase diagram as presented by Libowitz and Gibb[1] and by Chevallier, *et al.*[2] The vacancy–vacancy model by Libowitz[3] does not predict a critical temperature at 830° described by the latter authors. This critical temperature is also inconsistent with the two-phase equilibrium pressures observed by Mallett and Trzeciak[4] and reported to temperatures as high as 1400°. To resolve this conflict, additional considerations must be built into the statistical model for UH_3.

A further consideration is the recent findings of the effects of oxygen on both the kinetics[5] and thermodynamics[6] of this system. Experience with the kinetics of the uranium–hydrogen reaction cautions one to consider contaminant interactions, particularly interactions with oxygen. With sufficient oxygen contamination, the uranium–hydrogen reaction may actually cease far below stoichiometry. Oxygen background pressures as low as 10^{-7} Torr ($\sim 3 \times 10^{-5}$ Pa) have profound effects on the kinetics and presumably the thermodynamics of the system. In a report, Meusemann and Von Erichsen[6] conclusively demonstrate an effect of oxygen contamination on the thermodynamics of UH_3. Therefore, special attention is given to the effects of contamination in the present statistical model. This model is, therefore, quite similar to that used[5] to explain kinetics of the system as applied to the uranium side of the phase diagram. It accounts for the experimental data by Libowitz and Gibb[1] without assuming hydride vacancy–vacancy attractions.[3] It can also account for the data by Chevallier, *et al.*, with the assumption of slight metallic contamination.

The presented model by-passes some of the more questionable aspects of previous theories. One aspect is the assumption that at least the geometry of the metal lattice is unaffected by addition of hydrogen. This assumption allows the use of the van der Waal's "equal areas" criterion to generate two phases.[7,8] It is obvious, however, that the transformation from α-uranium to β-uranium hydride changes this lattice in a gross fashion; the change is not isomorphous. The present model, therefore, assumes α-uranium and β-uranium hydride are completely different phases. This not only frees the derivation from the assumption of vacancy–vacancy attractions to obtain phase separation (with a calculated critical point of ~1413°) but also allows stoichiometry for the hydrogen terminal solubility and the point of the maximum concentration of vacancies to be unsymmetrical with respect to the center of the phase diagram. Furthermore, in contrast to the model by Libowitz, the present treatment does not require that the energy of formation of a vacancy to vary with temperature.

The model by Libowitz is prominently used to substantiate the vacancy–vacancy attraction theory of ionic crystals as formulated by Anderson.[9] The model proposed in this paper, however, assumes no vacancy–vacancy attraction. Experimentally, there are enough conditions that may be varied to make a distinction. It is important to resolve this dilemma. However, resolution of this matter must await the accumulation of data at higher temperatures and pressures.

The concept of a mixed phase, with trace oxide ions behaving similarly to the hydride ions in the β-UH_3 phase, is central to the proposed model. In terms of the U–β-UH_3–UO_x ternary phase diagram (Figure 1), this means that the single β-UH_3 phase not only extends toward the uranium corner of the diagram but also toward the uranium oxide corner as well. This extension of the single phase for a finite distance from the corner point is *always* implied, even if it is much too small to be measured experimentally. To assume otherwise would rule out the concept of solubility.

II. Theory

Contaminant Modified. A. Symbols. The following symbols will be used in this discussion.

E_I	energy to form interstitial
E_V	energy to form vacancies
E_{VV}	energy of vacancy–vacancy attractions

E_X	energy released in replacing a hydride ion by an oxide ion in the lattice
k	Boltzmann's constant
K_1, K_2, K'	temperature dependent constants
m	stoichiometric number (*i.e.*, UH_m)
N	number of hydrogen lattice positions (*i.e.*, three times Avogadro's number per mole UH_3)
N_D	number of interstitial positions
N_I	number of interstitial hydrogens
N_S	number of sites the oxide ion can occupy
N_V	number of hydrogen vacancies
N_X	number of oxide ions replacing hydrogen
P_{H_2}	hydrogen pressure
P_{O_2}	oxygen pressure during hydride formation
q	a positive number equivalent to average number of near-by hydride lattice positions affected by the presence of a contaminant (*e.g.*, oxygen atom) such that vacancies will be unfavored (if favored q is negative)
R	gas constant (8.314 J mol^{-1} K^{-1} used here) (1 cal ≡ 4.184 J)
s	full stoichiometric number according to Libowitz
T	absolute temperature
Z_H	canonical partition function for hydrogen in the lattice
Z_M	canonical partition function for uranium in the lattice
Z_X	canonical partition function for oxygen in uranium hydride lattice
α	proportionality of the number of interstitial sites to the number of hydride ion positions
δ	negative deviation from stoichiometry
θ	ratio of oxide ion-to-hydrogen lattice positions
λ_H	activity of hydrogen
λ_M	activity of uranium
λ_X	activity of oxygen
ξ	a variable defined by eq 14
Ξ	grand partition function

B. Vacancy Model Modified by Oxygen Contamination. The model presented to account for the effect of oxygen on the kinetics of the hydrogen–uranium reaction[5] assumes an interference by oxygen within the crystal structure of the metal. Hydrogen, occupying interstitial positions, diffuses rapidly in the metal before nucleation and growth of the β-phase uranium hydride. Oxygen or other anions compete for these interstitial sites and modify the kinetics considerably. The present model, which describes the hydride phase, makes a similar assumption about the role of oxygen in the crystal structure. This assumption is that oxygen in trace quantities and at a low activity can substitute for hydrogen in the anionic lattice positions and subsequently can affect the behavior of other hydride sites in the immediate vicinity.

In the case of the uranium–hydrogen reaction, oxygen interstitials are established very slowly. This means that during the initial hydriding of metallic uranium the activity of the oxide ions is not equilibrated with the surroundings. It is reasonable to assume the same to be true for the measurements of Libowitz and Gibb. The greatest contamination by oxygen probably occurs during the creation of the hydride in the broad plateau region of the phase diagram. Knowing when this concentration is established is important in determining the energy of replacement of a hydrogen atom by an oxygen atom, since the replacement energy and the oxygen activity appear in the same mathematical term in the present statistical model.

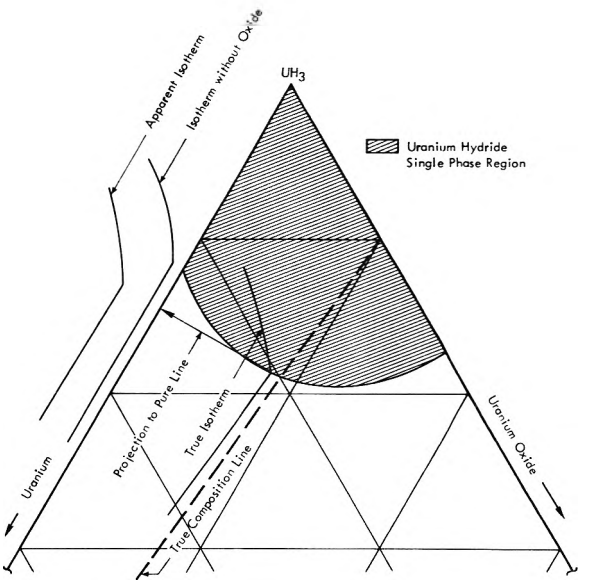

Figure 1. Schematic of the hydride corner of the uranium–β-uranium hydride–uranium oxide ternary diagram illustrating a region for the hydride phase. Isotherms drawn illustrate the uncontaminated *vs.* contaminated case. The true contaminated isotherm which occurs at the dashed line labeled true composition line is shown projected back to the U–β-UH_3 axis. This projection is labeled apparent isotherm and is compared to the isotherm that would be obtained in the absence of contamination.

It is reasonable to assume that the oxide ion in the lattice will affect the near-by hydride ions such that no vacancies will occur in those positions. This assumption originates from the fact that if the crystal structure of the uranium hydride is fixed then the primary determiner of the local electron densities is the uranium atom positions. The proton positions would be a secondary factor given their lower potential compared to the uranium cores. Surely, vacancies would be a very minor influence considering their low concentration. Thus, the creation of a vacancy would disturb the electron density very little in the vicinity of the vacancy; however, the absence of the proton would create a high effective negative charge. This would be very unfavorable in the vicinity of the localized negative charge associated with an oxide ion. The number of affected near-by positions will be left here as an arbitrary constant q. It will also be assumed that an oxide ion replaces a single hydride ion in the hydride lattice. The statistical fit is not very sensitive to this latter assumption and an assumption of double substitution yields nearly the same result.

Using single substitution and the parameter q, the grand partition function may now be written

$$\Xi = \sum_N \sum_{N_I} \sum_{N_S} \frac{(N - qN_X)!}{N_V!(N - qN_X - N_V)!} \frac{(N_D)!}{N_I!(N_D - N_I)!} \times \frac{N_S!}{N_X!(N_S - N_X)!} (\lambda_H Z_H)^{(N - N_V + N_I - N_X)} (\lambda_M Z_M)^{N/3} \times (\lambda_X Z_X)^{N_X} e^{-[(N_V E_V + N_I E_I + N_X E_X)/kT]} \quad (1)$$

The maximum term in Ξ may be obtained with respect to both N_V and N_I since they are in equilibrium at the time of the measurement. The maximum term in Ξ with respect to N_X, however, is determined for a previous time when the activity of the hydrogen, λ_H, was at the plateau pressure.

For N_V and N_I then

$$\frac{\partial \ln [\text{max term } \Xi]}{\partial N_V} = 0 = -\ln N_V + \ln (N - qN_X - N_V) - \ln \lambda_H Z_H - (E_V/kT) \quad (2)$$

and

$$\frac{\partial \ln [\text{max term } \Xi]}{\partial N_I} = 0 = -\ln N_I + \ln (N_D - N_I) + \ln \lambda_H Z_H - (E_I/kT) \quad (3)$$

If $N_I \ll N_D = \alpha N$, where α is only dependent on the crystal structure, then

$$\frac{N_V}{N} = \left(\frac{[1 - q\theta]}{\lambda_H Z_H + e^{-E_V/kT}} \right) e^{-E_V/kT} \quad (4)$$

with $\theta = N_X/N$, and

$$\frac{N_I}{N} = \alpha \lambda_H Z_H e^{-E_I/kT} \quad (5)$$

The negative deviation away from stoichiometry of three hydrogen atoms to one uranium atom, δ, may be written as

$$\delta = \frac{N_V}{N} - \frac{N_I}{N} + \theta \quad (6)$$

The extra θ accounts for the fact that one hydride position is removed from consideration by the original oxide substitution. With substitution one obtains

$$\delta = \theta + \left(\frac{[1 - q\theta]}{\lambda_H Z_H + e^{-E_V/kT}} \right) e^{-E_V/kT} - \alpha \lambda_H Z_H e^{-E_I/kT} \quad (7)$$

To simplify one may write

$$K_1/P_{H_2}^{1/2} = e^{-E_V/kT}/\lambda_H Z_H \quad (8)$$

and

$$K_2 P_{H_2}^{1/2} = \alpha \lambda_H Z_H e^{-E_I/kT} \quad (9)$$

to give the conceptually easier form of the equation for fitting data with m being the stoichiometric number of

$$m = 3\left(1 - \theta - \frac{(1 - q\theta)K_1}{P_{H_2}^{1/2} + K_1} + K_2 P_{H_2}^{1/2}\right) \quad (10)$$

The constants K_1 and K_2 both have a temperature dependence in the usual sense. The latter, K_2, may be considered a solubility coefficient for interstitial hydrogen in the uranium hydride phase. Below 650° this solubility is probably low; therefore, for the fitting to Libowitz' data the last term of eq 10 will be dropped. (The equation corresponds to the chemical formula $UH_m O_\theta$.)

There is uncertainty in calculating θ since it is unknown what the oxygen pressure was during the hydride formation. It is likely however that the oxygen activity is determined by the presence of solid uranium oxide and would depend on temperature in an exponential fashion. Assuming constant oxygen activity, one may find the differential of the maximum term Ξ during the formation of hydride with respect to N_X

$$\frac{\partial \ln [\text{max term } \Xi]}{\partial N_X} = 0 = -q \ln (N - qN_X) + q \ln (N - qN_X - N_V) - \ln N_X + \ln (N_S - N_X) - E_X/kT + \ln \lambda_X Z_X - \ln \lambda_H' Z_H \quad (11)$$

Here the primes are used to emphasize that the variables relate to the time of hydride formation. Assuming $N_X \ll N_S$ one obtains

$$\frac{N_X(N - qN_X)^q}{N_S(N - qN_X - N_V)^q} = \frac{\lambda_X Z_X}{\lambda_H' Z_H} e^{-E_X/kT} \quad (12)$$

Here, λ_H' is the hydrogen activity for the plateau pressure. Since it is assumed here that each hydride ion position is an oxide substitution site, then $N_S = N$. The value for the oxygen contamination should be much less than N; therefore, the approximation $N_X \ll N_S$ is valid. (Actually, the highest value found for N_X was less than 0.1 N.) From eq 12 it follows that

$$\theta = (1 - \xi)^q \frac{\lambda_X Z_X e^{-E_X/kT}}{\lambda_H' Z_H} = \frac{(1 - \xi)^q P_{O_2}^{1/2} K'}{P_{H_2}'^{1/2}} \quad (13)$$

where

$$\xi = \frac{N_V'}{N - qN_X} = \frac{K_1}{P_{H_2}'^{1/2} + K_1} \quad (14)$$

The constant K' also has an exponential dependence on $1/T$. The variable ξ is dependent on K_1 as well as the hydrogen plateau pressure. The term ξ is a small number compared to 1, however, and can be obtained by successive approximations while obtaining K' and K_1. Equation 13 expresses the oxygen contamination as either a function of an oxygen background pressure or more generally as simply an activity, which could be due simply to the presence of a mixed-in oxide phase.

Results and Conclusions

A. Raw Data Fit. Least-squares computer fits were made using Libowitz's data for eq 10 and 13 with the successive approximations for ξ made as mentioned. The plateau pressures used (for P_{H_2}) were those given by Libowitz and Gibb.[1] A shallow minimum for q around 20 to 24 was found in the least-squares analysis. Since the exact value had little effect on the fit, a value of $q = 22$ is chosen here for presentation. The values found for K' and K_1 are given by

$$R \ln K_1 = 95.27 - 96\,202/T \quad (15)$$

$$R \ln K' = 83.9(131.8) - 142\,900/T + \tfrac{1}{2} R \ln P_{H_2}' - \tfrac{1}{2} R \ln P_{O_2} \quad (16)$$

where pressures are given in Pa (atm in parentheses). The values that are calculated by these formula for K_1, ξ, and θ are given in Table I.

Fits were also made using Libowitz' theory and his plateau pressure data which may be written in present terminology as

$$\ln P_{H_2} = \ln P_{H_2}' + 2 \ln \frac{m}{s - m} + \frac{2E_{VV}}{kT}\left(\frac{2m}{s} - 1\right) \quad (17)$$

(which corresponds to a limiting chemical formula of UH_s). A non-linear least-squares routine was also used to fit this equation. The values for E_{VV} and the five values for s were very close to those values stated by Libowitz but gave a slightly lower mean square than if one used the latter. Both fits are shown in Figure 2 and, as can be seen, both are fairly good. A statistical analysis is given in the Appendix which shows that the present model is better than the Libowitz' model and is much better than the pure vacancy model. The overall number of parameters presently used is (1) 2 for K', (2) 2 for K_1, and (3) 1 for q. To explain the variation in s, according to Libowitz, one must generate again five parameters. Therefore, that model by Libowitz

TABLE I: Values of Parameters Calculated from Eq 13–16 and Plateau Pressures Given by Libowitz and Gibb as a Function of Temperature

T, °C	$10^3 P'_{H_2}$, Pa	K_1	$K' P_{O_2}^{1/2} / P'^{1/2}_{H_2}$	ξ	θ
450	1.44	0.01064	0.0003605	0.008786	0.0002969
500	3.57	0.02995	0.01679	0.0156	0.001188
550	8.40	0.07437	0.006482	0.02502	0.003712
600	16.3	0.1664	0.02144	0.03957	0.08823
650	29.8	0.3412	0.06232	0.05883	0.01642

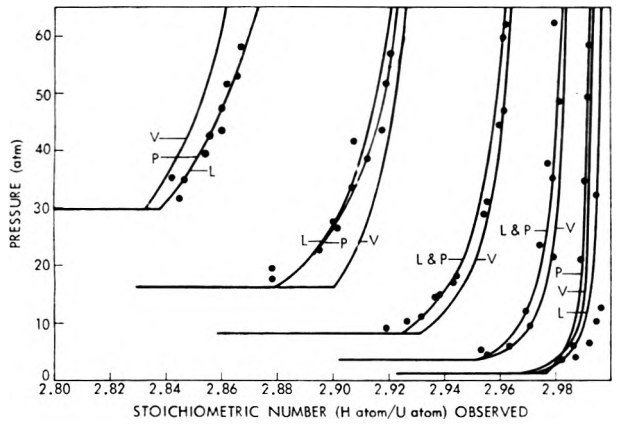

Figure 2. Pressure *vs.* stoichiometry for uranium hydride. Experimental points are compared to Libowitz' vacancy–vacancy attraction model (designated by L) and the present model with oxygen contamination (designated by P), and the pure vacancy model (designated by V). Isotherm temperature from left-to-right corresponds to 650, 600, 550, 500, and 450°.

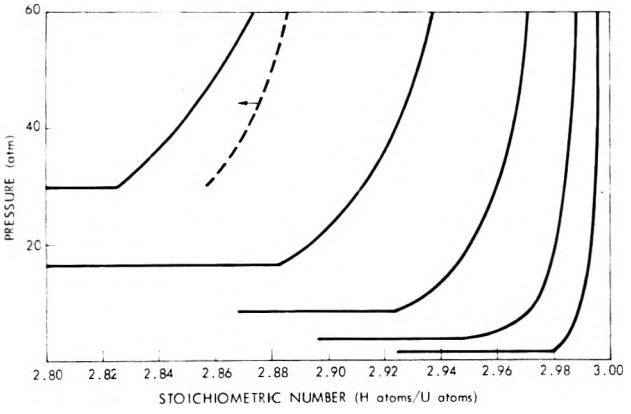

Figure 3. True phase diagram (portion) if oxide contamination model is correct. Dotted line shows effect oxygen contamination has on the filled hydride sites-to-uranium ratio to show the effect of oxygen solubility at 650°. Solid isotherm lines from left-to-right correspond to 650, 600, 550, 500, and 450°.

remains a six-parameter fit, since the parameter E_{VV} is considered as nearly constant. The problem involved with this latter model is the prediction of s as a function of temperature for extrapolation to high temperatures. This is needed in order to obtain the stoichiometry of the edge of the plateau on the hydride end of the phase diagram. If eq 10 represents a closer description of reality, then careful experimentation might eliminate oxygen contamination and thus eliminate θ. This would reduce eq 10 to a two-parameter model since q does not apply. Elimination of θ as a parameter out of eq 10 has a profound influence on the higher temperature isotherms. Figure 3 shows isotherms obtained by eliminating θ at the experimental temperatures.

B. Model Modified by Metal Contamination. It is well known that uranium and iron form eutectics and there is some solubility of iron in uranium.[10] The eutectics generated with UFe_2 and UFe_6 occur at 1080 and 726° and a peritectic decomposition occurs at 810°. The solubility of iron in pure uranium varies from 0.06 atomic per cent at 650° to approximately 2 atomic per cent at 810° and decreases at higher temperatures. The situation is even worse with uranium and stainless steel in the presence of hydrogen. A eutectic occurs below 700° (which has practical ramifications well known to those who have tried to purify hydrogen over a uranium chip bed contained in stainless steel) and the solubility of iron and chromium is increased. In the UH_3 phase this would create cation substitutions of chromium and iron for uranium ions.

Since both iron and chromium do not form hydrides as readily as uranium, the probable effect of their substitution for uranium in the hydride lattice would be to create hydrogen vacancies. The highest atomic ratio of hydrogen to iron, chromium, or nickel atoms reported to date is the $Ce_{0.3}La_{0.7}Ni_5H_7$[11] compound which has only a ratio of 1.4:1 (ignoring rare earth) as compared to 3:1 for UH_3. Thus, an equation similar to (10) could be derived with a negative q. If in uranium hydride these ions completely repelled the hydride ion, q could equal −12 since the cage structures for both types of uranium atoms in the β-uranium hydride structure contain 12 hydride ions.

A negative q moves the isothermal lines of Figure 3 further toward the uranium phase. Chevallier, *et al.*, contained their sample in a stainless steel container; therefore, the present model predicts that their data be shifted toward lower stoichiometry due to reaction between their sample and container.

C. Theoretically Generated Phase Diagram. According to the present model, the pressure relationship to stoichiometry for uncontaminated material is as shown in Figure 3. For this model oxygen changes the observed phase diagram in two ways. First, each oxygen atom displaces a hydrogen atom. Under conditions of observation on a molar basis, such as a Sieverts'-type experiment, this appears in the measurement directly. The term θ is observed in a Sieverts' experiment as a negative deviation in hydrogen stoichiometry. If experiments were carried out by mass measurements, then an additional weight of 16θ beyond the hydrogen weight of m would be observed. The second effect is the actual decrease in the hydrogen vacancies. This effect is the same regardless of the method of measurement. This oxygen-vacancy interaction is illustrated by the dashed line in Figure 3. Elimination of only the θ term from eq 10 gave an isotherm at 650° of a higher stoichiometry than the uncontaminated case. In other words, considering only the filled sites-to-uranium ratios, oxide contamination increases the stoichiometry at any particular pressure above the plateau pressure. On the ternary phase diagram the dashed line of Figure 3 corresponds to the isotherm on the dashed line of Figure 1. It will be noted from the shift in the 650° isotherm (illustrated with the dashed line in Fig-

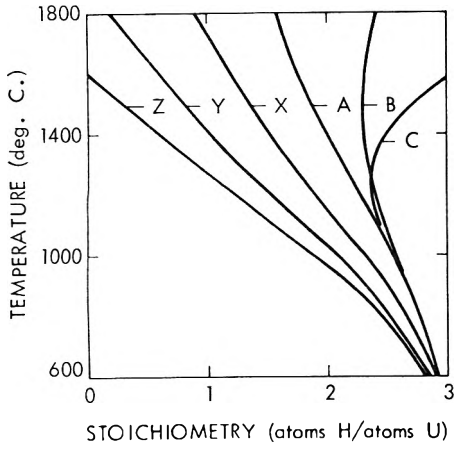

Figure 4. Plateau edge on the hydride side as calculated from the present model. Curve A is the uncontaminated case with no hydrogen solubility in the hydrice. Curves B and C assume some interstitial hydride solubility with the following ΔH_{sol} and ΔS_{sol}: (B) ΔH_{sol} = 41.84 kJ/mol (10 kcal/mol), ΔS_{sol} = −29.3 J mol^{-1} K^{-1} (−7 eu mol^{-1} K^{-1}); (C) ΔH_{sol} = 125.5 kJ/mol (30 kcal/mol), ΔS_{sol} = 25.1 J mol^{-1} K^{-1} (6 eu mol^{-1} K^{-1}). Curves X, Y, and Z assume iron contamination of 1, 2, and 3%, respectively. The iron is assumed to effect all nearest-hydride sites.

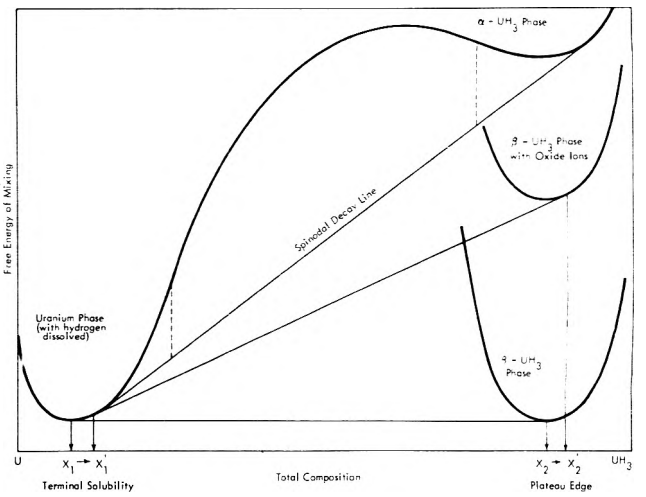

Figure 5. Schematic of the features one might find in the free-energy diagram corresponding to the proposed model. β-UH_3 is assumed to be a completely separate phase from uranium; whereas, α-UH_3 might be formed *via* a spinodal decomposition. Oxide contamination ra ses the free energy of the β-UH_3, thus causing the terminal solubility to increase and the vacancy population in the β-UH_3 to decrease.

ure 3) that the effect due solely to the oxide ion repulsion of vacancies is *not* trivial.

The present model may be used to extrapolate the stoichiometry of the pressure plateau edge to higher temperatures. This is the intersection of the calculated isotherm with the plateau pressures measured by Mallett and Trzeciak.[4] Comparisons of Figures 2 and 3 reveal that this edge, as observed by Sieverts' experiment, is lower for the contaminated case. The extrapolation, as presented in Figure 4, is dependent on the interstitial solubility assumed for hydrogen in the uranium hydride phase. Hydrogen solubility on interstitial sites of the hydride can displace the plateau edge to even higher stoichiometry. Two different sets of ΔS_{sol} and ΔH_{sol} were picked to illustrate this effect in Figure 4.

Even without solubility, a critical point seems unlikely since in order for one to occur the two plateau edges (on the uranium-rich and hydride-rich sides) must come together. Mallett and Trzeciak[4] reported a terminal solubility of hydrogen in liquid uranium at 1400° of stoichiometric number 0.6. According to the extrapolation, the stoichiometry of the other plateau edge at 1400° is at least 2.0. Extrapolation of Mallett and Trzeciak's data gives a terminal solubility of stoichiometry 1.5 at about 1800°. Thus, if the hydride remains solid, a critical point may not be achieved below approximately 1800° according to the present model.

Figure 4 also shows three cases where q is negative. This corresponds to metallic contamination as mentioned previously. Movement of this edge with a negative q makes the appearance of a critical point more likely. Deliberate iron contamination of a sample and measurement of the resulting phase diagram may resolve the problem presented by Chevallier's data.

D. Nucleation Vs. Spinodal Decomposition and the Model. One of the features of the kinetic model mentioned previously[5] but not considered until now is the nucleation step that would be necessary to start the growth of β-uranium hydride. The present model implies that β-uranium hydride and α-uranium are completely separate phases. That is, one single-valued equation is not sufficient to express the free energy as a function of composition. Thus, β-uranium hydride may not form from α-uranium by a simple spinodal decomposition. (A spinodal decomposition is a type of phase transformation involving no free-energy barrier.[12]) Libowitz' theory, however, implies that a simple spinodal decomposition is likely when α-uranium transforms to β-uranium hydride. One of the features of the spinodal decomposition mechanism, however, is that the two phases formed must be nearly isomorphous. α-Uranium is nearly isomorphous with the α-uranium hydride but not with β-uranium hydride.

Recent experiments on the kinetics of this system, however, indicate strongly some type of spinodal decomposition reaction is involved. First, the rate of hydriding is not strongly (if at all) dependent on the previous thermal history of a randomly oriented sample. The rates of hydriding have been measured on powders that had been annealed at temperatures ranging from 150 to 250°. The hydriding rates were not altered from what had been measured previously.[5] Thus, the sites for nucleation of β-uranium hydride are not the defects in the metal phase since defect density is dependent on prior heat treatment. Secondly, first-order (or nearly first-order) kinetics with respect to uranium prevails even when the pressure is very close to the plateau pressure. This would not be expected with the pure nucleation-and-growth mechanism. In that mechanism the first-order rate in the uranium would disappear with approach to equilibrium. This would be due to a switch in the rate-determining step from nucleation to growth. Since the dehydriding is zero order in uranium metal,[5] this switch would make the mechanism compatible with the thermodynamics. (The equilibrium in the plateau region has no dependence on the normalized uranium metal content.) These facts argue for a mechanism which involves a spinodal decomposition.

There is a reasonable compromise between the simple spinodal decomposition and the nucleation mechanism that is suitable for the uranium–hydrogen system. That is, a simple spindoal decomposition creates sites for nucleation. For this mechanism α-uranium transforms to α-urani-

TABLE II: Statistical Comparisons of the Various Models. Probability from *F* Distribution[a]

Model	Parameters[c]	Degrees of freedom residual	Mean square	Probability of identity to model
I. Pure vacancy	$A1^b$ = (20.56) 86.02 $B1$ = (20 974) 87 755	53	3.15×10^{-5}	
II. Present model	$A1^b$ = (22.77) 95.27 $B1$ = (22 993) 96 202 $A2$ = (20.04) 83.9 $B2$ = (34 160) 142 900 q = 22	50	1.09×10^{-5}	I = <0.5%
III. Libowitz six-parameter	E_{VV} = (−6700) 28 030 S_{450} = 3.0010 S_{500} = 2.9917 S_{550} = 2.9805 S_{600} = 2.9541 S_{650} = 2.9303	49	1.28×10^{-5}	I = <0.5% II = e
IV. Libowitz ten-parameter	$E_{VV_{450}}$ = (6700) 28 080 $E_{VV_{500}}$ = (6501) 27 200 $E_{VV_{550}}$ = (6400) 26 780 $E_{VV_{600}}$ = (6400) 27 780 $E_{VV_{650}}$ = (6601) 27 620 S_{450} = 3.0010 S_{500} = 2.9947 S_{550} = 2.9879 S_{600} = 2.9648 S_{650} = 2.9352	45 (Av[d]	1.09×10^{-5} 1.22×10^{-5})	I = <0.5% II = ~50% III = ≫25%

[a] Reference 17. [b] $R \ln K_1 = A1 - B1/T$ and $R \ln K' = A2 - B2/T + {}^1/_2R \ln P'_{H_2} - {}^1/_2R \ln P_{O_2}$. ($R$ = 8.314 J mol^{-1} K^{-1}, 1 cal = 4.184 J.) [c] Quantities in parentheses are in terms of cal and eu. Expressed in units of J/mol (1 cal = 4.184 J) where applicable, quantities in parentheses are in terms of cal. [d] This fit can be thought of as five separate two-parameter fits. This average value is over those five fits (not used in the F test). [e] A worse fit overall, F test not required.

um hydride *via* a spinodal decomposition. The β-uranium hydride grows on these sites of α-hydride.

In this mechanism the growth of the β-hydride depends on temperature and strain fields. The strain field may restrict its final size. The temperature will influence its rate of growth. One would expect to observe slower growth of β-uranium hydride at low temperatures. The thermodynamically unfavored α-uranium hydride would, therefore, predominate at low temperatures since there is no activation free-energy barrier for its formation.

An additional (and testable) prediction for this system is that oxide in the hydride phase will increase the terminal solubility of hydrogen in uranium. Considering only the effect of vacancy repulsions by oxide ions, or the third term of eq 10 (or the dashed line in Figure 3 for 650°), one must conclude that oxide ions shift the free energy of formation curve of the β-UH_3 phase upward relative to the pure phase. This shift is also upward relative to the free energy of formation of the uranium-dissolved hydrogen phase. This is illustrated (with exaggerated "open" curves for the free-energy curves) in Figure 5. A natural outcome of this shift is that the terminal solubility point must also increase. Figure 5 illustrates why one should come to this conclusion and the actual values of the free energies should not affect this conclusion. This, along with the previously mentioned kinetic effects,[5] should completely account for the hysteresis observed by some investigators[1,13] in the phase diagram.

Figure 5 also illustrates the above-postulated spinodal behavior for the α-UH_3.

IV. Conclusions

It will be difficult to differentiate between the model presented herein and the vacancy–vacancy model presented by Libowitz. Careful experimentation to directly address the oxygen contamination problem and measurements at higher pressure may resolve the question. If the present model is correct, a prominent example of Anderson's theory is eliminated. On the other hand, if the vacancy–vacancy model is found to be correct, then the kinetics of formation of the β-uranium hydride could occur by a spinodal decomposition reaction. This particular mechanism was not considered[5] previously since the structural changes from α-uranium to β-uranium hydride involved atom rearrangements greater than expected for a simple spinodal decomposition. Continuing kinetic studies, however, indicate that a spinodal decomposition may indeed be involved in the kinetics. If the present model holds then, a likely explanation for the hydriding is schematized as

$$\text{U + dissolved H} \xrightarrow[\text{decomposition}]{\text{spinodal}} \alpha\text{-UH}_3 \text{ nuclei}$$

$$\text{U + dissolved H} \xrightarrow[\text{nuclei}]{\text{growth on } \alpha\text{-UH}_3} \beta\text{-UH}_3 \text{ limited growth}$$

$$\alpha\text{-UH}_3 \xrightarrow{\text{very slowly}} \beta\text{-UH}_3$$

In addition to explaining the observed kinetics, this scheme accounts for the observation of pressure hysteresis,[13] the observed effects caused by contamination,[6] and increased abundance of α-UH_3 formed at low temperatures.[14,15]

Appendix I

The question might be raised as to whether the present fit is a justifiable improvement over the pure vacancy model[16] and if so, if a further refinement of the model to higher parameter models is also justified on purely statistical grounds. The answer to this question can be readily seen from the statistical analysis presented in Table II. It can be seen that there is a very highly significant improvement in the fit going from the pure vacancy model to the present model. This confirms what one would conclude by

inspection of Figure 1 in comparing the vacancy fit to the present fit. There is, however, absolutely no significant improvement when one goes from the present model to the six-parameter Libowitz model. In fact, according to the usual criterion that Prob (F) $\geq$ 5% indicates an insignificant improvement, the improvement to all models presented with more parameters than the present model is insignificant. Therefore, from a statistical standpoint, the most logical fit is the present one.

References and Notes

(1) G. G. Libowitz and P. R. T. Gibb, *J. Phys. Chem.*, **61**, 793 (1957).
(2) J. Chevallier, P. Desre, and J. Spitz, *J. Nucl. Mater.* **23**, 289 (1967).
(3) G. G. Libowitz, *J. Chem. Phys.*, **27**, 514 (1957).
(4) M. W. Mallett and M. J. Trzeciak, *Trans. Amer. Soc. Met.*, **50**, 981 (1958).
(5) J. B. Condon and E. A. Larson, *J. Chem. Phys.*, **59**, 855 (1973).
(6) H. Meusemann and L. Von Erichsen, BMFT-FBK73-18, 1973.
(7) J. R. Lacher, *Proc. Roy. Soc., Ser. A*, **161**, 525 (1938).
(8) A. L. G. Rees, *Trans. Faraday Soc.*, **50**, 335 (1954).
(9) J. S. Anderson, *Proc. Roy. Soc., Ser. A*, **185**, 69 (1946).
(10) M. Hansen, "Constitution of Binary Alloys," 2nd ed, K. Wmberko, Ed., McGraw-Hill, New York, N. Y., 1958, p 728.
(11) J. H. N. Van Vucht, F. A. Kuijpers, and H. C. A. M. Bruning, *Phillips Res. Rep.*, **23**, 133 (1970).
(12) J. W. Cahn, *Trans. Met. Soc. AIME*, **242**, 166 (1968).
(13) F. H. Spedding, A. S. Newton, J. C. Warf, O. Johnson, R. W. Nottorf, I. B. Johns, and A. H. Daane, *Nucleonics*, **4**, 8 (1946).
(14) R. N. R. Mulford, F. H. Ellinger, and W. H. Zachariasen, *J. Amer. Chem. Soc.*, **76**, 297 (1954).
(15) E. Wicke and K. L. Otto, *Z. Phys. Chem. (Frankfurt am Main)*, **31**, 2227 (1962).
(16) G. G. Libowitz and J. B. Lightstone, *J. Phys. Chem. Solids*, **28**, 1145 (1967).
(17) G. W. Snedecor and W. G. Cochran, "Statistical Methods," 6th ed, The Iowa State University Press, Ames, Iowa, 1967, Chapter 4, p 91.

Thermochemical Investigations of Hydrogen Bonding. An Improvement on the Ideal Associated Solution Approximation

Gary L. Bertrand

Department of Chemistry, University of Missouri—Rolla, Rolla, Missouri 65401

(Received August 16, 1974)

Publication costs assisted by the University of Missouri—Rolla

The application of the ideal associated solution approximation to calorimetric investigations of hydrogen bonding in binary solutions is considered from the viewpoint of solution thermodynamics. A simple model of nonideality is introduced to accommodate nonchemical contributions to the excess enthalpy of a binary solution containing a hydrogen-bonded complex. Application of the model to the chloroform + triethylamine system appears to be quite reasonable, and shows that relatively small contributions of nonideality can lead to large errors in hydrogen bonding parameters determined with the ideal associated solution approximation.

Introduction

As part of a continuing study on the fundamental assumptions of the various calorimetric methods of investigating association complexes in solution,[1] this paper considers the oldest method—that involving the ideal associated solution approximation. This method, which orginated with Dolezalek[2] and was severely criticized by van Laar and others,[3] has been applied to various excess properties of mixtures, most recently by Hepler, Fenby, and coworkers[4] for the study of the hydrogen bonds of chloroform with several bases. The basic idea of this method involves the treatment of a nonideal binary solution as if it were an ideal ternary (or higher order) solution, the nonideality arising from complexes existing in the solution. Hence, negative deviations from Raoult's law or exothermic heats of mixing are attributed to new chemical species in mixtures of the two components, and positive deviations from Raoult's law or endothermic heats of mixing are attributed to self-association of one of the components. The most obvious criticism of this approach centers on the fact that ideal binary solutions are extremely rare, particularly for polar components and components with considerable differences in their molar volumes. The probability of finding an ideal ternary solution of two components which are sufficiently polar to form a complex and a third component (the complex) which has a molar volume at least twice as large as one of the components must be considered extremely low.

One might expect that the likeliest components for ideal solutions would be isotopic isomers, but small excess enthalpies were observed in the chloroform + chloroform-d and acetone + acetone-d_6 systems.[5a] In applying a modification of the ideal associated solution approximation to the H_2O + D_2O + HDO system,[5b] we were careful to refer to the "apparent heat of formation" of HDO, and pointed out that even our very careful measurements were not of sufficient precision to detect subtle effects of nonideality which could have caused an error of almost 200% in our reported value for the enthalpy of the exchange reaction in solution.

Hepler and Fenby in their first paper[4a] considered the possibility of slight departures from ideality in terms of "physical" contributions, (ΔH_p), to the excess enthalpy of the chloroform + triethylamine system

$$\Delta\bar{H}^E = \Delta H_p + \Delta H_c \quad (1)$$

but reasoned that the molar excess enthalpy was so much larger than any "reasonable" value of ΔH_p, that these contributions could be neglected in comparison to the "chemical" contributions (ΔH_c) which arise from the formation of r moles of complex in one formal mole of solution with the molar enthalpy of complex formation (ΔH_r).

$$\Delta\bar{H}^E \cong \Delta H_c = r\Delta H_r \quad (2)$$

Their division of the excess enthalpy into "chemical" and "physical" contributions suggests a method of introducing "physical" interactions through a simple model of nonideality.

The Model

The simplest equation which might reasonably be expected to describe the "physical" or "nonideal" contributions to the enthalpy of a ternary solution (n_A, n_B, n_C), involves weighting factors for each component (Γ_i) and interaction parameters (A_{ij}) for each pair of components:

$$\Delta H_p = \frac{n_A\Gamma_A n_B\Gamma_B A_{AB} + n_A\Gamma_A n_C\Gamma_C A_{AC} + n_B\Gamma_B n_C\Gamma_C A_{BC}}{(n_A^0 + n_B^0)(n_A\Gamma_A + n_B\Gamma_B + n_C\Gamma_C)} \quad (3)$$

The enthalpy of formation of 1 mol of pure liquid complex (C) from pure liquids A and B is designated as ΔH_r^{id}, which will also apply to the enthalpy of complex formation in an ideal solution. Taking the formal amounts of A and B as n_A^0 and n_B^0, and formal mole fractions X_A^0 and X_B^0, gives

$$\Delta\bar{H}^E = \Delta H_p + r\Delta H_r^{id} \quad (4)$$

$$n_A = n_A^0 - n_C \qquad n_B = n_B^0 - n_C$$

$$r = n_C/(n_A^0 + n_B^0) \quad (5)$$

$$K_x = \frac{r(1-r)}{(X_A^0 - r)(X_B^0 - r)} \qquad K_x = K_x(T, X_A^0) \quad (6)$$

This group of equations obviously contains too many parameters for evaluation, but reasonable simplifications may be made. In models leading to equations of the form of (3), the use of molar volumes for weighting factors is quite common, and in any case, the assumption

$$\Gamma_C = \Gamma_A + \Gamma_B \quad (7)$$

appears reasonable. The solubility parameter treatment of Scatchard[6] and Hildebrand[3] provides a basis for approximations involving interaction parameters. The solubility parameter treatment gives

$$A_{ij} = (\delta_i - \delta_j)^2 \quad (8)$$

Assuming that the solubility parameter of the complex is the weighted mean of the solubility parameters of components A and B

$$\delta_C = \frac{\Gamma_A\delta_A + \Gamma_B\delta_B}{\Gamma_A + \Gamma_B} \quad (9)$$

allows elimination of two of the parameters of eq 3

$$A_{AC} = \frac{\Gamma_B^2 A_{AB}}{(\Gamma_A + \Gamma_B)^2} \qquad A_{BC} = \frac{\Gamma_A^2 A_{AB}}{(\Gamma_A + \Gamma_B)^2} \quad (10)$$

leaving only four parameters (K_x, ΔH_r^{id}, A_{AB}, and the ratio Γ_A/Γ_B) in the group of eq 3–6. The equilibrium constant might be evaluated by separate measurements (spectroscopic methods, for instance), but, as eq 6 indicates, the possibility exists that K_x may be composition dependent. This possibility does not affect the correctness of equations which include the quantity r, but could severely limit the application of these equations to real systems. Substitution of the approximations, eq 7 and 10 into eq 3 and 4, gives

$$\Delta H_p = \frac{X_A^0\Gamma_A X_B^0\Gamma_B A_{AB}}{(X_A^0\Gamma_A + X_B^0\Gamma_B)} - \frac{r\Gamma_A\Gamma_B A_{AB}}{(\Gamma_A + \Gamma_B)} \quad (11)$$

$$\Delta\bar{H}^E = r\left[\Delta H_r^{id} - \frac{\Gamma_A\Gamma_B A_{AB}}{(\Gamma_A + \Gamma_B)}\right] + \frac{X_A^0\Gamma_A X_B^0\Gamma_B A_{AB}}{(X_A^0\Gamma_A + X_B^0\Gamma_B)} \quad (12)$$

This equation can be applied very easily to experimental data if the interaction parameter A_{AB} and the ratio of weighting factors can be evaluated from independent measurements, since the square-bracketed term does not change with composition. This term represents the enthalpy of complex formation ($\Delta H_r'$) in mixtures of A, B, and C rather than in ideal solutions.

$$\Delta H_r' = \left[\Delta H_r^{id} - \frac{\Gamma_A\Gamma_B A_{AB}}{(\Gamma_A + \Gamma_B)}\right] \quad (13)$$

The weighting factors can be approximated by molar volumes, and the interaction parameter might be estimated from solubility parameters, but better estimates can in some cases be obtained from measurements of the partial molar excess enthalpy of each of the components in the other pure component and in the equimolar mixture. Before continuing with that development, however, a more important consideration arises—the effect of nonideality on the equilibrium constant.

Since slight variation in the equilibrium constant could have very large effects on the shape of the excess enthalpy curve, the possible effects of nonideality on the excess Gibbs' free energy of the system must be considered. The excess free energy can be divided into the contributions of "chemical" and "physical" interactions

$$\Delta\bar{G}^E + \Delta G_p + \Delta G_c \quad (14)$$

with

$$\Delta G_c = X_A^0 RT \ln\left[\frac{X_A^0 - r}{X_A^0(1-r)}\right] + X_B^0 RT \ln\left[\frac{X_B^0 - r}{X_B^0(1-r)}\right] + rRT \ln\left[\frac{K_x}{K_x^{id}}\right] \quad (15)$$

Assuming that ΔG_p can be described by an equation of the form of eq 3, with possibly different values of the weighting factors (Γ_i') and interaction parameters (A_{ij}'), but retaining the approximations of eq 7 and 10, leads to

$$RT \ln K_x = RT \ln K_x^{id} + \frac{\Gamma_A'\Gamma_B' A_{AB}'}{(\Gamma_A' + \Gamma_B')} \qquad K_x = K_x(T) \quad (16)$$

Equation 16 shows that this model leads to an equilibrium constant in solution which is not necessarily equal to the value in an ideal solution, K_x^{id} (which depends only on the properties of the pure liquids A, B, and C at a specified temperature), but which is nonetheless constant for all mixtures of A, B, and C. Excess free energy data might be used to evaluate Γ_A'/Γ_B' and A_{AB}', as well as K_x and K_x^{id}.

Returning now to the evaluation of the parameters of eq 12, this equation can be differentiated to obtain the formal excess partial molar enthalpy of component A, $(\bar{L}_A)_{X_A^0}$, in a solution of composition X_A^0

$$(\bar{L}_A)_{X_A^0} = \left(\frac{\partial \Delta H^E}{\partial n_A^0}\right)_{n_B^0, T, P} = \left[\frac{KX_B^0}{1 + K} - r\right] \times \left[\frac{\Delta H_r'}{1 - 2r}\right] + \left[\frac{X_B^0 \Gamma_B}{X_A^0 \Gamma_A + X_B^0 \Gamma_B}\right]^2 A_{AB} \Gamma_A \quad (17)$$

The partial molar excess enthalpy of component B, $(\bar{L}_B)_{X_A^0}$, can be obtained by reversing all subscripts (A ↔ B) in eq 17. The value of A_{AB} and the relative values of Γ_A and Γ_B can be estimated by considering the partial molar excess properties of the components in the pure solvents and in the equimolar mixture

$$(\bar{L}_A - \bar{L}_B)_{X_A^0=0.5} = \frac{\Gamma_A \Gamma_B (\Gamma_B - \Gamma_A) A_{AB}}{(\Gamma_A + \Gamma_B)^2} \quad (18)$$

$$(\bar{L}_A)_{X_A^0=0} - (\bar{L}_B)_{X_B^0=0} = (\Gamma_A - \Gamma_B) A_{AB} \quad (19)$$

The ratio of these quantities eliminates the interaction parameter, and

$$\frac{(\bar{L}_A)_{X_A^0=0} - (\bar{L}_B)_{X_B^0=0}}{(\bar{L}_A - \bar{L}_B)_{X_A^0=0.5}} = -\frac{(\Gamma_B + \Gamma_A)^2}{\Gamma_A \Gamma_B} \quad (20)$$

Obviously, this method of estimation will only be applicable to systems with a relatively large difference in the weighting factors for the two components, because of the difference term in both eq 18 and 19. For systems of components of similar molar volumes (expected to have similar weighting factors), extremely large "physical" contributions could be virtually undetectable by calorimetric methods. The chloroform ($\bar{V}$ = 81 cm^3 mol^{-1}) + triethylamine ($\bar{V}$ = 140 cm^3 mol^{-1}) system, however, provides an excellent example for this model of nonideality.

Application to the Chloroform + Triethylamine System

Matsui, Hepler, and Fenby[4b] measured the partial molar enthalpies of chloroform and triethylamine in the equimolar mixture and the pure solvents at 298.15°K: $(\bar{L}_T)_{X_T^0=0}$ = −11.55 kJ mol^{-1}, $(\bar{L}_T)_{X_T^0=0.5}$ = −4.217 kJ mol^{-1}, $(\bar{L}_C)_{X_C^0=0}$ = −12.68 kJ mol^{-1}, $(\bar{L}_C)_{X_C^0=0.5}$ = −3.950 kJ mol^{-1}. Application of eq 20 to these data gives Γ_T/Γ_C = 1.6, which agrees well (considering uncertainties in the experimental enthalpies and approximations in the model) with the ratio of molar volumes, 1.73. Substituting molar volumes for weighting factors in eq 18 and 19 gives A_{AB} = 0.019 kJ cm^{-3}, which is in reasonable agreement with the value of 0.014 kJ cm^{-3} calculated from the solubility parameters of triethylamine (15.2 J$^{1/2}$ cm$^{-3/2}$) and chloroform (19.0 J$^{1/2}$ cm$^{-3/2}$).

These estimates of the nonideality parameters for this system allow modification of eq 12 so that a simultaneous solution of K_x and $\Delta H_r'$ can be extracted from excess enthalpy data for this system with the treatment given by Hepler and Fenby[4a]

$$\Delta H_c' = \Delta \bar{H}^E - \frac{X_A^0 \bar{V}_A X_B^0 \bar{V}_B A_{AB}}{(X_A^0 \bar{V}_A + X_B^0 \bar{V}_B)} = r \Delta H_r' \quad (21)$$

substituting $\Delta H_c'$ and $\Delta H_r'$ for H^E and ΔH_r, respectively, in their eq 8. Treatment of their data for the excess enthalpy of the chloroform + triethylamine system at 298.15°K, along with the excess partial molar enthalpy data of Matsui, Hepler, and Fenby[4b] with A_{AB} = 0.019 kJ cm^{-3} gives K_x = 2.0 ± 0.5, $\Delta H_r'$ = −21.4 ± 2 kJ mol^{-1}, ΔH_r^{id} = −20.4 ± 2 kJ mol^{-1}. Values of $\Delta \bar{H}^E$ calculated with these values have approximately the same standard deviation as do values calculated with the ideal associated solution approximation, both of which appear comparable to the scatter of experimental data. The nonideality approximation naturally leads to better agreement with experimental values of the excess partial molar enthalpy. The equilibrium constant determined in this manner is in good agreement with the value determined by nmr spectroscopy (3 ± 1) in mixtures of chloroform and triethylamine[7] and with the value used in the ideal associated solution approximation (3.3[4b]).

The larger values (4–4.7) of the equilibrium constant reported for studies in cyclohexane are not necessarily relevant to chloroform + triethylamine mixtures. The enthalpy of complex formation determined with the nonideality approximation is in better agreement with the value of −17 kJ mol^{-1} determined from spectroscopic studies[7,8] than with the calorimetric values determined with the ideal associated solution approximation (−14.2 to −15.8 kJ mol^{-1}).[4a,b]

The actual contribution of physical/nonideal interactions to the excess enthalpy of this system which has been introduced by this model of nonideality can be calculated by substituting the calculated parameters in eq 11. This gives +0.28 kJ mol^{-1} as the nonideal contribution to the total excess enthalpy (−4.03 kJ mol^{-1}) of the equimolar mixture. Thus, this effect which is detectable (by this model) only because of the difference in the molar volumes of the components, and which amounts to only 7% of the total excess enthalpy, can lead to an error of 25% or more in the enthalpy of complex formation determined with the ideal associated solution approximation.

Conclusions

As was stated in an earlier work,[1b] the inclusion of estimated nonideality effects in the treatment of calorimetric data does not necessarily lead to greater reliability of the hydrogen bonding parameters. It is conceivable that other models might lead to results in better agreement with the results of the ideal associated solution approximation than with those reported here. A slight modification of the model presented here, using the Flory–Huggins equation for the entropy of mixing of molecules of different sizes, leads to an equilibrium constant based on volume fractions rather than on mole fractions, causing K_x to be composition dependent. Perhaps the major importance of the present approach lies in the demonstration that subtle effects of solution nonideality can lead to large uncertainties in the properties attributed to hydrogen bonds with the ideal associated solution approximation, completely independent of uncertainties estimated on the basis of statistical error analysis. To avoid the possibility that this work might give some advantage to the proponents of the spectroscopic methods of investigating hydrogen bonding over proponents of the calorimetric method, I must confess that I place an even lesser reliability on the results of spectroscopic investigations. As Hepler and Fenby[4] point out, these treatments also use the ideal associated solution approximation, along with the assumption of composition-independent properties of the various species in solution. The combination of spectroscopic equilibrium constants with calorimetric data for the evaluation of the enthalpy of complex formation has equal probability of reducing or compounding errors, and eliminates the possibility of detecting errors through differences in the results of indepen-

dent investigations. Agreement of equilibrium constants determined by calorimetric methods with those determined spectroscopically can provide greater confidence in the values, particularly if the two methods involve different ranges of composition.

Throughout this paper, reported values of ΔH_r and K_x have been referred to as "hydrogen bonding parameters" rather than as "properties of hydrogen bonds," because "properties" should be independent of the method of investigation, as these parameters certainly are not. The elevation of the results of investigations of association complexes in solution to the status of "thermochemical data" will require the same rigor of thermodynamic description and theoretical developments of extrapolation methods as those which have been applied to the properties of aqueous electrolyte solutions. Development and application of models such as the one described here are essential to the achievement of that goal.

Acknowledgment. I wish to thank Professor Loren G. Hepler for his helpful discussions and suggestions.

References and Notes

(1) (a) W. C. Duer and G. L. Bertrand, *J. Amer. Chem. Soc.*, **92**, 2587 (1970); (b) G. L. Bertrand and T. E. Burchfield in "Analytical Calorimetry III," J. F. Johnson, Ed., Plenum Press, in press. Presented at the 167th National Meeting of the American Chemical Society, Los Angeles, Calif., 1974.
(2) F. Dolezalek, *Z. Phys. Chem.*, **64**, 727 (1908).
(3) J. H. Hildebrand and R. L. Scott, "The Solubility of Nonelectrolytes," Dover Publications, New York, N.Y., 1964, Chapter VII.
(4) (a) L. G. Hepler and D. V. Fenby, *J. Chem. Thermodyn.*, **5**, 471 (1973); (b) T. Matsui, L. G. Hepler, and D. V. Fenby, *J. Phys. Chem.*, **77**, 2397 (1973); (c) N. F. Pasco, D. V. Fenby, and L. G. Hepler, *Can. J. Chem.*, **52**, 2139 (1974).
(5) (a) W. C. Duer and G. L. Bertrand, *J. Amer. Chem. Soc.*, **96**, 1300 (1974); (b) W. C. Duer and G. L. Bertrand, *J. Chem. Phys.*, **53**, 3020 (1970).
(6) G. Scatchard, *Chem. Rev.*, **8**, 321 (1931).
(7) C. M. Huggins, G. C. Pimentel, and J. N. Shoolery, *J. Chem. Phys.*, **23**, 1244 (1955).
(8) C. J. Creswell and A. L. Allred, *J. Phys. Chem.*, **66**, 1469 (1962).

Analysis of Aerosols from the Ozonolysis of 1-Butene by High-Resolution Field Desorption Mass Spectrometry

H.-R. Schulten and Ulrich Schurath*

Institut für Physikalische Chemie der Universität, 53 Bonn, West Germany *(Received July 29, 1974)*

The condensable products and aerosols generated by ozonolysis of 1-butene at low reactant concentrations in air, and in the presence of sulfur dioxide, have been investigated by high-resolution field desorption mass spectrometry (FDMS). A great number of molecular ions up to *m/e* 392 were recorded. The elemental composition of ions was established up to *m/e* 200, including several sulfur containing species. Aldehydes, organic acids, sulfuric acid, and some of its probable precursors have been identified. The mixed sulfur compounds support the assumption that SO_2 is oxidized by zwitterions in this system. The formation of hydrogen peroxide, recently reported by Pitts, *et al.*, has been confirmed, but only at low pressures. The results show that FDMS offers considerable capacities for the analysis of particulate matter in air, especially of highly polar compounds. A new direct sampling technique for aerosols takes advantage of the extremely low sample consumption of FDMS (submicrogram quantities).

Introduction

The ozonolysis of olefins in the gas phase produces an aerosol when the reactant concentrations are high enough to cause supersaturation of the products. Analyses of these condensable products by various analytical techniques have been reviewed in the literature for a number of olefins and reaction conditions.[1-3] Some of these products are expected to be formed by reactions of the so-called zwitterion resulting from the Criegee split of the primary cyclic ozonide. This primary reaction path has been well established by recent work in the liquid phase.[4] Secondary reactions of the zwitterion in the gas phase are of extreme interest, since ozone–olefin reactions occur in the atmosphere. In model calculations of photochemical smog formation[5,6] the zwitterion has been assumed to decompose into radicals which contribute to the initiation of oxidation chains, converting NO into NO_2, which results in a net increase of ozone under the action of sunlight. There is furthermore evidence that an intermediate of ozone–olefin reactions is capable of oxidizing atmospheric SO_2.[7,8] The oxidation product, sulfuric acid, is the most important source of condensation nuclei in the atmosphere.

Although most of the condensable products of ozone–olefin reactions are accounted for by aldehydes and organic acids of relatively high volatility, which are not expected to condense at low reactant concentrations, we have observed a viscous polymer-like product of very low volatility in flow tube experiments at 1–2 Torr total pressure, when low concentrations of gaseous olefins C_nH_{2n} ($n \geq 3$) were allowed to react with ozonized oxygen (6.5% ozone). When heated under vacuum, part of the condensate did not evaporate, but remained as a colorless resin. We have also observed that a chemiluminescent ozone detector, when operated with olefins such as 2-butene and isobutene instead of eth-

TABLE I: Experimental Conditions and Sample Collection at Atmospheric Pressure

Sample no.	Flow rates, ml min^{-1} 1-Butene	Ozone[a]	SO_2	Diluent gas (7.2 l. min^{-1})	Reaction time; collection mode
b	55	22		Ambient air	30 min; precipitation on emitter
c	12	22	60	Ambient air	30 min; precipitation on emitter; sample not analyzed (see text)
d	Variable flow rates; sample contains combined products from experiments b and c				60 min; acetone wash, emitter dipping technique
e	7.6	12	0.7	Dry synthetic air	20 min; precipitation on emitter

[a] The ozone flow rate was calculated from the measured oxygen flow rate and the percentage ozone deduced from its optical absorption at 2537 Å.

ylene, becomes rapidly contaminated by polymers which condense on the photomultiplier window, although the ozone concentrations reacting in the detector are extremely low. These observations as well as a fundamental interest in ozone–olefin reactions in the gas phase initiated a reinvestigation of the condensable reaction products. High-resolution field desorption mass spectrometry, combined with a novel sampling technique for aerosols, was chosen as the analytical method. The technique is being further developed to detect polar molecules and inorganic compounds in natural aerosols.[9]

High-resolution field desorption mass spectrometry is a powerful analytical tool for studying an extremely wide variety of compounds.[10] The technique yields, in contrast to electron impact mass spectrometry, very simple spectra which generally consist of only the parent ion and, depending on the polarity of functional groups in the molecule, of an ion corresponding to the protonated parent molecule. Little or no fragmentation is observed.[11] The method is therefore ideally suited for the analysis of mixtures.[12,13]

We wish to report on the analysis of condensable products and aerosols from the ozonolysis of 1-butene at low reactant concentrations in the absence and presence of SO_2.

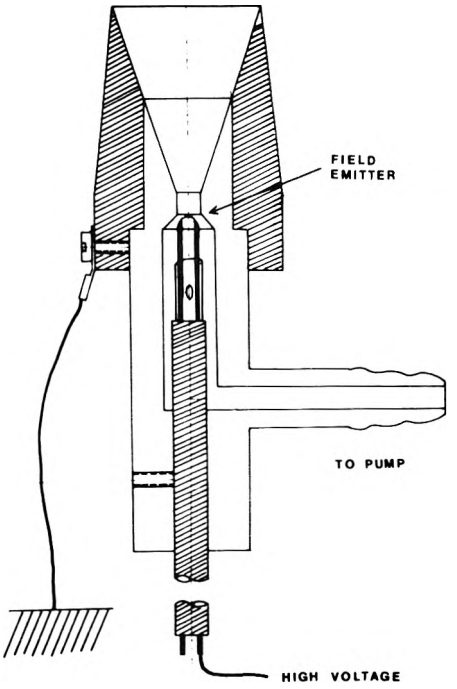

Figure 1. A device for the direct impactation of aerosols on the emitter wire of a field desorption mass spectrometer.

Experimental Section

The following reaction conditions and sampling methods have been used.

I. Low Pressure Reaction, Sample a. Ozonized oxygen of high purity (6.5% ozone) and 1-butene were pumped through a flow tube of 5 cm diameter and 30 cm length at flow rates of 170 and 50 Torr l. min^{-1}, respectively, at a total pressure of 1.6 Torr. Under these conditions, reaction products are observed to condense on the reaction tube walls. The products were collected on a cold finger protruding into the gas stream at the end of the tube, cooled to −30° to increase the deposition rate of the products. After 30 min the gas supplies were turned off, and the glass finger was allowed to warm to ambient temperature under vacuum conditions to evaporate any products of high volatility. The remaining colorless viscous liquid was directly applied to the field emitter by the dipping technique[14] and analyzed in the mass spectrometer.

II. Reaction at Atmospheric Pressure, Samples b–e. 1-Butene and ozonized oxygen were each premixed with either ambient air of average humidity or with dry synthetic air, and drawn through a 6-l. glass bulb serving as a mixed flow reactor at atmospheric pressure. Individual flow rates were controlled with calibrated flow meters. The air flow was set at 7.2 l. min^{-1}. Formation of an aerosol was observed at 13 ml min^{-1} of ozone and 3 ml min^{-1} of 1-butene, but higher flow rates were generally used for sample preparation, *cf.* Table I. To collect the aerosol droplets for mass spectrometric analysis, the aerosol was drawn from the mixed flow reactor through a plexiglass jet, Figure 1, which focussed the aerosol directly on the field emitter wire. The wire potential was kept 4.8 kV negative relative to the metallic brim of the plexiglass jet, which was grounded. In spite of the rather unsophisticated device, experiments with cigarette smoke as a test aerosol were successful in that the field emitter could be heavily loaded with aerosol droplets within a few minutes, covering the microneedles of the emitter completely. No damaging of the microneedles by the air blast has been observed. The collection efficiency of the device can be increased by improving the geometry of the jet relative to the emitter wire. No systematic study of the collection efficiency as a function of the wire potential has been made as yet.

The reaction of ozonized oxygen with 1-butene in air, using the mixed flow reactor, was repeated in the presence of SO_2, first with air as diluent gas, and second with dry synthetic air. Addition of SO_2 caused light scattering by

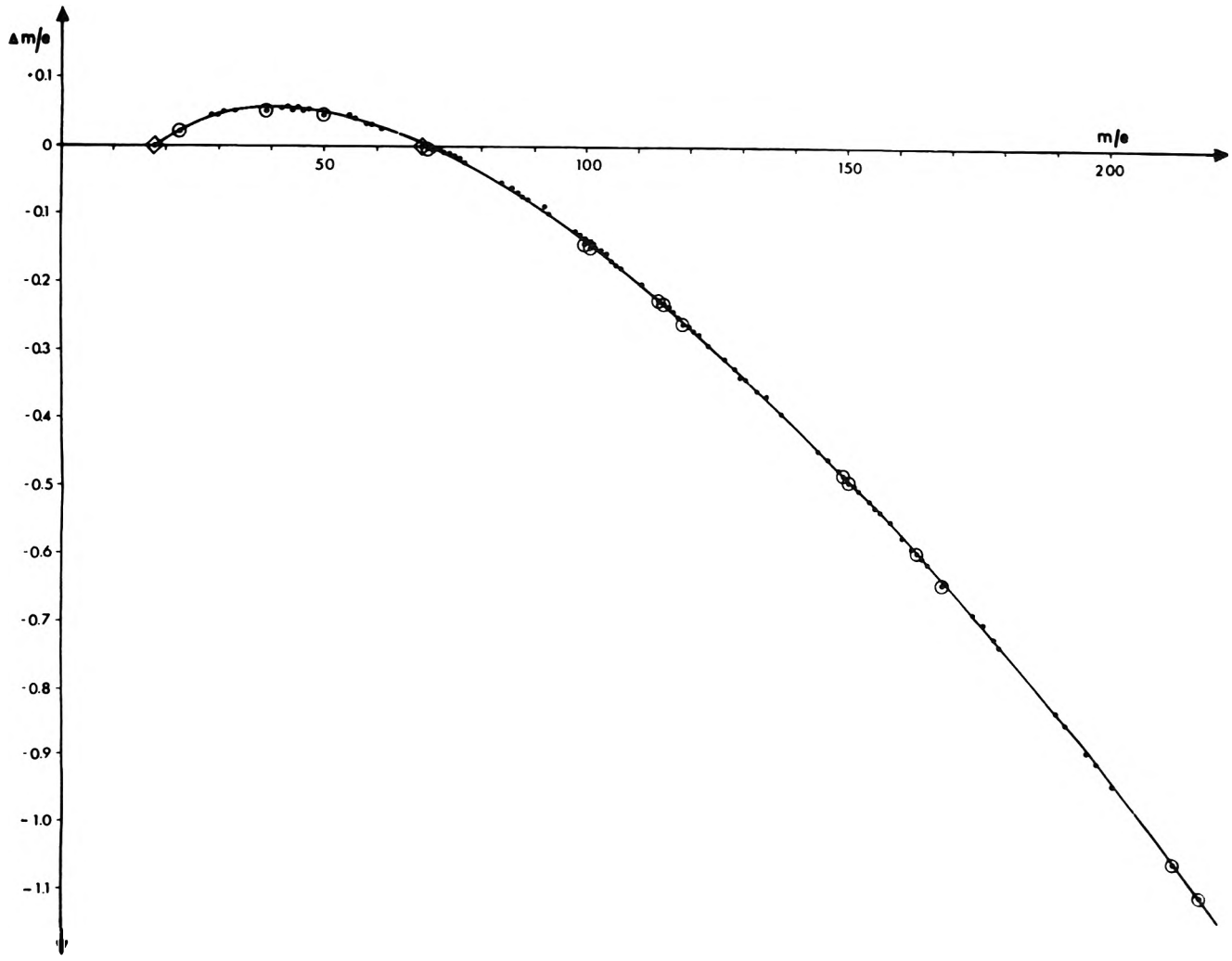

Figure 2. The difference $\Delta m/e$ between precision masses, calculated from the measured line positions by an interpolating program, and the precision masses of proposed ions, plotted as a function of m/e. Encircled dots are ions of known composition from the reference spectrum.

the aerosol to increase, in ambient air as well as in dry synthetic air, obviously by a reduction of particle size, due to the enormous increase of condensation nuclei from oxidized SO_2. Also, the rate of aerosol removal by wall deposition seemed to decrease. The aerosols produced in ambient air and in dry synthetic air, respectively, in the presence of SO_2, were collected on field emitter wires. However, only the dry sample (e) from the synthetic air experiment, *cf.* Table I, was suited for direct mass spectrometric analysis. Attempts to analyze aerosols from sample c and similarly prepared samples, after direct precipitation on the emitter, resulted in rupture of the wire when the high voltage for ion desorption was applied in the mass spectrometer. This was attributed either to corrosion by the dilute sulfuric acid or to discharges caused by sputtering. Instead, the reactor walls, which had been already contaminated by condensates from previous experiments in ambient air, also without SO_2, were flushed with reagent grade acetone. This solution of the combined products from experiments b and c was concentrated by pumping off the acetone solvent on the vacuum line, and drying the viscous product in a vacuum desiccator over P_2O_5 over night. This extract was applied to the emitter by the dipping technique as sample d.

Reaction conditions, gas flow rates, and collection modes of the samples prepared at atmospheric pressure are summarized in Table I. The field desorption mass spectrometer as well as details of the analytical procedure have been described in previous publications.[11] Mass spectra were recorded on vacuum evaporated AgBr plates (Ionomet Co.). Field desorption of nonvolatile material from the emitter in the ion source was enhanced by electric heating of the emitter wire. The temperature was slowly increased to about 80° (12-mA heating current) during the exposure of the plate.[13] The emission dropped to a low level after typically 12 min. After that, increasing the heating current to 30 mA did not raise the ion current significantly.

Results

The precise relative positions of mass spectral lines on the photographic plates as well as their intensities were measured on a home-built comparator system recently described.[11,13] The precision masses were deduced from the measured line positions relative to those of a field ionization reference spectrum of perfluorotributylamine with the help of an interpolating program on a PDP 8-E computer. Using the tabulated precision masses for ions of the elemental composition $C_xH_yO_z$, molecular formulae of the various ions could be deduced. Sulfur as a fourth element was taken into account in the case of spectra from samples d and e. The method is illustrated in Figure 2, which shows

TABLE II: Precision Masses, Molecular Formula, Densitometer Readings, and Proposed Parent Compounds of Ions Observed in the Mass Spectra of Samples a, b, d, and e

Precision mass	Molecular formula	Densitometer readings a	b	d	e	Proposed parent compounds (bp, °C)
29.003	CHO	50	8	35	52	Fragment of aldehyde, formaldehyde − H
30.011	CH_2O	50	8	60	60	Formaldehyde (−21)
31.018	CH_3O	60	50	52	60	Formaldehyde + H
29.039	C_2H_5	43	w	10	33	Fragment
32.998	HO_2	36			4	Fragment (O_2 is not observed!)
34.005	H_2O_2	18				Hydrogen peroxide (150.2)
42.011	C_2H_2O	20		w	15	Ketene (−56)
43.081	C_2H_3O	40	30	32	53	Ketene + H, acetaldehyde − H
44.026	C_2H_4O	52	30	48	53	Acetaldehyde (20.8)
45.034	C_2H_5O	60	40	31	55	Acetaldehyde + H
44.998	CHO_2	40	w	w	30	Fragment, formic acid − H (100.7)
46.005	CH_2O_2	50	w	52	60	Formic acid
47.013	CH_3O_2	52	43	38	60	Formic acid + H
56.026	C_3H_4O	w		6	45	Methylketene (mp −80)
57.034	C_3H_5O	46	30	31	55	Methylketene + H, propionaldehyde − H
58.042	C_3H_6O	54	35	52	58	Propionaldehyde (48.8)
59.050	C_3H_7O	54	60	33	55	Propionaldehyde + H
60.058	C_3H_8O	34				Alcohol?
59.013	$C_2H_3O_2$	22		25	42	
60.021	$C_2H_4O_2$	52	8	16	49	Acetic acid (117.9), methyl formate
61.029	$C_2H_5O_2$	54	33	3	35	The same + H
62.037	$C_2H_6O_2$	25				Acetaldehyde + H_2O
63.078	$C_2H_7O_2$	18				Acetaldehyde + H_3O
70.042	C_4H_6O	15		30	50	Ethylketene
71.050	C_4H_7O				20	The same + H, butyraldehyde − H
72.058	C_4H_8O	18		w	28	Butyraldehyde or ether (75.7)
73.065	C_4H_9O	45	w		6	The same + H
73.029	$C_3H_5O_2$	30	5	14	40	Propionic acid − H
74.037	$C_3H_6O_2$	35	w	30	50	Propionic acid (141)
75.044	$C_3H_7O_2$	52	50	5	40	Propionic acid + H
74.000	$C_2H_2O_3$				22	
75.008	$C_2H_3O_3$			27	40	
76.016	$C_2H_4O_3$			50	50	Formic acid + formaldehyde − cluster
77.024	$C_2H_5O_3$	30	3	15	35	The same + H
86.037	$C_4H_6O_2$			w	20	
87.045	$C_4H_7O_2$	36	8	33	50	Butanoic acid − H
88.052	$C_4H_8O_2$	44	w	10	27	Butanoic acid (163.5) expect in samples d, e
89.060	$C_4H_9O_2$	54	15			Butanoic acid + H
92.011	$C_2H_4O_4$			8	22	Dimer of formic acid, dimer zwitterion
93.019	$C_2H_5O_4$				8	The same + H
100.052	$C_5H_8O_2$			3	24	
101.060	$C_5H_9O_2$	36	w	32	40	
102.068	$C_5H_{10}O_2$	w			14	
103.076	$C_5H_{11}O_2$	37	5			
101.024	$C_4H_5O_3$				20	
102.032	$C_4H_6O_3$				15	
103.039	$C_4H_7O_3$	36	10	15	36	
104.047	$C_4H_8O_3$	w		3	20	Ozonide
105.054	$C_4H_9O_3$	42	25			
106.062	$C_4H_{10}O_3$	48	20			Butanoic acid + H_2O
107.070	$C_4H_{11}O_3$	19				Butanoic acid + H_3O
105.019	$C_3H_5O_4$			45	42	
106.027	$C_3H_6O_4$			16	20	
107.034	$C_3H_7O_4$	12		5	20	
115.040	$C_5H_7O_3$				29	
116.047	$C_5H_8O_3$			3	24	
117.055	$C_5H_9O_3$	37	5	2	27	
118.063	$C_5H_{10}O_3$	14		24	5	
119.071	$C_5H_{11}O_3$	10	w			
115.076	$C_6H_{11}O_2$	10			24	
117.091	$C_6H_{13}O_2$	10	w			
121.014	$C_3H_5O_5$			3	20	
122.022	$C_3H_6O_5$			33	28	
123.029	$C_3H_7O_5$				15	
117.019	$C_4H_5O_4$				17	
119.034	$C_4H_7O_4$	10	w		20	
120.042	$C_4H_8O_4$				4	

TABLE II: Continued

Precision mass	Molecular formula	Densitometer readings a	b	d	e	Proposed parent compounds (bp, °C)
121.050	$C_4H_9O_4$	20	w		4	
129.055	$C_6H_9O_3$				12	
133.014	$C_6H_{11}O_3$				27	
131.034	$C_5H_7O_4$				8	
133.050	$C_5H_9O_4$	12	w	w	30	
134.058	$C_5H_{11}O_4$	40	20			
135.066	$C_5H_{12}O_4$	8				
138.016	$C_3H_6O_6$			6	10	
145.050	$C_6H_9O_4$				15	
147.066	$C_6H_{11}O_4$				10	
151.024	$C_4H_7O_6$			5	30	
152.040	$C_4H_8O_6$			52	42	
153.040	$C_4H_9O_6$			3	20	
161.045	$C_6H_9O_5$				15	
179.056	$C_6H_{11}O_6$				18	
191.056	$C_7H_{11}O_6$				20	
199.024	$C_8H_7O_6$				22	

TABLE III: Sulfur Containing Ions in the Mass Spectrum of Sample e

Precision mass	Molecular formula	Densitom reading[a]	Densitometer reading of organic part of ion, from Table II column e
63.962	SO_2	Weak	
97.967	H_2SO_4	40 (32[a])	
98.975	H_3SO_4	32 (12[a])	
110.975	$SO_2 + CH_3O_2$	12	60
	$SO_3 + CH_3O$		62
124.991	$SO_2 + C_2H_3O_2$	8	35
	$SO_3 + C_2H_3O$		55
155.002	$SO_2 + C_4H_7O_3$	10	Not observed
	$SO_3 + C_4H_7O_2$		40
155.973	$SO_2 + C_2H_4O_4$	15 (weak[a])	22 (8[a])
	$SO_3 + C_2H_4O_3$		50 (50[a])
156.981	$SO_2 + C_2H_5O_4$	20 (weak[a])	8 (Not observed[a])
	$SO_3 + C_2H_5O_3$		35 (15[a])

[a] Densitometer readings of ions which are also observed in the mass spectrum of sample d are given in brackets.

the deviations of precision masses (dots) of ions proposed for the mass spectrum of sample e, and of known reference masses (encircled dots) from the calculated precision masses as obtained by interpolation, plotted as a function of *m/e*. The identification is considered correct when the deviations fall, within experimental scatter of less than ±5 millimass units, on a smooth line.

Mass spectra obtained from the analysis of samples a, b, and d, as explained in the Experimental Section, are plotted in Figure 3 for comparison. The mass spectrum of sample e has been omitted. It resembles the spectrum d rather closely, except from being more intense, *cf.* Table II. The peak heights are drawn proportional to the densitometer readings. Whenever more than one line was observed at a nominal mass position, this has been indicated by an asterisk. The peak height, in these cases, gives the intensity of the strongest line. The spectra in Figure 3 include mass numbers up to *m/e* 150. Considerably higher mass numbers, some with high intensities, appeared in the spectra of samples a, d, and e (highest observed *m/e* values were 269 for sample a, 392 for sample d, and 287 for sample e), indicating the presence of high molecular weight compounds or clusters, in accordance with the low volatilities of the aerosols.

The elemental composition of the observed ions $C_xH_yO_z$ in samples a, b, d, and e are listed in Table II. Ions of very low intensity (optical density <4) have been omitted. Sulfur containing ions are listed separately in Table III. The densitometer readings are included in the tables as a measure of the relative intensities. The ordering in Table II is basically by increasing mass number, however, groups of ions with constant numbers of carbon and oxygen atoms are lumped together to faciliate an overview of the results.

Acetone is injected into the mass spectrometer at the start of every analysis for emitter adjusting purposes. Therefore, a low intensity background line at *m/e* 58 ($C_3H_6O^+$) might be expected from this procedure which does, however, not account for the very high intensity of this ion in the spectra of Table II. Sample d does of course contain acetone from the elution process.

Discussion

Our findings, summarized in Tables II and III, have to be discussed in the light of previous analyses of olefin–ozone reaction products, among these a recent study by Pitts, *et al.*,[15] who detected stable intermediate products in a low pressure flow tube coupled to a photoionization mass spectrometer. The vapor pressures of the ozonolysis products of 1-butene, *cf.* the boiling points listed with the identified products in Table II, are generally high at room temperature, in contrast to the observed low evaporation rate of several types of condensates and aerosols, even at 10^{-5}

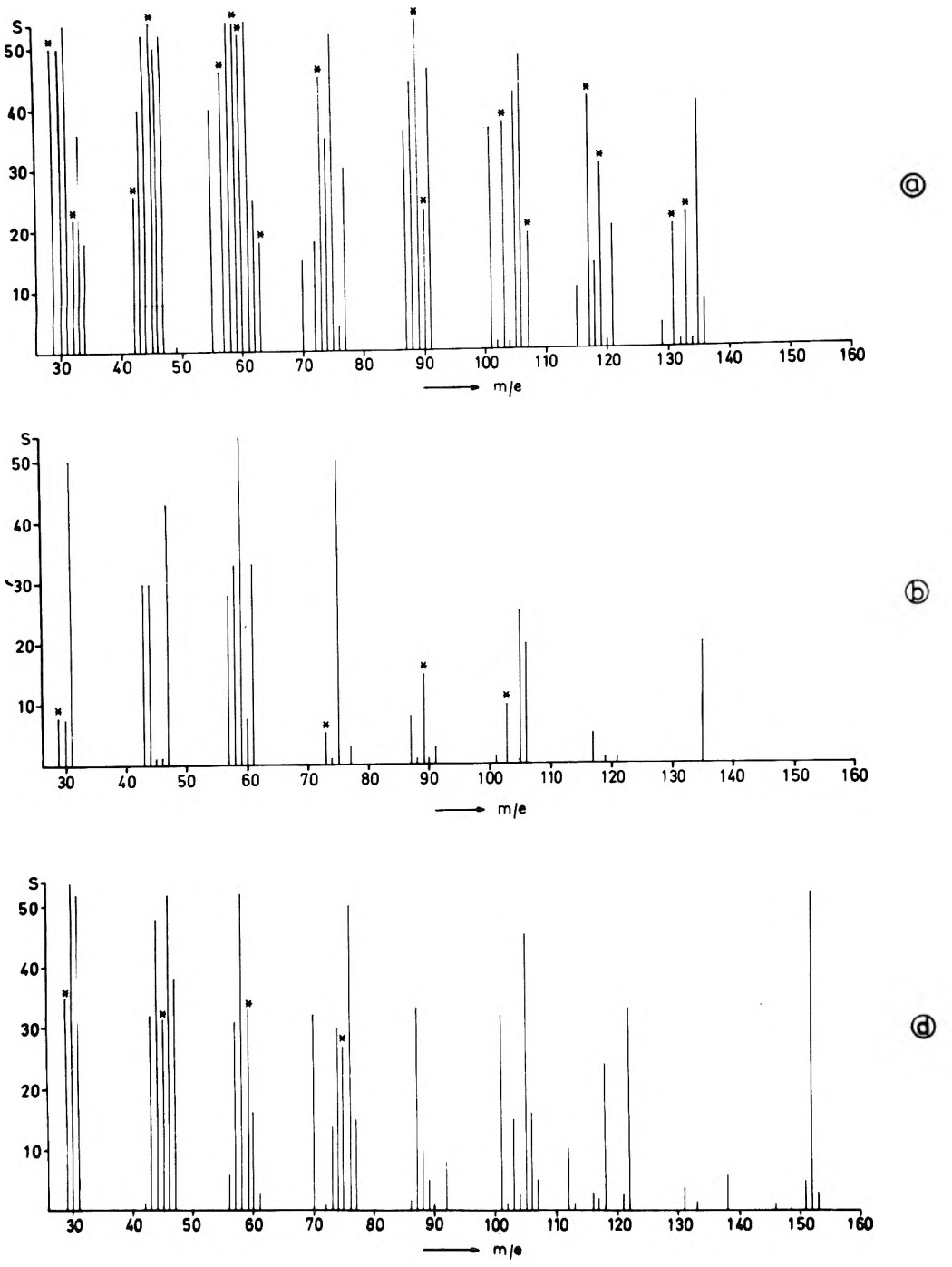

Figure 3. Field desorption mass spectra of condensable products and aerosols from the reaction of ozone with 1-butene, samples a, b, and d; see text and Table I for details of sample preparation and collection.

Torr in the ion source. This observation as well as the presence of complex ions in the higher mass region leads us to the conclusion that the vapor pressure of the aerosol is reduced by structures of high molecular weight, probably condensates or aggregates of aldehydes and acids held together by strong hydrogen bonds, which also give rise to the high viscosity, and reduce the activities of otherwise volatile products in the solution. This is in accordance with Cvetanović's observation of "free" and "bound" carbonyl products.[2]

On attributing parent compounds to the various ions listed in Table II, allowance had to be made for a number of reactions commonly observed in field desorption work, such as formation of $(M + H)^+$ ions due to protonation.[11] The relatively high $(M-H)^+$ ion intensities may be taken as further evidence of strong intermolecular bonding.[16] More complex reactions (formation of cluster ions, *e.g.*, addition of H_3O^+, especially in sample a), may in part account for some of the ions in the higher mass range. No parent ions were proposed whenever the number of isomers consistent with the elemental composition of an ion was too great to make a decision. We are, however, confident on the basis of recent experiences with complex mixtures[12] and biopolymers,[13,16] that these ions are not accounted for by fragmentation or pyrolysis of a polymer. The high oxygen content of all ions is evidence against simple chain polymerization

of the olefin, stressing the importance of secondary reactions of oxygen-containing primary products, including zwitterions.

Several of the products listed in Table II confirm the findings of other investigators. Formaldehyde, acetaldehyde, propionaldehyde, but only traces of butyraldehyde have been detected by Cvetanović.[2] Formic acid was also identified in that study, but no analysis for other acids was carried out. Ketenes as products of other olefins were reported by Scott, *et al.*,[17] and by Pitts, *et al.*[15] The abundance of formic acid and propionic acid is evidence in favor of a rearrangement of the "zwitterion" or biradical into carboxyl compounds, probably *via* a cyclic peroxidic structure, which has been calculated to be energetically favorable.[18] The rearrangement of zwitterions into acids is expected to be favored at high pressures. Accordingly, extremely low acid yields, but high CO yields, have been recently observed in the ozonolysis of propene at 22 mTorr total pressure.[19] The abundance of C_2 products, such as acetaldehyde, acetic acid, and ketene, stresses the importance of abnormal ozonolysis reactions, *e.g.*, splitting of the primary ozone–olefin complex of 1-butene into C_2 fragments, or degradation of the C_3 zwitterion.

The most reasonable interpretations of the ions $C_2H_2O^+$, $C_3H_4O^+$, and $C_4H_6O^+$ in Table II are ketene and its homologs, which may be derived from the acids or their zwitterion precursors by loss of one water molecule. These ions are in fact most abundant in the spectrum of sample e which was produced under anhydrous conditions, and contained sulfuric acid as a dehydrant.

H_2O_2 is an interesting product, since HO_2 radicals are its most probable precursors, and these are also important oxidizing chain carriers in photochemical air pollution. H_2O_2 was, however, only detected in the low pressure experiment, in agreement with Pitts, *et al.*,[15] being absent at atmospheric pressure. The weak HO_2^+ ion in sample e is probably due to fragmentation of a peroxidic compound. The absence of H_2O_2 at high pressures may be accounted for by collisional stabilization of a HO_2 precursor which decomposes at low pressures.

The presence of an ozonide among the products cannot be excluded on the basis of our data, but this is certainly not an important stable product. The $C_4H_8O_3^+$ ion can equally be accounted for by an α-keto-hydroperoxide which was proposed as a relatively stable precursor of some ozonolysis products.[20]

Table III lists all sulfur containing ions which have been detected in sample e, some of which were also present in sample d. Most intense are the ions $H_2SO_4^+$ and $H_3SO_4^+$, providing direct evidence of free sulfuric acid production in this system. Since SO_2 does not react with pure ozone,[1,8] the oxidizing agent must be a product of the ozone–olefin reaction. So far, no intermediate products of this oxidation process have been reported in the literature. Table III includes five sulfur containing organic ions. These cannot, however, be attributed to stable derivatives of sulfuric acid or sulfurous acid. In Table III, these ions have been formally split into $SO_2 + C_xH_yO_z$, or $SO_3 + C_xH_yO_{z-1}$, where the organic formula implies only a residue. It is found that most of the organic residues, preferentially of the type $C_xH_yO_{z-1}$, are also observed as separate ions of high intensity in the spectra. One might speculate that $CH_3SO_4^+$ (*m/e* 110.957) and $C_2H_5SO_4^+$ (*m/e* 124.991) are protonated addition products of SO_2 and the zwitterions CH_2OO or C_2H_4OO, respectively, thus providing direct evidence of intermediary reaction products in the system. These and other mixed ions in Table III may likewise be interpreted as mixed anhydrides of sulfurous or sulfuric acid with formic, acetic, and propionic acid, but a more detailed discussion seems not warranted on the basis of the available information.

Acknowledgment. The authors thank U. Nitschke, Bonn, for his excellent technical assistance in recording the field desorption mass spectra.

H.-R.S. thanks the "Deutsche Forschungsgemeinschaft" for supplying the computer (PDP 8-E) for precise mass measurements, and the "Landesamt für Forschung des Landes Nordrhein-Westfalen" for providing the double-focussing mass spectrometer.

Financial support of part of this work by the "Bundesminister des Inneren" under Grant No. U III 2-320-01-7/72 is gratefully acknowledged.

References and Notes

(1) P. A. Leighton, "Photochemistry of Air Pollution," Academic Press, New York, N.Y., 1961.
(2) T. Vraaski and R. J. Cvetanović, *Can. J. Chem.*, **38**, 1063 (1960).
(3) Y. K. Wei and R. J. Cvetanović, *Can. J. Chem.*, **41**, 913 (1963).
(4) C. W. Gillies, R. P. Lattimer, and R. L. Kuczkowski, *J. Amer. Chem. Soc.*, **96**, 1536 (1974).
(5) H. Niki, E. E. Daby, and B. Weinstock, *Advan. Chem. Ser.*, **No. 113** (1972).
(6) T. A. Hecht and J. H. Seinfeld, *Environ. Sci. Technol.*, **3**, 1175 (1972).
(7) R. A. Cox and S. A. Penkett, *J. Chem. Soc., Faraday Trans. 1*, **68**, 1735 (1972).
(8) K. H. Becker, U. Schurath, V. Kriesche, H. Seitz, and K. Löbel, Annual Report 1973, Institut für Physikalische Chemie, University of Bonn, Project No. U III 2-320-01-7/72 of the Bundesministerium des Innern.
(9) U. Schurath and H.-R. Schulten, to be submitted for publication.
(10) H.-R. Schulten and D. E. Games, *Biomed. Mass Spectrom.*, **1**, 120 (1974), and references cited therein.
(11) H.-R. Schulten and H. D. Beckey, *Org. Mass Spectrom.* **7**, 861 (1973).
(12) H.-R. Schulten, H. D. Beckey, H. L. C. Meuzelaar, and A. J. H. Boerboom, *Anal. Chem.*, **45**, 191 (1973).
(13) H.-R. Schulten, H. D. Beckey, A. J. H. Boerboom, and H. L. C. Meuzelaar, *Anal. Chem.*, **45**, 2358 (1973).
(14) H. D. Beckey, *Int. J. Mass Spectrom. Ion. Phys.*, **2**, 500 (1969).
(15) R. Atkinson, B. J. Finlayson, and J. N. Pitts, Jr., *J. Amer. Chem. Soc.*, **95**, 7592 (1973).
(16) H.-R. Schulten, "New Approaches to the Identification of Microorganisms," Part A, "New Technologies in the Automation of Microbiological Identification Routines," Heden/Illeni, Ed., Wiley, New York, N.Y., 1974, pp 117–125.
(17) W. E. Scott, E. R. Stephens, P. L. Hanst, and R. C. Doerr, *Proc. Amer. Petrol. Inst.*, **37**, III, 171 (1957).
(18) Tae-Kyu Ha, H. Kühne, S. Vaccani, and Hs. H. Günthard, *Chem. Phys. Lett.*, **24**, 172 (1974).
(19) K. H. Becker, U. Schurath, and H. Seitz, *Int. J. Chem. Kinet.*, in press.
(20) H. E. O'Neal and C. Blumstein, *Int. J. Chem. Kinet.*, **V**, 397 (1973).

Optical Spectra of Sodium, Potassium, Rubidium, and Cesium in Binary Solutions of Ethylenediamine and Hexamethylphosphoramide[1]

Paula S. Childs and Robert R. Dewald*

Department of Chemistry, Tufts University, Medford, Massachusetts 02155 *(Received July 29, 1974)*

The optical absorption spectra of the alkali metals Na, K, Rb, and Cs in binary solutions of ethylenediamine and hexamethylphosphoramide were studied at room temperature. The maximum of the spectrum of e_{sol}^- was found to be located between the reported maxima in the pure solvents, and its position was dependent on the composition of the binary solution. The peak position for the M^- species was found to be dependent on both the metal and the solvent composition. A correlation of the absorption maxima of all species with dielectric properties was found. The spectra of Na^-, K^-, Rb^-, and Cs^- obey criteria of a charge-transfer-to-solvent transition. The high-energy sides of the e_{sol}^- spectra were found to be consistent with bound–continuum transition.

Introduction

The physical and chemical properties of alkali metal solutions in polar solvents have been extensively studied by numerous investigators.[2-15] Metal–amine solutions (except Li) appear to contain at least two species: solvated electrons (including ion pairs of solvated electrons) and a diamagnetic species, identified as M^-.[9,14,16] Solutions resulting from the dissolution of the alkali metals (except Li and Na) in ethylenediamine (EDA) exhibit optical absorption spectra with two absorption maxima.[2,15] The location of the peak in the visible–near-infrared region (M band) is dependent on the metal, whereas the peak in the infrared region (S band) is independent of the metal, and occurs at 1280 nm[2,15] (no ir peak has been observed for Na). Optical absorption spectra exhibiting two maxima were reported for alkali metal–hexamethylphosphoramide (HMPA) solutions.[6,17] The absorbing species responsible for the S band in metal–EDA solutions has been identified as the solvated electron, e_{sol}^-, and this assignment was further substantiated by the pulse radiolysis method.[18] Moreover, the assignment of the 2200–2250-nm peak (S band) in HMPA as an absorption due to the solvated electron has been verified by a number of investigators.[6,17,19,20]

Studies of alkali metals dissolved in binary solutions of ethylamine–methylamine[8] and ethylamine–ammonia[21] have recently been reported. The M band observed in these mixtures was identified as a charge-transfer-to-solvent absorption of the M^- species.[8,21] However, the extensive overlap between the M and S bands in the latter binary system did not allow quantitative analysis of the M band as a function of composition.[21]

Using the pulse radiolysis method, the optical spectra of solvated electrons have been studied in a number of binary systems including alcohols–alkanes,[22] ether–EDA,[23,24] H_2O–NH_3,[17,25] H_2O–EDA,[17] H_2O–THF,[24] H_2O–alcohol,[26] and EDA–HMPA.[20] In all cases, the solvated electron absorption peak position in the binary mixtures was intermediate to those in the pure solvents.

This study was undertaken to examine the optical spectra of solutions of alkali metals in mixtures of ethylenediamine and hexamethylphosphoramide as a function of composition and dielectric properties of the solvent system.

Experimental Section

The alkali metals were obtained in highest purity from the following sources: Na, K, and Rb from the United Mineral and Chemical Corp.; Cs was a gift from the Dow Chemical Co. The metals were further purified by a high vacuum distillation process described elsewhere.[2]

Ethylenediamine (Matheson Coleman and Bell, 98-100%) was purified by a fractional freezing process,[27] then refluxed in a dry nitrogen atmosphere to aid in the removal of ammonia, and finally distilled *in vacuo* onto Na–K alloy. The EDA immediately formed a deep blue solution which discharged its color after several days. The middle fraction of the bleached solution was then distilled onto a mirror of distilled Na–K. Several days later, the EDA was distilled into glass breakseal tubes and stored. Hexamethylphosphoramide (a gift from the Dow Chemical Co.) was purified by a procedure similar to one described elsewhere,[6] and stored in breakseal tubes. Both solvents were prepared and used for spectra determinations using high vacuum techniques in a borosilicate glass system, without the use of ground joints or stopcocks. Mixtures of solvents were prepared from volumetric amounts of the pure solvents contained in the calibrated breakseal tubes. All glassware (except optical cells) was cleaned following a reported procedure.[2,6]

For the optical measurements, borosilicate absorption cells of 0.10-mm nominal path length (American Instrument Co.) were sealed to a borosilicate apparatus similar to one described previously.[6] It was constructed to allow examination of the blue solutions separated from any undissolved metal. A Cary 17 recording spectrophotometer was used to record the optical absorption spectra from about 300 to 3000 nm. A matched cell containing purified solvent *in vacuo* was placed in the reference beam. All measurements were made at room temperature (~25°). A WTW Diplometer DMOI (Kahl Scientific Instrument Corp.) equipped with MFL 2/s and MFL 3/s cells[28] was used to determine the static dielectric constants of pure solvents and binary mixtures at 2 MHz and 25.0 ± 0.1°. Refractometric measurements on these solvents were made using an Abbe refractometer (Bausch and Lomb Corp.) at 25.0 ± 0.1°.

TABLE I: Summary of Spectra Data

Mole fraction of HMPA	Absorption max in mixtures of EDA and HMPA, cm^{-1}					Width at half-height for e_{sol}^-, cm^{-1}	Static dielectric constant D_s	Refractive index n_D
	e_{sol}^-	Na^-	K^-	Rb^-	Cs^-			
1.00	4550 ± 100[a]	13,330 ± 90[b]	10,750 ± 60[b]	10,310 ± 80[b]	9000 ± 120[b] sh	3600 ± 300[c]	28.8	1.4570
0.72	4870 ± 130	13,660 ± 90	10,930 ± 60	10,530 ± 80	9100 ± 130 sh	4150 ± 300	23.9	1.4557
0.52	5260 ± 140	13,930 ± 100	11,110 ± 60			4500 ± 400	20.6	1.4552
0.51	5290 ± 140	13,990 ± 100	11,240 ± 60	10,750 ± 90	9470 ± 130 sh	4600 ± 400	20.4	1.4551
0.33	6100 ± 190	14,410 ± 100	11,360 ± 60	10,930 ± 90		5100 ± 600	17.5	1.4545
0.19	6450 ± 210	14,660 ± 110	11,550 ± 70	11,110 ± 90	9600 ± 120	5800 ± 400	15.6	1.4540
0	7810 ± 310	15,150 ± 115	11,330 ± 70	11,240 ± 100	9700 ± 110	6800 ± 500	13.0	1.4533

[a] Estimated average error from three or more scans for each metal. [b] Estimated average error from three or more scans [c] Estimated average error from spectra of sodium and cesium metals.

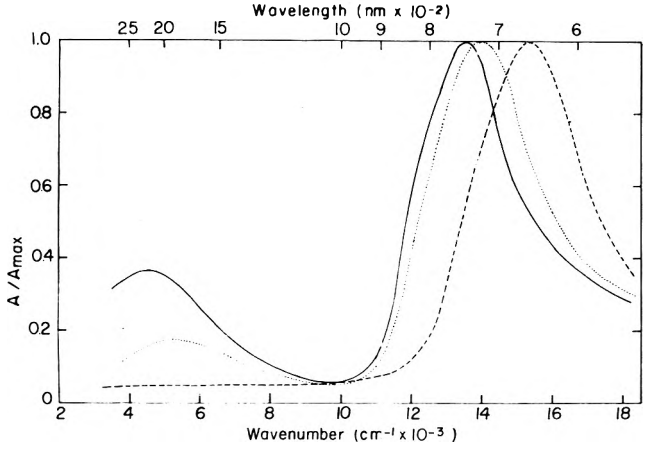

Figure 1. Optical absorption spectra of sodium metal in pure HMPA (—), pure EDA (– – –), and a binary mixture of 51 mol % HMPA (• • • •) at 25°.

Results and Discussion

A summary of the absorption maxima observed is given in Table I. The positions of the absorption maxima were difficult to define precisely because of the broad half-widths (3750–6500 cm^{-1}). The values of the dielectric constants and refractive indices given in Table I were obtained by interpolation, since these parameters were found to be monotonic functions of solvent composition.

Spectra were evaluated by plotting A/A_{max} *vs.* wavenumber. This method allowed for a comparison of solutions of varying concentrations.[2] The spectra were corrected for decomposition during the scan, since the decomposition was found to be a smooth function of time. The rate of decomposition varied with the metal. Sodium solutions were most stable, at times taking as long as 24 hr to discharge the blue color. Potassium and rubidium solutions had an average half-life of 1 hr, whereas cesium solutions bleached within 1 hr. In all cases, M bands decomposed more rapidly than the infrared peaks for the metal solutions in the binary solvent systems.

Figure 1 shows representative absorption spectra for sodium in pure EDA, pure-HMPA, and mixture of 51 mol % HMPA in EDA. Some features are particularly important. The solvated electron and Na^- absorption bands in the binary mixture are located between the corresponding maxima in the pure solvents. Overlap of the bands is minimal, facilitating analysis of the bands. The relative intensity of the solvated electron absorption increases with increasing HMPA concentration. The same trends were also observed for K, Rb, and Cs solutions. Unfortunately, except for the Na solutions, there was extensive overlap of the M and S bands.

The absorption maxima of the metal solutions as a function of a solvent composition are shown in Figure 2. The M^- species maxima are linear functions of solvent composition. It should be pointed out that the position of the Cs^- band was determined from the position of a shoulder. The shift in absorption maxima for the e_{sol}^- species is shown to be strongly influenced by the composition of the binary mixtures. Also, as shown in Figure 2, the same trend in the shift of the absorption maximum of the solvated electron with composition in the binary system was observed using the pulse radiolysis method.[20]

According to the theoretical interpretation of charge-transfer-to-solvent (ctts) spectra by Stein and Treinin,[30] variation of E_{max} with changes in solvent is given by the following expression

$$h\nu_{max} = E_X - L_X + \frac{e^2}{r_0}\left(\frac{1}{2} + \frac{1}{2D_{op}} - \frac{1}{D_s}\right) - \frac{e^2}{2R_e}\left(1 - \frac{1}{D_{op}}\right) - \frac{\pi^2 m e^4}{2h^2}\left(\frac{1}{D_{op}} - \frac{1}{D_s}\right)^2$$

where E_X and L_X are the respective electron affinity and solvation energy of the X radical associated with X^- ion undergoing a ctts transition. D_{op} and D_s are optical and static dielectric constants of the solvent. R_e is the mean distance of the electron in the excited ctts state and r_0 is the radius parameter characterizing the ionic cavity. The important term in the above equation is the third on the right-hand side[30,31] which contains r_0. Hence, to the first approximation the theory predicts that a plot of E_{max} *vs.* $(\frac{1}{2} + \frac{1}{2}D_{op} - 1/D_s)$ should be linear. The correlation of the absorption maxima for the M^- species is shown in Figure 3. Using the method of least squares, values of 2.5 ± 0.1, 4.5 ± 0.3, 5.0 ± 0.5, and 6.5 ± 1.4 Å were determined for the radius parameter, r_0, for Na^-, K^-, Rb^-, and Cs^-, respectively. These r_0 values are in agreement, within experimental error, with the values estimated by Matalon, *et al.*,[21] and the trend of increasing r_0 values from Na^- to Cs^- is as expected. Moreover, there is a linear correlation (not shown) of the absorption maxima of the K^-, Rb^-, Cs^-, and e_{sol}^- species with Na^- which is in agreement with the prediction of the ctts theory.[29] Recently, Fox and Hayon[32] have shown that there is a good linear correlation for the absorption maxima of solvated electrons in some 30 different solvents or solvent mixtures *vs.* the absorption maxima of the iodide ion in the same medium. They concluded that the electronic transitions of the solvated electron paralleled those of the ctts transitions of the iodide ion. Thus, Figure

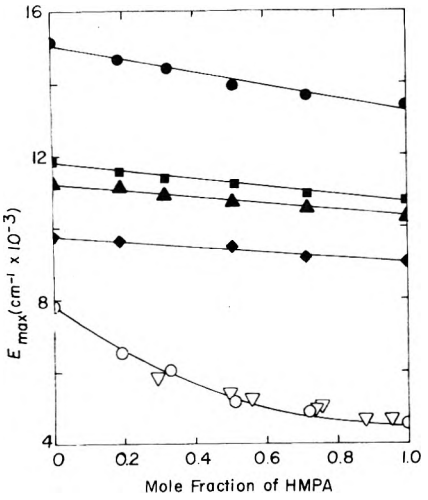

Figure 2. The variation of composition with peak position: ●, Na^-; ■, K^-; ▲, Rb^-; ♦, Cs^-; O, e_{sol}^-; ∇, e_{sol}^- by pulse radiolysis.[18,20]

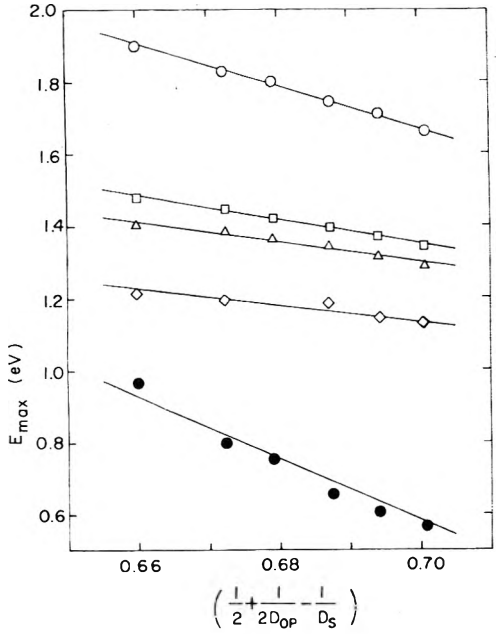

Figure 3. Plot of E_{max} (eV) *vs.* $(1/2 + 1/2D_{op} - 1/D_s)$ for Na^- (O), K^- (□), Rb^- (△), Cs^- (◊), and e_{sol}^- (●) in the pure solvents and various binary mixtures of EDA and HMPA.

3 also shows a correlation of the absorption maxima of e_{sol}^- in the binary mixtures. The radius parameter (ctts theory) for e_{sol}^- was found to be 1.7 ± 0.4 Å as determined by the method of least squares.

Figure 4 shows another correlation between the dielectric properties of the binary solvent system and E_{max} for e_{sol}^-, namely, the function $\beta = 1/D_{op} - 1/D_s$. This parameter appears in the Landau polaron theory[33,34] and modified continuum models.[35] It should be noted from Figure 4 that the correlation is equally linear with β or β^2, within experimental error. These correlations are in contrast to observations of solvated electrons in a number of other binary mixtures.[23,36]

The variation with composition of the half-width of the absorption bands for Na^- and e_{sol}^- is shown in Figure 5. The invariance of the half-width of the Na^- band with composition is striking. This invariance could suggest selective solvation by EDA in the binary systems studied.

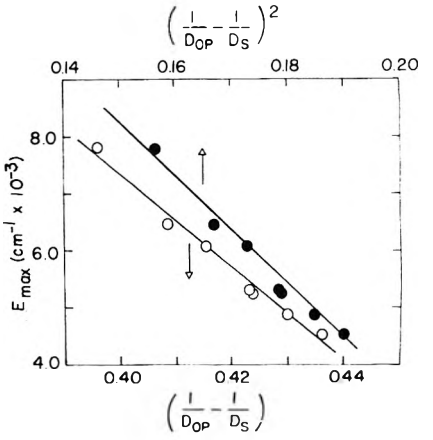

Figure 4. Plots of E_{max} for the solvated electron *vs.* $1/D_{op} - 1/D_s$ and $(1/D_{op} - 1/D_s)^2$ for the pure solvents and mixtures.

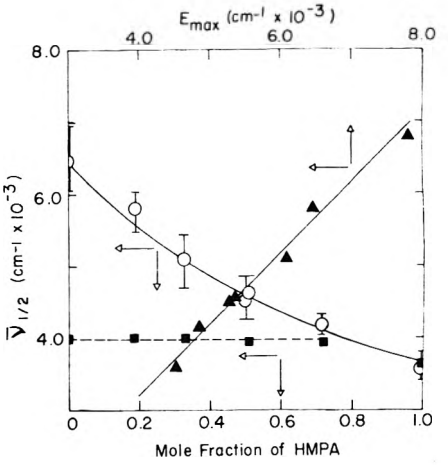

Figure 5. Variation of half-widths ($W_{1/2}$) for e_{sol}^- (O) and Na^- (■) with composition and the relation between half-width and peak position for e_{sol}^-, ▲.

HMPA is known to solvate negative ions extremely weakly.[5] Therefore, it appears that the ctts transition for Na^- in the binary mixtures is characteristic of the transition in pure EDA as far as half-width is concerned. Unfortunately, overlap is too extensive to determine the half-width for the K^-, Rb^-, and Cs^- bands with any certainty.

The variation with composition of the half-width of the e_{sol}^- band was difficult to determine precisely, due to broad half-width of the bands and a small dependence on metal concentration. In spite of these difficulties, the variation of the half-width of e_{sol}^- with composition is significant, Figure 5. This variation is similar to that observed for e_{sol}^- in H_2O–NH_3 mixtures.[18] We also conclude[18] that this variation can not be accounted for by a simple substitution model based upon a small solvation number for the solvated electron. Theoretical models, although providing valuable insight into the nature of solvated electrons[35,37] and ctts transitions,[31] do not account yet for the shape of the absorption band in any quantitative fashion.[38] In a recent paper, Kestner and Jortner[37] discussed possible sources of line broadening which included medium polaron modes, contribution of several types of cavities, and distortion of the cavity from its spherical shape. On the other hand, Lugo and Delahay[38] were successful in a phenomenological fitting of the solvated electron spectrum in HMPA by superposition of four gaussian distributions and one bound-

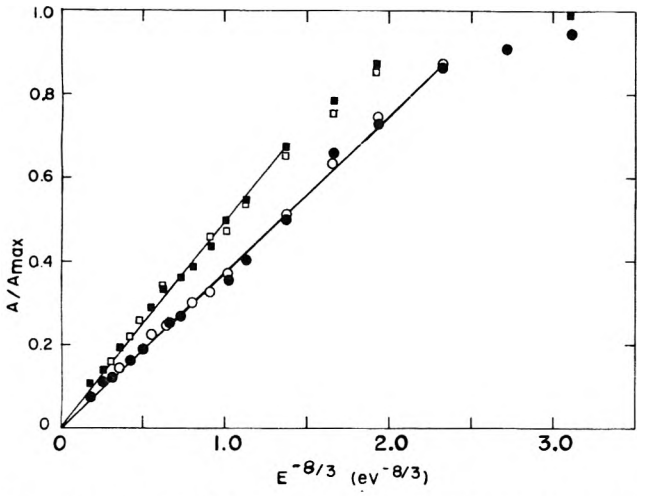

Figure 6. The normalized experimental absorbancy plotted against $E^{-8/3}$ for solvated electron. ■ and □ represent Cs and Na metal in 0.51 mole fraction HMPA. ● and ○ represent Cs and Na metal in 0.72 mole fraction HMPA.

continuum band. Unfortunately, their resolution of the e_{sol}^- band in EDA is tentative due to insufficient experimental data. Moreover, convincing experimental evidence has been recently presented that the spectra obtained for $Na–NH_3$ solutions and for $Na–NH_3–NaI$ solutions fulfill the expectations of a two absorber model.[39] In Figure 5, the linear correlation of the absorption maxima to the half-width is to be noted. This correlation indicates that whatever property (or properties) affects the absorption maximum of e_{sol}^- in the binary system has a similar effect on the half-width. From the above discussion, many factors are suspected to contribute to line shapes. The results shown in Figure 4 and 5 suggest that for this particular binary solvent system, medium polaron modes are important factors in determining peak position and half-width. This, however, does not rule out the possibility that the observed e_{sol}^- band in the HMPA–EDA mixtures is a superposition of two or more bands and that energy levels, band amplitudes, widths, etc. associated with one or more of these bands are characterized by the dielectric properties of the media.

Delahay[40] has shown that plots of experimental absorbances in the high-energy tail of e_{sol}^- *vs.* $E^{-8/3}$ should give a straight line passing through the origin. Such linear plots have been presented by Lugo and Delahay[38] for the solvated electron in a number of solvents including HMPA. Figure 6 shows plots of A/A_{max} *vs.* $E^{-8/3}$ for e_{sol}^- in two binary mixtures. The linearity of these plots should be noted and these results suggest a bound–continuum transition.[38] We also noted (not shown) plots of mole fraction of HMPA *vs.* $E_{max}^{-8/3}$ were linear for Na^-, K^-, Rb^-, Cs^-, and e_{sol}^-. It is hoped that the experimental results presented here will be helpful in the future development of better theoretical understanding of solvated electrons.

Acknowledgment. This work was supported by the National Science Foundation.

References and Notes

(1) (a) Abstracted from the Ph.D. Thesis of P. S. Childs, Tufts University, 1974. (b) Presented in part at the 166th National Meeting of the American Chemical Society, Chicago, Ill., 1973.
(2) R. R. Dewald and J. L. Dye, *J. Phys. Chem.*, **68**, 121 (1964).
(3) K. Bar-Eli and T. R. Tuttle, Jr., *J. Chem. Phys.*, **40**, 2508 (1964).
(4) M. Ottolenghi, K. Bar-Eli, and H. Linschitz, *J. Chem. Phys.*, **43**, 206 (1965).
(5) H. Normant, *Angew. Chem., Int. Ed. Engl.*, **6**, 1046 (1967).
(6) J. M. Brooks and R. R. Dewald, *J. Phys. Chem.*, **72**, 2655 (1968).
(7) D. Huppert and K. H. Bar-Eli, *J. Phys. Chem.*, **74**, 3285 (1970).
(8) G. Gabor and K. Bar-Eli, *J. Phys. Chem.*, **75**, 286 (1971).
(9) M. G. Debacker and J. L. Dye, *J. Phys. Chem.*, 75, 3092 (1971).
(10) B. Baron, P. Delahay, and R. Lugo, *J. Chem. Phys.*, **55**, 4180 (1971).
(11) J. L. Dye, M. G. Debacker, J. A. Eyer, and L. M. Dorfman, *J. Phys. Chem.*, **76**, 839 (1972).
(12) K. Bar-Eli and G. Gabor, *J. Phys. Chem.*, **77**, 323 (1973).
(13) J. W. Fletcher, W. A. Seddon, J. Jevcak, and F. C. Sopchyshyn, *Chem. Phys. Lett.*, **18**, 592 (1973).
(14) M. T. Lok, F. J. Tehan, and J. L. Dye, *J. Phys. Chem.*, **76**, 2975 (1972).
(15) I. Hurley, T. R. Tuttle, Jr., and S. Golden in "Metal-Ammonia Solutions," J. J. Lagowski and M. J. Sienko, Ed., Butterworths, London, 1970, p 449.
(16) J. L. Dye, *Accounts Chem. Res.*, **1**, 306 (1968).
(17) R. Catterall, L. P. Stodulski, and M. C. R. Symons, *J. Chem. Soc. A*, 437 (1968).
(18) J. L. Dye, M. G. Debacker, and L. M. Dorfman, *J. Chem. Phys.*, **52**, 6251 (1970).
(19) E. Saito, in ref 15, p 485.
(20) E. A. Shaede, L. M. Dorfman, G. J. Flynn, and D. C. Walker, *Can. J. Chem.*, **51**, 3905 (1973).
(21) S. Matalon, S. Golden, and M. Ottolenghi, *J. Phys. Chem.*, 73, 3098 (1969).
(22) R. R. Hentz and G. Kenney-Wallace, *J. Phys. Chem.*, **76**, 2931 (1972).
(23) F. Y. Jou and L. M. Dorfman, *J. Chem. Phys.*, **58**, 4715 (1973).
(24) L. M. Dorfman, F. Y. Jou, and R. Wageman, *Ber. Bunsenges. Phys. Chem.*, **75**, 681 (1971).
(25) R. Olinger and U. Schindewolf, *Ber. Bunsenges. Phys. Chem.*, **75**, 693 (1971).
(26) S. Arai and M. C. Sauer, Jr., *J. Chem. Phys.*, **44**, 2297 (1966).
(27) L. H. Feldman, R. R. Dewald, and J. L. Dye, *Advan. Chem. Ser.*, **No. 50**, 163 (1965).
(28) We appreciate the cooperation of the Department of Chemistry at Wellesley College, Wellesley, Mass., for loaning us the dielectric constant cells.
(29) I. Burak and A. Treinin, *Trans. Faraday Soc.*, **59**, 1490 (1963).
(30) G. Stein and A. Treinin, *Trans. Faraday Soc.*, **55**, 1086 (1959).
(31) M. J. Blandamer and M. F. Fox, *Chem. Rev.*, **70**, 59 (1970).
(32) M. F. Fox and E. Hayon, *Chem. Phys. Lett.*, **25**, 511 (1974).
(33) R. Platzman and J. Franck, *Z. Phys.*, **138**, 411 (1954).
(34) J. Jortner, *J. Chem. Phys.*, 30, 839 (1959).
(35) D. A. Copeland, N. R. Kestner, and J. Jortner, *J. Chem. Phys.*, **53**, 1189 (1970).
(36) L. M. Dorfman and F. Y. Jou in "Electrons in Fluids," J. Jortner and N. R. Kestner, Ed., Springer-Verlag, Heidelberg, 1973, p 447.
(37) N. R. Kestner and J. Jortner, *J. Phys. Chem.*, **77**, 1040 (1973).
(38) R. Lugo and P. Delahay, *J. Chem. Phys.*, **57**, 2122 (1972).
(39) G. Rubinstein, T. R. Tuttel, Jr., and S. Golden, *J. Phys. Chem.*, **77**, 2872 (1973).
(40) P. Delahay, *J. Phys. Chem.*, **55**, 4188 (1971).

A Spectral Study of Matrix-Isolated *ms*-Tetraphenylporphines. Isolation of an Iron(II) Complex

John J. Leonard and Frederick R. Longo*

Drexel University, Chemistry Department, Philadelphia, Pennsylvania 19104 *(Received May 15, 1974)*

Tetraphenylporphine (TPP), tetraphenylchlorin (TPC), tetraphenylbacteriochlorin (TPBC), the Zn, Cu, Ni, and Co complexes of TPP, and Fe(III)TPPCl were studied in *n*-octane matrices. TPP was also studied in matrices of Ar and SF_6. Fe(II)TPP was isolated by the Knudsen deposition technique from Fe(II)TPP(piperidine)$_2$. None of the tetraphenylporphines in any of the matrices studied exhibited the sharp absorption peaks or quasilines reported for porphines, tetrabenzporphines, and phthalocyanines. Calculations show that quasilines arising from metalloporphyrin pair splitting are probably not observable under the conditions of our experiments at 23°K. The matrix spectra of Fe(II)TPP are interpreted in terms of interactions with host molecules, Ar, *n*-C_8H_{18}, O_2, N_2, and NH_3.

Introduction

In a previous paper[1] we reported results of our absorption spectral study of matrix-isolated porphine, zinc porphine, and copper porphine. The matrix spectra exhibited many features which were absent in the room temperature solution spectra. Similar effects had been reported for phthalocyanines and tetrabenzporphines.[2] These results were interpreted in terms of metal porphine pair formation and the resulting Davydov splitting of the excited states. In this paper, we report the results of our study of matrix-isolated tetraphenylporphines (TPP) in matrices of *n*-octane, argon, and sulfur hexafluoride. Also, we have isolated a ferrous tetraphenylporphine with no axial ligands, and have recorded spectra in oxygen, nitrogen, ammonia, and the above three matrices.

Expermental Section

The Knudsen deposition technique employed in these experiments and the method of taking the absorption spectra were described previously.[1] Tetraphenylporphine was prepared and purified by the method of Adler, *et al.*[3] Metal tetraphenylporphines were prepared and purified by a previously reported method.[4] *meso*-Tetraphenylchlorin was prepared as follows. To 100 ml of pyridine were added 1.0 g of TPP and 1.00 ml of N_2H_4–H_2O; 3.00 ml of 30% H_2O_2 solution was added dropwise over a 10-min period. The solution was refluxed for 35 min, then placed in a refrigerator overnight. The solvent was evaporated under vacuum; the residue was dissolved in about 200 ml of chloroform and chromatographed on a column (d = 2.5 cm, h = 35 cm) of basic alumina. No distinct fractionation appeared on the column but pure tetraphenylchlorin (TPC) comes off in the first few fractions followed by fractions progressively richer in TPP. Visible absorption spectra were taken of all fractions and those whose absorbance at 650 nm was 5 to 7 times greater than at 598 nm were combined and rechromatographed. Fractions from the second chromatography whose visible spectrum agreed with the literature[5] were combined and the TPC was precipitated by gently boiling off the chloroform while methanol was slowly added. Approximately 250 mg of pure TPC (25%) was obtained. *meso*-Tetraphenylbacteriochlorin (TPBC) was prepared by the method of Whitlock, *et al.*[6] The bipiperdine complex of Fe(II)TPP was prepared by a method described by A. D. Adler in a private communication. Fe(III)TPPCl (0.5 g) was dissolved in 50 ml of piperidine at room temperature. The solution was allowed to stand for 10 min; then the piperidine was removed under vacuum leaving pure Fe(II)TPP(piperidine)$_2$. The Mössbauer spectrum of the material agreed with that in the literature.[7] We could detect no Fe(III)TPPCl by ordinary chemical and spectral examination.

Results

The results of the study of TPP, tetraphenylchlorin (TPC), and tetraphenylbacteriochlorin (TPBC) are summarized in Table I and Figure 1. TPP, its reduced derivatives, and its metal derivatives (Zn, Cu, Ni, Co, Fe(II), and Fe(III)Cl) were all studied in a *n*-octane matrix. TPP was also studied in matrices of argon and sulfur hexafluoride. No quasilines were observed for any of the above compounds under any of the conditions used in this study. The bands are sharper in the matrix spectra than in the room temperature solution spectrum, and they broaden with increasing temperature as would be expected. For comparison, the bandwidth at half-maximum for Q_x(0–0) of TPP in benzene solution is approximately 20 nm, while it is 3 nm in an agron matrix at 23°K.

Shoulders did appear in the TPP spectrum in the Ar and SF_6 matrices. There is a shoulder to the red of the 420-nm peak which may indicate a splitting of the main transition. The Q_y(1–0) band has a definite shoulder to the blue when recorded in an Ar matrix. In the SF_6 matrix-isolated sample, this shoulder and one to the red of Q_x(1–0) were present. These results seem to confirm the contention of many that the visible bands observed in solution spectra at room temperature are merely envelopes of several vibronic transitions.

The peak positions for TPP and its reduced derivatives were independent of deposition temperature and mole ratio in the region 500:1 to 5000:1. For TPP in octane with mole ratios less than 500:1 there appears to be a red shift as the concentration of TPP increases. This would be expected; the TPP thin film spectrum which was recorded in this study, in agreement with that reported by Assour,[8] shows peaks to the red of those observed in benzene solution or in the other matrices used in this study. Therefore, as the

TABLE I: Matrix Isolated TPP, TPC, and TPBC

Compd; matrix; temp, °K; mole ratio	Band	Wavelength, nm	Half-Width, nm 77°K	Half-Width, nm 135°K	Remarks
TPP; octane; 77, 135; 2500:1	"400"	400.0	7.0	8.5	
	Soret	420.0	19.0	22.0	
	"480"	482.0	12.0	13.0	
	$Q_y(01)$	515.5	18.5	19.0	
	$Q_y(00)$	551.5	14.0	16.0	
	$Q_x(01)$	585.0	9.0	10.5	
	$Q_x(00)$	646.0	9.0	10.0	
TPP; argon; 23; 3000:1		394.0	2.5		
		412.0	10.0		
					blue shd
		510.0	15.0		
		544.0	8.0		
		585.0	6.0		
		645.0	3.0		
TPP; SF_6; 23; 3000:1					
		475.0	10.0		
		510.0	15.0		blue shd
		541.0	10.0		
		585.0	8.0		red shd
		645.5	6.0		
TPC; *n*-octane; 77, 135; 2500:1	"400"	403.0	9.0	9.5	
	Soret	421.0	14.0	16.0	
	$Q_x(01)$	516.5	17.0	20.8	
	$Q_x(00)$	547.5	16.0	16.5	
	$Q_y(01)$	592.0	10.0	11.0	
	$Q_y(00)$	650.5	10.0	12.0	
TPBC; *n*-octane; 77, 135; 3000:1		353.6	10.5	11.0	
		377.0	8.4	10.0	
		520.5	17.0	17.5	
		723.8	9.5	11.0	

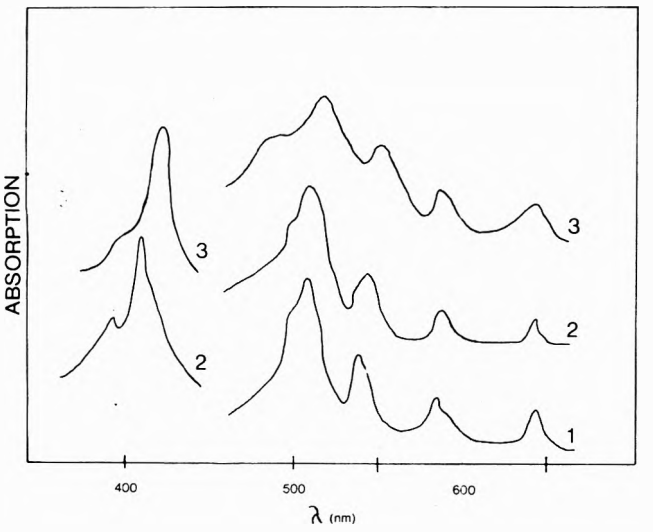

Figure 1. Absorption spectra of matrix-isolated TPP: (1) SF_6 matrix, 23°K, 3000/1; (2) Ar matrix, 23°K, 3000/1; (3) *n*-octane matrix, 77°K, 2500/1.

TABLE II: (Metal)TPP (*n*-Octane Matrix)

Compd; mole ratio	Wavelength, nm	Half-width, nm 77°K	Half-width, nm 135°K
ZnTPP; 4000:1	404.8	8.0	
	427.0	14.0	
	555.0	20.0	25.0
	595.0	9.0	11.0
CuTPP; 3500:1	393.0	7.5	
	418.4	13.5	
	539.0	20.0	22.0
	577.0	10.0	10.5
NiTPP; 4000:1	420.0	14.5	
	519.0	15.0	17.5
	551.0		
CoTPP	420.0	16.0	
	536.0	20.0	23.0
	572.0		
Fe(III)TPPCl	409.0	14.0	
	513.0	15.0	
Fe(II)TPP	421.0	18.0	
	542.0	15.0	15.0
	588.5	6.0	6.5

concentration of TPP increases, TPP–TPP interactions become stronger and cause the red shift, as observed in the thin film. There are clearly two bands in the Soret region of the TPP and TPC matrix spectra, at about 420 and 400 nm.

The results of the study of metal TPP's in *n*-octane matrices are summarized in Table II and Figure 2. Again the peak positions were independent of deposition temperature and mole ratio in the region 500:1 to 5000:1. The absorption bands are sharper than in the room temperature solution spectra and broaden with increasing temperature as expected. Trends observed in the room temperature solution spectra still remain in the matrix spectra. There were no extra bands as observed by Lucia, *et al.*,[9] for copper phthalocyanine isolated in an argon matrix. The metal TPP spectra show no quasilines as were reported by Bajema[2] for free base and metal phthalocyanines and tetrabenzporphines in argon matrices, and by us[1] for metalloporphines in Ar, SF_6, and *n*-octane matrices.

The Fe(II)TPP was obtained when the Fe(II)TPP(piper-

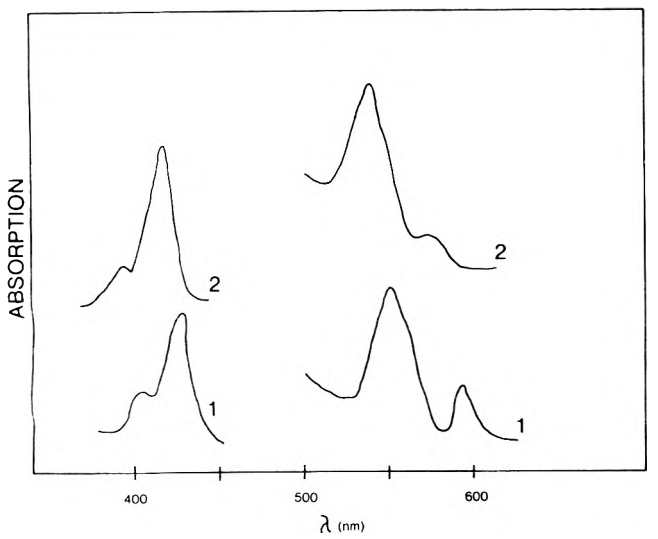

Figure 2. Absorption spectra of MTPP's 77°K: (1) ZnTPP, *n*-octane matrix, 4000/1; (2) CuTPP, *n*-octane matrix, 3500/1.

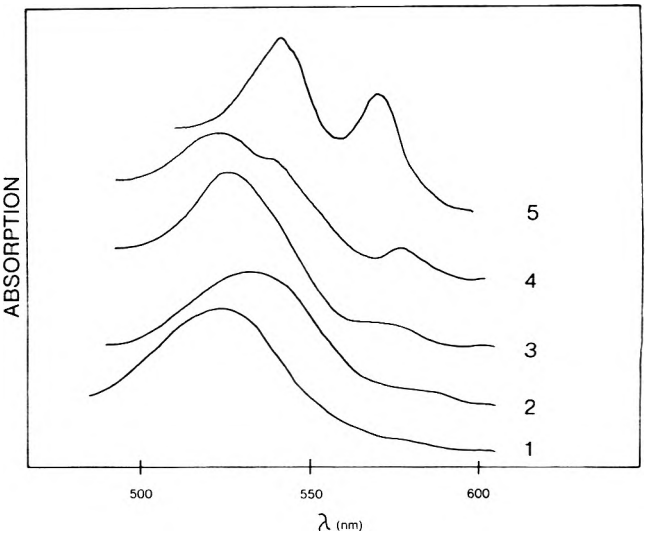

Figure 3. Absorption spectra of Fe(II)TPP at 23°K: (1) Ar matrix, 2500/1; (2) *n*-octane matrix, 3000/1; (3) N_2 matrix, 3000/1; (4) O_2 matrix, 3000/1; (5) NH_3 matrix, 3000/1.

idine)$_2$ complex was heated to 300° in the Knudsen cell. (A similar result was reported for MnTPP complexes.)[10] Several observations support the contention that Fe(II)TPP has been isolated. During the out gassing before deposition was begun, there was always a sharp increase in the system pressure from about 10^{-5} to 10^{-3} Torr; then just as sharply, the pressure dropped. This step increase then decrease in pressure was not observed during the out gassing of any of the other porphyrins in any of the other experiments. The visible spectrum of Fe(II)TPP in *n*-octane at 77°K has an absorption maximum at 542 nm and a very weak one at 589 nm. The energy spacing between these two peaks is approximately 1200 cm^{-1} which is the spacing observed between the Q(0–0) and Q(0–1) bands of Zn(II)TPP and Cu(II)TPP as well as other simple metal porphyrins. If the system is allowed to warm to room temperature after the spectrum of the matrix isolated sample is recorded, and opened to the atmosphere, the visible spectrum of the film remaining on the target has a broad maximum at about 550 nm. The benzene solution spectrum of the film washed from the target window agrees with that reported by Dorough, *et al.*,[11] for the Fe(III)TPPOH complex, the expected product of air oxidation of Fe(II)TPP.

Once the identity of Fe(II)TPP was established, it was studied in matrices of Ar, NH_3, O_2, N_2, and *n*-octane. The visible region exhibits one or two relatively broad bands depending on the matrix. In argon at 20°K there is a single band with a maximum at 521 nm. Another band in the region of 560–570 nm develops and increases in intensity as we proceed from Ar through *n*-octane, N_2, O_2, to NH_3. We shall refer to the longer wavelength band as band I and to the shorter wavelength as band II.

Discussion

For TPP the bands in Ar are shifted to the blue of those in *n*-octane and slightly to the blue of those in SF_6. Bajema[2] found that the Soret band of copper octaethylporphine isolated in an argon matrix was to the blue of the Soret of the same compound in a methane matrix. A detailed treatment of spectral shifts in matrix-isolation spectroscopy has been developed by Robinson.[12] The theory is quite complicated, but the one simple generality that can be drawn from the theory is that for simple matrices, the blue shift should decrease with increasing host size. Thus, our results and Bajema's results are in agreement with this aspect of Robinson's theory.

TABLE III: Matrix-Isolated Fe(II)TPP

Matrix; Temp, °K; mole ratio	Wavelength, nm	Half-width, nm	I/II	Remarks
NH_3, 23;	430.0	30.0		
3000:1	537.0	20.0	0.63	
	567.5	13.0		
NH_3; 77;				
3000:1	537.0	20.0	0.62	
	567.5	13.0		
Ar; 23;	400.0	25.0		
2500:1	521.0	15.0	0.00	
O_2; 23;	407.0	28.0		
3000:1	519.0	35.0	0.22	shd, 538
	576.0			
N_2; 23;	410.0	28.0		
3000:1	524.0	28.0	0.05	
Octane; 23;				
3000:1	542.0	32.0	0.05	
	588.5	6.0		

In the Soret region of the TPP spectrum, one is tempted to identify the 400-nm band with the oppositely polarized Soret transition predicted by the theory.[13] This band is probably masked by the more intense 420-nm Soret band in room temperature solution spectra where the latter is much broader. However, the 1200-cm^{-1} energy spacing between the two bands is approximately equal to the spacing between the vibronic bands in the visible spectrum. The 400-nm band is also present in the spectra of ZnTPP and CuTPP in octane matrices (see Figure 3). Since there is only one doubly degenerate Soret transition in metal porphyrins of D_{4h} symmetry, the 400-nm band must be a vibronic of the Soret transition in the metal TPP's. However, one cannot dismiss it as vibronic in the free base spectra, especially in light of the polarization study reported by Anex and Umans[14] on crystalline TPP. They examined the polarization in the reflectance spectra and found two mutually perpendicular polarizations in the Soret region. The

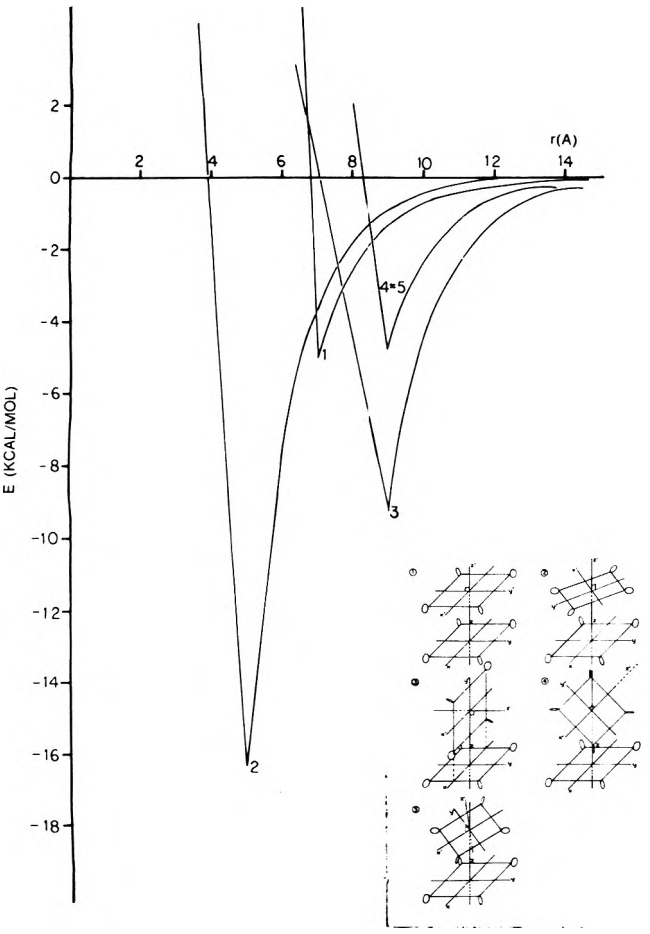

Figure 4. Potential curves. Sketches indicate relative orientation of porphine planes.

broadness of the two bands prevented resolution into two distinct peaks but the y-polarized absorption appeared around 400 nm while the x-polarized absorption was around 420 nm. Thus in the free base spectra, the 400-nm band may be $B_y(0\text{–}0)$ or an overlap of $B_y(0\text{–}0)$ and $B_x(1\text{–}0)$. With this in mind, several attempts were made to anneal samples hoping to reveal a split or shoulder but nothing was found. The band is much sharper in argon but still no splitting or shoulder is noticeable.

Following the procedure described previously,[1] we calculated stable geometries for metal TPP pairs. The results are shown in Figure 4. The most stable structure has the porphine planes parallel, 5 Å between centers and twisted 45° to minimize steric crowding of the phenyl groups. This twisting appears to lower the energy by about 11 kcal/mol (structure 2 in Figure 4). The second most stable structure occurs at 9 Å distance between centers with the porphine planes mutually perpendicular (structure 3 in Figure 4). A 45° dihedral angle between the porphine planes gives a less stable structure. For the intense Soret transition for which the dipole–dipole approximation[1] should be adequate, we calculate a Davydov splitting +1518 cm^{-1} for structure 2, and ±184 cm^{-1} for structure 3.

All absorption peaks observed in this work are about an order of magnitude broader than those observed previously for porphine and its copper and zinc derivatives.[1] The 184-cm^{-1} splitting for structure 3 would not be detectable and the ±1518-cm^{-1} splitting for structure 2 should be but we did not observe it. In our earlier pair potential calculations for porphine[1] a stable structure was predicted which would have a spectrum similar to that observed experimentally in several different matrices indicating that guest–host interactions could not have significantly affected the geometry of the pair. In the case of TPP and its metal derivatives, the bulky phenyl groups which may be appreciably twisted with respect to the porphine plane[15,16] may make guest–host interactions much more significant so that no pairing may be occurring or one of the less stable configurations (structure 3, 4, or 5) may now be the most stable. Such a structure would result in a splitting too small to be detected.

Several theoretical calculations on iron porphyrins have been reported.[17-20] The work of Pullman, *et al.*, and Ohno, *et al.*, is limited since their calculations made use of a limited set of basis orbitals. Gouterman, *et al.*, improved the calculation by including all valence orbitals of all atoms. Several ferrous and ferric porphine complexes with other ligands were also treated and the effects of planarity of the Fe porphyrin were also investigated. The uncomplexed ferrous compound was calculated to have a triplet ground state if planar and a quintet ground state if nonplanar (Fe atom about 0.4 Å out of plane). The calculations predicted no stable complex with molecular nitrogen, and a low spin complex with H_2O. Two oxygen complexes were predicted, high spin with the O–O axis perpendicular to the porphine plane (calculated to be unstable) and low spin with the O–O axis parallel to the porphine plane.

Low spin complexes typically have two rather sharp bands in the visible spectrum, while high spin complexes exhibit a broad diffuse absorption in visible with one or two poorly defined maxima, the most intense occurring around 550 nm.[20] The argon matrix-isolated sample should correspond to the unliganded form and it does exhibit a broad diffuse absorption in the visible. With the expected blue shift, the spectrum is remarkably similar to that of deoxyhemoglobin or myoglobin.[21] Similar results were observed in the n-octane matrix, as would be expected. Ammonia is a strong ligand and one would expect formation of a low spin complex; thus there are two distinct absorptions in the visible for the ammonia matrix-isolated sample. The spectrum is quite similar to that of low spin carboxyhemoglobin or myoglobin.[21] The oxygen matrix spectrum shows a broad absorption characteristic of high spin complex (maxima at 519 nm) with a shoulder at 538 nm and a peak at 576 nm characteristic of a low spin oxygen complex (O–O axis parallel to porphyrin plane) and either the high spin unliganded Fe(II)TPP or the oxygen complex with the O–O axis normal to the porphyrin plane. Only the low spin oxyhemoglobin has been observed, but in the oxygen matrix the oxygen crystal lattice may force formation of the less stable high spin complex. The N_2 matrix spectrum suggests that a very weak high spin complex is obtained.

Acknowledgment. J. J. Leonard was supported during the course of this investigation by an NIH predoctoral fellowship 5-Fol-GM-48947-02.

References and Notes

(1) See J. J. Leonard and F. R. Longo, *J. Amer. Chem. Soc.*, **95**, 8506 (1973).
(2) L. Bajema, M. Gouterman, and B. Meyer, *J. Mol. Spectrosc.*, **27**, 225 (1968).
(3) A. D. Adler, F. R. Longo, J. Finarelli, J. Assour, and J. Goldmacher, *J. Org. Chem.*, **32**, 476 (1967).
(4) A. D. Adler, F. R. Longo, F. Kampus, and J. Kim, *Inorg. Nucl. Chem.*, **32**, 2443 (1970).

(5) D. W. Thomas and A. E. Martell, *J. Amer. Chem. Soc.*, **78**, 1338 (1956).
(6) H. W. Whitlock, R. Hanauer, M. Y. Oester, and D. K. Bower, *J. Amer. Chem. Soc.*, **91**, 7485 (1969).
(7) L. Epstein, D. K. Stoaub, and C. Maricondi, *Inorg. Chem.*, **6**, 1720 (1967).
(8) J. M. Assour, private communication.
(9) E. A. Lucia, F. D. Vercerame, and G. Taddei, *J. Chem. Phys.*, **52**, 2307 (1970).
(10) A. Yamamoto, L. Philips, and M. Calvin, *Inorg. Chem.*, **7**, 847 (1968).
(11) G. D. Dorough, J. R. Miller, and F. M. Huennekens, *J. Amer. Chem. Soc.*, **73**, 4315 (1951).
(12) G. W. Robinson, *J. Mol. Spectrosc.*, **6**, 58 (1961).
(13) M. Gouterman, *J. Chem. Phys.*, **30**, 1139 (1959).
(14) B. S. Anex and R. S. Umans, *J. Amer. Chem. Soc.*, **86**, 5026 (1964).
(15) (a) J. M. Robertson, *J. Chem. Soc.*, 1195 (1936); (b) J. M. Robertson, *ibid.*, 1809 (1939).
(16) J. Webb and E. B. Fleischer, *J. Chem. Phys.*, **43**, 3100 (1965).
(17) B. Pullman, C. Spanjaard, and G. Berthier, *Proc. Nat. Acad. Sci. U.S.*, **73**, 1011 (1960).
(18) K. Ohno, Y. Tanabe, and F. Sasaki, *Theor. Chim. Acta*, **1**, 378 (1963).
(19) M. Zerner and M. Gouterman, *Theor. Chim. Acta*, **4**, 44 (1966).
(20) M. Zerner, M. Gouterman, and H. Kobayashi, *Theor. Chim. Acta*, **6**, 363 (1966).
(21) E. Antonini and M. Brunori, "Hemoglobin and Myoglobin in Their Reactions with Ligands," North-Holand Publishing Co., Amsterdam, 1971, Chapter 1.

Excited State Quenching Activity of d^6 Metallocenes and a Detailed Study of Ruthenocene Luminescence

Mark S. Wrighton,* Laddawan Pdungsap, and David L. Morse

Department of Chemistry, Massachusetts Institute of Technology, Cambridge, Massachusetts 02139 *(Received June 17, 1974)*

Publication costs assisted by the National Science Foundation

Quenching of electronically excited benzil and ruthenium(2,2′-bipyridine)$_3^{2+}$ by d^6 metallocenes of Fe, Ru, Os, and Co has been investigated. Consistent with quenching by electronic energy transfer, the quenching rates correlate with the position of the lowest accessible triplet state in absorption in the metallocene compared to the excitation energy available in the donor. Luminescence from pure solids of ruthenocene and 1,1′-diacetylruthenocene at 25°K has been measured and the emission maximum at ~17,000 cm^{-1} is red shifted by nearly 10,000 cm^{-1} from the first singlet → triplet absorption maximum. The emission intensity in each case is temperature dependent and for ruthenocene both lifetimes (127 μsec at 28°K) and quantum yields (0.027 ± 0.005 at 28°K) have been measured revealing that the decreasing emission efficiency at higher temperatures is due principally to a faster rate of nonradiative decay. The structured emission of ruthenocene shows two vibrational progressions separated by 162 ± 10 cm^{-1} with vibrational spacings of 327 ± 10 and 340 ± 10 cm^{-1} associated with the ring–metal stretch found at 330 cm^{-1} in the Raman.

Since the geometrical structural characterization of ferrocene in 1952[1] investigations of the electronic structure of metallocenes have been numerous,[2-6] and it is now established[2] that the lowest excited states of the d^6 complexes are ligand field states. Even so, important aspects of the photochemical and photophysical behavior of these substances remain unresolved.[7] The effective energetic position of the lowest excited state is key to further progress in understanding the excited state chemistry. Ferrocene itself has been the object of most detailed studies and it now appears that early literature reports[3a,5] of its luminescence are in error.[8] The quenching ability of ferrocene has also created some interest in that anthracene triplet excited states (triplet energy, E_T = 14,700 cm^{-1})[9] are deactivated by ferrocene at a diffusion-controlled rate[10] even though the lowest singlet → triplet absorption maximum in ferrocene is at approximately 18,600 cm^{-1}.[2]

We have undertaken two lines of investigation to begin further characterization of the lowest excited states in metallocenes: (1) determination of the quenching ability of several metallocenes having large variations in excited state energy in comparison to the donor and (2) study of metallocenes which are found to luminesce upon optical excitation. In this report we describe our results for several metallocenes of the d^6 electronic configuration.

Experimental Section

Spectra. All uv–visible absorption spectra were recorded on a Cary 17 spectrophotometer. Low-temperature (77°K) absorption spectra were obtained using an all quartz dewar with optical quality flats for windows. The sample was dissolved in EPA and placed in a round quartz cell placed in direct contact with liquid nitrogen. The emission spectrometer used for the emission studies is an Aminco-Bowman spectrophotofluorometer set up for emission measurements in the 300–900-nm range and equipped with a grating blazed at 750 nm. The detectors used were either a Hamamatsu R136 PMT operated at 800 V and 25° or an RCA 7102 PMT operated at 1200–1500 V and cooled with a Dry Ice–2-propanol bath. Both the emission and excitation monochromators were calibrated using a low-pressure Hg lamp and readings are found to be within 3 nm of the expected values. The relative sensitivity of the entire detection system (and for both PMT detectors) has been calibrated in the range 300–600 nm using the Rhodamine B quantum counter[11] and over the entire 300–900-nm range

TABLE I: Quenching Activity of Several d^6 Metallocenes

Quencher	Lowest absptn max quencher $cm^{-1} \times 10^{-3}$ (ϵ)	k_q for benzil (solvent), M^{-1} sec^{-1} ± 10%	k_q for $Ru(bipy)_3^{2+}$ (solvent), M^{-1} sec^{-1} ± 10%
Ferrocene	22.72 (90)	1.2×10^{10}(isooctane)	5.9×10^9(EtOH)
Acetylferrocene	22.37 (290)	9.3×10^9(isooctane)	3.4×10^9(EtOH)
Benzoylferrocene	21.74 (740)	1.1×10^{10}(isooctane)	7.4×10^9(EtOH)
Cobalticinium perchlorate	24.69 (200)	2.0×10^9(CH_3CN)	1.5×10^8(EtOH:H_2O, 1:1 v/v)
Ruthenocene	31.25 (220)	1.4×10^8(isooctane)	$<10^7$(EtOH)
1,1′-Diacetylruthenocene	30.30 (770)	2.5×10^7(isooctane)	$<10^7$(EtOH)
Acetylosmocene	29.76 (770)	4.2×10^8(isooctane)	$<10^7$(EtOH)

by a standard lamp[12] obtained from and calibrated by E, G & G, Inc. of Salem, Mass. The standard lamp is a 200-W tungsten halogen lamp operated at 6.50 A having serial no. B115A and was calibrated from NBS standards QM 197, QM 198, QM 199. Thus, the emission spectra shown in the figures are corrected for detector response. Temperature variation of the sample was achieved using a Cryogenic Technology, Inc. Spectrim II sample conditioner. The temperature indicator was checked for accuracy by using a hydrogen pressure thermometer calibrated by Cryogenic Technology, Inc. Temperatures reported below 100°K are ±3°K.

Materials. The ferrocenes and ruthenocene were obtained commercially. Purity was checked by optical absorption spectra and melting points; sublimation or recrystallizations were carried out until pure. Ruthenocene samples were carefully purified by several sublimations and material from several sources was used to ensure that the luminescence from ruthenocene is real. Acetylosmocene and 1,1′-diacetylruthenocene was generously supplied by Professor M. Rausch of the University of Massachusetts, Amherst. The cobalticinium perchlorate is the same material used in a previous absorption spectral study.[2a] Solvents were commercially obtained and emission lifetimes of the donors in the degassed solvents employed verified that no quenchers were present. Benzil was purified by recrystallization from Et_2O, and $Ru(bipy)_3Cl_2$ was obtained from Baker Chemical Co. and used after recrystallization.

Quenching Studies. Solutions of the donor at a constant concentration and the quencher were placed in 13 × 100 mm test tubes with constrictions and freeze–pump–thaw degassed in at least three cycles. Generally, 500 nm was the excitation wavelength for studies using $Ru(bipy)_3^{2+}$ as the donor and the benzil was excited at 420 nm. The luminescence spectrum of each sample was measured and the relative emission yields determined as a function of quencher concentration and plots of the ratio of emission yields without quencher (ϕ_0) to the yield with quencher (ϕ) against quencher concentration are linear and the line passes through $\phi_0/\phi = 1.0$ at zero quencher concentration. Typical plots are shown in Figure 1. The quenching constant, k_q, can be determined from the slope of the plot, $k_q\tau$, after determination of the donor lifetime in the absence of quencher, τ. This value was determined for each donor for each quenching experiment. The lifetime for benzil phosphorescence in isooctane is near 0.2 msec in each case and the $Ru(bipy)_3^{2+}$ lifetime is near 0.9 μsec. Generally, the value of k_q given in Table I is the average of two separate determinations differing by no more than 15%.

Luminescence Lifetimes. Lumiscence lifetimes, τ, were measured using a TRW Model 75A decay time fluorometer equipped with a Xenon Corp. Nanopulser excitation source. The RCA 931A PMT detector was powered by a

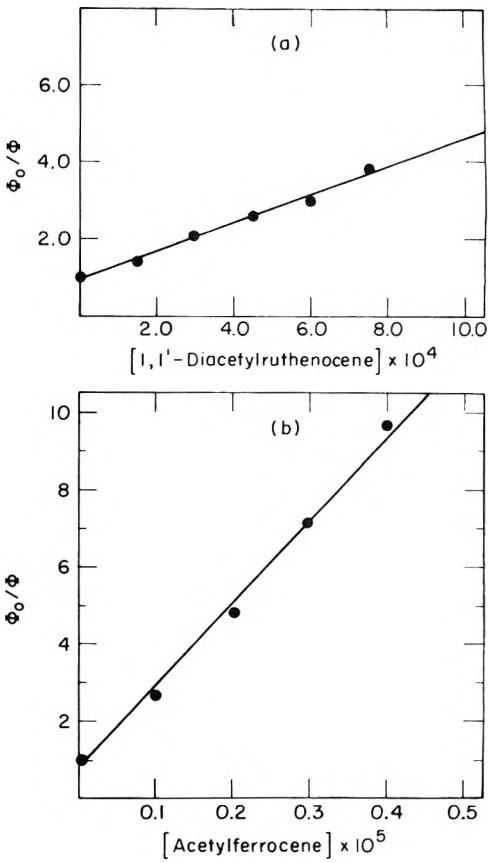

Figure 1. (a) Stern–Volmer plot for quenching of benzil phosphorescene by 1,1′-diacetylruthenocene at 25°. Measured lifetime of the benzil at zero quencher concentration is 0.15 msec; the excitation wavelength is 420 nm; solvent is isooctane; and the benzil concentration is $\sim 10^{-2}$ *M*. (b) Stern–Volmer plot for quenching of benzil phosphorescence by acetylferrocene at 25°. The conditions are the same as above except the measured lifetime of the benzil at zero quencher concentration is 0.21 msec.

Kepco Model 2500 ABC regulated high-voltage supply. Output from the PMT following the ~20-nsec excitation pulse was monitored by a Tektronix 453 oscilloscope and recorded with a Polaroid camera. Plots of log (emission intensity) against time were linear in every case over at least two lifetimes. The value of τ is taken as the time required for the luminescence intensity to decay to $1/e$ of its original value.

Luminescence of Ruthenocene and 1,1′-Diacetylruthenocene. The luminescence of the pure 1,1′-diacetylruthenocene was recorded as a function of temperature using the Aminco and the Spectrim II. The RCA 7102 PMT detector was used and the following emission slits were used: a 0.5 mm slit ~0.5 in. from the sample; a 0.5 mm slit at the entrance to the emission monochromator; and a 0.5 mm slit at

the entrance to the PMT housing. No structure of the emission band was detected. The emission lifetime could not be measured with our equipment due to the weak intensity of the emission.

Ruthenocene emission spectra were recorded under the same conditions as above except the detector used was the Hamamatsu R136 PMT. The emission quantum yield of the ruthenocene was measured by a previously reported method.[13] The ruthenocene was diluted with KBr and mixed by grinding. A point-by-point 298°K reflectance spectrum was recorded by monitoring the diffuse reflectance of the KBr–ruthenocene powder relative to KBr as the reflectance standard and this spectrum was retaken upon cooling the sample to 28°K. These data are collected by using the excitation beam of the Aminco as the excitation source and at room temperature the solid state sample holder accessory for the Aminco was used to hold the sample in a quartz cuvette. In this case the excitation beam is incident normal to the powder surface and a portion of the diffuse reflected light is collected by a mirror and directed into the emission monochromator of the Aminco. The same point-by-point reflectance data for KBr–ruthenocene was obtained at room temperature upon placing the powder on the copper cold tip (a thin layer of silicone grease was used for thermal conduction and adhesion) of the Spectrim II and directing some diffuse reflectance into the emission monochromator. Upon cooling to 28°K the ruthenocene luminescence is easily detected, and the temperature dependence of the luminescence (relative intensity and lifetime) appears to be the same as for the pure solid ruthenocene. Since the emission has the same angular distribution as diffuse reflected light then the area under the emission curve divided by the area between the reflectance curves of pure KBr and KBr–ruthenocene is the quantum yield after correction for spectral response. The quantum yield should be essentially independent of the fraction of light absorbed and this is proven by the linear plot of relative emission intensity against per cent light absorbed and the line passes through zero, Figure 4. The emission yield was determined to be 0.025 and 0.029 in two completely separate determinations exciting at 370 and 400 nm, respectively.

Results

(*a*) *Quenching Studies.* Metallocenes having the d^6 electronic configuration of Fe, Ru, Os, and Co have been used as quenchers of electronically excited benzil and ruthenium(2,2′-bipyridine)$_3^{2+}$ = Ru(bipy)$_3^{2+}$. Both of these donors exhibit luminescence in fluid solution at 25°, and quenching activity is conveniently measured by monitoring the decline in emission intensity as a function of metallocene concentration. For benzil only the phosphorescence is quenched at concentrations of quenchers employed. For all of the quenchers studied the quenching obeys Stern–Volmer kinetics[14] and some typical Stern–Volmer plots are shown in Figure 1. Quenching constants obtained by monitoring emission intensity are identical with those obtained by determination of emission lifetimes of the donor at variable quencher concentrations. Biacetyl (which has a triplet energy nearly isoenergetic with benzil) also phosphoresces in fluid solution at room temperature and quenching by both ferrocene and ruthenocene yields rate constants for quenching which are comparable to the values for benzil. The data are summarized in Table I. One general trend emerges: the best quenchers have the lowest absorption maxima.

TABLE II: Vibrational Band Maxima for Ruthenocene Emission

Band max, cm^{-1} for 1st progression	$\Delta(\nu_n - \nu_{n+1})$, cm^{-1}	Band max, cm^{-1} for 2nd progression	$\Delta(\nu_n' - \nu_{n+1}')$, cm^{-1}
19,800			
	350		
19,450			
	300		
19,150			
	350		
18,800			
	350		
18,450			
	390	18,300	
18,060			350
	310	17,950	
17,750			350
	300	17,600	
17,450			300
	330	17,300	
17,120			300
	270	17,000	
16,850			300
	370	16,700	
16,480			420
	360	16,280	
16,120			360
		15,920	
			Av 340.0
	300		
15,820			
	320		
15,500			
	200		
15,300			
	400		
14,900			
Av	326.7		

(*b*) *Emission Studies.* Luminescence from both ruthenocene and 1,1′-diacetylruthenocene has been detected upon electronic excitation. All of our detailed studies of the emission have been carried out on the solids, but ruthenocene luminescence is also observable in EPA glasses at 77°K. The absorption of ruthenocene at 298 and 77°K in EPA and the emission spectrum of the pure solid at 28°K are shown in Figure 2. The spectral distribution of the emission is independent of the excitation energy at least below 33,000 cm^{-1}. As seen in Figure 2 the luminescence maximum of ruthenocene is near 17,000 cm^{-1} and is highly structured. There appear to be two vibrational progressions, and the maxima for the two progressions are given in Table II. The progressions are separated by 162 ± 10 cm^{-1} and the average vibrational splittings for the progressions are 327 ± 10 and 340 ± 10 cm^{-1}.

The ruthenocene luminescence intensity and lifetime are strongly dependent on the sample temperature. The luminescence red shifts slightly upon warming from 25°K and the vibrational structure becomes much less pronounced. Figure 3 depicts the effect of temperature on the relative emission quantum yield and the emission lifetime. Particularly noteworthy is the fact that the lifetimes fall on the same curve as for the relative quantum yields. More clearly stated, the ratio of the emission quantum yields at temperatures T and T' is equal to the ratio of lifetimes at these same temperatures. This result is compatible with a temperature-independent radiative decay constant since the emission quantum yield, ϕ, is given by expression 1 and the emission lifetime, τ, by expression 2 where k_r and k_{nr} are

TABLE III: Luminescence Data for Ruthenocene

T, °K	Emission max, $cm^{-1} \times 10^{-3}$	Lifetime,[a] μsec ± 10%	Φ ± 20%[b]	k_r, sec^{-1} ± 25%	k_{nr}, sec^{-1} ± 25%
28	~17.0	127	0.027	2.13×10^2	7.66×10^3
40	~17.0	68	0.017	2.50×10^2	1.45×10^4
50	~17.0	37	0.009	2.43×10^2	2.68×10^4
60	~17.0	20	0.004	2.00×10^2	4.98×10^4

[a] Except for 28°K data are interpolated from plot of τ *vs.* T. [b] Except for 28°K data are calculated from the relative quantum yield and the absolute yield at 28°K.

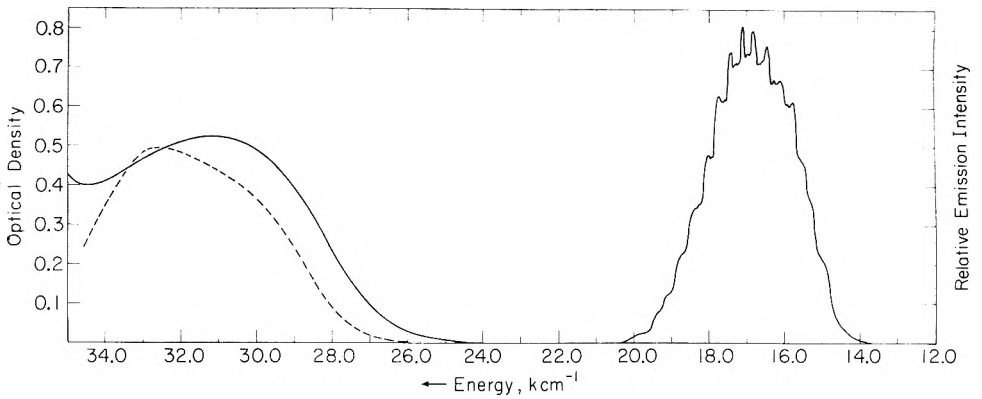

Figure 2. Absorption of ruthenocene in EPA at 298 (—) and 77°K (- - -) (left curves) and emission (right curve) of the pure solid ruthenocene at 28°K.

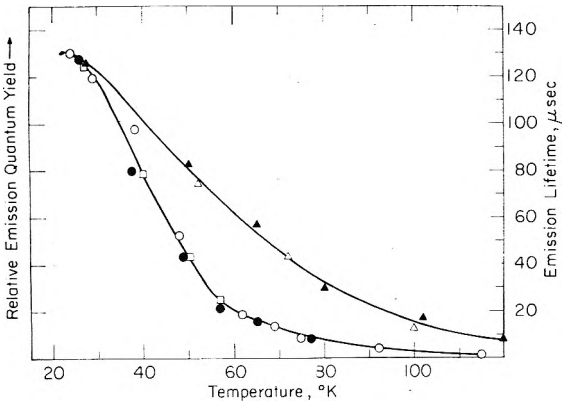

Figure 3. Separate determinations of relative emission quantum yields of ruthenocene (O and □) and ruthenocene emission lifetimes (● and right scale) as a function of temperature. Separate determinations of relative emission quantum yields of 1,1′-diacetylruthenocene (△ and ▲). The relative emission yields are all normalized at 28°K, but the absolute yield for the 1,1′-diacetylruthenocene is substantially less than that for ruthenocene.

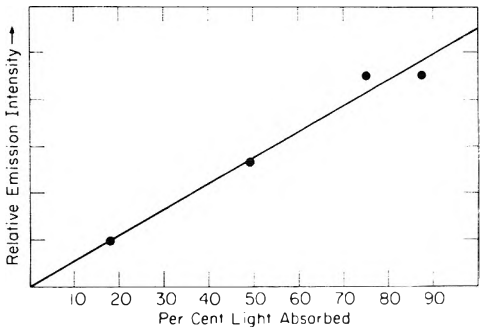

Figure 4. Plot of relative observed emission intensity of KBr diluted ruthenocene as a function of per cent light absorbed. Variation in per cent light absorbed was achieved by variation in the excitation wavelength in the range 350–430 nm. The relative emission intensity has been corrected for variation in the excitation light intensity in the 350–450-nm range.

$$\phi = k_r/(k_{nr} + k_r) \quad (1)$$

$$\tau = 1/(k_{nr} + k_r) \quad (2)$$

the radiative and nonradiative decay constants, respectively. To determine the values for the decay constants requires an absolute quantum yield determination in addition to the data given above. The emission yield of ruthenocene diluted with KBr has been measured to be 0.027 ± 0.005 at 28°K using a technique recently reported.[13] As shown in Figure 4 the emission intensity is proportional to the per cent light absorbed by the ruthenocene, as expected. Representative values of k_r and k_{nr} at several temperatures are given in Table III along with other luminescence data for ruthenocene. The errors in such constants are very large especially in view of the facts that $k_{nr} \gg k_r$ and we are dealing with powdered samples. The significant result is that it is the increase in k_{nr} which gives smaller lifetimes and emission yields at higher temperatures.

The luminescence of 1,1′-diacetylruthenocene is much weaker than that of ruthenocene and we could detect no structure on the emission band at comparable resolving conditions to those used for ruthenocene at temperatures as low as 25°K. The absorption of 1,1′-diacetylruthenocene at 298 and 77°K in EPA and the temperature-dependent luminescence spectrum of the pure solid are shown in Figure 5. The spectral distribution of the emission is independent of the excitation energy below 33,000 cm^{-1}. The emission maxima at ~16,300 cm^{-1} at 28°K is fairly close to that for ruthenocene. However, the shape of the plot of relative emission quantum yield against temperature is different than that for ruthenocene as seen in Figure 3. The emission of the 1,1′-diacetylruthenocene is too weak to enable us to measure the emission lifetime with our equipment.

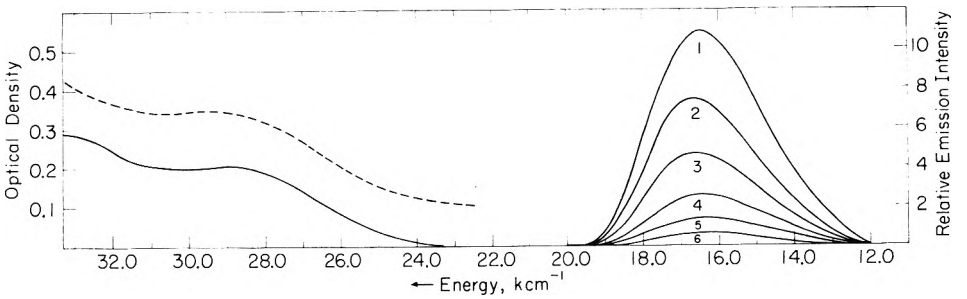

Figure 5. Absorption (left curves) in EPA at 298°K (—) and 77°K (- - - - - and displaced by 0.1 OD) and emission (right curves) as a pure solid of 1,1′-diacetylruthenocene. Emission curve 1 is at 27°K, curve 2 at 50°K, curve 3 at 65°K, curve 4 at 80°K, curve 5 at 102°K, and curve 6 at 122°K.

Discussion

The absorption spectra of the d^6 metallocenes have been measured and discussed previously.[2] We adopt the assignment of Sohn, Hendrickson, and Gray[2a] for the lowest expected absorption as the $^1A_{1g} \rightarrow {}^3E_{1g}$. The emission is associated with this absorption. Crosby, Hager, Hipps and Stone[15] have independently discovered and measured the luminescence of ruthenocene and they find results comparable to those reported here. The temperature dependence of the emission is interpreted[15] as due to thermal equilibration of the spin–orbit levels arising from $^3E_{1g}$ (A_{2g}, A_{1g}, E_{1g}, E_{2g}) with emission occurring from the Boltzmann distribution of four levels with four sets of k_r and k_{nr}. We concur with the essential features of this interpretation but find, additionally, that the large increase in decay constants is in k_{nr} for the various higher lying levels. The apparent constancy of the value of k_r does not support the spin–orbit model in that each spin–orbit state should have its own value of k_r, but one cannot say *a priori* how large such variations should be. The error (±25%) in our k_r values is such that a definitive statement cannot be made. Actually, the data could be fitted to a one level emitting system with strongly temperature-dependent k_{nr} values. There is no compelling reason, however, to abandon the spin–orbit scheme especially if the temperature dependence arises from intramolecular effects. A reasonable test of the spin–orbit model would be a double resonance experiment but this is beyond our own capability.

The splitting of the vibrational bands (~334 cm^{-1}) compares very favorably with the ring–metal stretching vibration (a_{1g}) found at 330 cm^{-1} in the Raman.[16] The rather weak overlap of absorption and emission in both ruthenocene and 1,1′-diacetylruthenocene suggests a substantial distortion in the excited compared to ground state. This excited state distortion is thought to be a symmetrical expansion of the molecule maintaining the ground state symmetry.[15]

The energetic position of the lowest excited state is required to interpret the quenching activity of the metallocenes, and now for ruthenocene and 1,1′-diacetylruthenocene we have a direct measure of the energetic position of the relaxed excited state. The other d^6 metallocenes have electronic spectra which are very similar to the ruthenocene except for band positions,[2] thus, we can crudely relate the relaxed excited state energy of ruthenocene to the other d^6 metallocenes. As seen in Table I the ferrocenes have the lowest absorption followed by cobalticinium, acetylosmocene, and the ruthenocenes. The quenching of the benzil phosphorescence (corrected phosphorescence maximum at 25° = 17,600 cm^{-1}) and the $Ru(bipy)_3^{2+}$ luminescence (corrected emission maximum at 25° = 15,700 cm^{-1}) by the various metallocenes follows the ordering of the lowest excited state in the metallocene with lower energy excited states in the quencher yielding higher quenching constants. Further, the benzil is quenched more effectively than the $Ru(bipy)_3^{2+}$ by the metallocenes except that the ferrocenes deactivate both donors at essentially diffusion-controlled rates. These energetic considerations are consistent with electronic energy transfer as the quenching mechanism in these cases.[14] The fact that Ru- and Os-containing metallocenes do not quench as effectively as the Fe-containing compounds is inconsistent with the notion that the heavy metal complexes exert an external heavy atom perturbation on the donor excited state which for benzil is clearly a triplet and could be deactivated by such a perturbation. Quenching by a charge-transfer interaction would not necessarily be expected to correlate with the relative energy of states in the donor and quencher. The observation[17] that styrylferrocene undergoes benzophenone triplet sensitized cis–trans isomerization lends further evidence to support our general conclusion that quenching of the donors produces the lowest electronically excited state ($^3E_1$) in the metallocene. The consistency of our results using $Ru(bipy)_3^{2+}$ is wholly in accordance with an earlier finding that it behaves as a normal triplet donor when the quencher has low-energy triplets accessible.[18]

One point remains to be made and it concerns the distortion in the excited state of the metallocene. The distortion of the ruthenocene excited state manifests itself by giving rise to a substantially red-shifted emission (~17,000 cm^{-1}) compared to the $^1A_{1g} \rightarrow {}^3E_{1g}$ absorption maximum at 26,000 cm^{-1}.[2] Further, we see that the quenching activity of ruthenocene is very poor for $Ru(bipy)_3^{2+}$ whose emission substantially overlaps the ruthenocene, and the benzil triplet is poorly deactivated even though the phosphorescence maximum of benzil is at *higher* energy than that of ruthenocene. Similar relationships were pointed out[19] for the quenching of biacetyl triplets by $Co(CN)_6^{3-}$. Such data are consistent with the conclusion that for quenching to be fast the metallocene must have a nondistorted, spectroscopic triplet state accessible with the excitation energy available in the donor, and in general the emission of the transition metal complex will serve only as a guide to the donor energy necessary to achieve electronic energy transfer. This consideration will be generally important for low-spin d^6 complexes as the emission is often red shifted considerably from the corresponding absorption implicating large distortions upon electronic excitation.

Acknowledgment. We thank the National Science Foundation for support of this research, M.W. acknowledges support as a Fellow of the Alfred P. Sloan Foundation

1974–1976, and L.P. thanks the Agency for International Development, U.S. Department of State, for financial support. We thank Professor R.J. Silbey of MIT for valuable discussion, the authors of ref 15 for a preprint of their work prior to publication, and Professor M. Rausch of the University of Massachusetts for providing authentic samples of 1,1′-diacetylruthenocene and acetylosmocene.

References and Notes

(1) (a) G. Wilkinson, M. Rosenblum, M. C. Whiting, and R. B. Woodward, *J. Amer. Chem. Soc.*, **74**, 2125 (1952); (b) E. O. Fischer and W. Pfab, *Z. Naturforsch. B*, **7**, 377 (1952).
(2) (a) Y. S. Sohn, D. N. Hendrickson, and H. B. Gray, *J. Amer. Chem. Soc.*, **93**, 3603 (1971); **92**, 3233 (1970); (b) Y. S. Sohn, D. N. Hendrickson, J. H. Smith, and H. B. Gray, *Chem. Phys. Lett.*, **6**, 499 (1970).
(3) (a) D. R. Scott and R. S. Becker, *J. Chem. Phys.*, **35**, 516 (1961); (b) *J. Organometal. Chem.*, **4**, 409 (1965); (c) *J. Phys. Chem.*, **69**, 3207 (1965).
(4) A. T. Armstrong, D. G. Carroll, and S. P. McGlynn, *J. Chem. Phys.*, **46**, 4321 (1967).
(5) J. J. Smith and B. Meyer, *J. Chem. Phys.*, **48**, 5436 (1968).
(6) P. B. Stephenson and W. E. Winterrowd, *J. Chem. Phys.*, **52**, 3308 (1968).
(7) For a review of metallocene photochemistry *cf.* R. E. Bozak, "Photochemistry in the Metallocenes," in "Advances in Photochemistry," Vol. 8, J. N. Pitts, Jr., G. S. Hammond, and W. A. Noyes, Jr., Ed., Wiley, New York, N.Y., 1971, pp 227–244.
(8) A. Müller-Goldegg and J. Voitländer, *Z. Naturforsch A*, **23**, 1236 (1968).
(9) D. P. Craig and I. G. Ross, *J. Chem. Soc.*, 1589 (1954).
(10) A. J. Fry, R. S. H. Liu, and G. S. Hammond, *J. Amer. Chem. Soc.*, **88**, 4781 (1966).
(11) W. H. Melhuish, *J. Opt. Soc. Amer.*, **52**, 1256 (1962).
(12) J. N. Demas and G. A. Crosby, *J. Phys. Chem.*, **75**, 991 (1971).
(13) M. S. Wrighton, D. S. Ginley, and D. L. Morse, *J. Phys. Chem.*, **78**, 2229 (1974).
(14) N. J. Turro, "Molecular Photochemistry," W. A. Benjamin, New York, N.Y., 1965.
(15) G. A. Crosby, G. D. Hager, K. W. Hipps, and M. L. Stone, *Chem. Phys. Lett.*, **28**, 497 (1974).
(16) E. R. Lippincott and R. D. Nelson, *Spectrochim. Acta*, **10**, 307 (1958).
(17) J. H. Richards and N. Pisker-Trifunac, *J. Paint Technol.*, **41**, 363 (1969).
(18) M. Wrighton and J. Markham, *J. Phys. Chem.*, **77**, 3042 (1973).
(19) M. Wrighton, D. Bredesen, G. S. Hammond, and H. B. Gray, *Chem. Commun.*, 1018 (1972).

Phosphorescence and Electron Paramagnetic Resonance of Triplet-State Naphthalene–Tetracyanobenzene Charge-Transfer Complexes

A. M. Ponte Goncalves* and R. J. Hunton

Department of Chemistry, The Pennsylvania State University, University Park, Pennsylvania 16802 *(Received August 26, 1974)*

Publication costs assisted by the Petroleum Research Fund

Phosphorescence spectra of naphthalene–tetracyanobenzene complexes at 77 K in EPA and 3-methylpentane glasses, and in 1:1 single crystals, reveal an important effect of excitation wavelength and environment on the nature of the emitting triplet state. The phosphorescence and epr spectra, and their lifetimes, show that at least two distinctly different types of triplet states may be populated in EPA glasses: locally excited triplet states (on the naphthalene moiety of the complexes) and triplet states with considerable charge-transfer character. Earlier phosphorescence and epr results, at first sight contradictory, are discussed in view of the experiments reported here. These results are discussed in terms of different complex geometries, excited state multiple complexes, and intersystem crossing channels dependent on excitation wavelength.

Introduction

Until a few years ago investigations of the phosphorescence of organic charge-transfer (CT) complexes failed to produce evidence of triplet states with a measurable CT contribution.[1] Excitation in the CT absorption band of many complexes results in a phosphorescence which is very similar to that of the donor alone, but which has a somewhat less resolved structure and a shorter lifetime. The decrease in triplet state lifetime is attributed to the perturbation caused by the presence of the acceptor.[1] The pioneering work of Iwata, *et al.*,[2] represents the first reported observation of triplet states with unambiguous CT character. These authors observed that the phosphorescence of complexes between 1,2,4,5-tetracyanobenzene (TCNB) and several aromatic hydrocarbons is considerably red-shifted with respect to the phosphorescence of either component alone. The assignment of these emissions to CT triplet states was later confirmed by electron paramagnetic resonance (epr) experiments,[3] which showed that the electron spin in these triplet states is delocalized over both molecules of the complex.

The case of the complex between naphthalene and TCNB presents an intriguing problem because of the conflicting conclusions derived from published phosphorescence and epr results. Iwata, *et al.*,[2,4] reported that the phosphorescence of this complex at 77 K, in ether–isopentane glasses and in 1:1 single crystals, closely resembles that of naphthalene. They concluded therefore that the triplet state of the naphthalene–TCNB complex, like those of many other complexes investigated earlier,[1] must be almost entirely localized in the naphthalene moiety. More recently, however, Krebs, *et al.*,[5] investigated the epr spectrum of the naphthalene–TCNB triplet state in an oriented liquid crystal matrix and in single crystals, and in both in-

stances found conclusive evidence of large CT contribution to the triplet state of the complex. (They reported also that excitation in the CT absorption did not give rise to naphthalene locally excited triplet states.) In spite of the apparently clear contradiction between these results and the conclusions of Iwata, *et al.*,[2,4] the naphthalene–TCNB complex is still frequently invoked as an example of a locally excited triplet state.[6–9]

In order to resolve this question we have investigated in some detail the phosphorescence spectra and lifetimes of the naphthalene–TCNB complex at 77 K in rigid glasses and in single crystals. The epr spectra and decay times in EPA glasses were also investigated, and the results of these experiments are in agreement with our phosphorescence results. It is shown in what follows that at least two distinctly different types of triplet states exist for the naphthalene–TCNB complex, as a consequence of different local environments. The possibility of intersystem crossing channels which depend on the excitation wavelength, and of complexes comprising more than two molecules, is discussed.

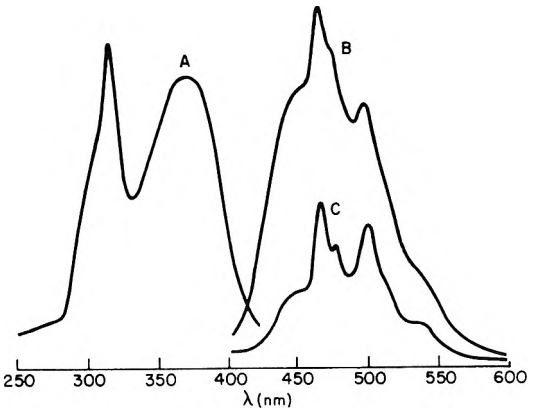

Figure 1. Excitation spectrum of the CT fluorescence (A) and total emission spectra (B, C) of an EPA glass containing naphthalene and TCNB. Spectrum A was detected at 420 nm, and spectra B and C were excited at 380 and 280 nm, respectively. Excitation at 280 nm also results in the ultraviolet fluorescence of the uncomplexed molecules, which is not shown in the figure. Curves B and C are to the same scale.

Experimental Section

The luminescence measurements were performed with an Aminco-Bowman spectrofluorimeter which could be equipped with a phosphoroscope. The excitation light was supplied by a Hanovia 150-W xenon arc lamp, and the detector was an RCA 1P21 photomultiplier tube. All optical spectra were obtained at 77 K, and were not corrected for instrumental response. The epr experiments were performed with a Varian E-12 spectrometer, with the sample temperature at approximately 90 K. The triplet states were generated for the epr measurements by light from a 1000-W AH-6 mercury arc lamp (General Electric). In some epr experiments this light was filtered by a long-pass filter with less than 0.001% transmittance for wavelengths shorter than 350 nm. Use of the filter ensured, therefore, that only CT complexes were directly excited.

The TCNB was obtained from Frinton Laboratories and was recrystallized twice from ethanol before use. Scintillation grade naphthalene-h_8 from Eastman Kodak was purified by 100 passes in a zone refiner, and naphthalene-d_8 from Merck Sharp and Dohme was used as received. All solvents were supplied by Matheson Coleman and Bell, and were checked for background emissions before use. The EPA solvent (a 5:5:2 ether–isopentane–ethanol mixture) was used as received. Chromatoquality 3-methylpentane (3MP) was purified by distillation and passage through an activated alumina column. Unless otherwise stated the EPA solutions used in the luminescence measurements were 5×10^{-3} *M* in naphthalene and 5×10^{-4} *M* in TCNB. The 3MP solutions were 5×10^{-3} *M* in naphthalene and saturated with TCNB, and were filtered before use. In every case the solutions were degassed by several freeze–pump–thaw cycles. All luminescence spectra were obtained with glasses containing naphthalene-h_8, but the phosphorescence lifetimes were measured with glasses containing naphthalene-d_8. The epr experiments were performed with EPA solutions saturated with the complex and filtered before use. Naphthalene-d_8 was used in all epr experiments. Initial cooling to 77 K always resulted in clear glasses with no visible indication of solute segregation, but some complex usually precipitated after repeated thermal cycling. All solutions were discarded before precipitation became apparent. The 1:1 naphthalene–TCNB single crystals were grown by slow evaporation of equimolar solutions of naphthalene-h_8 and TCNB in spectroquality acetone.

Results

Phosphorescence. Excitation at 380 nm (CT absorption band) of an EPA glass containing naphthalene and TCNB results in total emission B of Figure 1. This emission is composed of a broad, structureless, fluorescence which originates in the excited CT singlet state, on which is superimposed a structured phosphorescence. A similar emission is obtained by excitation at considerably shorter wavelengths, as shown in curve C of Figure 1 for excitation at 280 nm. The excitation spectrum of the CT fluorescence (detected at 420 nm) is shown in curve A of Figure 1. The origin of the shorter wavelength peak in the excitation spectrum will become apparent later, but it can be seen from the outset that the excited CT singlet state may be reached by absorption not only in the CT band but also further into the ultraviolet.

Phosphorescence spectra of an EPA glass containing naphthalene and TCNB are shown in Figure 2, for excitation at the wavelengths indicated. If the excitation is made at or below 320 nm the observed phosphorescence includes a less intense, structureless, component which originates in TCNB triplet states. This component[10] is clearly seen in Figure 2 for excitation at 300 and 320 nm. Excitation at 310 nm or shorter results also in a stronger phosphorescence which is identical with that obtained from an EPA glass containing only naphthalene. If the excitation is made at 320 nm the phosphorescence is unmistakably different from that of naphthalene, if only in a slight blurring of the structure. Similar spectra (without the TCNB phosphorescence) are obtained by excitation at longer wavelengths, up to 380 nm. This type of phosphorescence has been previously reported by Iwata, *et al.*,[2] who used broad-band excitation in the CT absorption band. Because of its similarity to the naphthalene phosphorescence, this emission was assigned to locally excited triplet-state naphthalene within the complex. This is the only phosphorescence previously observed from naphthalene–TCNB complexes and its assignment appeared, therefore, to be in contradiction with the unambiguous CT contribution observed in the subsequent epr results of Krebs, *et al.*[5] We found, how-

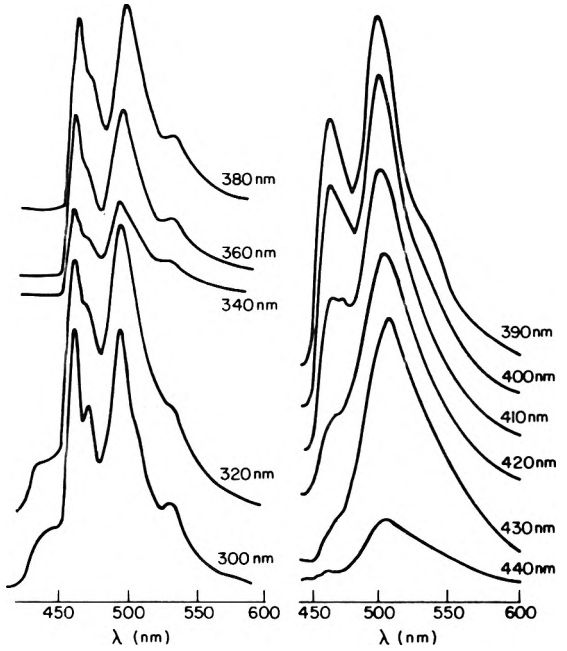

Figure 2. Phosphorescence spectra of an EPA glass containing naphthalene and TCNB, obtained with excitation at the wavelengths indicated. The spectra on the left-hand side of the figure are all to the same scale.

ever, that excitation above 380 nm leads to phosphorescence spectra which become progressively more red-shifted as the excitation is made at longer wavelengths. At the visible edge of the CT absorption band the phosphorescence no longer resembles at all that of naphthalene, and we attribute its origin to triplet states with large CT contribution. This trend is shown in Figure 2, and remains unchanged when the naphthalene concentrations are varied from 5×10^{-2} to 5×10^{-4} M. We see that at least two distinctly different types of complex triplet states may be populated in EPA glasses, regardless of naphthalene concentration. The importance of this point will become clear in the Discussion.

The phosphorescence lifetime of an EPA glass containing naphthalene-d_8 and TCNB depends critically on the excitation wavelength. Excitation between 320 and 380 nm leads to slightly varying lifetimes[11] which cluster around 11 sec. This value can be contrasted to that obtained when the excitation is made below 310 nm, 18 sec, which corresponds to uncomplexed naphthalene phosphorescence. Excitation at wavelengths longer than 380 nm leads to progressively shorter lifetimes, until the value of 8 sec is reached for 420-nm excitation.

A totally different situation arises when the complex phosphorescence is investigated in 3MP glasses. Figure 3 shows two phosphorescence spectra obtained with the same 3MP sample, in both cases with excitation at 380 nm. Spectrum A was recorded first, the sample was then warmed to room temperature and cooled again to 77 K, after which spectrum B was obtained. These two spectra represent extremes in a variety of phosphorescence spectra observed in 3MP glasses. Within these limits the spectra varied unpredictably from glass to glass, even for those obtained using the same sealed sample. No dependence of the phosphorescence on excitation wavelength was observed in any case. Spectrum A was obtained in the vast majority of experiments, and spectrum B or intermediate spectra could be observed in, perhaps, one out of every ten glasses formed.

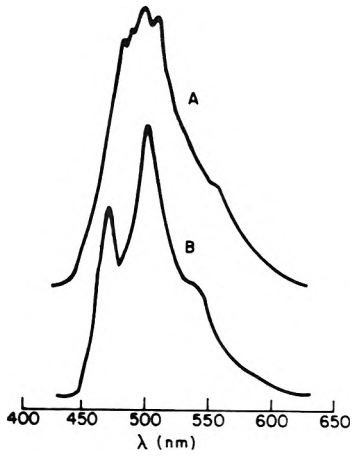

Figure 3. Phosphorescence spectra of 3MP glasses containing naphthalene and TCNB. The two spectra, both excited at 380 nm, were obtained with the same sample. After spectrum A was recorded the sample was warmed to room temperature and then cooled to 77 K, after which spectrum B was obtained.

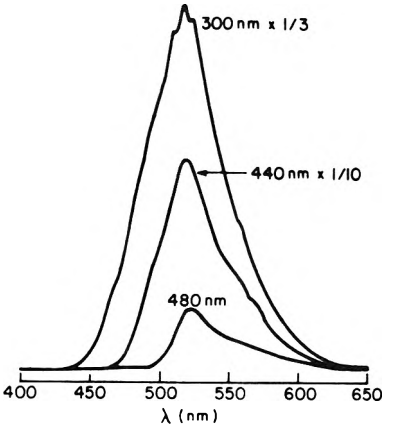

Figure 4. Phosphorescence spectra of a 1:1 naphthalene–TCNB single crystal, excited at the wavelengths indicated.

As the freeze–thaw cycles were repeated with the same sample, no trend was observed favoring either spectrum. Neither could we determine any set of experimental parameters, such as cooling rate and solute concentration, which led to the systematic observation of a particular phosphorescence. It should be noted that a detailed investigation of 3MP glasses was made difficult by the low solubility of the complex in this solvent. This fact led us to suspect that spectrum A in Figure 3 might result from microsegregated complexes, and spectrum B from complexes dispersed in the 3MP glass. However, the lack of concentration dependence of the phosphorescence spectra in both EPA and 3MP would appear to indicate that this is not the case.

We examined also the phosphorescence of 1:1 single crystals, for two reasons. First, because the original report of Iwata, *et al.*[4] seemed to contradict the single crystal epr results of Krebs, *et al.*[5] Second, if the red-shifted phosphorescence spectra in EPA and 3MP glasses were simply due to the formation of microcrystals of complex, then a similar spectrum should be obtained with 1:1 single crystals. Phosphorescence spectra of a naphthalene–TCNB single crystal at 77 K are shown in Figure 4, for excitation at the wavelengths indicated. The spectra vary slightly from crystal to crystal, but we were never able to observe the short-wave-

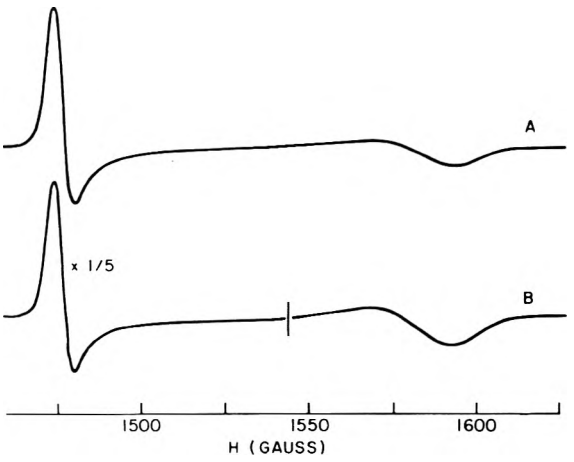

Figure 5. The $\Delta m = 2$ region of the epr spectrum of an EPA glass containing naphthalene-d_8 and TCNB, excited by light from a mercury arc lamp. Spectrum A was recorded with a long-pass filter inserted in the path of the exciting light, and spectrum B was obtained without the filter. The two spectra are to the same scale, except for the left-hand side of curve B which was recorded with five times lower amplification.

length tail reported by Iwata, *et al.*,[4] which had led them to assign the emission to a locally excited naphthalene triplet state. Our phosphorescence measurements clearly indicate that the complex triplet state in the crystal has a marked CT character, in agreement with the epr results.[5] As can be seen in Figure 4, the maximum of the emission changes only slightly with excitation wavelength, but the change in the onset of the phosphorescence is very marked. It should be noted that excitation at short wavelengths (300 nm in Figure 4) does not appear to lead to naphthalene emission. We may conclude from these spectra that the red-shifted phosphorescence observed in EPA and 3MP glasses is not due to the formation of similar 1:1 microcrystals, since the crystal emissions have maxima at noticeably longer wavelength. This alone does not, of course, rule out aggregation which might perhaps lead to a disordered molecular arrangement, of even simply to a different crystal structure.

Electron Paramagnetic Resonance. In order to establish further the existence of the two distinct types of complex triplet states just discussed, we investigated the epr spectrum of EPA glasses containing naphthalene-d_8 and TCNB. Similar experiments with 3MP glasses were unsuccessful, probably because of the lower solubility of the complex in this solvent. The epr experiments were performed either with excitation in the CT absorption band only (through a long-pass filter), or with the full mercury spectrum. In the first instance the only observed epr signals were those due to so-called $\Delta m = 2$ transitions, which are shown in curve A of Figure 5. Excitation without the filter produced the $\Delta m = 2$ epr signals shown in curve B of the same figure, but resulted also in $\Delta m = 1$ signals due to uncomplexed naphthalene molecules (not shown in the figure). Either type of excitation leads to the appearance of two $\Delta m = 2$ peaks. The position of the lowest field signal is indistinguishable from that found for uncomplexed naphthalene triplet-state molecules. The highest field signal corresponds to a triplet state with a large CT contribution, as indicated by the small value measured for the parameter[12] $D^* = 0.053$ cm^{-1}. This value is identical with that reported earlier[5] for 1:1 single crystals.

The line shapes of the $\Delta m = 2$ epr signals are slightly different in the two modes of excitation. Also, and most importantly, the decay times are different for the two types of excitation. The lowest field peak has decay times of 12 and 17 sec for excitation with and without the long-pass filter, respectively. The corresponding decay times for the higher field peak are 8 and 7 sec. These measurements clearly show that the low-field signal in spectrum A is not due to triplet-state uncomplexed naphthalene molecules, which might have been populated through energy transfer. Its lifetime closely resembles the phosphorescence lifetime of the locally excited complex triplet states (11 sec), rather than that of uncomplexed naphthalene molecules (18 sec). This signal corresponds therefore to locally excited complex triplet states. The decay time of the low-field peak in spectrum B enables us to assign it to uncomplexed naphthalene triplet states. The higher field peaks of spectra A and B correspond clearly to more than one type of CT complex triplet state, since line shape and lifetime depend on the mode of excitation. The appearance of more than one such CT triplet state had already been reported for complexes in a liquid crystal matrix.[5] It should be noted, however, that Krebs, *et al.*,[5] detected these CT triplet states but did not find any evidence of a localized triplet state such as the one reported here.

Comparison between epr and phosphorescence results in EPA glasses leads us to associate the lower field epr signal with the phosphorescence spectra excited between 320 and 380 nm (locally excited complex triplet states). The higher field epr signals, obtained in both modes of excitation, appear to correspond to the phosphorescence spectra excited above 380 nm (CT triplet states). Unfortunately the epr signals are not strong enough to permit narrow band excitation, and therefore do not allow a more detailed investigation of this correspondence.

Discussion

We have shown that the nature of the triplet state of naphthalene–TCNB complexes depends critically on the environment. This observation removes the apparent contradiction between some of the earlier phosphorescence[2] and epr[5] results, since those experiments were performed in very different host matrixes. Also, our phosphorescence spectra of 1:1 single crystals clearly point to a triplet state with a large CT contribution, and are therefore at variance with the measurements reported by Iwata, *et al.*,[4] and in agreement with the epr results of Krebs, *et al.*[5]

The data presented here do not permit a determination of the nature of the observed environment effect on the complex triplet states. However, some general conclusions may be drawn from these results. In particular, the behavior observed in 3MP glasses allows us to exclude the possibility of a trivial solvent–solute interaction as the cause for the drastically different complex triplet states observed in this matrix. The obvious dependence of the phosphorescence on the glass formation, together with the low solubility of the complex in this solvent, leads us to suppose that aggregation effects may be involved in some manner. On the other hand, the systematic red-shift of the phosphorescence maximum in 1:1 single crystals clearly shows that any aggregation effects in 3MP do not correspond simply to the formation of 1:1 microcrystals. Caution must be exercised before assigning the observed environment effect to aggregation, since no concentration dependence of the observed phosphorescence could be found. The same cautionary remark applies to the EPA spectra, which were found to be

unaffected by a change in naphthalene concentration of two orders of magnitude. Nevertheless, these observations still do not rule out the possibility that aggregation is responsible for the stabilization of the CT triplet state. A most persuasive argument favoring this interpretation lies in the similarity between the CT phosphorescence in glasses and that observed in 1:1 single crystals.

The manner in which aggregation might be responsible for stabilization of the CT triplet state can only be, at this stage, a matter of speculation. One attractive possibility is the formation of triple (or even more extended) excited state complexes.[13-17] The phosphorescence results of Briegleb, *et al.*,[15] are of especial interest, since these authors observed a red-shifted phosphorescence in glasses with CT complexes involving naphthalene. At low naphthalene:acceptor concentration ratios the phosphorescence is identical with naphthalene emission, but at high concentration ratios, and with excitation in the CT absorption band, the phosphorescence is considerably red-shifted in a manner similar to that observed in the present work. Brieglieb, *et al.*,[15] attributed this phosphorescence to naphthalene triplet excimer emission originating in triple complexes of two naphthalene and one acceptor molecules. It appears reasonable to rule out a similar possibility in the present study, since changing the naphthalene:TCNB concentration ratio by two orders of magnitude did not affect the observed spectra.

The effect of lattice interactions in stabilizing the CT triplet state in 1:1 single crystals is undoubtedly a strong one, since excitation in the naphthalene absorption band does not lead to any naphthalene phosphorescence. Investigation of a variety of other 1:1 single crystals of complexes of aromatic donors with TCNB shows[18] that this is generally true.

The effect of excitation wavelength found in EPA glasses could be explained by the presence of a variety of complex configurations, each with a different absorption spectrum. Again, the lack of concentration dependence appears to cast some doubt as to the validity of this picture. A possible explanation for this behavior is that excitation in the visible edge of the CT absorption band leads to formation of the CT triplet state, but that excitation at shorter wavelengths provides the complex with enough excess vibrational energy for dissociation to take place prior to emission. This possibility of two excitation-dependent intersystem crossing channels appears reasonable in the light of experimental evidence[6,9,19] that the complex triplet state is formed in many cases from the nonrelaxed excited CT singlet state.

Acknowledgments. Acknowledgment is made to the donors of the Petroleum Research Fund, administered by the American Chemical Society, and to the Research Corporation, for support of this research. The epr spectrometer used in this work was purchased with the aid of a grant from the National Science Foundation.

References and Notes

(1) R. Foster, "Organic Charge-Transfer Complexes," Academic Press, New York, N.Y., 1969, p 82.
(2) S. Iwata, J. Tanaka, and S. Nagakura, *J. Chem. Phys.*, **47**, 2203 (1967).
(3) H. Hayashi, S. Iwata, and S. Nagakura, *J. Chem. Phys.*, **50**, 993 (1969).
(4) S. Iwata, J. Tanaka, and S. Nagakura, *J. Amer. Chem. Soc.*, **89**, 2813 (1967).
(5) P. Krebs, E. Sackmann, and J. Schwarz, *Chem. Phys. Lett.*, **8**, 417 (1971).
(6) N. Tsujino, H. Masuhara, and N. Mataga, *Chem. Phys. Lett.*, **15**, 357 (1972).
(7) M. Yagi, S. Nagakura, and H. Hayashi, *Chem. Phys. Lett.*, **18**, 272 (1973).
(8) D. Haarer and N. Karl, *Chem. Phys. Lett.*, **21**, 49 (1973).
(9) M. Ottolenghi, *Accounts Chem. Res.*, **6**, 153 (1973).
(10) The excitation spectrum of TCNB phosphorescence in EPA glasses is identical with the short wavelength peak of curve A of Figure 1. The sharp short wavelength cut-off is due to the high optical density of the glass at the onset of the naphthalene absorption. The presence of this peak in the excitation spectrum of the CT fluorescence means that excitation of TCNB in the glass leads to formation of the excited CT singlet state. Experiments at various concentrations seem to rule out the possibility of energy transfer from uncomplexed TCNB molecules. These results point, therefore, to a localized excitation of the TCNB moiety as a possible first step in the formation of the excited CT singlet state. This possibility had already been discussed in ref 4 for 1:1 single crystals.
(11) The decays are not always single exponentials. The values given here are average values.
(12) It was assumed that $g = 2.003$. The parameter D^* is defined by $D^* = (D^2 + 3E^2)^{1/2}$.
(13) H. Beens and A. Weller, *Chem. Phys. Lett.*, **2**, 140 (1968).
(14) G. Briegleb, H. Schuster, and W. Herre, *Chem. Phys. Lett.*, **4**, 53 (1969).
(15) Z. Teitelbaum, R. Potashnik, and M. Ottolenghi, *Mol. Photochem.*, 3, 107 (1971).
(16) N. Tsujino, H. Masuhara, and N. Mataga, *Chem. Phys. Lett.*, **21**, 301 (1973).
(17) H. Masuhara and N. Mataga, *Chem. Phys. Lett.*, **22**, 305 (1973).
(18) R. Gillies, R. J. Hunton, and A. M. Ponte Goncalves, unpublished results.
(19) H. Masuhara, N. Tsujino, and N. Mataga, *Chem. Phys. Lett.*, **12**, 481 (1972).

Electron Spin Resonance Studies of the e_{aq}^- Adduct to Fumaric Acid[1,2]

Om P. Chawla and Richard W. Fessenden*

Radiation Research Laboratories, Center for Special Studies and Department of Chemistry, Mellon Institute of Science, Carnegie-Mellon University, Pittsburgh, Pennsylvania 15213 *(Received May 2, 1974)*

Publication costs assisted by Carnegie-Mellon University and the U. S. Atomic Energy Commission

Esr spectra are reported for the mono- and dianion forms of the e_{aq}^- adduct to fumaric acid. Two forms of the monoanion, $[HO_2CCH{=}CHCO_2H]\cdot^-$, differing in the location of the protons on the carboxyl oxygens were found. Both have essentially the same pK_a value of 8.1 for dissociation to the dianion radical. With the identification of the mono- and dianions it is possible to correlate each of the esr spectra previously reported to a particular state of ionization of the radical. In several instances more than one spectrum had been observed at a particular pH, depending upon whether rapid exchange of the carboxyl protons occurred. The reactions of the trianion radical $[^-O_2CCH{=}CHCO_2^-]\cdot^-$ with water to form $^-O_2CCH_2\dot{C}HCO_2^-$ and for electron transfer from $(CH_3)_2\dot{C}O^-$ to fumarate are also reported. The latter reaction allowed production of such high signal intensities that the ^{13}C hyperfine constants ($a^C(2)$ = 4.39, $a^C(2)$ = 2.04 G) of $[^-O_2CCH{=}CHCO_2^-]\cdot^-$ could be determined.

Introduction

Radicals formed by one electron reduction of fumaric and maleic acids have been studied by a number of workers using steady-state esr,[3-5] pulse optical absorption,[6] and conductiometric[7] techniques. In spite of the effort expended on these systems some disagreement still exists as to the esr spectra and pK values for the various forms and it is one purpose of the present paper to provide some additional esr data to clarify the situation. In addition, we wish to report several new reactions discovered during the course of this work and involving fumarate and maleate.

pK Values

The esr results of Anderson, *et al.*,[5] and Neta and Fessenden,[4] the pulsed conductivity experiments of Lilie and Fessenden,[7] and the pulse radiolysis experiments of Hayon and Simic[6] are all substantially in agreement in the maleic acid system. Esr spectra clearly attributable to HO_2C-$\dot{C}H{=}CH\dot{C}(OH)_2$ in strong acid (pH 1), $[HO_2C$-$CH{=}CHCO_2H]\cdot^-$ at pH 4–5 and 6–7, and $[^-O_2CCH{=}CH$-$CO_2H]\cdot^-$ at pH 7 and above (to pH 14) have been reported. Subsequent conductivity experiments[7] have confirmed the fact that the last carboxyl proton does not dissociate significantly at least to pH 12. These various results are summarized in Table I.

Much more confusion exists with fumaric acid. Anderson, *et al.*,[5] noted a number of changes in the esr spectrum of the reduced form over the pH region 1–6 and they attributed the spectrum at pH 5–6 to $[^-O_2CCH{=}CH$-$CO_2H]\cdot^-$. Neta[3] reported the spectrum to be the same at pH 6.9 and 12 and assumed that the radical was fully dissociated over that region. The conductivity results,[7] however, showed the pK for last dissociation (II to I in Figure 1) to be 10.7 and pulse optical experiments[6] have supported this value. The work to be described below demonstrates that there are indeed changes in the esr spectrum over this pH region and also helps to explain some of the other spectra observed at lower pH.

Esr experiments were carried out using previously described techniques of photolysis[8] and radiolysis.[9] The photolytic experiments used SO_3^{2-} as the source of electrons.[8] When 15 mM Na_2SO_3 and 1.3 mM fumaric acid at pH 12.2 were photolyzed three sets of lines were observed: the g = 2.00307 singlet of $\dot{S}O_3^-$, a 1:2:1 triplet described by $a^H(2)$ = 6.48 G and g = 2.00352, and a doublet of triplets with $a^H(1)$ = 20.38, $a^H(2)$ = 23.59 G, and g = 2.00329. With an N_2O saturated solution the latter two sets of lines disappeared showing that the corresponding radicals arise from the reaction of e_{aq}^- with fumarate. The triplet spectrum is that which was observed by Neta[3] and is ascribed to $[^-O_2C$-$CH{=}CHCO_2^-]\cdot^-$ (designated as I in Figure 1) formed directly by e_{aq}^- attachment. The doublet of triplets has the same parameters as have been found for the succinate radical, $^-O_2CCH_2\dot{C}HCO_2^-$ (radical V),[3] and is assigned accordingly. As will be discussed below this latter radical is produced by a protonation of $[^-O_2CH{=}CHCO_2^-]\cdot^-$ by water. The spectra of radicals I and V decreased in intensity with pH in a parallel fashion to pH 9.5–9.6 where they became too weak to observe. Between pH 9.6 and 12.0 the central line of the triplet (I) was broader than the outer two lines and as a consequence did not have twice the peak height of the outer pair of lines. Between pH 8.5 and 10.6 another set of lines appeared which could be described by $a^H(1)$ = 9.11, $a^H(1)$ = 3.61, $a^H(1)$ = 0.43 G, and g = 2.00346. These lines were present simultaneously with those of I and V from pH 9.5 to 10.6. Below pH 9.5 only these new lines were present. This spectrum is assigned to $[HO_2CCH{=}CH$-$CO_2^-]\cdot^-$ (radical II) with the 0.43-G splitting belonging to the carboxyl proton. Although the ethylenic protons have very different splittings of 3.61 and 9.11 G as a result of the asymmetry produced by the protonation of one carboxyl group, the sum of these two values (12.72 G) is very similar to the sum for radical I (12.98). A similar asymmetry has been observed for the monoanion radical of maleate (see Table I).

The difference in splitting by the two ethylenic protons provides a mechanism for broadening the central line of the triplet of the trianion form (I). A transformation from I to II and back again by protonation–dissociation effectively shifts the two components of the central line of the triplet to rather different positions. The kinetics and equilibrium concentration ratio determine the magnitude of the effect.

TABLE I: Summary of Esr Data on e_{aq}^- Adducts to Fumaric and Maleic Acids

Form of radical	pK_a	Esr Spectrum: pH		Hyperfine constants	g factor	Ref
Fumaric acid						
$HO_2CC(H)=C(H)\dot{C}(OH)_2$		1–3		$a^H(2) = 6.0$ (broad central line)[b]	2.0036	5
⇵	~3[a]					
$[HO_2CC(H)=CCO_2H]\cdot^-$		4–5		$a^H(2) = 6.25$, $a_{OH}^H(2) = 0.5$	2.0035	5
		5–6		$a^H(2) = 6.25$	2.0035	5
		6.9		$a^H(2) = 6.61$	2.00357	3
⇵	8.1	4.6–9	IV[c]	$a^H(2) = 6.41$, $a_{OH}^H(2) = 0.66$	2.00350	*d*
			III	$a^H(2) = 6.32$, $a_{OH}^H(1) = 0.63$, $a_{OH}^H(1) = 0.36$	2.00354	*d*
$[HO_2CC(H)=CCO_2^-]\cdot^-$		7–11	II	$a^H(1) = 9.09$, $a^H(1) = 3.64$, $a_{OH}^H(1) = 0.47$	2.00350	*d*
⇵	10.7,[e] 10.9[a]					
$[^-O_2CC(H)=CCO_2^-]\cdot^-$		>9.6	I	$a^H(2) = 6.48$	2.00352	*d*
		~12		$a^H(2) = 6.61$	2.00357	3
				$a^H(2) = 6.81$	2.0035	*f*
Maleic acid						
$[HO_2CC(H)=CCO_2H]\cdot$		1		$a^H(2) = 6.4$, $a_{OH}^H(1) = 1.1$	2.0035	5
⇵	~4[a]					
$[HO_2CC(H)=CCO_2^-]\cdot$		4–5		$a^H(1) = 7.9$, $a^H(1) = 5.1$, $a_{OH}^H(1) = 0.6$	2.0035	5
		6–7		$a^H(1) = 8.12$, $a^H(1) = 5.06$, $a_{OH}^H(1) = 0.76$, $a_{OH}^H(1) = 0.59$	2.00341	4
⇵	5–6[a]					
$[^-O_2CC(H)=CCO_2^-]\cdot$		5–7		$a^H(2) = 6.6$, $a_{OH}^H(1) = 0.6$	2.0035	5
	>14[g]	9.2–14		$a^H(2) = 6.74$, $a_{OH}^H(1) = 0.65$	2.00347	4

[a] Value of pK_a taken from ref 6. [b] The broad central line and the absence of any carboxyl proton splitting must be the result of an acid-catalyzed exchange of those protons, see ref 5. [c] Two symmetric isomers are possible. It is not known to which these parameters pertain. [d] This work. [e] From conductivity results, ref 7. [f] Values for solution in liquid NH_3, I. H. Elson, T. J. Kemp, D. Greatorex, and H. D. B. Jenkins, *J. Chem. Soc., Faraday Trans. 2*, **69**, 1402 (1973). [g] Based on the fact that only the one set of lines is observed in 1 *M* KOH solution.

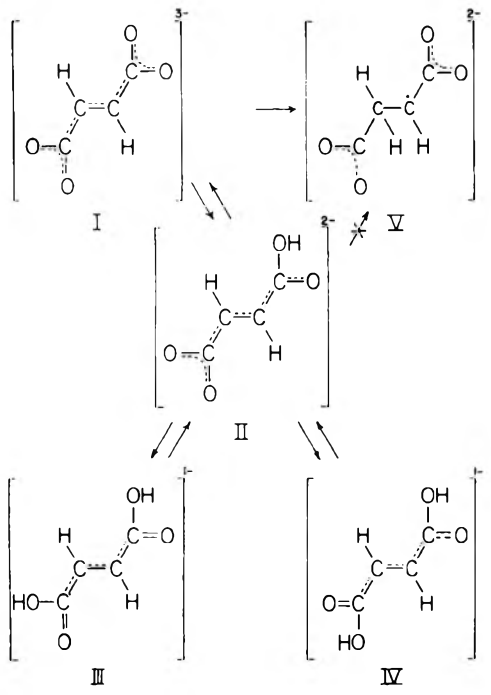

Figure 1. Reactions observed at pH >6 for the various e_{aq}^- adducts to fumarate. Note that two possible isomers of the dianion and three of the monoanion radicals are possible. Lines of only one dianion and two monoanions were seen. Except for the unsymmetrical species III the exact position of the carboxyl protons is not known.

This process will also affect the outer lines of the triplet spectrum but the effect will be smaller because the sum of the two large splittings is similar in I and II. Collapse of the OH proton splitting also leads to a degree of line broadening for all lines of both I and II. The p*K* for this equilibrium (10.7) is such that the dianion form is partially dissociated before a pH is reached where the reaction $OH^- + II \rightleftarrows I + H_2O$ can cause observable broadening (above about pH 10).[10] This fact in turn keeps the maximum degree of line broadening relatively small. No detailed study of the broadening was made.

Experiments at lower pH where the signals tended to be weaker were more readily carried out using radiolysis as the source of e_{aq}^-. The solutions contained 1.3 m*M* fumaric acid and 11 m*M* *t*-BuOH as OH scavenger and, over the range pH 8.5–12.2, duplicated the photolysis results for radicals I and II. (Lines from $^-O_2CCH_2\dot{C}HCO_2^-$ and ^-O_2C-$CH(OH)\dot{C}HCO_2^-$ were also present.)[11] Below pH 8 (1 m*M* phosphate was used as buffer) new lines appeared and below 7.0 the lines of II completely disappeared. The new lines consist of two sets each with a large triplet of about 6.4 G with, in one case a small triplet of 0.66 G and in the second case two doublets of 0.63 and 0.36 G (see Figure 2). These two spectra can be assigned to radicals IV and III respectively in Figure 1; the exact hyperfine parameters are given in Table I. The same structure as in Figure 2 persisted at pH values of 5.3 and 4.6 with a slight broadening of the lines at pH 4.6 (with 10 m*M* fumarate). With a higher concentration of fumarate (20 m*M*) at pH 4.6 considerable

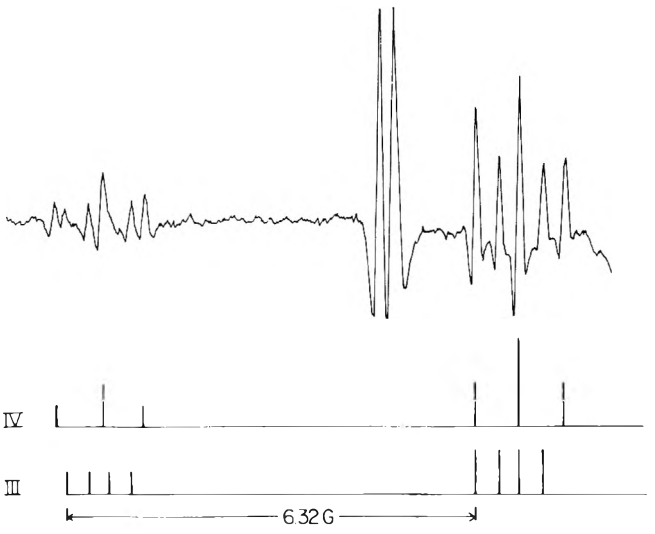

Figure 2. Second-derivative esr spectrum taken during radiolysis of 1.3 m*M* fumarate at pH 6.1 (0.5 m*M* phosphate buffer). The complete spectrum of the e_{aq}^- adducts consists of three groups of lines of which the low-field two are shown. The third group is under the peak from the irradiated silica cell and is not observable. The two stick spectra represent the two monoanion radicals III and IV. The large doublet near the center is from the OH adduct to fumarate. The observed line width (which has some contribution from the field modulation) is about 0.14 G.

broadening occurred so that the low-field line group appeared as a triplet. Under these latter conditions the central group remained as in Figure 2 but had approximately 1.5–2 times the line width. Because of the weakness of the lines no detailed study of this broadening was made.

The existence of two distinct spectra of radicals with the formula $[HO_2CCH{=}CHCO_2H]\cdot^-$ shows that the interconversion between the isomers is not rapid enough to cause line broadening except at the higher solute concentrations. There are three possible isomers for the monoanion of which two are represented by III and IV in Figure 1. The structure given for IV is one of the two symmetric ones but there is no way to decide which actually is correct. The equivalence of the splittings of the ethylenic protons for the unsymmetrical isomer III is somewhat surprising but demonstrates that the position of the proton on the oxygens of a given carboxyl group has little effect on the OH proton splitting. This result is in contrast to the large asymmetry occurring when one carboxyl group is dissociated. The large difference in splittings by the carboxyl protons in the two positions is peculiar but the indirect nature of the mechanism for this splitting precludes any detailed discussion but can probably account for the difference.[12]

It is now possible to discuss the pK values for the e_{aq}^- adduct to fumaric acid. There is no disagreement on the pK of 10.7–10.9 as both the conductivity[7] and optical results[6] agree. The esr data reported here are also in accord with such a value but direct determination of the pK from these data is difficult because of the line broadening associated with the equilibrium II $\rightleftarrows$ I. The coexistence of lines from radicals II, III, and IV over the pH range 7–9 shows that there must be a pK in this interval. Because equilibration among the various forms must be more rapid than the chemical decay it is possible to use the relative concentrations of the forms to determine the pK. At pH 8.1 the concentration[13] of II is equal to that of III and IV taken together so this value must be the pK. (The relative concentrations of III and IV were similar from pH 7.3 to 8.9 with that of IV about one-third higher. Clearly the two forms have very similar pK values.) The pulse radiolysis experiments[6] did not find a corresponding change in absorption at 360 nm showing that the optical spectra of the various forms involved in this pH region do not differ significantly. The conductivity experiments[7] were carried out only down to pH ~9 so that a pK of 8 would not have been found. Extension of that method to pH 8 is not possible because buffers cannot be used.

The previous esr results which gave a spectrum showing only a single triplet splitting at pH 5–6[5] and 6.9[3] can only be explained by the assumption that high buffer concentrations caused a rapid proton exchange which collapsed the carboxyl proton splittings.[14] The spectrum reported by Anderson, *et al.*,[5] for pH 4–5 which has a triplet structure caused by the two carboxyl protons is probably the same as reported here for III and IV together. A slight broadening of the lines would cause the complex structure shown in Figure 2 to reduce to a ~0.5-G triplet as was seen for the end line group with 20 m*M* fumarate solutions. The change in the spectrum from pH 1–3 to 4–5 (see Table I) and the line broadening seen at pH 3 show the first pK to be between these ranges in support of the value of ~3 suggested by Hayon and Simic.[6] These pK values are summarized in Table I.

The data in Table I show that the one-electron reduction product of fumaric acid or fumarate displays a full sequence of protonations on the carboxyl groups and that distinct esr spectra can be assigned to the four forms from neutral radical to trianion. With maleic acid only the three forms from neutral radical to dianion are known in aqueous solution.

Protonation of $[^-O_2CCH{=}CHCO_2^-]\cdot^-$ on Carbon

The formation of $^-O_2CCH_2\dot{C}HCO_2^-$ (V) in photolysis shows rather clearly that the electron adduct to fumarate can protonate on carbon and its appearance only when the trianion form is present suggests that the rate of protonation is higher for the trianion than for the dianion. However, several other factors may also affect the concentration of V. Because the concentration of the e_{aq}^- adduct as measured by the total signal height is less with the dianion form its lifetime is shorter and less time is available for reaction to form V. In addition it might be expected that disappearance by reaction with the dianion is faster than that by reaction with the trianion. The unobservability of V at lower pH may be the result of these two factors rather than to a lower rate of protonation for the dianion. Radiolysis experiments have the advantage that greater signal intensities can be produced but here formation of V by addition of H atoms to fumarate is a problem. A number of experiments are possible but the most useful involved formate as a scavenger for OH and part of the H atoms. With 1.5 m*M* fumarate and 50 m*M* formate most of the H and OH radicals react with formate to produce CO_2^- which then adds to the fumarate to give the adduct $(^-O_2C)_2CH\dot{C}HCO_2^-$. An experiment at pH 9.0 (1 m*M* $Na_2B_4O_7$) showed approximate relative concentrations[13] of 60, 4.4, and 40 for the CO_2^- adduct, V, and the fumarate dianion radical, respectively. When the solution was saturated with N_2O to scavenge e_{aq}^- the concentration of dianion decreased[15] by about a factor of 10, that of the CO_2^- adduct increased to 240, and that of V remained unchanged to within ~10%. A similar experiment at pH 10.0 showed 40

units of the CO_2^- adduct, 6.0 units of V, and about 60 units total of the di- and trianions before addition of N_2O and similar values to the pH 9.0 experiment after addition of N_2O. Thus at pH 10.0 a significant decrease in concentration of V (about 1.6 units) occurred upon scavenging e_{aq}^- while at pH 9.0 a change of less than about 0.4 units was found. As in the photolytic experiments it is difficult to use these data to determine whether the trianion protonates on carbon more rapidly than the dianion as is suggested by a superficial examination. The best argument involves the fact that at pH 10.0 the di- and trianions should be in rather rapid equilibrium with a larger amount of the former present (based on the pK) so that the various radical lifetimes should not be significantly different than in the pH 9.0 experiment. Therefore, the increase of concentration of V[16] from 4.4 at pH 9.0 to 6.0 at pH 10.0 must come mainly from the protonation on carbon of the trianion. The rate constant for this reaction is estimated to be $<10^3$ sec^{-1}. On the basis of the differences between the two pH values it would appear that protonation of the dianion is at least fourfold slower.

The results above show that these radicals undergo normal acid–base equilibria involving the carboxyl groups independently of the protonation on carbon. The idea that the rate of protonation on carbon is lower for species with lower total charge is further supported by the fact that the monoanion radicals of fumaric and maleic acids exist as such at pH ~4 where protonation (on carbon) by H^+, if it were to occur, could be quite rapid. This idea also lead us to suppose that a similar situation should exist for the doubly and singly charged anion radicals of acrylate for which puzzling kinetic behavior had been observed.[17] Pulse conductivity experiments were undertaken[18] and those results when taken with the optical data[17] show that the radical dianion $[CH_2{=}CHCO_2^-]\cdot^-$ protonates to $CH_3\dot{C}HCO_2^-$ with a half-life of <0.1 μsec while the monoanion $[CH_2{=}CHCO_2H]\cdot$ does so with a half-life of about 10 μsec.[17] In this case the effect of the total charge is very pronounced and clearly established.

Electron Transfer from $(CH_3)_2\dot{C}O^-$

Hayon and Simic[6] have reported measurements of the rates of electron transfer from $\dot{C}O_2^-$ and $(CH_3)_2\dot{C}OH$ to maleic and fumaric acids. They found measurable rates of transfer to the acids themselves, to the monoanionic forms, and to dimethylfumarate. No significant transfer to the dianionic forms was found at pH 10. Lack of transfer from $\dot{C}O_2^-$ is consistent with the observation of an adduct by esr.[3] Because the basic form of the radical derived from isopropyl alcohol $[(CH_3)_2\dot{C}O^-]$ is a better reducing agent than the neutral form[19] electron transfer is more likely in the former case. Esr experiments confirm that transfer from $(CH_3)_2\dot{C}O^-$ to fumarate and maleate does occur. The radical $(CH_3)_2\dot{C}O^-$ was produced either by photolysis of aqueous 5% acetone and 10% isopropyl alcohol or by radiolysis of similar solutions in both cases at about pH 13. With 2.5 mM fumarate in the photolytic experiment large signals from $[^-O_2CCH{=}CHCO_2^-]\cdot^-$ were observed along with lines from $^-O_2CCH_2\dot{C}HCO_2^-$. The lines from $[^-O_2CCH{=}CHCO_2^-]\cdot^-$ were so strong as to allow the ^{13}C containing radicals to be observed at a signal-to-noise ratio of at least 5:1. Two sets of lines at an intensity of 1% of those of the ^{12}C species were found since the carbon atoms occur symmetrically in pairs. The two carbon hyperfine constants are a^C = 4.39 and 2.04 G. These small values, demonstrate the delocalization of the unpaired electron in the radical and are similar to those of radicals derived from ascorbic acid derivatives.[20] The high radical concentration shows that electron transfer can compete with decay of $(CH_3)_2\dot{C}O^-$.

A similar photolysis experiment carried out with maleate gave a rather different result. In this case comparable concentrations of *both* the maleate dianion and fumarate trianion radicals were present.[21] This result is qualitatively different than that obtained when e_{aq}^- is used to reduce maleate either in the photolysis of SO_3^{2-} or in radiolysis. In those experiments no detectable intensity of the fumarate trianion radical was found (its concentration was <1% that of the maleate species). Several explanations can be given for the formation of the fumarate trianion. However, the finding in radiolytic experiments (also using 5% acetone and 10% isopropyl alcohol) that 0.027 mM of intentionally added fumarate in the presence of 4.5 mM maleate produced comparable signal intensities of the two radicals[21] clearly shows that electron transfer to fumarate is considerably faster than to maleate (by as much as 100 times faster). Thus the observed result in photolytic experiments can arise from secondary reactions involving small amounts of fumarate formed by photolytic isomerization or upon radical–radical disappearance.[22] Small amounts of fumarate should not have any significant effect in experiments with e_{aq}^- because the rates of reaction with maleate and fumarate are more nearly comparable (1.7×10^9 *vs.* 7.5×10^9 M^{-1} sec^{-1}).[23]

References and Notes

(1) Supported in part by the U. S. Atomic Energy Commission.
(2) From the Ph.D. dissertation of O. P. Chawla, Carnegie-Mellon University, Aug 1973.
(3) P. Neta, *J. Phys. Chem.*, **75**, 2570 (1971).
(4) P. Neta and R. W. Fessenden, *J. Phys. Chem.*, **76**, 1957 (1972).
(5) N. H. Anderson, A. J. Dobbs, D. J. Edge, R. O. C. Norman, and P. R. West, *J. Chem. Soc. B*, 1004 (1971).
(6) E. Hayon and M. Simic, *J. Amer. Chem. Soc.*, **95**, 2433 (1973).
(7) J. Lilie and R. W. Fessenden, *J. Phys. Chem.*, **77**, 674 (1973).
(8) O. P. Chawla, N. L. Arthur, and R. W. Fessenden, *J. Phys. Chem.*, **77**, 772 (1973).
(9) K. Eiben and R. W. Fessenden, *J. Phys. Chem.*, **75**, 1186 (1971).
(10) G. P. Laroff and R. W. Fessenden, *J. Phys. Chem.*, **77**, 1283 (1973).
(11) The OH adduct is formed because the amount of *t*-BuOH is not sufficient to scavenge all OH radicals in competition with fumarate.
(12) The reader is reminded that the two protons on the same end carbon of allyl radical show splittings differing by 1 G out of about 14 G, R. W. Fessenden and R. H. Schuler, *J. Chem. Phys.*, **39**, 2147 (1963).
(13) No differences in line width were evident so the total signal height for a given radical was taken to represent its steady-state concentration.
(14) An experiment with 0.13 *M* phosphate and 0.1 *M* fumaric acid showed the carboxyl proton structure to be a broad singlet at pH 7.1 in accord with the observations by Neta.[3] The beginnings of this effect were also seen at pH 4.6 with 20 m*M* fumarate (see text).
(15) The amount of fumarate used is sufficient to react with some e_{aq}^- even in the presence of N_2O.
(16) It is actually the comparison of the results without and with N_2O at the two pH values which is important.
(17) E. Hayon, N. N. Lichtin, and V. Madhavan, *J. Amer. Chem. Soc.*, **95**, 4762 (1973).
(18) R. W. Fessenden and O. P. Chawla, *J. Amer. Chem. Soc.*, **96**, 2262 (1974).
(19) J. Lilie, G. Beck, and A. Henglein, *Ber. Bunsenges. Phys. Chem.*, **75**, 458 (1971); K.-D. Asmus, A. Wigger, and A. Henglein, *ibid.*, **70**, 862 (1966).
(20) G. P. Laroff, R. W. Fessenden, and R. H. Schuler, *J. Amer. Chem. Soc.*, **94**, 9062 (1972).
(21) Photolytic experiments gave equal signal heights for both radicals for about a 2:1 concentration ratio in favor of the maleate dianion. Radiolytic experiments on the same solution showed about a 10:1 ratio in favor of the maleate species. In both cases only a weak flow-rate dependence was found.
(22) Because of the involvement of such secondary reactions, the situation here does not appear to be related to that reported for the isomerization of stilbene [G. Levin, T. A. Ward and M. Szwarc, *J. Amer. Chem. Soc.*, **96**, 270 (1974)].
(23) M. Anbar, M. Bambenek, and A. B. Ross, *Nat. Ref. Data Ser., Nat. Bur. Stand.*, **No. 43** (1973).

Spectroscopic Studies of Ionic Solvation. XVI. Lithium-7 and Chlorine-35 Nuclear Magnetic Resonance Studies in Various Solvents

Yves M. Cahen, Paul R. Handy, Eric T. Roach, and Alexander I. Popov*

Department of Chemistry, Michigan State University, East Lansing, Michigan 48824 *(Received January 10, 1974; Revised Manuscript Received September 9, 1974)*

Publication costs assisted by Michigan State University

Chemical shifts of lithium-7 nucleus were measured in 11 nonaqueous solvents against 4.0 *M* aqueous lithium perchlorate solution. Lithium perchlorate, chloride, bromide, iodide, triiodide, and tetraphenylborate were used. The shifts ranged from +2.80 ppm for acetonitrile, down to −2.54 ppm for pyridine. In dimethyl sulfoxide and dimethylformamide no evidence for contact ion pairing was observed. Formation of contact ion pairs was particularly evident in tetrahydrofuran, nitromethane, and tetramethylguanidine. The large broadening of the ^{35}Cl resonance of the perchlorate ion in these solvents is in agreement with the above explanation. In contrast to sodium-23 nmr, no correlation was found between limiting chemical shifts in different solvents and the Gutmann donor numbers of these solvents.

Introduction

Previous studies in this laboratory[1] and elsewhere[2-4] have shown that sodium-23 nmr offers a very sensitive probe of the environment of sodium ions in various solvents and solvent mixtures. It was of interest to us to extend such studies to salts of other alkali metal ions in order to determine the influence of the cation on the ionic equilibria and ionic species present in various nonaqueous solvents.

The exchange of ions between different environments is usually rapid with respect to the nmr time scale, resulting in only one resonance signal at an average frequency determined by the magnetic shielding and lifetime of the nucleus in each of the sites. Alteration of parameters such as concentration, counterions, and solvent produces changes in the relative proportion and type of environment which may be reflected by alteration of the nmr spectra on chemical shift and/or line shape, and/or line width of the observed resonance.

The properties of ^{7}Li nucleus are quite favorable for nmr studies. The resonance lines of Li^{+} ion in solutions are exceptionally narrow and chemical shift can be measured with considerable accuracy.

Nuclear magnetic resonance studies on simple lithium salts in different solvents have been rather sparse. Craig and Richards[5] report on ^{7}Li spin–lattice relaxation rates for lithium chloride solutions in water, methanol, formic acid, and dimethylformamide and observe, *inter alia*, that no significant variation in the chemical shifts was observed with a change in salt concentration or in the solvent. Subsequent studies by Maciel, *et al.*,[6] and by Akitt and Downs,[7] however, showed that the frequency of the ^{7}Li resonance is quite sensitive to the environment. The chemical shifts in different solvents range from 2.90 ppm upfield (from water) in acetonitrile, to 2.26 ppm downfield in pyridine. The above studies also indicated that in certain solvents, the chemical shift was influenced by the anion of the lithium salt.

Very few results are available on chlorine nmr in nonaqueous solvents and particularly on lithium perchlorate solutions. Dodgen, *et al.*,[8] reported the ^{35}Cl chemical shift of $HClO_4$ at -946 ± 6 ppm from concentrated aqueous HCl solution with a line width of 0.15 ± 0.005 G, *i.e.*, 62.5 Hz. The same observations were made by Saito[9] for the chemical shift. In the latter case the line width was less than 0.1 G, *i.e.*, ~42 Hz.

The relatively narrow line width of the ^{35}Cl resonance for perchlorate solutions is probably due to the highly symmetrical electronic density around the nucleus and one can expect its broadening when the perchlorate ion is involved in interactions, such as contact ion pair formation, which will destroy such symmetry.

In this paper we report the influence of the solvent, of the concentration, and of the counterions on the ^{7}Li chemical shifts. We also report ^{35}Cl nmr line width of lithium perchlorate solutions in methanol, acetone, tetrahydrofuran, tetramethylguanidine, and acetonitrile.

Experimental Section

A. Reagents. Lithium perchlorate and lithium chloride (Fisher) were dried at 190° for several days. Water content was found to be, respectively, 0.2 and 0.6 wt %. Lithium iodide (K & K Laboratories) was purified by recrystallization from acetone and dried under vacuum over P_2O_5 2 days at room temperature, 1 day at 56.3°, and 2 days at 82°. The purified salt contained 0.1 wt % of water. Lithium bromide (Reagent grade, Matheson Coleman and Bell) was dried at 190° for 3 days and contained 0.3 wt % of water. Lithium tetraphenylborate was prepared from $NaBPh_4$ (J. T. Baker) by methathesis reaction,[10] then dried over P_2O_5 under vacuum for 12 hr at room temperature followed by 24 hr at 82°. The purified salt contained 0.1 wt % of water. After drying, all the lithium salts were stored in a drybox under dry nitrogen atmosphere.

Solutions of lithium triiodide were prepared by the addition of equimolar amounts of iodine to a lithium iodide solution in a given solvent. Reagent grade iodine (Baker) was used as received.

B. Solvents. Nitromethane (spectroscopic grade, Aldrich) was fractionally distilled and dried over freshly activated 5A Linde molecular sieves for 24 hr. Water content was found to be <50 ppm. Dimethyl sulfoxide (Baker, re-

agent grade) was dried over molecular sieves for 2 days: water content <25 ppm. Acetone (Fisher) was distilled over Drierite and further dried over molecular sieves. Methanol (analyzed reagent grade, Matheson Coleman and Bell) was first fractionally distilled from calcium hydride and then from magnesium turnings in a nitrogen atmosphere: water content <40 ppm. Dimethylformamide (Fisher) was vacuum distilled from P_2O_5: water content <100 ppm. Propylene carbonate (Aldrich) was dried over activated molecular sieves for 2 days. Tetrahydrofuran (Baker, analyzed reagent) was fractionally distilled from calcium hydride in a nitrogen atmosphere: water content <100 ppm. Acetonitrile (Baker, analyzed reagent) was refluxed over calcium hydride and then fractionally distilled over granulated barium oxide: water content <100 ppm. Pyridine was refluxed over granulated barium oxide and then fractionally distilled in a nitrogen atmosphere. Tetramethylguanidine was refluxed over granulated barium oxide and then fractionally distilled: water content 85 ppm. Acetic acid (Baker) was purified by six fractional freezings.

Analyses for water in salts and solvents, where possible, were carried out with an automatic Karl Fischer titrator Aquatest II from Photovolt.

C. Solutions. In view of the hygroscopicity of solvents and of lithium salts, all solutions were prepared and the nmr tubes were filled in a drybox under nitrogen atmosphere.

D. Nmr Measurements. Lithium spectra were obtained using a Varian Associates DA-60 spectrometer operating at a field of 1.4092 T and a frequency of 23.3 MHz. The spectrometer was frequency locked to an aqueous 4.0 *M* $LiClO_4$ solution contained in a 1-mm melting point capillary and centered in the 5-mm nmr tube by Delrin spacers. Line widths were on the order of 0.25 Hz (0.01 ppm) and chemical shifts were measured with respect to the lock with a Hewlett Packard 5245 L frequency counter. The accuracy of measurement was ±0.2 Hz. Magnetic susceptibility corrections were calculated on the basis of published values of magnetic susceptibilities of the various solvents; several of these values were checked using a Guoy balance, and several others were confirmed by using the method of Live and Chan,[11] the additional data coming from measurements made with a superconducting solenoid nmr spectrometer constructed in this laboratory. Chlorine spectra were obtained using the DA-60 spectrometer operating at a field of 1.0378 T and a frequency of 4.33 MHz. Modulation frequencies in the ranges 20–30 and 800–1000 Hz were used, depending on the line width to be observed. Care was taken to avoid modulation broadening; the modulation amplitude was progressively reduced until the width of the resonance being observed showed no further narrowing. The radio frequency power and sweep rate were also optimized. All experiments were done at room temperature (25°). Cylindrical nonspinning sample tubes of about 15-mm diameter were used. Spectra were calibrated using the high-frequency sidebands in the case of relatively narrow lines. Line widths were determined with an estimated accuracy of ±10% as an average of two to four measurements.

Viscosities of lithium perchlorate solutions were measured with an Ostwald viscosimeter at 25° in a constant temperature bath.

Results and Discussion

The results of our lithium-7 nmr studies are shown in Figures 1–6 and in Table I. In dimethylformamide the ^7Li chemical shifts for lithium perchlorate, chloride, bromide, and iodide are essentially independent of the counterion and of the concentration. Somewhat similar behavior is found in propylene carbonate, methanol, and dimethyl sulfoxide. In tetrahydrofuran, there is little concentration dependence but a significant difference in the chemical shifts of various lithium salts. Acetonitrile and nitromethane solutions show considerable dependence of the ^7Li chemical shift on the concentration and on the counterion.

Since the limit of detection of ^7Li resonance with our in-

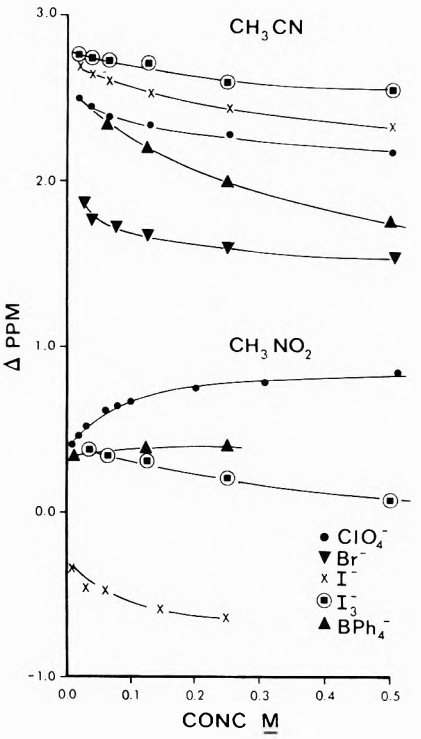

Figure 1. Lithium-7 chemical shifts in acetonitrile and nitromethane.

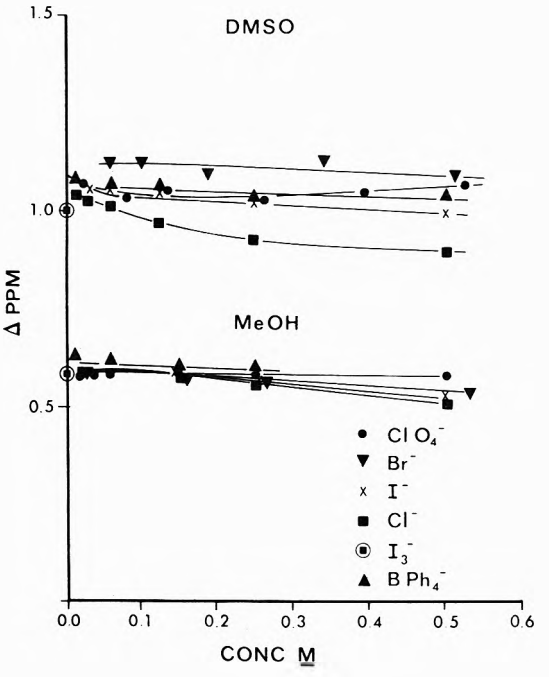

Figure 2. Lithium-7 chemical shifts in dimethyl sulfoxide and methanol.

TABLE I: Limiting Chemical Shifts of ^{7}Li in Various Solvents

Solvent	δ, ppm[a]	Donor no.[b]	Dielectric constant (25°)
Acetonitrile	+2.80	14.1	37.5
Dimethyl sulfoxide	+1.01	29.8	46.68
Propylene carbonate	+0.61	15.1	65.0
Tetrahydrofuran	+0.60	20.0	7.58
Methanol	+0.54	25.7[c]	32.7
Nitromethane	+0.36	2.7	35.87
Acetic acid	+0.03		6.2
Dimethylformamide	−0.45	30.9	36.71
Tetramethylguanidine	−0.63		11
Acetone	−1.34	17.0	20.7
Pyridine	−2.54	33.1	12.4

[a] *Vs.* 4.0 *M* aqueous $LiClO_4$ as external standard. Corrected for bulk susceptibility. [b] Reference 14. [c] Reference 1.

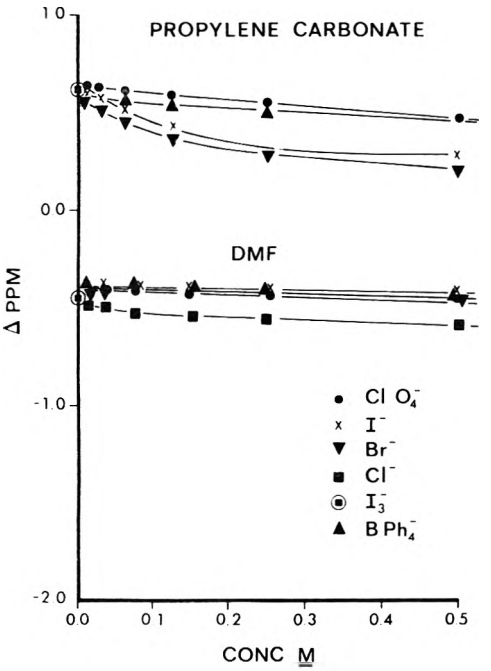

Figure 3. Lithium-7 chemical shifts in propylene carbonate and dimethylformamide.

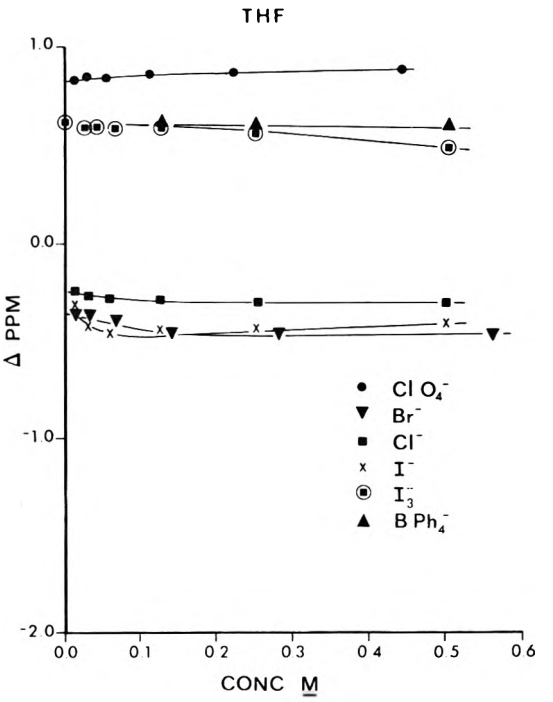

Figure 4. Lithium-7 chemical shifts in tetrahydrofuran.

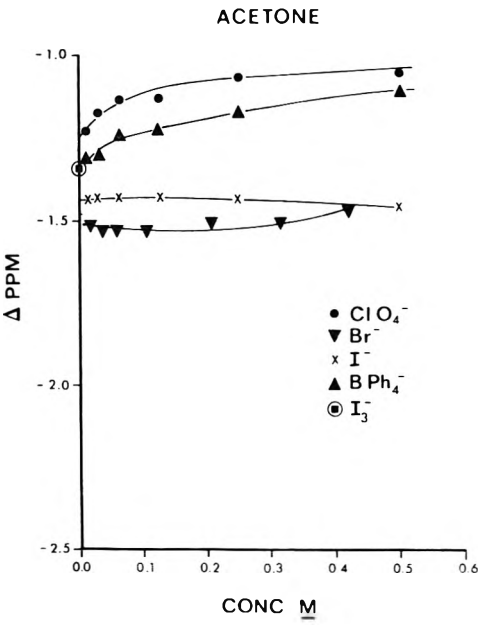

Figure 5. Lithium-7 chemical shifts in acetone.

strument is ~0.01 *M*, it was difficult to establish the limiting chemical shifts of Li^+ ions in such solvents as acetonitrile, THF, nitromethane, and acetone where ion pair formation was especially evident. It has been shown previously by electrical conductance measurements that, in general, the triiodide salts behave as strong electrolytes in nonaqueous solutions.[12] It was found that the chemical shifts of lithium triiodide were essentially independent of concentration in all solvents tried and, therefore, the values of the chemical shifts in 0.02 *M* LiI_3 solutions are reasonably close to the limiting chemical shifts of the Li^+ ion in the same solvents. It should be noted that in cases where extrapolations of chemical shifts to infinite dilution are possible, the value obtained for LiI_3 agrees well with the extrapolated value (for example, in dimethylformamide, methanol, and propylene carbonate).

The chemical shift values obtained in this investigation agree reasonably well with those reported by Maciel, *et al.*,[6] and by Akitt and Downs.[7] Our values, however, seem to be uniformly displaced by ~0.2 ppm towards higher field. We feel that this difference may be due to the fact that our values are corrected for the bulk susceptibility of the solvents.

It should be noted that in most solvents with low or intermediate solvating ability, the ^{7}Li chemical shifts are strongly influenced by the presence of even small amounts of water. It has been shown by Akitt and Downs[7] that the addition of small amounts of water to lithium perchlorate solutions in pyridine results in a sharp upfield shift of the ^{7}Li resonance. We find that the effect is even more drastic in nonsolvating solvents such as nitromethane. Since most organic solvents cannot be obtained completely anhydrous, it is obvious that meaningful chemical shifts for Li^+ ion in

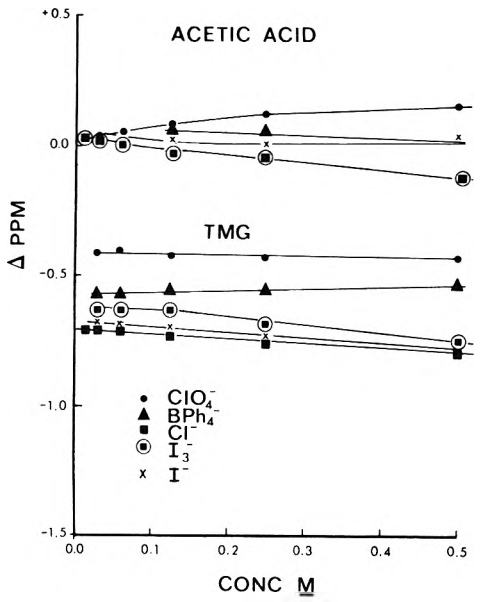

Figure 6. Lithium-7 chemical shifts in acetic acid and tetramethylguanidine.

such cases can only be obtained if the concentration of water is much smaller than the concentration of the salt.

It has been previously observed[1,13] that the contact ion pair equilibrium strongly depends on the donor ability of the solvent molecule as well as on the bulk dielectric constant of the medium. Although nitromethane has a high dielectric constant of 36, its donor ability is very low and on Gutmann's scale,[14] its donor number is 2.7. We see from Figure 1 that the chemical shifts of lithium perchlorate and lithium iodide are concentration dependent and, therefore, that there is contact ion pair formation. There is also some evidence for contact ion pair formation in lithium iodide and bromide solutions in propylene carbonate (Figure 3) (dielectric constant 65, donor number 15.1). These results are in agreement with the data obtained with ^{23}Na nmr in propylene carbonate solutions where the chemical shifts of sodium bromide and of sodium thiocyanate are strongly concentration dependent.[15] On the other hand, in dimethylformamide, with a high dielectric constant of 36.7 and a donor number of 30.9, there is very little influence of the chemical shift on the counterion or on concentration (Figure 3). In fact, the chemical shifts for the perchlorate, bromide, and iodide are essentially superimposable and only the chloride shows some evidence of contact ion pair formation.

Tetrahydrofuran is an interesting solvent in that it has a low dielectric constant of 7.58 but a respectable donor number of 20.0. The similarity of the chemical shifts for the chloride, bromide, and iodide (Figure 4) and the fact that they are downfield from the perchlorate may indicate contact ion pair formation. The low dielectric constant would preclude any ion pair dissociation in the concentration limits used (0.01–0.6 *M*). In fact, conductance measurements reported in a previous paper[1] showed that sodium–anion ion pairs do not dissociate in the same concentration range.

In the case of acetic acid solutions (Figure 6) we see very little concentration or counterion dependence of the ^{7}Li chemical shift. In fact, the greatest difference we observe is ~0.2 ppm between 0.5 *M* solutions of the perchlorate and the triiodide. Acetic acid, however, is a solvent of low dielectric constant (6.3 at 25°) and it is natural to expect that

TABLE II: Line Broadening of ^{35}Cl Resonance in $LiClO_4$ Solutions

Solvent	Concn, *M*	$W_{1/2}$ (obsd), Hz[a]	η(cP sample)/ η(cP solvent)	$W_{1/2}$ (corr), Hz[a]
Acetone	0.00		1.00	
	0.26	11	1.12	10
	0.52	16	1.21	13
	1.00	27	2.07	13
Methanol	0.00		1.00	
	0.49	19.4	1.30	15
	1.00	19.4	1.38	14
Tetrahydrofuran	0.00		1.00	
	0.26	53	1.19	44
	0.49	63	1.39	45
	1.44	202	3.15	64
Nitromethane	0.00		1.00	
	0.26	85	1.04	82
	0.51	120	1.16	103
	1.01	173	1.37	131
Tetramethylguanidine	0.00		1.00	
	1.00	280	5.53	51
Acetonitrile	0.00		1.00	
	0.26	15	1.09	14
	0.50	27	1.26	21
	1.00	26	1.68	22

[a] Width at half-height.

there will be a considerable amount of ionic association in this medium. It seems reasonable to assume that in this case we have largely solvent-separated ion pairs and that a very slight concentration dependence indicates an equilibrium between solvent-separated ion pairs and a small amount of contact ion pairs. At the limiting concentration of 0.01 *M* essentially only solvent-separated ion pairs exist in solution. This assumption is strongly supported by a previously reported observation from this laboratory that in acetic acid solution the frequency of the lithium ion vibration in a solvent cage *is independent of the nature of the counterion* and comes at 390 cm^{-1} for ^{7}Li salts and at 407 cm^{-1} for ^{6}Li salts.[16] On the other hand, it has been shown that the frequency of the solvation band is anion dependent when the anion penetrates the inner solvation shell to form a contact ion pair.[17]

We mentioned above that we attribute the concentration dependence of the ^{7}Li chemical shifts to the formation of contact ion pairs, *i.e.*, to cases where the anion directly replaces a solvent molecule or molecules in the *inner* solvation shell of the cation. It seems reasonable to assume that gross variations in the chemical shift of an alkali metal ion is a direct influence of the change in its immediate chemical environment, *i.e.*, it reflects the influence of its nearest neighbors. It has been shown, for example, that nmr techniques for the determination of solvation numbers of ions invariably yield numbers indicative of the inner solvation shell. Thus the hydration number of magnesium(II) ion was found to be six by nmr measurements[18] while the electrical conductance technique, which also reflects the contribution of the outer solvation[19] shell, yields a solvation number of 14–15. Evidence for the contact ion pair formation, in the case of lithium perchlorate–acetone system, was also obtained from the behavior of the 935-cm^{-1} Raman band corresponding to the symmetrical stretch of the ClO_4^- ion (ν_1, A_1).[20]

The results of the ^{35}Cl nmr study are shown in Table II. In general, in dilute solutions the width and half height of

the ^{35}Cl resonance was 10–20 Hz as compared with 45 or 65 Hz reported previously for aqueous solutions. It is seen that there is a considerable broadening of the ^{35}Cl resonance with increasing concentration of the salt in nitromethane and to some extent in tetrahydrofuran and tetramethylguanidine. On the other hand, very little concentration dependence is evident in acetone, methanol, or acetonitrile solutions.

It seems to us that the concentration-dependent broadening of the ^{35}Cl resonance is indicative of contact ion pair formation for the reasons given below.

In theory, spin–lattice relaxation mechanisms may be divided into five categories:[21] dipole–dipole relaxation, chemical shift anisotropy, scalar coupling, spin rotation relaxation, and quadrupole relaxation. Since the observed relaxation time is assumed to be T_1 equals T_2 in the motional narrowing limit, the observed results may be expressed as

$$\frac{1}{T_1} = R_{1\,\mathrm{expt}} = R_{1\,\mathrm{dip-dip}} + R_{1\,\mathrm{scalar}} + R_{1\,\substack{\mathrm{chem}\\\mathrm{shift}\\\mathrm{anis}}} + R_{1\,\mathrm{spin\ rot}} + R_{1\,\mathrm{quad}} \quad (1)$$

In general, the relaxation mechanisms have a Hamiltonian operator

$$H_c = -hI \cdot T_c \cdot O \quad (2)$$

where I is the spin of interest, O is a physical quantity which interacts with I to provide the relaxation mechanism, and T_c is the coupling interaction tensor. For the case of the dipole–dipole relaxation mechanism

$$H_c = hI \cdot T \cdot S \quad (3)$$

where S is the nuclear spin of the species coupled to the spin of the nucleus of interest. Clearly, this relaxation mechanism is negligible when compared to the smallest observed R_1 for ^{35}Cl in the $^{35}ClO_4^-$ anion. Since the interaction falls off as r^{-3}, where r is the distance between spins, dipole–dipole interactions between ^{35}Cl and nuclei other than nearest neighbors need not be considered, at least to a first approximation.

For chemical shift anisotropy to be a significant relaxation mechanism, the chemical shift of the species must vary radically with orientation in the magnetic field. The ClO_4^- anion cannot satisfy this criterion, since even a fairly large deviation from T_d symmetry does not seem to affect chemical shift significantly.

Scalar coupling of the first kind is due to the effects of chemical exchange of the species of interest, or of nuclei directly coupled to it. This is of no relevance to ^{35}Cl resonance of the ClO_4^- anion, since the nonexchanging oxygens shield the chlorine effectively from chemical exchange effects. In contrast, scalar coupling of the second kind would be due to magnetic field fluctuations at the chlorine nucleus due to motion of the ^{17}O nuclear spins, which should be negligible compared to the observed R_1 as a consequence of the extreme magnetic dilution of ^{17}O.

In the isotropic molecular reorientation limit, the contribution from the spin rotation mechanism may be expressed as

$$R_{1\,\substack{\mathrm{spin}\\\mathrm{rot}}} = (2\pi IkT/h^2)C_{\mathrm{eff}}{}^2\tau_\theta \quad (4)$$

where I is moment of inertia of the ClO_4^- anion, C_{eff} is the spin rotation coupling constant, and τ_θ is the angular correlation time. A calculation using the largest reasonable estimates of τ_θ and C_{eff} shows that $R_{1\,\mathrm{spin\ rot}}$ is several orders of magnitude smaller than the smallest observed $R_{1\,\mathrm{expt}}$.

The term involving quadrupole relaxation may be expressed as

$$R_1 = R_2 = \frac{3}{40}\frac{2I+3}{I^2(2I-1)}\left(1+\frac{\eta^2}{3}\right)\left(\frac{e^2Qq}{h}\right)^2\tau_c \quad (5)$$

where I is the nuclear spin of the observed species, η is the asymmetry parameter, e^2Qq/h is the quadrupole coupling constant, and τ_c is the translational correlation time. For $^{35}ClO_4^-$, the asymmetry parameter is zero, or at most very small for small distortions from T_d symmetry, and the terms involving the nuclear spin are of course constant. Therefore concentration dependence of $R_{1\,\mathrm{quad}}$ must depend on the influence of concentration on either the correlation time, τ_c, or the quadrupole coupling constant, or both. For pure T_d symmetry, e^2Qq/h is zero, since this term may also be expressed as $(eQ/h)(\partial^2V/\partial Z^2)$,[22] and the electric field gradient at the chlorine nucleus is obviously zero for pure tetrahedral symmetry. Therefore, for the quadrupole relaxation mechanism to make any contribution to R_1, some distortion from T_d symmetry must be involved. This distortion and, of course, any change in $R_{1\,\mathrm{quad}}$ would be due to an ion pair phenomenon rather than classical solvation or bulk viscosity effects. Also it should be noted that changes in the electric field gradient at the chlorine nucleus affect the $R_{1\,\mathrm{quad}}$ as the square of the perturbation, while τ_c is influential only to the first power. Several authors have assumed that this effect on the translational correlation time might be minimized by using a correction term linear in bulk viscosity, but recently[23,24] this correction term has been questioned on the basis that bulk viscosity does not accurately reflect changes in τ_c, especially for relatively high concentrations ($>10^{-2}$ M). Despite this, the correction is still useful in predicting the sign and order of magnitude of the change in $R_{1\,\mathrm{quad}}$ due to the concentration effects on τ_c.

In conclusion, it seems that the ^{35}Cl nmr data support our assumption that the concentration-dependent ^7Li chemical shifts are indicative of the contact ion pair formation. It is, of course, possible that the second nearest neighbors (solvent shared ion pairs) may slightly influence the chemical shift of the alkali nucleus, however, the predominant effect must be due to the nearest neighbors. Similar results were recently obtained by Stengle and coworkers[25] who have studied sodium, lithium, and particularly magnesium perchlorates in nonaqueous solvents by ^{35}Cl nmr.

An interesting difference was observed in the relation between the ^{23}Na and ^7Li chemical shifts in different solvents to the Gutmann's donor numbers.[14] It was pointed out in previous publications that a plot of the limiting ^{23}Na chemical shifts *vs.* donor numbers yield a respectable straight line. It is interesting to note that no such correlation is observable with the ^7Li chemical shifts in different solvents (Table I). For example, the limiting chemical shift of a poor donor, nitromethane, is between the limiting chemical shifts of two excellent donors, dimethyl sulfoxide and pyridine.

Several workers[2] have pointed out that in the case of sodium, the paramagnetic screening constant is dominant over the diamagnetic screening constant. For lithium, however, this is not the case; the diamagnetic and paramagnetic terms are of the same order of magnitude, and tend to cancel one another.[26] For this reason, effects such as ring currents and neighbor-anisotropy effects become more important for lithium chemical shifts, as pointed out by Maciel, *et al.*[6] For example, in the case of pyridine, the deshielding of the lithium nucleus may be accounted for by

the effect of the circulating π electrons, if it is assumed that the lithium nucleus is coordinated with the nitrogen in the plane of the ring. Conversely, the upfield shift of lithium when coordinated to acetonitrile may be attributed to a strong neighbor-anisotropy effect analogous to the extraordinary shielding of acetylene protons.

Acknowledgment. The authors gratefully acknowledge the support of this work by a grant from the National Science Foundation.

References and Notes

(1) M. S. Greenberg, R. L. Bodner, and A. I. Popov, *J. Phys. Chem.*, **77**, 2449 (1973), and references listed therein.
(2) E. G. Bloor and R. G. Kidd, *Can. J. Chem.*, **46**, 3425 (1968).
(3) C. Deverell and R. E. Richards, *Mol. Phys.*, **10**, 551 (1966).
(4) A. L. Van Geet, *J. Amer. Chem. Soc.*, **94**, 5583 (1972).
(5) R. A. Craig and R. E. Richards, *Trans. Faraday Soc.*, **59**, 1972 (1963).
(6) G. E. Maciel, J. K. Hancock, L. F. Lafferty, P. A. Mueller, and W. K. Musker, *Inorg. Chem.*, **5**, 554 (1966).
(7) J. W. Akitt and A. J. Downs in "The Alkali Metals Symposium," The Chemical Society, London, 1967, p 199.
(8) K. Jeffrey Johnson, J. P. Hunt, and H. W. Dodgen, *J. Chem. Phys.*, **51**, 4993 (1969).
(9) Y. Saito, *Can. J. Chem.*, **43**, 2532 (1965).
(10) D. N. Bhattacharyya, C. L. Lee, J. Smid, and M. Szwarc, *J. Phys. Chem.*, **69**, 608 (1965).
(11) D. H. Live and S. I. Chan, *Anal. Chem.*, **42**, 791 (1970).
(12) A. I. Popov and N. E. Skelly, *J. Amer. Chem. Soc.*, **76**, 5309 (1954).
(13) U. Mayer and V. Gutmann, *Struct. Bonding (Berlin)*, **12**, 113 (1972).
(14) V. Gutmann, "Coordination Chemistry in Nonaqueous Solvents," Springer-Verlag, Vienna, 1968, p 19.
(15) M. S. Greenberg, D. M. Wied, and A. I. Popov, *Spectrochim. Acta, Part A*, **29**, 1927 (1973).
(16) M. K. Wong and A. I. Popov, *J. Inorg. Nucl. Chem.*, **33**, 1203 (1971).
(17) (a) M. S. Greenberg, D. M. Wied, and A. I. Popov, *Spectrochim. Acta, Part A*, **29**, 1927 (1973); (b) W. F. Edgell, A. T. Watts, J. Lyford, and W. M. Risen, *J. Amer. Chem. Soc.*, **88**, 1815 (1966); (c) A. T. Tsatsas, R. W. Sterns, and W. M. Risen, *ibid.*, **94**, 5247 (1972).
(18) N. A. Matwiyoff and H. Taube, *J. Amer. Chem. Soc.*, **90**, 2796 (1968).
(19) A. P. Zipp, *J. Phys. Chem.*, **78**, 556 (1974).
(20) M. K. Wong, W. J. McKinney, and A. I. Popov, *J. Phys. Chem.*, **75**, 56 (1971).
(21) T. C. Farrar and E. D. Becker, "Pulse and Fourier Transform NMR," Academic Press, New York, N.Y., 1971, Chapter 4.
(22) A. Abragam, "The Principles of Nuclear Magnetic Resonance," Oxford University Press, London, 1961, p 313 *ff*.
(23) M. St. J. Arnold and K. J. Packer, *Mol. Phys.*, **14**, 241 (1968).
(24) T. E. Burke and S. I. Chan, *J. Magn. Resonance*, **3**, 55 (1970).
(25) T. R. Stengle, personal communication.
(26) C. J. Jameson and H. S. Gutowsky, *J. Chem. Phys.*, **40**, 1714 (1964).

On the Debye Scattering Factor for Polydisperse Gaussian Chains

Raymond L. Arnett

3460 Birkerød, Denmark *(Received March 4, 1974; Revised Manuscript Received October 4, 1974)*

The z average of the Debye factor, $P(u)$, for random coils is found to be $P_z = 2(u_n - 1 + (e^{-u})_n)/u_n u_w$ in the absence of polymer swelling by the solvent; the subscripts n, w, and z imply number, weight, and z averages, respectively. An approximate expression for $(e^{-u})_n$ is given in terms of the moments of the polymer molecular-weight distribution, and this approximation compares favorably with exact values calculated for three different distribution functions. It is shown that the asymptotic expression for P_z proposed by others has a very limited validity in scattered-light experiments on polydisperse polymers.

I. Introduction

The factor, $P(u)$, developed by Debye[1] to account for the change with viewing angle in amount of light scattered by dilute solutions of large molecules is

$$P(u) = 2\frac{u - 1 + e^{-u}}{u^2} \qquad u = \left(\frac{4\pi n}{\lambda}\right)^2 s^2 \sin^2\frac{\theta}{2} \tag{1}$$

for monodisperse random coils (gaussian chains). Here n is the refrative index of the scattering medium; λ is the wavelength (vacuum) of light scattered at the angle, θ, from the incident beam; and s is the root-mean-square molecular radius of the scattering molecule.

It is observed that the angular dependence of the amount of light scattered is substantially influenced by polydispersity, and by its nature, in the solute. Hence the shape of an experimental $P(u)$ curve contains information (through s^2) about the distribution of sizes present. Over the past 2 decades a number of proposals have been made to extract this distribution information. Earlier Zimm[2] had shown that with a polydisperse solute, the appropriate average of (1) is the z average, defined by either of

$$P_z = (MP)_w/M_w = (M^2P)_n/M_nM_w \tag{2}$$

where the subscripts n, w, and z denote the number, weight, and z averages, respectively, and M is molecular weight. The initial slope of P_z (or of $(P_z)^{-1}$, as the data are plotted) gives $(s^2)_z$ and this, together with M_w, are two pieces of information about the distribution of sizes which have long been extracted from scattered-light data.

The first to suggest a means of getting more distribution information from the shape of $(P_z)^{-1}$ was Benoit[3] who, following the work of Zimm,[2] pointed out that the asymptote approached by $(P_z)^{-1}$ would give M_n and a ratio s^2/M which has the same kind of average for s^2 as for M. The quantity normally displayed with the experimental data is $(M_wP_z)^{-1}$; the asymptote for this quantity is given by either of the equivalent relations

$$(u_w + u_w/u_n)/2M_w = (1 + u_n)/2M_n$$

Thus the slope of the asymptote gives us $(s^2)_w/M_w = (s^2)_n/M_n$ while the intercept at $\theta = 0$ gives M_n. Following this work came the results[4] of an experiment which seemed to confirm the analysis. Later the analysis on the asymptote was extended[5] to include non-gaussian chains (chains where the gaussian statistics are perturbed by good solvents).

Some years later Carpenter[6] reported on a scattered-light study of polypropylene. On using Benoit's technique, Carpenter found that the intercept of the asymptote yielded a value of M_n which was off by a factor of 2 from the experimental value determined osmotically. This was so even though the value of u was considerably extended by using several wavelengths of incident light in order to bring the measurements into the asymptote region. Carpenter also found that the expressions[5] intended for chains perturbed by good solvents does not give any improvement. After this, Kratoichvil[7] calculated the z average of $P(u)$ for two different distribution functions, the γ distribution and a generalized exponential distribution, and warned that $(P_z)^{-1}$ achieves the asymptotic behavior only at very high values of u_w, which are more inaccessible to measurement. Also the relatively low curvature of the $(P_z)^{-1}$ dependence leads one to mistake a part of the dependence in the region of high angles for an asymptote, and thus that the value regarded as M_n may differ from the correct one by as much as a multiple. The next year, Shultz and Stockmayer[8] reported results of prior calculations of the z average of gaussian chains having a γ distribution. These authors also issue a warning that experimental data are not likely to fall on the asymptote so that extrapolation to the intercept would give an "M_n" appreciably in error but that the slope of the data at the asymptote end of $(M_w P_z)^{-1}$ is sufficiently close to the true slope of the asymptote that good values of the ratio, s^2/M, may be obtained. This present work will confirm both of these findings of Shultz and Stockmayer, not only for a γ distribution of gaussian chains but for a discrete distribution and truncated logrithmic-normal distributions as well.

This technique initiated by Benoit is graphical and calls for the geometrical construction of what is hoped to be the asymptotic line as well as a line tangent to the $(M_w P_z)^{-1}$ data at $u = 0$. The intercepts and slopes of these two straight lines were to provide the four quantities, M_w, $(s^2)_z$, M_n, and s^2/M, which would in fact give three moments in the unknown molecular-weight distribution from one experiment (truly a worthwhile goal). However if now we accept what appears to be conclusive (both by experiment and by calculation) evidence that data from normal scattered-light experiments do not reach the asymptotic portion of the $(M_w P_z)^{-1}$ curve, then what other techniques are open to us to extract the distribution information contained in the curve? Carpenter's[6] finding, augmented by the subsequent cited work, is that the real difficulty does not stem from the fact that good solvents perturb the gaussian statistics to the point where relation 1 is no longer valid but rather from the fact that in an ordinary light-scattering experiment the data simply do not extend far enough to reach the asymptote and hence cannot define it. To circumvent this practical difficulty, Carpenter proposed choosing, by trial and error, various distribution functions with which to calculate the z average of $P(u)$ and compare these calculated averages with the observed. Carpenter's proposal also involvec the determination of M_n by means of an additional experiment (osmotic pressure measurement) and adjusting parameters in the trial distribution functions so that they gave the observed M_n and M_w (from the scattered-light experiment). This is not a straightforward technque and departs from the goal of learning all the distribution information from the single scattered-light experiment. The presnt work takes up this problem again and offers an alternative solution.

II. Further Comments on the Asymptote Problem

As was indicated in our introductory remarks, Zimm[2] pointed out that the reciprocal of the function given by relation 1 has the asymptote

$$\lim_{u \to \infty} P^{-1}(u) = (u + 1)/2$$

an exact, linear relation having both a slope and intercept of ½. Benoit's[3] subsequent arguments extending Zimm's work to polydisperse substances has u sufficiently large so that e^{-u} becomes negligible compared to unity and $P(u)$ is approximated by

$$2(u - 1)/u^2$$

Then taking the reciprocal of the z average of this, he obtained

$$(P_z)^{-1} = (u_w + u_w/u_n)/2$$

as the asymptote for polydisperse polymer (a straight line having slope ½ and intercept $u_w/2u_n$). As we shall see, implicit in these arguments is that *all* values of u in the polymer be large. This is a very limiting restriction in the valid use of the asymptotic relation for it requires *a priori* knowledge about the polymer which is usually not available.

Let us go back to the complete expression for gaussian chains given by (1). There is no problem in obtaining the z average of this; by using the algebra of averages as given by (2), we immediately obtain

$$P_z = 2\frac{u_n - 1 + (e^{-u})_n}{u_n u_w} \tag{3}$$

as an expression for the z average of the complete function, $P(u)$. This expression is exact as long as u (through s^2) is proportional to M. The conditions (experimental) which ensure this also ensure the gaussian statistics necessary for (1). Now we can begin to understand why the asymptote of $(P_z)^{-1}$ is so difficult to obtain through experiment. It is $(e^{-u})_n$ which must become negligibly small compared to unity before the asymptote is reached. The fact that the number average of e^{-u} (rather than some higher and hence more effective average) is involved in the exact z average of $P(u)$ explains why the exponential term does not decay to a negligibly small quantity in most experimental applications.

The reciprocal of (3) is

$$(P_z)^{-1} = \frac{r_0}{2}\left(u_n + \frac{\delta}{1 - \delta/u_n}\right) = \frac{1}{2}\left(u_w + \frac{\delta r_0}{1 - \delta/u_n}\right) \tag{4}$$

where $r_0 \equiv u_w/u_n = M_w/M_n$ and $\delta \equiv 1 - (e^{-u})_n$, $0 \leq \delta \leq 1$. Relation 4 is valid for all points on the $(P_z)^{-1}$ curve including the point at $u_n = 0$. As u_n increases from zero, δ increases from zero and approaches unity. Depending on the nature of the distribution which controls $(e^{-u})_n$, and remembering that as u_n increases from 0 to ∞, δ changes its value by only unity, and noting that as δ slowly increases, 1

$- \delta/u_n$ also slowly increases, there will be a value of u_n for which greater values will leave $\frac{1}{2}/(1 - \delta/u_n)$ changing so slowly as to be effectively constant compared to changes in u_n. At this point the slope of $(P_z)^{-1}$ *vs.* u_w will have nearly the value of the slope of the asymptote (= ½) even though the quantity $\delta/(1 - \delta/u_n)$ is appreciably smaller than its asymptotic value of unity. These are the same conclusions reached by Shultz and Stockmayer.[8]

Sample calculations of the z averages of $P(u)$ for various distribution functions provide dramatic illustrations of the above mentioned conclusions. Figure 1 shows by two examples how a geometrical interpretation of scattered-light data, using what is hoped to be the asymptote, can lead the experimenter to incorrect results. Let us assume the investigator here had prior knowledge of the ratio s^2/M so that with his new knowledge of M_w from this experimental study he can, from his measurements, make the plots of $(P_z)^{-1}$ *vs.* u_w shown in the figure. Consider first the set of three dashed lines. This set is for an essentially monodisperse, high-molecular-weight polymer (having a discrete distribution) and our investigator is not surprised to find the upward curvature his data display, characteristic of monodisperse polymer. He draws the initial tangent (at $u_w = 0$) and finds its slope to be 0.336. He knows this slope should be $u_z/3u_w$ and so concludes that u_z/u_w (= M_z/M_w) is 1.01 for his polymer (in keeping with the expectation of monodisperse polymer). (The actual curve was calculated for a two-component blend that was 99.3% (by weight) pure in the high-molecular-weight component and had an M_z/M_w of 1.0070.) Our investigator now notices that for $u_w >$ *ca.* 8, the slope of his curve is constant at ½ within his ability to determine it from his measurements. (The actual slope is 0.5003 at $u_w = 13.4$.) He concludes his data extend into the asymptotic region and again draws a tangent having a slope of ½ and learns that the intercept of this is 0.588. If this intercept is interpreted as $M_w/2M_n$, as it would be for the true asymptote, then M_w/M_n is found to be 1.18 (a value which may be construed to be quite consistent with the shape of the curve and the value of M_z/M_w already found). However it is in error by more than a factor of 3. The curve was calculated for a polymer having $M_w/M_n = 3.3766$, $M_z/M_w = 1.0070$, $M_{z+1}/M_z = 1.0000$. At the point where the slope is 0.5003, the value of $(e^{-u})_n$ is 0.714, a number certainly not negligible compared to unity! The reader should appreciate that the arrangement of this illustration provides a better check on the asymptote for the experimenter can choose as the asymptote not only the place where the curve has attained a constant slope, but in addition, a constant slope having the correct value of ½. If the ratio s^2/M was not already known it could be obtained from this curve with an error of less than 0.1% coming from the fact that the asymptote had not been reached by the data; however, the value of M_n so obtained would be in error by a factor of more than 3.

The set of three solid lines in Figure 1 is calculated for a polymer having a γ distribution of molecular weights with $M_w/M_n = 8$, $M_z/M_w = 1.875$, $M_{z+1}/M_z = 1.4667$. The slope of the tangent at $u_w = 0$ is found to be 0.625 giving the correct value of M_z/M_w. The slope of the curve, $(P_z)^{-1}$ *vs.* u_w, is only 2% greater than ½ at $u_w = 16$ and in that neighborhood the curve drawn through experimental points would not be distinguished from one having a constant slope of ½. A straight line of slope ½ drawn through the curve at $u_w = 17$ has an intercept of 1.54 which would be interpreted as $M_w/M_n = 3.08$ (instead of the correct

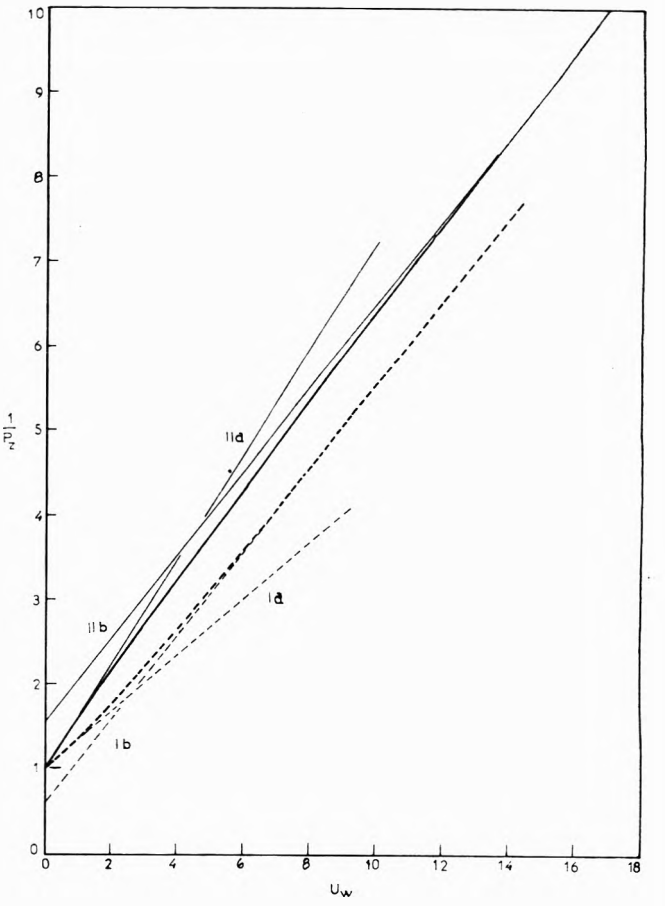

Figure 1. Incorrect conclusions possible from geometrical interpretation of angular dependence of scattered light. (See text. Ia, slope = 0.336; Ib, slope = ½, intercept = 0.588; IIa, slope = 0.625; IIb, slope = ½, intercept = 1.54.)

value, 8) for the polymer by the assumption of the asymptote. The value of $(e^{-u})_n$ at $u_w = 17$ is 0.674 and is, in fact, still greater than 0.6 at $u_w = 38$ where $(P_z)^{-1}$ has risen to 21 times its zero angle value. Further, $(e^{-u})_n = 0.53$ at $(P_z)^{-1} = 48$ and the true slope of the $(P_z)^{-1}$ *vs.* u_w curve is 0.503 at this point, yet the value of M_n deduced from the intercept of a tangent to the curve even at this (experimentally) extreme point would be in error by more than 100%.

It is apparent from these examples that something better than this geometrical approach involving the asymptote is needed

III. An Alternative Proposal

The considerations which follow recognize that the data collected in scattered-light experiments will not define the asymptote of $(P_z)^{-1}$ in order for geometrical interpretations to be made, and therefore that whatever distribution information is contained in the observed $(M_w P_z)^{-1}$ curve must be extracted by means of a relation which is appropriate for the data in the region where they exist. The true z average, (3), has, of course, to be the basis for that relation. The procedure followed here is to find an approximate expression for $(e^{-u})_n$. This will be done, not by using some distribution function in order to calculate the number average of e^{-u} (it is this distribution function which is the unknown), but by giving an expression for $(e^{-u})_n$ in terms of several moments of the unknown distribution function. Since this is an analytic approach rather than a geometric one, it is anticipated that the parameters (moments of the

distribution) in the expression for $(e^{-u})_n$ will be determined, together with M_w, by a least-squares fitting of the function to the data for $(M_w P_z)^{-1}$.

To follow this route requires that the approximate expression for $(e^{-u})_n$ be quite good in view of how it is combined in (3) and in view of the fact that we shall want our result to be valid over the whole range of P_z $(1 \geq P_z \geq 0)$ just as in (3). The early part of the curve is the most restricting ($P_z \simeq 1$). For example, for $e^{-x} \simeq 0.9$, if we approximate e^{-x} by an expression which has an error of only 0.1%, the combination, $x - 1 + e^{-x}$, has an error of amost 19% (x without error); for e^{-x} known to 0.1% at $e^{-x} \simeq 0.95$, $x - 1 + e^{-x}$ has an error of 75%. Nevertheless, it has been possible to give an expression for $(e^{-u})_n$ good enough so that the error in the approximated P_z is within the normal errors of measurement in the scattering of light.

The function to be averaged, being the exponential, suggests that it be expanded in terms of functions which themselves have exponential behavior. One such function is obviously the exponential function itself; thus we consider the series

$$a_1 e^{-b_1 u_n} + a_2 e^{-b_2 u_n} + \ldots \tag{5}$$

where the a_i, b_i are to be determined. Further, since the exponential function is the limit

$$e^{-u_n} = \lim_{q \to 0} (1 + q u_n)^{-1/q} \qquad q \neq 0 \tag{6}$$

we also consider the series

$$p_1(1 + q_1 u_n)^{-1/q_1} + p_2(1 + q_2 u_n)^{-1/q_2} + \ldots \tag{7}$$

and take a linear combination of (5) and (7) to represent $(e^{-u})_n$, *i.e.*

$$(e^{-u})_n = \chi[a_1 e^{-b_1 u_n} + a_2 e^{-b_2 u_n}] + (1 - \chi)[p_1(1 + q_1 u_n)^{-1/q_1} + p_2(1 + q_2 u_n)^{-1/q_2}] \tag{8}$$

The question of how to put the a_i, b_i, p_i, and q_i in terms of moments of the distribution is solved for us by the need to make the right member of (8) an excellent approximation of the left member, particularly at low values of u_n. For small values of the argument, a power series expansion is valid. The series expansion of the left member of (8) is

$$(e^{-u})_n = 1 - u_n + (u^2)_n/2! - (u^3)_n/3! + (u^4)_n/4! - \ldots$$

which, in view of the algebra of averages (and an obvious extension thereof) as given by (2), becomes

$$(e^{-u})_n = 1 - u_n + u_n u_w/2! - u_n u_w u_z/3! + u_n u_w u_z u_{z+1}/4! - \ldots$$

This last relation may be rewritten as

$$(e^{-u})_n = 1 - u_n + r_1 u_n^2/2! - r_0^2 r_1 u_n^3/3! + r_0^3 r_1^2 r_2 u_n^4/4! - \ldots \tag{9}$$

involving the dimensionless ratios, r_0, r_1, r_2, defined by

$$r_0 \equiv \frac{u_w}{u_n} = \frac{M_w}{M_n}; \qquad r_1 \equiv \frac{u_z}{u_w} = \frac{M_z}{M_w}; \qquad r_2 \equiv \frac{u_{z+1}}{u_z} = \frac{M_{z+1}}{M_z}$$

It is immediately clear now how the a_i, b_i, p_i, and q_i of (8) must be determined; the right member of (8) is to be expanded in a power series of u_n and made identical with the right member of (9) by equating coefficients of equal powers of u_n. For by doing this, the right member of (8), which is an approximation, becomes an increasingly better approximation (because the right member of (9) becomes an increasingly better approximation) as u_n becomes smaller, as we must have in order for the numerator of (3) to give a good value for P_z. The fraction, χ, in (8) will be left undetermined at this stage. It will be fixed later to reduce the deviation of the right member of (8) (at larger values of u_n) from exact values of $(e^{-u})_n$ determined from several distribution functions.

For now we set the series, (5), identical with χ times the right member of (9). Closed form expressions for the a_i, b_i are possible only if (5) is limited to the two terms shown. The values of a_1, a_2, b_1, b_2 which make (5) identical with χ times the first four terms of (9) are

$$\begin{aligned} a_1 &= \chi\{1 + (r_0 r_1 - 3 + 2/r_0)/[(r_0 r_1 - 1)^2 - 4(r_0 - 1)(r_1 - 1)]^{1/2}\}/2 \\ a_2 &= \chi - a_1 \\ b_1 &= 1 - [(r_0 - 1)a_2/a_1]^{1/2} \\ b_2 &= 1 + [(r_0 - 1)a_1/a_2]^{1/2} \end{aligned} \tag{10}$$

It is comforting to note that the set of relations, (10), does not present any difficulties in the limit of monodisperse polymer where $r_0 = r_1 = 1$. In this case

$$a_1 = a_2 = \chi/2 \qquad b_1 = b_2 = 1$$

and the series (5) reduces to e^{-u} as it must. Further it may be noted that the argument of the radical in (10) is nonnegative (hence the a_i, b_i are real) as long as r_0 and r_1 are not less than unity. This is the physically real situation.

The series, (7), is now expanded to give the remainder of (9). Again only two terms of the series are used. The remainder of (9) to be accounted for is $1 - \chi$ times the first four terms of (9); however, a redundancy in two equalities, coming from equating coefficients of like powers of u_n, requires the inclusion of the r_2 term in (9) to determine each of p_1, p_2, q_1, q_2. Allowing for the contribution of the series (5) in that term, the expressions for the p's and q's, which with (5) give the first five terms of (9) exactly, are

$$\begin{aligned} p_1 &= (1 - \chi)[1 + C/(4r_0 S^3 + C^2)^{1/2}]/2; \qquad p_2 = 1 - \chi - p_1 \\ q_1 &= r_0 - 1 - (r_0 S p_2/p_1)^{1/2}; \qquad q_2 = r_0 - 1 + (r_0 S p_1/p_2)^{1/2} \\ C &= r_0^2[r_1^2(r_2 - \chi) - \chi(r_1 - 1)^2/(r_0 - 1)]/6(1 - \chi) + r_0[2r_0 - r_1(2r_0 - 7/6)/2 - 3/2] + 1/4 \\ S &= [r_0(r_1 - 1) - (r_0 - 1)]/2 \end{aligned} \tag{11}$$

For monodisperse polymer, the set, (11), becomes

$$p_1 = 1 - \chi, \quad q_1 = 0, \quad p_2 = 0$$

so that in view of (6) the series yields $(1 - \chi)e^{-u}$ for $r_0 = r_1 = r_2 = 1$, and the approximation, (8), then gives

$$(e^{-u})_n = e^{-u}$$

as we desire for proper behavior.

It is clear that either of the series, (5) or (7), would suffice to give the first several terms of (9) exactly. The purpose of combining both series is to introduce the additional parameter, χ, whose numerical value can be adjusted to

make the deviation from truth of the approximation, (8), minimal in the region of u_n between $u_n \to 0$ and $u_n \to \infty$.

The expressions presented above are not pleasant to contemplate. Nevertheless, computers handle them unemotionally.

IV. Comparison of Approximate with Exact Values of P_z

Relations 3, 8, 10, and 11 provide a means of determining M_w/M_n, M_z/M_w, M_{z+1}/M_z, and $(s^2)_n$ in addition to M_w from suitable experiments in the scattering of light. These five quantities are perhaps best determined by a least-squares fit of $(M_wP_z)^{-1}$ (P_z given by (8) in (3)) to the experimental observations of $(Kc/R_\theta)_{c=0}$. The quantities K, c, and R_θ are the usual optical constant in light scattering, the solute concentration, and Rayleigh's ratio, respectively. The five parameters to be determined by the data give the first four moments in the unknown distribution (by number) function and a mean-square radius for the dissolved polymer.

It remains now to determine how far from truth the proposed approximation, (8) in (3), for P_z is. For this test we use three different distribution functions to compute exact z averages of $P(u)$; two of these are continuous distributions and one, a discrete distribution. Several different sets of the four parameters r_0, r_1, r_2, and $(s^2)_n$ are used to specify each of the distribution functions in order to obtain exact P_z values under many different conditions. Corresponding approximate values of P_z, using the same sets of the four parameters, are calculated from (3), (8), (10), and (11) with differing values assigned to χ for comparison with the exact values of P_z.

One of the continuous distribution functions we use is the γ distribution. Its frequency function, for distribution by number, is

$$(m/M_n)^m M^{m-1}/\Gamma(m)e^{-mM/M_n}, \quad m = 1/(r_0 - 1)$$

and permits of a closed form expression for $(e^{-u})_n$. In terms of the ratio, r_0, the expression for P_z is

$$P_z = \frac{2}{r_0}\frac{u_n - 1 + [1 + (r_0 - 1)u_n]^{-1/(r_0-1)}}{u_n^2}$$

In this distribution, r_1 and r_2 are not independent quantities; they are fixed, once r_0 is fixed, by the relations

$$r_1 = (2r_0 - 1)/r_0, \qquad r_2 = (3r_0 - 2)/(2r_0 - 1), \quad r_0 \neq 1$$

Only a very limited range of values for r_1 and r_2 is possible ($1 \leq r_1 < 2$; $1 \leq r_2 < 1.5$) with this distribution.

In order to provide a test with larger values of r_1 and r_2, we use the truncated logarithmic-normal distribution whose frequency function, $p(M)$, for distribution by number, is

$$p(M) = \frac{(2\pi \ln r)^{-1/2}}{\Phi(U') - \Phi(L')}M^{-1}\exp\left[-\frac{(\ln M/\mu)^2}{2 \ln r}\right]$$

where r is the single value each of r_0, r_1, r_2, ... would have if the log-normal distribution were not truncated

$$U' = (\ln U/\mu)/(\ln r)^{1/2}, \quad L' = (\ln L/\mu)/(\ln r)^{1/2}$$

L and U are the lower and upper bounds, respectively, of molecular weight, M, found in the polymer, μ is a parameter related to the M_n of a non-truncated log-normal distribution by $M_n = \mu r^{1/2}$, and $\Phi(x)$ is defined by

$$\Phi(x) \equiv (2\pi)^{-1/2}\int_{-\infty}^{x} e^{-t^2/2}\,dt$$

The mth moment of this distribution is

$$\frac{\Phi(U' - m\sqrt{\ln r}) - \Phi(L' - m\sqrt{\ln r})}{\Phi(U') - \Phi(L')}u^m r^{m^2/2}$$

from which the ratios r_0, r_1, and r_2 are readily found. The expression for r_0, for example, is

$$r_0 = \frac{[\Phi(U' - 2\sqrt{\ln r}) - \Phi(L' - 2\sqrt{\ln r})][\Phi(U') - \Phi(L')]}{[\Phi(U' - \sqrt{\ln r}) - \Phi(L' - \sqrt{\ln r})]^2}r$$

A selection of values of the four distribution parameters, r, μ, L, and U, fixes the values of r_0, r_1, r_2, and $(s^2)_n$. This same set of values is then used in the approximate expression for $(e^{-u})_n$ while the exact value is determined from the numerical integration of

$$\int_L^U p(M)e^{-uM}\,dM$$

where $u = aM$. Finally, both the approximate and exact values of $(e^{-u})_n$ are inserted in (3) to obtain the respective values of P_z.

For the discrete distribution, the number average of e^{-u} is calculated from $\Sigma_i X_i e^{-aM}$ where X_i is the mole fraction of polymer having molecular weight, M_i. The exact z average of $P(u)$ for this distribution is again obtained by using this value for $(e^{-u})_n$ in (3). The discrete distribution is unique, among the three we use, in that it permits of distributions for which $r_1 > r_0$.

Since the number average of e^{-u} for the γ distribution is identical in form with the second of our approximate series, we use only the truncated log-normal distribution in order to explore the best value for χ. In Figure 2 we display those values of χ which make complete agreement between the exact and approximate calculations of P_z. These preliminary computations were made for a number of different sets of values for r_0, r_1, and r_2, two of which are shown in the figure. The value of χ giving agreement varies with the values of P_z, but the variation is less as the amount of truncation becomes less. Also, for this situation, a greater fraction of the exponential series (larger χ) is needed. In the comparisons which follow, the approximate calculations of P_z are made with $\chi = 0.4$.

Comparisons of approximate with exact values of the z averages of $P(u)$ for a number of different sets of ratios, r_0, r_1, and r_2, are shown in Figure 3. Here the exact values were calculated from the truncated log-normal distribution function. The disagreement shown is less than 7% throughout the complete range of P_z; the abcissa in the figure is the true value of P_z. As was ensured by the method of introducing r_0, r_1, and r_2, the agreement is better for smaller values of u_n (P_z closer to unity) so that excellent values of $(s^2)_z$ ($= r_0r_1(s^2)_n$) would be obtained by using the approximate formula.

Even though a distribution may be fixed by knowledge of all of its moments, fixing the three ratios, r_0, r_1, and r_2, still leaves a distribution effect in the z average of $P(u)$ as Figure 4 shows. Here almost the same set of values for r_0, r_1, and r_2, in the two distribution functions, γ and trun-

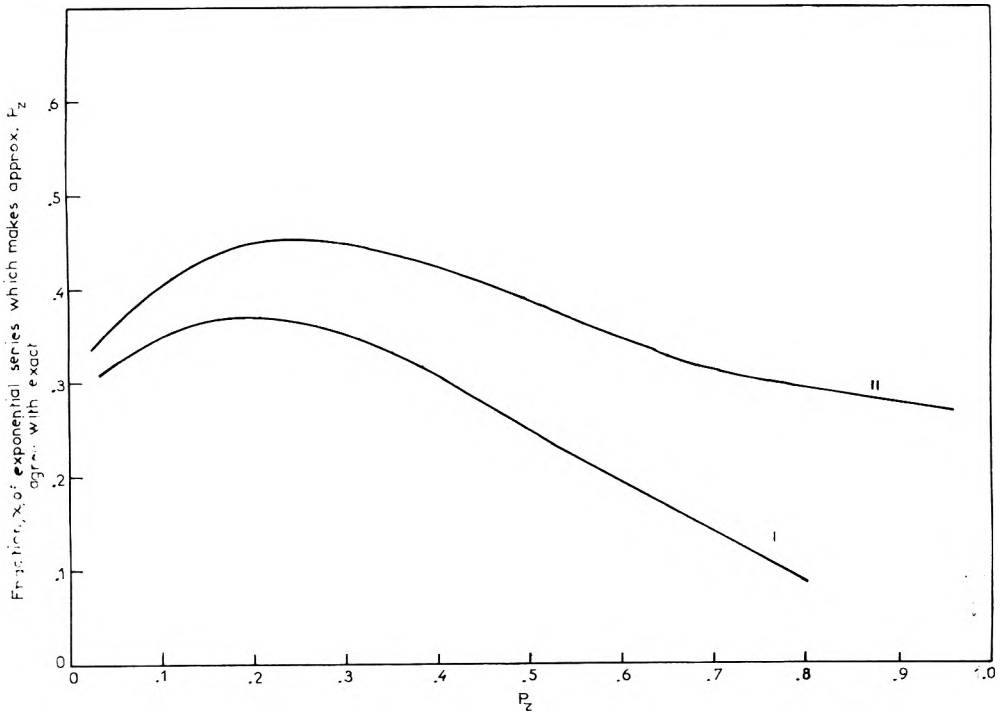

Figure 2. Fraction, χ, of exponential series which makes approximate z averages of $P(u)$ agree with true value.

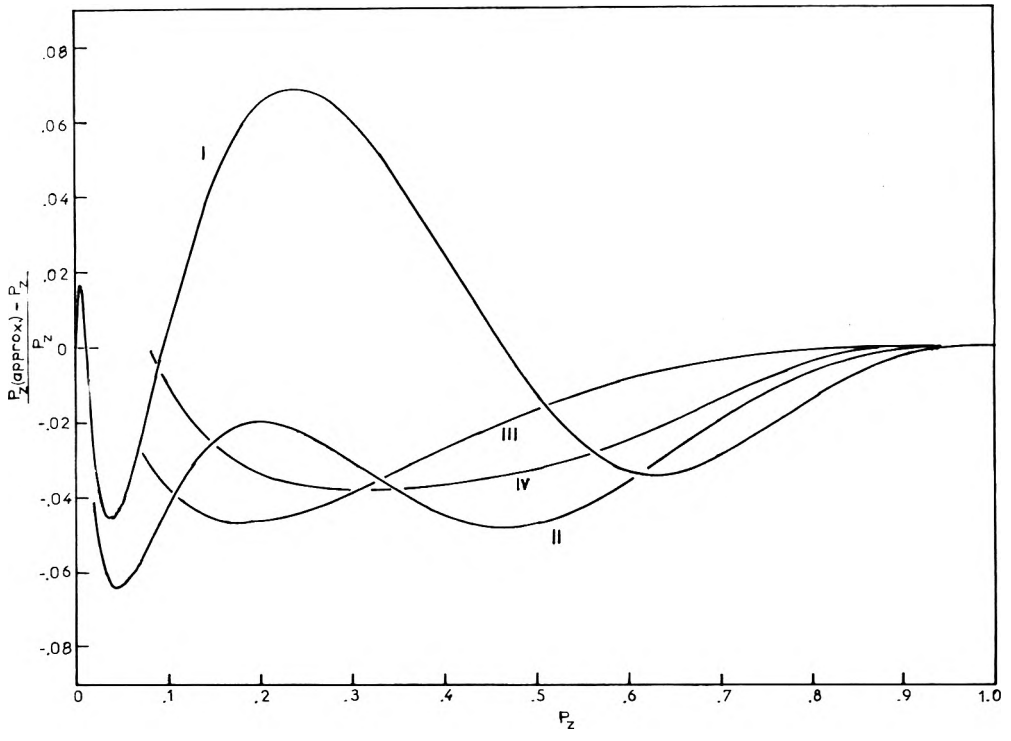

Figure 3. Comparison of approximate calculation of P_z (having $\chi = 0.4$) with true value of truncated log-normal distribution. (I, $r_0 = 50.0$, $r_1 = 27.7$, $r_2 = 4.9$; II, $r_0 = 49.9$, $r_1 = 12.4$, $r_2 = 2.4$; III, $r_0 = 8.1$, $r_1 = 2.1$, $r_2 = 1.4$; IV, $r_0 = 8.0$, $r_1 = 7.6$, $r_2 = 5.2$.)

cated log-normal, give some difference in the true value of P_z. The deviation of the approximate value from truth is still acceptable in both cases considering the present quality of scattered-light experiments.

No comparison with the discrete distribution is shown because, in general, the approximate calculation gives almost exact agreement even when $r_1 > r_0$. For example, in a distribution having $r_0 = 3.8$, $r_1 = 77.9$, $r_2 = 1.4$ (such as would occur for an essentially monodisperse polymer having a trace of much higher molecular weight impurity), the approximate formula deviates from the exact by less than 0.001% throughout the range of P_z.

An examination of relation 4 reveals that the intial portion of the curve $(M_w P_z)^{-1}$ *vs.* $((4\pi n/\lambda) \sin \theta/2)^2$ contains information about the higher moments in the molecular-weight distribution; that is, it is from this portion of the

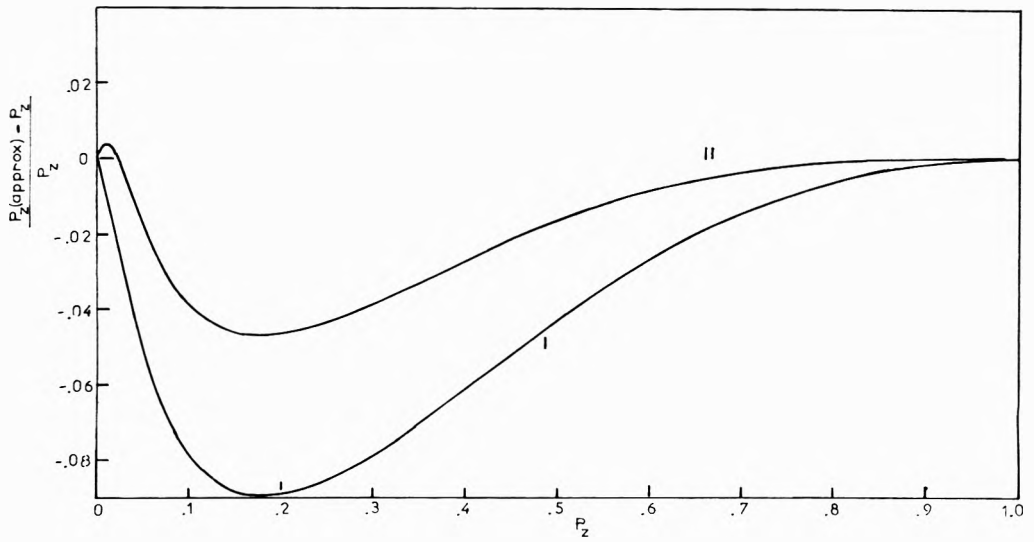

Figure 4. Comparison of approximate calculation of P_z (having $\chi = 0.4$) with true values. (I, γ distribution, $r_0 = 8.0$, $r_1 = 1.9$, $r_2 = 1.5$; II, truncated log-normal distribution, $r_0 = 8.1$, $r_1 = 2.1$, $r_2 = 1.4$.)

curve that we can learn M_w, $(s^2)_z$, and r_2. After the quantity $\delta/(1 - \delta/u_n)$ becomes effectively constant, that is, after the curve has attained a nearly constant slope, then the curve contains information about r_0 and r_1. Both of these pieces of information can be extracted because the value of δ will be known through (8). However, without a means of estimating $(e^{-u})_n$ from the experimental curve, a means which relation (8) provides, the only information which can be obtained is M_w, $(s^2)_z$, and s^2/M, equivalent to M_w, r_1, $(s^2)_z$.

Acknowledgment. The author is grateful to I. C. K. Andresen who provided not only the facilities to dc this work, but the inspiration as well.

References and Notes

(1) P. Debye, *J. Phys. Colloid Chem.*, **51**, 18 (1947).
(2) B. H. Zimm, *J. Chem. Phys.*, **16**, 1099 (1948).
(3) H. Benoit, *J. Polym. Sci.*, **11**, 507 (1953).
(4) H. Benoit, A. M. Holtzer, and P. Doty, *J. Phys. Chem.*, **58**, 635 (1954).
(5) C. Loucheux, G. Weill, and H. Benoit, *J. Chim. Phys.*, **55**, 540 (1958).
(6) D. K. Carpenter, *J. Polymer Sci., Part A-2*, **4**, 923 (1966).
(7) P. Kratochvil, *J. Poly. Sci., Part C*, **23**, 143 (1968).
(8) A. R. Shultz and W. H. Stockmayer, *Macromolecules*, **2**, 178 (1969).

Heteroconjugation of Inorganic Anions in Nonaqueous Solvents. III. Complexes of Polymolybdates and -tungstates with Chloral Hydrate

Lajos Barcza and Michael T. Pope*[1]

Department of Chemistry, Georgetown University, Washington, D.C. 20007 *(Received June 3, 1974)*

Heteroconjugates of 1,1-dihydroxy-2,2,2-trichloroethane (chloral hydrate) with a number of polyanions in nitrobenzene solution have been investigated by nmr spectroscopy. The computed formation constants (at 37°) of the 1:1 complexes are as follows: $Mo_6O_{19}^{2-}$, 1.76; $PMo_{12}O_{40}^{3-}$, 3.11; $SiMo_{12}O_{40}^{4-}$, 24.7; $PW_{12}O_{40}^{3-}$, 1.30; ClO_4^-, 2.55 M^{-1}. These figures provide the first direct quantitative measure of hydrogen bonding involving heteropoly anions and demonstrate the very low charge densities on the surface of such anions.

Introduction

In the first paper of this series,[2] we pointed out the importance of investigating the interactions of heteropoly anions with neutral organic molecules in homogeneous solution. The structures of isopoly and heteropoly anions resemble fragments of metal oxide lattices and the behavior of such complexes in solution may be used as a model for metal oxide catalyst–substrate interactions. Since hydrogen-bonded complexes involving heteropoly anions are very weak, simple "chelate"-type donors such as pyrocatechol were initially studied. Only indirect evidence for complex formation with pyrocatechol could be observed with polymolybdates owing to irreversible oxidation–reduction reactions.[3] In the present work we have used the nonreducible geminal diol, chloral hydrate (1,1-dihydroxy-2,2,2-trichloroethane) as the H-bond donor.

Experimental Section

The preparation and purification of the heteropoly salts and solvent are described elsewhere.[2,4] Chloral hydrate (Fisher) was used without further purification. Solutions for nmr measurements were prepared freshly by direct weighing and contained TMS as an internal standard.

Results

The chemical shift of the α-methylene protons of the tetrabutylammonium ion was found to be unaffected by the presence of various concentrations of the anions investigated and indicates that no significant ion pairing of these species occurs in nitrobenzene.

Although the chemical shift of the two hydroxy protons of chloral hydrate was measured for the determination of the extent of heteroconjugation, the peak of third hydrogen could also be observed. The ratios of the heights of the integrated signals were always 2:1 in the concentration range investigated (15–900 mM). The chemical shift of the two hydroxy protons was independent of concentration in solutions more dilute than 0.1 M, but small downfield shifts could be observed in more concentrated chloral hydrate solutions. Assuming that hydrogen-bonded dimers are formed in such solutions, the dimerization constant (in nitrobenzene at 37°) is calculated to be 0.164 ± 0.039 M^{-1}. Because of the limited solubilities of the polyanion salts in nitrobenzene, it was only necessary to take dimerization of the chloral perchlorate into account for the perchlorate solutions. The concentration ranges used were as follows: tetrabutylammonium perchlorate, [A^-], 10–250 mM; chloral hydrate, [H_2B], 15–125 mM; mole ratios [A^-]/[H_2B], 0.5–5. For these solutions the relative chemical shifts, Δ, ranged from 0.02 to 0.65 ppm. The corresponding figures for the polyanions were as follows: [A^{n-}], 10–60 mM ($Mo_6O_{19}^{2-}$), 7–28 mM (12-heteropoly anions); [A^{n-}]/[H_2B], 0.3–4.

The heteroconjugation constants

$$K = [AH_2B^{n-}]/[A^{n-}][H_2B]$$

were calculated by the interative procedure described previously.[4]

In this procedure the relative chemical shift of the fully complexed chloral hydrate, $\Delta_{AH_2B^{n-}}$, is also determined. This parameter could be calculated with reasonable accuracy only for the 12-molybdosilicate complex, and its value, $\Delta_{AH_2B^{4-}}$ = 1.39 ppm, was used in the calculations for the other polyanions. Using this value, and the heteroconjugation constants listed in Table I, it was possible to reproduce the observed chemical shifts to within the limits of measurement for all the solutions studied.

Discussion

The formulation of chloral hydrate as a geminal diol is well established by X-ray analysis,[5,6] cryoscopy,[7] and ^{17}O and ^1H nmr.[8] The equilibrium constant for $Cl_3C \cdot CHO + H_2O \rightleftharpoons Cl_3C \cdot CH(OH)_2$ is 2.8×10^4 at 25° in water.[9] That the situation is similar in nitrobenzene solutions is shown by the constancy of the ratio of the proton nmr signals. The formation constant for the perchlorate complex with chloral hydrate is similar to that observed[3] for the corresponding vicinal diol, ethylene glycol, but is much smaller than that for the aromatic diol, pyrocatechol (20.6 M^{-1}). On the other hand, although the stabilities of chloral hydrate complexes of perchlorate and 12-molybdophosphate are similar, we could detect no complex formation of the heteropoly anion with pyrocatechol.[2,10] Part of this failure may lie in smaller chemical shifts, $\Delta_{AH_2B^{n-}}$, for the fully complexed H donor. The $\Delta_{AH_2B^-}$ value for the perchlorate–chloral hydrate complex is about three times larger than that for the perchlorate–catechol complex. However, even allowing for this factor, and for solubility limitations, it is evident that H-bonded pyrocatechol complexes of polyanions are not as stable as those of perchlorate.[11]

The formation constants listed in Table I provide the first direct quantitative demonstration of the very low surface charge densities of isopoly and heteropoly anions. Unlike the perchlorate ion, the surface oxygen atoms of poly-

TABLE I: Formation Constants of Heteroconjugates of 1,1-Dihydroxy-2,2,2-trichloroethane with Some Inorganic Anions in Nitrobenzene at 37°

Anion	K, M^{-1}
ClO_4^-	2.55 ± 0.39
$Mo_6O_{19}^{2-}$	1.76 ± 0.41
$PMo_{12}O_{40}^{3-}$	3.11 ± 0.63
$SiMo_{12}O_{40}^{4-}$	24.7 ± 2.7
$PW_{12}O_{40}^{3-}$	1.30 ± 0.45

anions are of two types, terminal and bridging.[12] It seems likely that protonation or hydrogen bonding would take place at the bridging oxygen atoms, since the terminal oxygens are strongly polarized toward the interior of the anion by π bonding to the metal atoms.[13] The differences in stabilities of the molybdate complexes cannot simply be accounted for in terms of electrostatic (−4 *vs.* −3) arguments, but also show influences of the central atom upon the surface charge density. The central atom has elsewhere been shown to affect reduction potentials and spectroscopic properties of 1:12 heteropoly anions.[14] Finally we note the variation between the complexes of $PMo_{12}O_{40}^{3-}$ and $PW_{12}O_{40}^{3-}$. We have pointed out elsewhere[15] that, other things being equal, heteropoly molybdates are somewhat stronger Brønsted bases than the corresponding heteropoly tungstates, and the present results are consistent with this.

Acknowledgments. The support of this research by AFOSR, through Grant No. AF70-1833, is gratefully acknowledged.

References and Notes

(1) Author to whom correspondence should be addressed.
(2) L. Barcza and M. T. Pope, *J. Phys. Chem.*, **77**, 1795 (1973).
(3) L. Barcza and M. T. Pope, manuscript in preparation.
(4) L. Barcza and M. T. Pope, *J. Phys. Chem.*, **78**, 168 (1974).
(5) S. Kondo and I. Nitta, *X-Sen*, **6**, 53 (1950) [*Chem. Abstr.*, **45**, 3237 (1951)].
(6) K. Ogawa, *Bull. Chem. Soc. Jap.*, **36**, 610 (1963).
(7) S. R. Jain and S. Soundararajan, *Tetrahedron*, **20**, 1589 (1964).
(8) P. Greenzaid, A. Luz, and D. Samuel, *J. Amer. Chem. Soc.*, **89**, 749 (1967).
(9) L. C. Gruen and P. T. McTigue, *J. Chem. Soc.*, 5217 (1963).
(10) Upon heating the solutions of molybdates and pyrocatechol, reduction of the polymolybdates occurred. In the case of hexamolybdate a stoichiometric reaction produced 1,2-benzoquinone (ref 3).
(11) Earlier results with pyrocatechol led us to state that 12-molybdosilicate and -phosphate anions were less subsceptible to hydrogen bonding than was perchlorate anion (ref 2). The present results show that this statement is not necessarily valid for chloral hydrate complexes.
(12) In the Keggin (1:12 heteropoly anion) structure there are two types of bridging oxygen atom.
(13) A referee has pointed out that Strandberg interpreted long Mo–O distances in $H_6PMo_9O_{34}^{3-}$ as evidence for protonated terminal oxygens (*Acta Chem. Scand., Sect. A*, **28**, 217 (1974)). This seems reasonable, but the molybdenum atoms in question each have *two* terminal oxygen atoms. In the Keggin and $Mo_6O_{19}^{2-}$ structures each metal has a single unshared oxygen. Reduction of charge density on the oxygen by π bonding is expected to be more efficient in the latter case.
(14) M. T. Pope, *Polym. Prepr., Amer. Chem. Soc., Div. Polym. Chem.*, **13**, 787 (1972).
(15) E. Papaconstantinou and M. T. Pope, *Inorg. Chem.*, **6**, 1152 (1967).

COMMUNICATIONS TO THE EDITOR

Evaluation of Dielectric Permittivity by Time Domain Spectroscopy

Publication costs assisted by the Materials Science Program, Brown University, with support from the National Science Foundation

Sir: We present here simple formulas for evaluating complex permittivity $\epsilon^*(i\omega)$ at frequencies $\nu = \omega/2\pi$ from Laplace transforms of voltage pulses $V_0(t)$ and $R(t)$ incident on and reflected from a dielectric sample in coaxial lines, as observed by time domain spectroscopy (tds).[1]

From transmission line and network theory,[2] the input admittance y_{IN} of a dielectric sample in length d of coaxial line terminated by an admittance y_d is $y_{IN} = (y_o + y_d)/(1 + Z_s y_d)$, where $y_o = i\omega C_c d((\tanh x)/x)$ and $Z_s = i\omega L_c d((\tanh x)/x)$ are the open-circuit admittance and short-circuit impedance of the dielectric section, C_c and L_c are the geometric capacitance and inductance per unit line length, $x = i\omega\epsilon^{*1/2}d/c$, and $c = (L_c C_c)^{-1/2}$. y_{IN} is related to the transforms $v_0(i\omega)$ and $r(i\omega)$ of $V_0(t)$ and $R(t)$ by $y_{IN} = G_c(v_0 + r)/(v_0 - r)$, as the input voltage is $v_0 - r$ for our sign convention and the input current is $G_c(v_0 + r)$, where $G_c = (C_c/L_c)^{1/2}$.

For a sample inserted in a matched line, $y_d = G_c$, and combining the preceding equations gives

$$\epsilon^* - 1 = \left(\frac{2c}{d}\right)\frac{r/i\omega v_0}{1 - i\omega(r/i\omega v_0)}(x \coth x + i\omega d/c) \quad (1)$$

The approximation $x \coth x = 1 - \frac{1}{3}(\omega d/c)^2\epsilon^*$ gives an explicit solution for ϵ^* valid for $(1/45)(\omega d/c)^4\epsilon^{*2} \ll 1$. The transform of the incident pulse in commercial equipment can be approximated to quite high frequencies by $V_0/i\omega v_0 = (\omega T_r/2)\cot(\omega T_r/2) + i(\omega T_r/2)$, corresponding to a finite ramp with rise time T_r to the final value V_0.

An alternative, often preferable, method is to place the sample at the end of an open coaxial line, as proposed by Iskander and Stuckly.[3] We take $y_d = 0$ and an effective sample length d, larger than the length in the line because of end effects (by 1.5–2 mm for a 7-mm line). This gives a

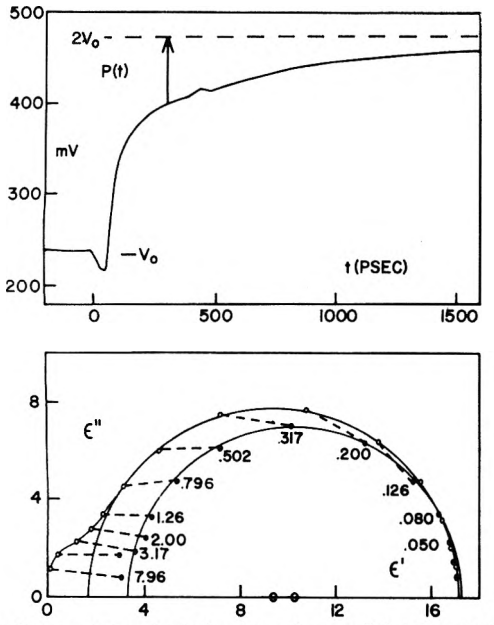

Figure 1. Upper plot: reflected voltage from a 3.4-mm sample of 1-butanol at 23° terminating a 7-mm coaxial line, as recorded from a Hewlett-Packard Type 181 tds system with 40-psec rise time. Lower plot: complex plane plot of $\epsilon^* = \epsilon' - i\epsilon''$. Open circles are calculated from $\epsilon^* = (c/d)(p/2i\omega v_0)$. Solid circles are calculated from eq 2. Numbers opposite points are frequencies in gigahertz; the dashed lines connect points for the same frequency.

simple formula for ϵ^* in terms of $p(i\omega) = r(i\omega) + v_0(i\omega)$, *i.e.*

$$\epsilon^* = \left(\frac{c}{d}\right)\frac{p/2i\omega v_0}{1 - i\omega(p/2i\omega v_0)}\, x \coth x \qquad (2)$$

The usefulness of both methods has been tested using polar liquids with relaxation time in the range 300–2000 psec (1 psec = 10^{-12} sec). As an example, the observed response $P(t) = R(t) + V_0(t)$ for a 3.4-mm sample of 1-butanol at 23° terminating a 7-mm line is shown in the upper part of Figure 1, and complex plane loci of $\epsilon^* = \epsilon' - i\epsilon''$ are shown in the lower part. The open circles are from values of $(c/d)(p/2i\omega v_0)$, corresponding to a thin-sample or lumped-circuit approximation, while the solid circles result from the more general formula (2). The corrections change the apparent frequency of Debye relaxation from 0.24 to 0.310 GHz and its high-frequency intercept ϵ_∞ from 1.7 to 3.4, with the corrected values in good agreement with other steady-state and tds results. The artifact in the uncorrected result of a second higher frequency process centered at 5 GHz is removed to the accuracy of numerical evaluation of $p(i\omega)$ from $P(t)$. Scatter in the corrected values above 2 GHz is primarily the result of this evaluation, made by simple summation of values of $P(n\Delta)\exp(-i\omega n\Delta)$ with time interval $\Delta = 40$ psec.

In our analysis, no assumptions about the form of ϵ^* have been made, exact account has been taken of the nonlinear relation of y_{IN} to $r(i\omega)$ and $v_0(i\omega)$, and effects of propagation ($x \coth x \neq 1$) can be usefully approximated in a simple way. Satisfactory results are obtained for much larger samples and reflection signals than in thin-sample[4] or lumped-capacitance[3] approximations and without recourse to computerized sampling, fast Fourier transforms, or iterative solutions used in other more general methods.

Acknowledgments. This work was supported by the Brown University Materials Science Program and the National Science Foundation. Special thanks are due to T. Copeland for the computer programs used to evaluate $p(i\omega)$.

References and Notes

(1) For a comprehensive review, see M. J. C. vanGemert, *Philips Res. Rep.*, **28**, 530 (1973).
(2) See for example G. P. Harnwell, "Principles of Electricity and Electromagnetism," McGraw-Hill, New York, N.Y., 1938, Chapter 14.
(3) M. F. Iskander and S. S. Stuckly, *IEEE Trans. Instrum. Meas.*, **21**, 425 (1972).
(4) H. Fellner-Feldegg, *J. Phys. Chem.*, **76**, 2116 (1972).

Chemistry Department **Robert H. Cole**
Brown University
Providence, Rhode Island 02912

Received October 10, 1974

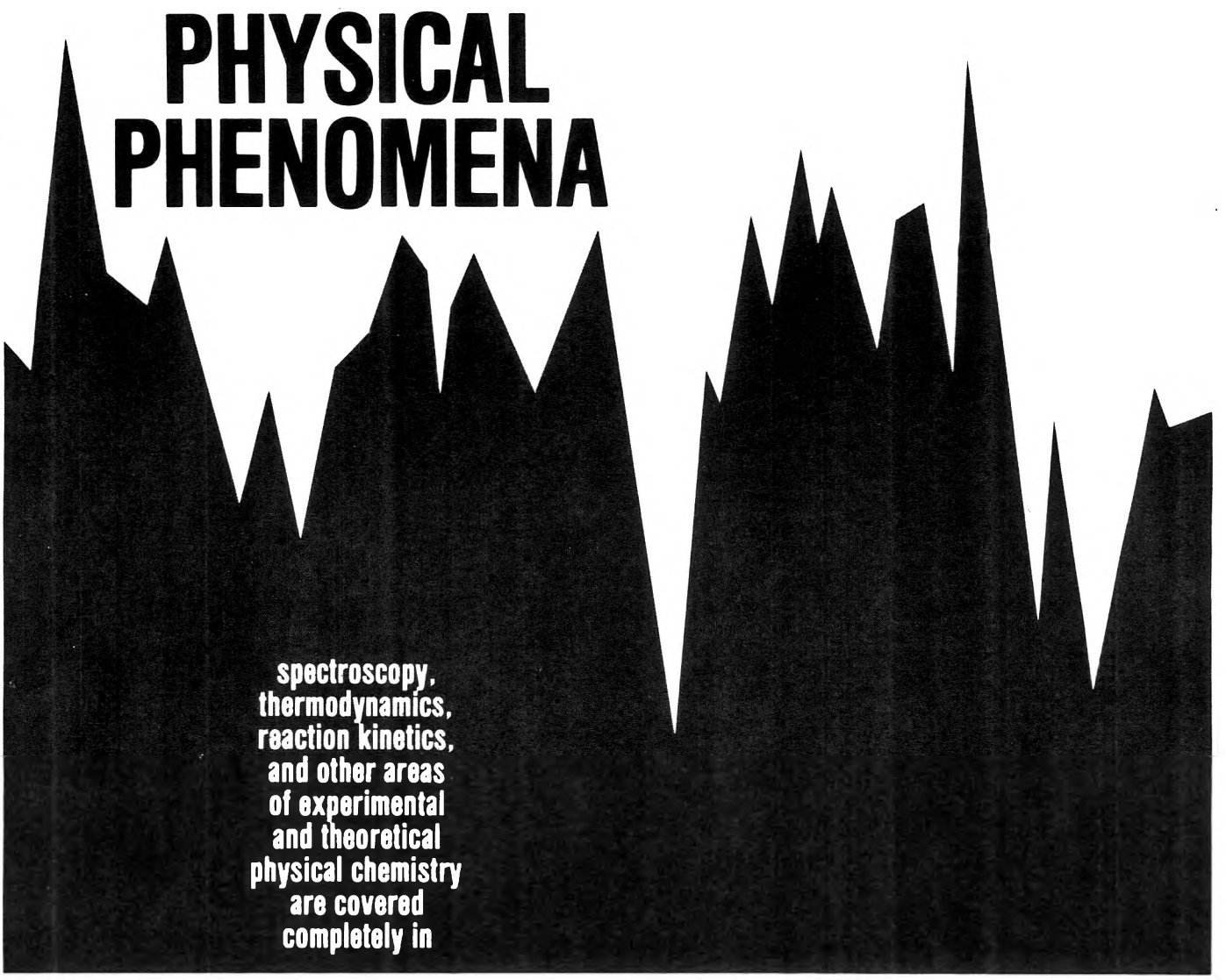

THE JOURNAL OF PHYSICAL CHEMISTRY

The biweekly JOURNAL OF PHYSICAL CHEMISTRY includes over 25 papers an issue of original research by many of the world's leading physical chemists. Articles, communications, and symposia cover new concepts, techniques, and interpretations. A "must" for those working in the field or interested in it, the JOURNAL OF PHYSICAL CHEMISTRY is essential for keeping current on this fast moving discipline. Complete and mail the coupon now to start your subscription to this important publication.

The Journal of Physical Chemistry
American Chemical Society
1155 Sixteenth Street, N.W.
Washington, D.C. 20036

1975

Yes, I would like to receive the JOURNAL OF PHYSICAL CHEMISTRY at the one-year rate checked below:

	U.S	*Canada***	*Latin America***	*Other Nations***
ACS Member One-Year Rate*	☐ $20.00	☐ $24.50	☐ $24.50	☐ $25.00
Nonmember	☐ $80.00	☐ $84.50	☐ $84.50	☐ $85.00

Bill me ☐ Bill company ☐ Payment enclosed ☐

Air freight rates available on request

Name _____

Street _____ Home ☐ Business ☐

City _____ State _____ Zip _____

Journal subscriptions start on January '75

*NOTE: Subscriptions at ACS member rates are for personal use only. **Payment must be made in U.S. currency, by international money order, UNESCO coupons, U.S. bank draft, or order through your book dealer.

Famous Scientists

Tape Cassettes From The American Chemical Society

ENERGY

- ☐ **Optical Communications** J. Cook, B. Deloach, A. D. Pearson **The Promise of Hydrogen** J. Russell
- ☐ **Energy in the Future** Dr. P. Donovan **Solar Homes for the Future**
- ☐ **Coal's New Face** Dr. B. Lee **More Power, Less Pollution** Dr. D. Bienstock
- ☐ **Cleaning a Dirty Fuel** H. Feldman **From Wastes to Energy** H. Feldman
- ☐ **Energy: A Critique** Dr. D. Abrahamson **Puzzles of Air Pollution** A. Levy
- ☐ **Fusion: Prospects & Pitfalls—Parts I & II** Dr. H. Furth & Dr. H. Forsen
- ☐ **Antidote to the Energy Crisis** G. Long **Chemicals In the Environment** Dr. S. Epstein
- ☐ **Fusion and Fission: An Appraisal** Dr. J. L. Tuck **The Prospects for Energy** Dr. M. K. Hubert

ENVIRONMENT

- ☐ **Putting Potatoes in Plastics** Dr. G. Griffin **Lead Poisoning in Children** D. Darrow
- ☐ **New Look in Phosphorus Removal** Dr. G. Levin **A Solution for Metals** T. Chapman
- ☐ **Turning Insects Against Themselves** D. Lazare **Updating Aluminum** Dr. A. Russell
- ☐ **Energy and Environmental Thrift** Dr. S. Berry **Tracing the Skeleton's Image** Dr. T. Raby
- ☐ **Come Rain, Come Shine, I.** C. Hosler **Come Rain, Come Shine, II.** Dr. S. Schneider
- ☐ **Seafood From Waste** J. Huguenin **Underwater World of Communications** Dr. J. Atema
- ☐ **Water Supply of The Future** Dr. I. Kugelman **The Secrets of Salmon** Dr. A. Hasler
- ☐ **Cleaner Water Through Chemistry** D. Parker **Bromine Chloride: A Better Disinfectant** Dr. J. Mills
- ☐ **Man & Nature in South Florida** R. McCluney **The Slick Factor in Ocean Pollution** Dr. E. Corcoran
- ☐ **The Damaged Air—I** **The Damaged Air—II**
- ☐ **How Smells Shape Up** Dr. J. Amoore **Urban Auto Design**
- ☐ **Tough Filaments of Fragile Liquid** J. Bacon **Electricity from Rooftops** Dr. C. E. Backus
- ☐ **The Struggle for Clean Water—I** **The Struggle for Clean Water—II**
- ☐ **The Oil Mystery** H. Bernard **The Language of Odors** Dr. S. Freeman
- ☐ **The Muskegon County Experiment** Dr. W. Bauer & Dr. J. Sheaffer **The Sophisticated Dowser** Dr. R. Parizek
- ☐ **The Lonely Atom** Dr. P. Skell **How Green the Revolution** L. Brown
- ☐ **Mercury: Another Look, Part I** Dr. J. Wood **Mercury: Another Look, Part II** Dr. J. Wood & D. G. Langley
- ☐ **The Troubles with Water** Dr. D. Okun **Pure Oxygen for Polluted Water** Dr. J. McWhirter
- ☐ **Bubble Machines & Pollution Finders** Dr. K. Patel & Dr. L. Kreuzer **The Steam Engine: A Modern Approach** Dr. W. Doerner & Dr. M. Bechtold
- ☐ **Insects: The Elements of Change—Parts I & II** Dr. C. M. Williams
- ☐ **New Weapons Against Insects** Dr. G. Staal & Dr. J. Siddall **Moths, Drugs, & Pheromones** Dr. W. Roelofs
- ☐ **The Lead Issue** H. Mayrsohn & M. H. Hyman **Smog: An Environmental Dilemma** Dr. J. Pitts
- ☐ **The Fusion Torch** Dr. B. East und & Dr. W. Gough **The Impermanent Plastic** Dr. J. Guillet

CANCER RESEARCH

- ☐ **Cancer & Chemicals—Parts I & II** Dr. C. Heidelberger
- ☐ **Screening for Cancer Agents** Dr. B. Ames **Narcotics & the Brain** Dr. A. Goldstein
- ☐ **Chemicals Combating Cancer** Dr. D. Grassetti **Chemical Essence of Beer & Ale** Dr. R. Palamand
- ☐ **Cancer Research I—Perspective & Progress** Dr. F. Rauscher **Cancer Research II—Viruses** Dr. R. Gallo & Dr. G. Todaro
- ☐ **Cancer Research III—Chemotherapy** Dr. C. G. Zubrod **Cancer Research IV—Immunology** Dr. P. Levine
- ☐ **Cancer Research V—Environmental Agents** Dr. U. Saffiotti **Cancer Research VI—NCI Roundtable**

SCIENCE

- ☐ **The Seas in Motion** Dr. W. Broecker **Rumbles in the Earth** Dr. C. Scholz
- ☐ **The View from Space** Drs. R. Madole & R. Anderson **The Attraction of Magnets** D. Kelland
- ☐ **Cosmic Ray Astronomy** Dr. P. Meyer **The Reactor Never Lies** T. Raby
- ☐ **Neutron Activation Analysis and Ancient History** Dr. E. Sayre **Neutron Activation Analysis: From History to Hair** Dr. and Mrs. A. Gordus
- ☐ **Wine From Native American Grapes—Parts I & II** Dr. A. Rice
- ☐ **Community Needs: New Emphasis in Research** Dr. H. G. Stever **Aspirin vs. Prostaglandins** Dr. J. Vane
- ☐ **A Breakdown in Plastics—Parts I & II** Drs. J. Guillet & G. Scott
- ☐ **Protein: The Next Big Production?** Dr. S. Tannenbaum **Clean Energy: A One-Way Dream** Dr. J. R. Eaton
- ☐ **Science, Scientists, & the Public Interest—Parts I & II**
- ☐ **Nitrosamines: A Reappraisal** Dr. P. Issenberg **The Emperor of Ice Cream** Dr. W. Arbuckle
- ☐ **Ethics and Genetics** Dr. R. F. Murray **The American Diet: A Critique** Dr. A. Schaefer
- ☐ **Probing Creation** Dr. M. A. Coler **New Directions in U.S. Science** Dr. W. McElroy
- ☐ **Aspirins, Enzymes, & Fragrant Redheads** An Essay Report **Vitamin D: A New Dimension** Dr. H. DeLuca
- ☐ **Pica (Lead Poisoning)** Dr. J. J. Chisolm, Jr. **Technology in the Nursery** Dr. W. J. Dorson
- ☐ **Engineering Microbes** Dr. E. Gaden **Liquid Crystals: A Bright Promise** Dr. G. Heilmeier
- ☐ **Hot Brines in the Red Sea** Dr. D. Ross **Complete Corn** Dr. E. T. Mertz
- ☐ **Lively Xenon** Dr. N. Bartlett **The Repressor Hunt** Dr. M. Ptashne
- ☐ **The New Prospectors** Dr. W. Prinz **A Sober Look at Alcoholism** Dr. J. Mendelsohn
- ☐ **Probing the Active Site** Dr. D. Pressman **The Puzzle of Diversity** Dr. O. Smithies
- ☐ **Help for the Have Nots** Dr. H. Brown **The Closing Circle** Dr. P. Cloud

BIO-MEDICAL

- ☐ **Monitoring High Risk Pregnancies** Drs. G. Stiles & J. Hobbins **Progress in Enzyme Replacement Therapy** Dr. R. Brady
- ☐ **Safety for Premature Infants** Dr. J. Morrison **Help for the Critically Ill** Dr. J. Moylan
- ☐ **Pinpointing Hepatitus Viruses** Dr. R. Purcell **New Key to Heart Disease** Dr. A. Gotto
- ☐ **Nature's Own Toxicants in Foods** Dr. J. M. Coon **Added, Not Intended** Dr. H. Kraybill
- ☐ **Seventy-Two Per Minute, I** Dr. L. Harmison **Seventy-Two Per Minute, II** Dr. N. Rasor
- ☐ **Filling the Molar Gap** Dr. J. Cassel **Two Drugs, More or Less** Dr. K. Hussar
- ☐ **A Tilt at Genetic Ills** V. Aposhian **Binding the Catalysts of Life** Dr. H. Garfinkel
- ☐ **Early Prenatal Diagnosis of Genetic Disease** Dr. M. L. Moss **From Mother to Child** Dr. M. Horning & Dr. R. Hill
- ☐ **Insulin & Diabetes—I** Dr. G. Cahill **Insulin & Diabetes—II** Dr. G. Cahill
- ☐ **Stalking the Molecules of Memory** Dr. L. Iverson **Immunotherapy** Dr. K. Bagshawe
- ☐ **Engineering Enzymes** Dr. V. Edwards **On Drugs, Plasticizers, & Mass Spec** Dr. G. W. A. Milne
- ☐ **Body Metal** Dr. T. Clarkson **Judging Technology** Dr. E. G. Mesthene
- ☐ **Prospects for the Living Filter** Dr. R. Parizek **Coral Designs** Dr. E. White
- ☐ **Bones, Teeth, & Ceramics** T. Driskell **PCBs: The Accidental Pollutants** Dr. H. Enos
- ☐ **Birth Control: Problems & Prospects** Dr. C. Djerassi **Hormones, Terpenes, & the German Air Force** Dr. A. J. Birch
- ☐ **Prospects for Implants** Dr. D. Lyman **New Dimensions for Polymers** Dr. A. Michaels
- ☐ **Fabricating Life** An Essay Report **New Ways to Better Food** Dr. R. W. F. Hardy
- ☐ **Chemistry of the Mind: Schizophrenia** Dr. L. Stein **Chemistry of the Mind: Depression** Dr. J. Elkes
- ☐ **The Molecules of Memory** Dr. W. L. Byrne & Dr. A. M. Golub **The Matter with Memory** Dr. J. McGaugh
- ☐ **Dissonant Harmony** Dr. D. Harman **Why We Grow Old** Dr. H. Curtis
- ☐ **New Materials for Spare Parts** Dr. V. Gott & Dr. A. Rubin **Against Individuality** Dr. R. Reisfeld & Dr. B. Kahan
- ☐ **A Richness of Lipids** Dr. R. O. Brady **Life: Origins to Quality** Dr. S. Miller
- ☐ **The Nitrogen Fixer** Dr. E. v. Tamelen **Prostaglandins: A Potent Future** Dr. E. J. Corey & Dr. S. Bergstrom
- ☐ **A Glass Revolution** Dr. S. D. Stookey **A View of Genes** Dr. N. Davidson
- ☐ **Chemical Evolution** Dr. R. Doolittle **An Evolving Engine** Dr. R. E. Dickerson

NOBEL PRIZE WINNERS

- ☐ **Dr. L. Pauling** The Committed Scientist **Dr. J. Bronowski** Science and Man
- ☐ **Dr. G. Seaborg** The Atomic World of Glenn Seaborg **Dr. G. Wald** Vision, Night Blindness, & Professor Wald
- ☐ **Dr. M. Calvin** The Search for Significance—Parts I & II

OUTER SPACE

- ☐ **Mapping Molecular Fossils** Dr. M. Rossman **Beginnings of Life** Dr. S. Fox
- ☐ **Man in the Solar System** Dr. W. R. Downs **From Meteorites to Man** Dr. E. Anders
- ☐ **In Search of Life: Planetary Evolution** Dr. I. Rasool **In Search of Life: Chemical Evolution** Dr. C. Ponnamperuma
- ☐ **Molecules in Space** Dr. D. Buhl & Dr. L. Snyder **Chemistry Among the Stars** Dr. B. Donn
- ☐ **Molecules Meeting Molecules** Dr. J. Richards **The Neutrinos of the Sun** Dr. R. Davis

	ACS Members	Nonmembers	Order from:
Single cassette	*$5.59	$6.59	American Chemical Society
Any Eight cassettes	$4.20/cassette	$5.20/cassette	1155 16th Street, N.W.
Any 20 or more cassettes to one address		$4.00/cassette	Washington, D.C. 20036
10% Discount if payment accompanies order			ATTN: A. Poulos